UNIVERSITÀ
DEGLI STUDI
FIRENZE

Scuola di Ingegneria

DIEF - Department of Industrial Engineering of Florence

DOTTORATO DI RICERCA IN

Ingegneria Energetica e Tecnologie Industriali Innovative

DEVELOPMENT OF A NEW COMBUSTOR LINERS THERMAL DESIGN PROCEDURE THROUGH LOW ORDER CODES AND UNCERTAINTY QUANTIFICATION TOOLS

Scientific Area: ING-IND/08 – Macchine a Fluido

PhD Candidate
Ing. Poggiali Matteo

Tutor
Prof. Ing. Facchini Bruno

Academic Supervisor
Dr. Ing. Andreini Antonio

PhD School Coordinator
Prof. Ing. Manfrida Giampaolo

XXXIII PhD School Cycle - 2017-2020

To my loved ones,
anchor of my life

Acknowledgements

And in the end,
it is not the years in your life that count.
It is the life in your years.
(Abraham Lincoln)

Abstract

Turbomachinery plays an important role in the propulsion and heavy-duty industry. Improving the efficiency and reliability of gas turbines continue to be an important driver in the development of modern engines and power generation. There are two straightforward and effective methods for improving the performance of a gas turbine engine. One is increasing the engine pressure ratio to raise the thermal efficiency, the other is increasing the outlet temperature of a combustor to raise the specific thrust. Therefore, the gas turbine combustors working conditions are moving towards higher temperature rise and higher heat capacity. Therefore, the design requirements for a combustor become stricter, such as a wider working range, shorter length, and smaller distribution of outlet temperature. Simultaneously, the combustor is required to have a longer life and lower pollutant emission.

In this scenario, a fundamental role is played by the cooling system. The definition of the most appropriate scheme represents one of the most challenging tasks in the combustor since it directly determines the components life.

During the design and subsequent optimization phases of a combustor cooling system, the designer must consider several uncertainties related to manufacturing, geometry and operating conditions. These gaps can be very impacting on the system performance, so it is obvious that the design becomes a matter of optimization of the whole system. This requires an accurate assessment of trade-offs to meet all requirements.

The design choices made in the first phases influence the following developments and it is essential to have a tool as efficient and flexible as possible to rely on. During the initial stages, *1-D* codes are still widely used in industrial practice, and a low-order approach is preferred over high-fidelity simulations. These tools are important for designers because they allow having a good understanding of the problem, in relatively short times and with low general costs. Although these analyses have a good predictive level, they are often used when input quantities that characterize the problem are roughly known. These gaps lead to the inclusion of uncertainties within the code, which propagate and eventually influence the solution. The final common objective is to optimize the various components to find out the configuration in which the machine is independent from the uncertainties that may afflict it, thus arriving at a robust design.

The aim of this thesis is the development of a numerical procedure for the preliminary thermal design of combustor liners (*Therm-1D/Dakota*). This procedure is based on the coupling of a one-dimensional tool

(*Therm-1D*), developed by *DIEF* of the University of Florence, and a software that allows uncertainty quantifications analyses (*Dakota*).

This has allowed the development of an innovative, faster, and more reliable procedure for the preliminary design and optimization of combustor cooling systems that is able to estimate the uncertainties affecting the results of this numerical simulations. In this way, the output quantities are as independent as possible from input uncertainties.

Contents

List of Figures

List of Tables

Nomenclature

Acronyms

ACARE	*Advisory Council for Aeronautics Research in Europe*
AFRL	*US Air Force Research Lab*
AM	*Additive Manufacturing*
BC	*Boundary Conditions*
CFD	*Computational Fluid Dynamics*
CHT	*Conjugate Heat Transfer*
CIAM	*Central Institute of Aviation Motors*
CJ	*Chapman-Jouguet*
CPC	*Constant Pressure Combustion*
CVC	*Constant Volume Combustion*
DOE	*Design of Experiment*
FAR	*Fuel Air Ratio*
FEM	*Finite Element Model*
ICAO	*International Civil Aviation Organization*
IR	*Infrared Thermography*
LEMCOTEC	*Low EMission COre-engine TEChnologies*
LHS	*Latin Hypercube Sampling strategy*
LP	*Lean Premixed*
MC	*Monte Carlo method*
PCE	*Polynomial Chaos method*
PDC	*Pulse Detonation Combustors*
PDE	*Pulse Detonation Engine*
PGC	*Pressure Gain Combustion*
PIV	*Particle Image Velocimetry*
PM	*Particulate Matter*
PSP	*Pressure-Sensitive Paint*
RANS	*Reynolds Averaged Navier Stokes*

RDC	*Rotating Detonation Combustors*
RDE	*Rotating Detonation Engine*
RQL	*Rich-Quench-Lean*
SC	*Stochastic Collocation method*
SCALAR-E	*identifies the coolant mass fraction originating from the effusion holes*
SFC	*Specific Fuel Consumption*
SOPRANO	*Soot Processes and Radiation in Aeronautical inNOvative combustors*
TBC	*Thermal Barrier Coating*
TP	*Test Point*
TU	*Technische Universität Berlin*
UQ	*Uncertainty Quantification*
ZND	*Zel'dovich-Neumann-Doring*

Greek symbols

α	*Inclination Angle*	*[deg]*
ε	*Emissivity*	*[-]*
η	*Effectiveness*	*[-]*
θ	*Non-Dimensional Temperature*	*[-]*
λ	*Thermal conductivity*	*[W m^{-1} K^{-1}]*
μ	*Dynamic viscosity*	*[Pa s]*
μ	*Mean value*	*[-]*
ρ	*Density*	*[kg m^{-3}]*
σ	*Boltzmann constant - Standard Deviation*	*[-]*
ϕ	*Equivalence Ratio*	*[-]*

Symbols

∞	*Bulk conditions*	*[-]*
Ar	*Aspect Ratio*	*[-]*
BR	*Blowing Ratio*	*[-]*
C	*Oxygen Concentration*	*[%]*
C_1	*Gas Side Convection*	*[W]*
C_2	*Coolant Side Convection*	*[W]*
C_d	*Discharge coefficient*	*[-]*
D	*Diameter*	*[m]*
d	*Effusion holes diameter*	*[m]*

d_d	*Dimple diameter, Pin-fin diameter, Impingement Jet hole diameter*	*[m]*
D_h	*Hydraulic Diameter*	*[m]*
DR	*Density Ratio*	*[-]*
e	*Rib height, Dimple depth*	*[m]*
e^+	*Roughness Reynolds Number*	*[-]*
f	*Friction Factor*	*[-]*
h	*Heat Transfer Coefficient*	$[W\ m^{-2}\ K^{-1}]$
$H(e^+)$; $G(e^+)$	*Heat transfer Roughness Function*	*[-]*
I	*Momentum Flux Ratio*	*[-]*
l	*Effusion holes length*	*[m]*
m	*Mass flow rate*	$[kg\ s^{-1}]$
M	*Blowing ratio*	*[-]*
N	*Sampling dimension*	*[-]*
NHFR	*Net Heat Flux Reduction*	*[-]*
Nu	*Nusselt Number*	*[-]*
OPR	*Overall Pressure Ratio*	*[-]*
P	*Pressure*	*[Pa]*
Pr	*Prandtl Number*	*[-]*
P/T	*Pilot-to-total fuel split*	*[-]*
q	*Wall heat flux*	$[W\ m^{-2}\ K^{-1}]$
R	*Generic response function*	*[-]*
$R(e^+)$	*Friction Roughness Function*	*[-]*
R_1	*Gas Side Radiative heat load*	*[W]*
R_2	*Coolant Side Radiation*	*[W]*
Re	*Reynolds Number*	*[-]*
s	*Entropy*	*[kJ/(kmol·K)]*
S	*Curvilinear Abscissa*	*[-]*
St	*Stanton Number*	*[-]*
S_x , S_y	*Pitch*	*[m]*
T	*Temperature*	*[K]*
t	*Effusion plate thickness*	*[m]*
TIT	*Turbine Inlet Temperature*	*[-]*
Tu	Turbulence	[-]
v	*velocity*	$[m\ s^{-1}]$
VR	*Velocity Ratio*	*[-]*
x	*value*	*[-]*
Z	*Channel height*	*[m]*

Subscripts

∞	*Bulk conditions*
0	*Total – Reference*
ad	*Adiabatic*
an	*Annulus*
aw	*Adiabatic wall*
casing	*Casing*
cold	*Cold Side*
cool	*Coolant*
E	*Enhancement*
r2	*Evaluated for a duct with two ribbed walls*
r4	*Evaluated for a duct with four ribbed walls*
g	*Gas*
hot	*Hot Side*
hs	*Heat sink*
is	*isoentropic*
main	*Main flow – Hot Side – Mainstream*
ov	*Overall*
smooth	*Smooth channel*
turb	*Presence of turbulators*
w	*Wall*

Introduction

Turbomachinery plays an important role in the propulsion and land-based power generation industry. Improving the efficiency and reliability of gas turbines continue to be an important driver in the development of modern engines and power generation. As stated by *Lefebvre* [1], developments in the art and science of gas turbines have traditionally taken place gradually and continuously, rather than through dramatic change. However, during the last three decades, the more demanding request for engine improvements in overall efficiency and power output caused a rapid acceleration in the development of more performing systems.

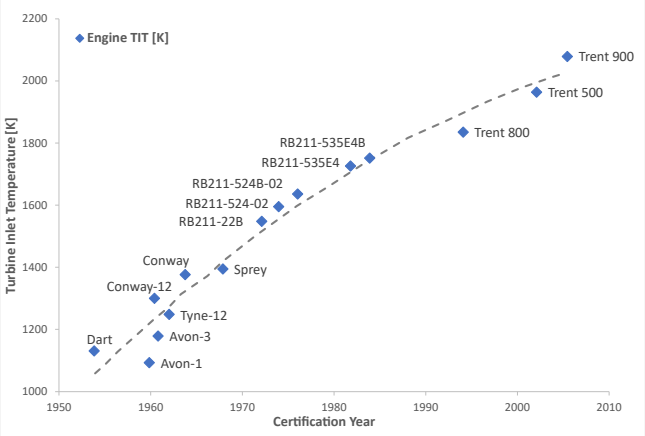

Figure 1 - Evolution of turbine inlet temperature over the years (Figure reproduced by data from Rolls Royce jet engine.)

The demand for more efficient gas turbines with increased specific power output is directly related to the possibility to realize compressors with high compression ratios and high efficiency and to build components capable of withstanding high temperatures. In fact, for a conventional gas turbine cycle, the thermal efficiency is mainly a function of the overall pressure ratio (OPR) and the turbine inlet temperature (TIT). This tendency is also shown in Figure 1 and Figure 2 which show the trends of TIT and OPR over the last 50÷70 years for aeroengines.

Overall pressure ratio and turbine inlet temperature directly affects the design of the combustor and the high pressure turbine, which are the most critical components from a thermal point of view.

According to *Lefebvre* [1], the increase in the overall pressure ratio allows to obtain substantial reductions in engine fuel consumption. Unfortunately, increasing the OPR raises the radiative heat transferred to the liner walls; also, increasing the pressure ratio causes an increase in combustor inlet temperature, thus reducing the capability of the annulus air to cool the walls. On the other hand, an increase of turbine inlet temperature directly affects the overall efficiency of the engine; therefore, the necessity of increasing the TIT calls for improvements in combustor pattern factor in order to maintain the integrity of the downstream hot sections.

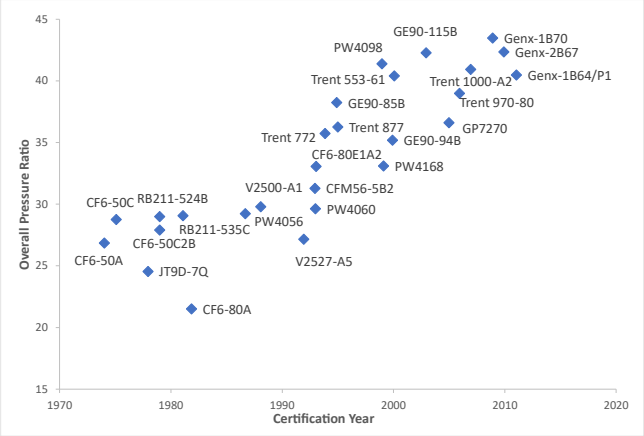

Figure 2 - Engine overall pressure ratio increment. (Data Source: the engine certification data sheet of International Civil Aviation Organization (ICAO))

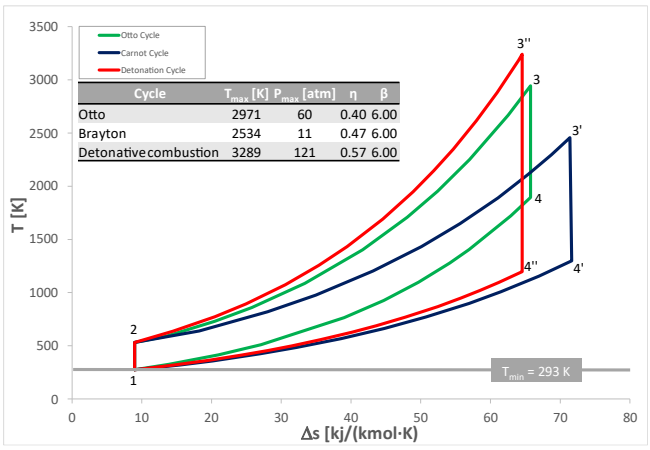

Figure 3 - T-s diagrams, comparison of combustion systems

Moreover, as noted by *Mellor* in [2], as combustor operating temperatures have been increased, component durability and life expectations have also risen, thus the operating time before combustor maintenance has exponentially grown.

According to *Lefebvre* [1], another fundamental point for the improvement of turbomachinery is the introduction of new combustion technologies. In order to improve the performance of gas turbine systems, one of the most important alternatives recently investigated is the possible modification of the thermodynamic cycle at the base of the system. It can be seen from the comparison in Figure 3 that the use of a combustion system based on new concepts (detonating combustion – red line) can lead to greater

efficiencies as well as lower increases in entropy. This system is not yet in use but should be the object of further investigation considering its potentiality.

The Figure 3 shows three cycles (*Otto, Carnot, Zel'dovich*) realized at the same T_{min} and pressure ratio. In the same image there is also a table that lists the values of the thermal efficiency of the cycles, their maximum temperature, maximum pressures. The foregoing confirms the comparison of the considered three cycles in the entropic diagram. It is shown that at the same degree of compression the detonation cycle has higher thermal efficiency than the Brayton and Otto cycle.

However, detonation is a phenomenon which is difficult to manage due to its instability and complexity of the flow field. Also, during this combustion process, a huge amount of energy at high pressure and temperature is released, considerably stressing the combustor structure. One of the biggest issues in rotating detonation combustors (RDCs) comes from the complexity and the high frequency of the flow field inside the combustion annulus, combined with its strength and high energy release due to the detonation phenomenon. These two aspects lead to the problem of heat fluxes to the combustor walls.

Therefore, it is evident that the need to develop more powerful and efficient gas turbine systems leads all the components of the hot path, combustor and turbine, to undergo stronger thermal stresses that could lead to dangerous damages and failures. And this happens both when OPR and TIT are increased and when new combustion technologies are introduced.

Figure 4 shows the historical trend in TIT and the development of maximum allowable metal operating temperature. The average increase in TIT has been around 19 K/year, which is substantially higher than the increase in operating metal temperature of around 5 K/year [3]. This discrepancy is compensated by the ever more sophisticated cooling techniques. When the TIT exceeds the allowable metal operating temperature significantly, a large amount of bleed air is required to cool all the components of the hot path.

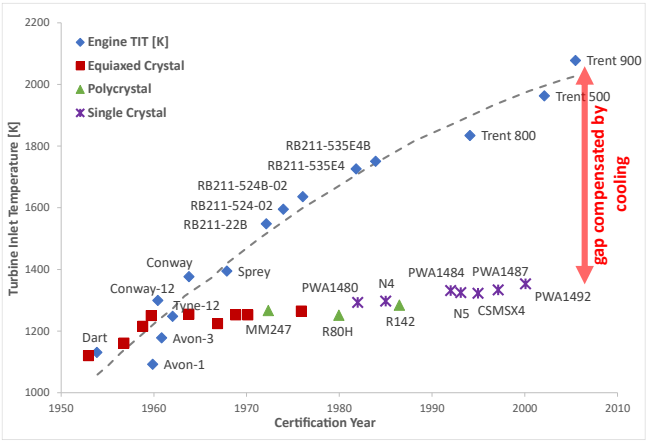

Figure 4 - Evolution of turbine inlet temperature and metal operating temperature over the years (Figure reproduced by data from Rolls Royce jet engine.)

The bleed air used for cooling does not completely participate in the main cycle, thereby imposing penalties on the cycle performance.

For these reasons, the design of efficient cooling systems becomes mandatory and the definition of the most appropriate cooling scheme represents one of the most challenging tasks in the combustor and turbine design since it directly determines the component's life. It is therefore critical to efficiently use the coolant

air and maximize the cooling effectiveness per unit mass of injected coolant [4]. It is also evident comparing Figure 1 and Figure 4, that engineers have continually pushed the TIT to higher values and beyond the material limits of the hot gas path components, and this gap has always been covered by the continuous improvement of cooling systems. Indeed, through active cooling technologies, designers have nearly doubled the inlet temperature of gas turbines since the beginning of the previous century [5,6].

During the design phases of the cooling scheme, due to its importance in providing adequate life and performances of the whole system, uncertainties are not to be underestimated. Among the most important, it is worth to mention those related to manufacturing, geometry, but also the ones imposed by the operating conditions.

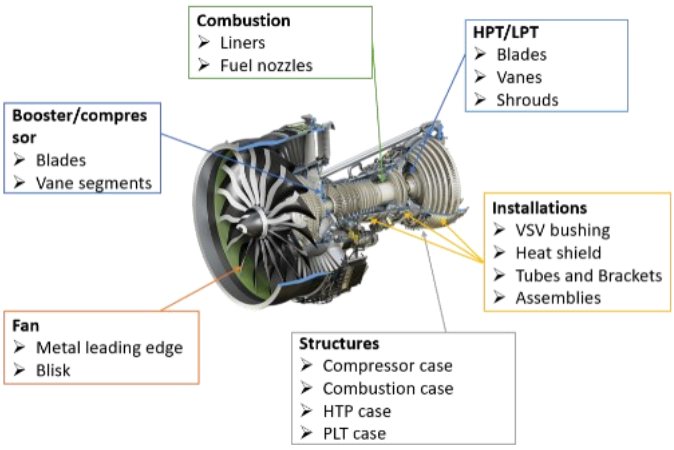

Figure 5 - Turbomachinery components produced with AM

As a matter of fact, another aspect that has certainly contributed to turbomachinery evolution has been the technological development related to materials and manufacturing processes that led to a significant improvement in reliability. Nowadays, this growth is aided by the onset of new technologies, as Additive Manufacturing (AM) which is a manufacturing process that is gaining importance in the production of turbomachinery components. There are several applications of this technology for the production of many components, as shown in Figure 5. This also involves the liners of the combustors and therefore their cooling systems.

Of course, AM provides increased design flexibility, shorter production periods, the realization of very complex geometries, and therefore possible economic advantages. Turbomachinery designers have found innovative and creative ways to design parts thanks to the AM process. On the other hand, as it is known each manufacturing process is associated with a certain tolerance that depends on the process itself [7]. In this context, these methods still present significant critical issues for this type of application [8,9]. This causes a further increase in the geometrical uncertainties that must be taken into account during the design phases of cooling systems, as they affect performance. The combustor is very sensitive to changes in the efficiency of the cooling system; this, in turn, is closely dependent on geometric tolerances; so, the various uncertainties inherent in the manufacturing processes used have a great impact on the performance of the system.

Moving on to the operating conditions, for *Heavy Duty* applications the first question mark is related to the real working conditions. In fact, these machines tend to work more and more often in off-design conditions compared to the nominal design conditions. Transient operation is of critical importance for machines and in this phase, the greatest uncertainties related to the operation and internal temperatures are found in this phase [10]. As far as aero engines are concerned, in the work of *Massini & Montomoli* [11], the most important uncertainties are discussed. Focusing on the combustion chamber, the great uncertainty within the combustors is related to the temperature profile at the outlet that goes to invest the first stage of the turbine. Although the TIT is a key parameter for the performance of the entire machine, it is difficult to measure it directly because of the problems related to the high temperature and pressure values; the typical conditions of the combustor exit are around 1800-2300 K with pressures up to 40 bar [12]. For the cooling of the combustor walls, the level of internal turbulence is a key parameter, which, however, is usually estimated only by numerical simulations.

So, it's clear that all of these factors become more crucial when considering combustors. Combustors are the core component of the gas turbines systems and operate at high energy intensity. Compared to other engine components such as the turbine blades, the liners must survive high temperature and thermal gradients, that undermine their durability.
With these assumptions, it is immediately clear that the design and development of more efficient cooling systems are essential to ensure further development of turbomachinery systems.
For this reason, it is immediately comprehensible that from the early stages of design it is necessary to have the most powerful and flexible tool to rely on.

Aim of the work

The main objective of this research is the development of a numerical procedure for the preliminary thermal design of combustor liners (*Therm-1D/Dakota*). This procedure is based on the coupling of a one-dimensional tool that solves the radial heat transfer inside the combustor and obtains the liner wall temperature (Therm-1D) and a software that allows uncertainty quantifications analyses (Dakota). This has allowed the development of an innovative, faster, and more reliable procedure for the preliminary design and optimization of combustor cooling systems.

Based on the above discussion to ensure the life of the combustor it is therefore necessary to:

- Keep liner temperatures below critical
- Have acceptable temperature gradients
- Reduce the thermomechanical stresses to which this component is subjected

For this reason, the development of an effective cooling system is fundamental. At the same time, it is crucial to take into account all those uncertainties that such evaluations involve:

- Manufacturing process [8,9]
- Geometry [7]

- Boundary Conditions [10,11]
- Modeling [13]

All these factors just described have a strong impact on the performance in turbomachinery. With these assumptions, it is necessary to have more reliable tools for the cooling system preliminary design. So, it becomes mandatory to create a new procedure that considers all the uncertainties involved during that phase.

During the initial stages, many parameters are often approximately known. Exploring the entire design space is extremely important to better understand the system behavior and it is critical to know the most promising first attempt configurations, which will then be refined with computational fluid dynamics and finally validated with experimental tests. The considerable cost and time associated with experimental campaigns and numerical simulation make such an approach unsuitable during the preliminary stages of combustor design. Tools combining *0-D* and *1-D* approaches [14,15] based on the procedure described by *Lefebvre* [1] are able to quickly solve Conjugate Heat Transfer (CHT) problems with acceptable accuracy. So, *1-D* codes are still widely used in industrial practice, and a low-order approach is preferred over high-fidelity simulations.
The one-dimensional tool used during this research (Therm-1D), developed by *DIEF* of the University of Florence, solves the conjugated fluid-wall calculation by imposing the condition of the radial thermal equilibrium of the liner, neglecting the heat transfer in the circumferential and axial direction. The whole procedure is carried out iteratively.
The main inputs are the main geometric features and boundary conditions. The code may be dependent on uncertainties in these parameters.

In this context, uncertainty quantification plays an important role. With the introduction of this methodology within the design procedure it is possible to define components that are not intrinsically influenced by possible geometric variations and boundary conditions: this procedure is called *Robust Design*. As reported by *Iaccarino* [16], in order to obtain the real predictive capacity of the simulation and, in turn, the correct validation, it is necessary a rigorous evaluation of the uncertainties that are introduced into the numerical code; in the same way, as it happens for the tests carried out in the laboratory. Non-intrusive UQ methods allow to determine the propagation of uncertainties within a numerical code, so it is possible to know how much an input variable affects the final solution and probabilistic information can be obtained using a discrete approach. Some UQ software has procedures for dealing with variables that are not independent from each other. This allows to introduce correlated variables and still obtain distributions from independent variables. This feature is very useful for the study of uncertainties in systems that solve heat transfer since it is often complicated to identify only independent variables.

The integrated tool *Therm-1D/Dakota* is necessary to obtain a robust design, i.e., within the limits of the capabilities of the code, having the output quantities as independent as possible from uncertainties. Thus,

the evaluations made are released from what are the uncertainties related to the behavior of the code and those dependent on the input data.
These methodologies, if correctly used, can lead to a complete understanding of how the mathematical model approximates and solves the real physical problem.

Thesis Outline

The dissertation will be organized as follows:

- **Chapter 1:**

  Here are described the tools and procedures that will be used during the entire investigation. Also, the fundamentals for understanding the UQ methodologies that will be discussed are provided.

- **Chapter 2:**

  To better explain the context into which the work has been carried out the RQL, Lean and RD combustor are presented.

  The cooling technologies to manage the thermal loads are been here described. The chapter is focused on the description of those analyzed during the dissertation.

- **Chapter 3:**

  In this chapter, the first application of the coupled procedure described above is presented. This application was performed with a triple purpose. The first aim is to increase the level of experience in the use of UQ techniques applied to one-dimensional codes. The second purpose is to verify the accuracy of the uncertainty propagation methods and the relative sampling grids, comparing the spectral methods with the Monte Carlo method. The third purpose is to carry out a critical analysis of the Therm-1D procedure, analyzing the main input or tuning parameters, those that introduce the greatest uncertainties in the system response.

- **Chapter 4:**

  In this chapter, a new procedure is developed for a faster and more reliable setup of the input boundary conditions to the Therm-1D tool. The analysis is related to the thermo-fluid dynamic conditions in the combustion chamber. The procedure is developed and validated for a combustor liner realized in AM and cooled with effusion cooling techniques. Here, the UQ analysis is aimed to define a robust design associated with the developed procedure.

- **Chapter 5:**

  Here a heat transfer problem analysis and an assessment of air cooling feasibility for Rotating Detonation Combustors have been done. Thus, with Therm-1D/Dakota procedure, different cooling system fluid network layouts were modeled and their performances have been evaluated varying the characteristic parameters of every solution adopted, to highlight what are the main influencing aspects relative to each heat transfer augmentation solution. Once that these parameters have been found, Uncertainty

Quantification and Sensitivity Analysis has been performed to evaluate how the variation of each one of them, singularly and overall, could affect cooling system performances. From these analyses it has been possible to build several operational maps that show the behavior of the different tested layouts, giving a guideline to possible improvements in the cooling system design operations.

Chapter 1

Methodologies

Introduction

A reliable design tool for the thermal management of hot gas path components is vital to improve the capabilities and fulfill all the technical requirements demanded to a modern combustor. The development process of a new product is characterized by several steps, in which it evolves from a simple concept to its final configuration. The process could be thus subdivided into different phases: the concept design, the preliminary design and the detailed design, after which the actual performances of a prototype are usually verified utilizing experimental tests. Each phase is characterized by intermediate checks aimed at confirming if the targets are fulfilled and, in case, revising the design.
As a consequence, an appropriate trade-off between speed and accuracy must be identified during the development of the design tools. Concept design usually consists in *0D* analyses, whereas in the preliminary design the geometry is studied employing equivalent *1D* flow networks and simplified *2D* CFD/FEM models, that exploit correlative approaches aimed at approximatively estimating pressure losses and heat transfer. These phases are characterized by the investigation of many geometries, often using optimization codes to identify the most promising configurations able to provide the required performance. Afterward, more detailed (and onerous) investigations are carried out through *3D* CFD analyses, to verify the validity of the design choices before the manufacturing of a prototype.

As introduced, one-dimensional codes are still a fundamental tool for the design of complex systems, such as cooling schemes for combustor chambers or turbine blades. They are based on the use of engineering simplified models that are linked to each other to represent the whole combustor cooling system. Such type of codes are characterized by a wide library of elements used to describe the different parts of the system, from simple models to represent an orifice or a straight pipe to more complex models used to represent cooling arrangements, such as impingement or effusion cooling.
They rely on simplified models that describe the different parts of the system, from simple orifices, straight and curved pipes to more complex models representing impingement plates, effusion cooled or double-wall liners. For each model, the one-dimensional Navier-Stokes equations, including dedicated correlations that describe the phenomena of pressure drop and heat transfer, are employed. To provide a solution of the whole system, the single models are coupled together giving rise to a cooling system fluid network, whereas

appropriate boundary conditions must be provided to the metallic parts to calculate the temperature distribution of the investigated components.

The main strength of such type of *1D* codes lies in the short time needed to model the system and to run the simulation: this aspect makes them a powerful tool especially in the preliminary stages of the design procedure, usually aimed at testing several arrangements at various working conditions to identify the most promising solution and to draw the guidelines for the following more detailed investigations. Also, thanks to their ability to easily set boundary conditions and manage complex geometries, they may be used to perform the design of experiment (DOE) calculations to indicate useful correlations or trends and the relative importance of the operating parameters. In such context, the effort required for additional CFD simulations, with the related modification of the CAD and generation of a new mesh, would be unbearable.

On the other hand, the use of this kind of tools has to take into account some native limitations of the one-dimensional approach: these meanly deal with both the impossibility to describe with high accuracy a fully three-dimensional flow, like swirling flows in the combustor chamber or cold recirculating flows at the end of the annulus, and with the uncertainty of empirical correlations, which is commonly lower than 10% only within their (usually narrow) range of validity.

However, the relevance of the *1D* codes for the cooling system design remains evident. In particular, this is even more essential for a system based on impingement or effusion: in fact, such dense arrays of small holes require a significant calculation cost in a simulation with CFD codes.

Even if many efforts have been made to develop lower-order approaches aiming at reducing the number of mesh elements, such as those based on localized mass sources in the region of hole discharge [17], *1D* codes remain the first choice for the preliminary design phases, so it becomes mandatory to update these tools.

A further aspect of the computational approaches (low order codes included), that should not be underestimated, is related to the fact that the initial real problem is modeled to be solved, i.e. this becomes a deterministic exercise, as described by *Maître & Knio* [18] and reported as a scheme in Figure 1.

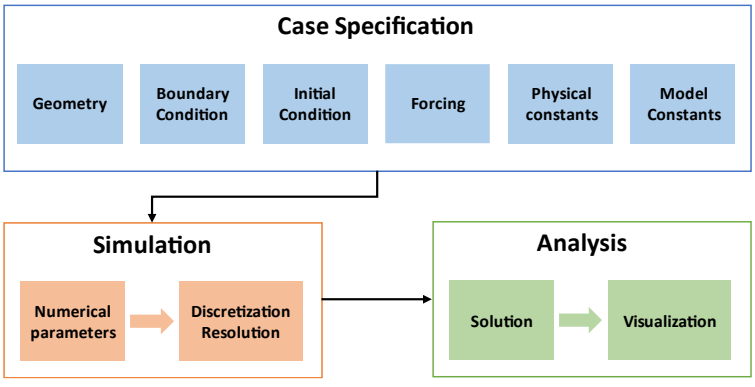

Figure 1.1 - Schematic procedure of a deterministic simulation [18]

It is known that each production process is associated with a certain tolerance that depends on the manufacturing process, but these aspects are usually not included in the computational analysis. The

uncertainties present in numerical simulations are not only geometric in nature, but it is also sufficient to consider all those parameters assumed as input or boundary conditions that have been measured. Therefore, the measurements will always be affected by uncertainty.

With the introduction of the uncertainty quantification in the design procedure it is possible to define components that are not intrinsically influenced by possible geometric and boundary conditions variability; this procedure is called robust design.

Uncertainty quantification (UQ) is the science that quantitatively identifies uncertainty to reduce it, both in experimental and computational applications, and aims to determine the probability of certain results when some system input parameters are not exactly known. In the numerical field, the propagation of uncertainty within the codes is evaluated. This type of study has been developed mainly in recent years because only in this period the availability of computational resources has promoted the development and application of this procedure.

As reported by *Iaccarino* [16], to obtain the real predictive capacity of the simulation and, in turn, the correct validation, it is necessary the rigorous evaluation of the uncertainties that are introduced into the numerical code.

The general objective of UQ analyses is to investigate the impact of uncertainties on a quantity of interest obtained as a response from the system, to define a confidence interval for the results obtained and to assess the probability that a certain result will occur; the whole process leads to a better risk assessment analysis and therefore helps the designer in the decision-making process.

To implement this procedure, it is necessary to adopt an approach that is no longer deterministic but probabilistic; this does not affect the standard procedure necessary to set up a simulation but introduces considerable difficulties in the various phases Figure 1.2 [18].

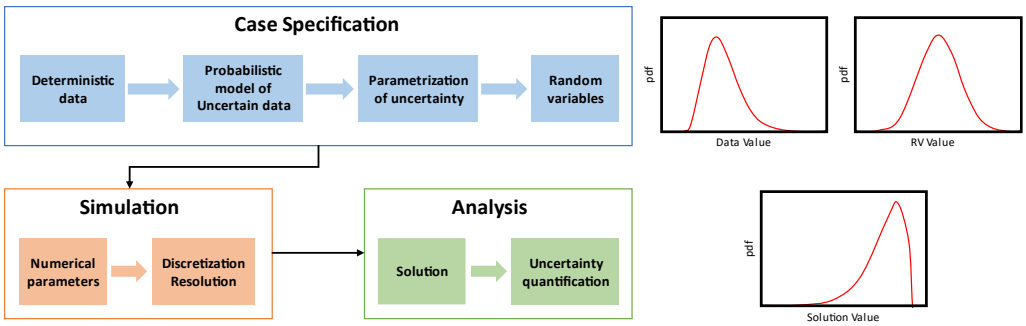

Figure 1.2 - Schematic procedure of a probabilistic simulation [18]

This type of result can be subsequently used for reliability studies, which is not the case for those obtained by deterministic approaches; this aspect is particularly important for both heavy-duty machines [19,20] and aero-engines [21].

The range of uncertainty of the result will be a function of those uncertainties imposed as an input; this can be further investigated through sensitivity analyses [22,23]. This information is extremely important for robust design and optimization because it allows to focus the design only on the components that most affect the response function.

Due to all the design requirements described in the opening chapter, it is mandatory to implement a new procedure that takes into account the effects of uncertainties related to input parameters from the early design phases. For this reason, it is essential to move from a deterministic approach to a probabilistic approach also for low-order codes.

The coupled procedure realized, that will be described in this chapter, has allowed obtaining an output that is no longer a deterministic distribution, but rather a range and most of all it is a statistical evaluation of occurrence, not least the possibility to perform sensitivity analysis to uncertain input variables.

Therm-1D Procedure

This chapter describes the in-house *1D* thermal methodology (*Therm-1D*) currently used by the *University of Florence* and *GE Avio Aero* for the preliminary design of combustor cooling systems [24]. The procedure already existed, but the development and improvement of its functionality was continued during the activities of this research. The tool allows the estimation of flow split within the combustion chamber and liner wall temperature, through the solution of an equivalent flow network and a wide database of correlations.

This code was developed starting from a well-proven approach for the thermal analysis of blades and vanes cooling systems. This tool is capable of estimating radiative and convective heat loads on both gas and coolant sides of the liners, to predict the metal temperature. The thermal calculation is based on the approach proposed by *Lefebvre et al* [1,25–27] and later improved by *Kretschmer et al.* [28] and *De Champlain et al*. [29].

As described in Figure 1.3, the methodology relies on the balance among different mechanisms of heat transfer: radiative and convective heat loads on the gas side (*R1* and *C1*), radiative heat load toward the casing (*R2*), and convective heat load between metal and coolant (*C2*), while Q*HS* indicated the contribution of heat removal for the sink effect. The energy balance in steady-state condition implies that (neglecting heat conduction in axial and circumferential directions):

Energy balance in steady-state conditions:

$$C_1 + R_1 = C_2 + R_2 + Q_{HS} = K_{1-2} \tag{1.1}$$

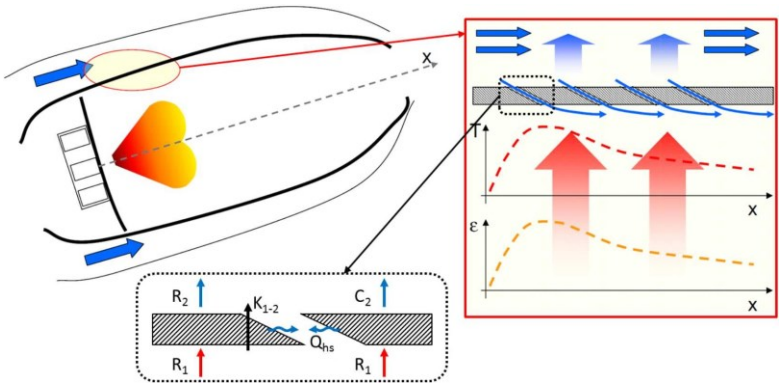

Figure 1.3 - Conceptual illustration of 1D thermal analysis [1]

Gas side heat loads are evaluated from a given description of the flame conditions in terms of *FAR*, temperature, velocity, and pressure. Moreover, the heat sink effect (Q_{HS}) is accounted for applying, for each row, heat removal given by the calculated heat transfer coefficient and adiabatic wall temperature inside the holes.

The analysis of the coolant fluid network is performed using a one- dimensional steady code, *Icons1D*, developed starting from an in-house code used in several works [30–34]. The representation of a cooling system consists of a fluid network made up connecting basic components, each one dedicated to model a particular region of the combustor. Specifications of the geometrical characteristics of a single component, such as holes diameter, pitch, length, roughness, inclination angle, and so on, can be custom selected. Coolant is considered a perfect gas subject to wall friction and heat transfer and the flow field is solved in the subsonic regime, using correlations to determine HTC, friction factor, cooling effectiveness, etc. The user can specify boundary conditions for the fluid network in terms of inlet and outlet pressure or mass flow rate, depending on design specifications. Through the resolution of the fluid network, Icons-1D provides coolant side boundary conditions for thermal calculation; also, it estimates the heat sink effect of cooling holes.

Heat load on the gas side and radiative heat transfer between the liner and the casing are estimated by *Cowl* following the approach suggested by *Lefebvre* [1] and more recently improved by *Andreini et al* [24]; afterward, cold side and hot gas side boundary conditions are read by the thermal solver for the resolution of the Fourier law within the metal and the wall temperature is finally calculated. Since the mass flow rate and pressure drop are wall temperature-dependent, an iterative overall procedure is required; also, an internal loop is included to accelerate the procedure convergence.

Convergence is achieved when differences in temperatures, pressures, and mass flow remain unchanged or below an error set by the user. To have a better comprehension of the overall procedure and to clearly

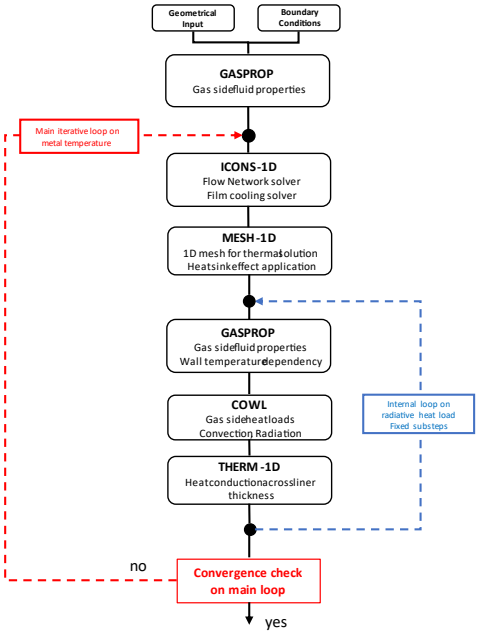

Figure 1.4 – Therm-1D: procedure flow chart

describe the connections among the different involved codes, a schematic flow chart is reported in Figure 1.4. Further details on the procedure can be found in [24] [35]. The estimation of thermal loads is carried out utilizing a correlative approach, therefore the choice of the employed correlations plays a key role in the prediction as accurate as possible of metal temperature.
Here below are reported the equations implemented within the code.

Gas side radiation

The radiative heat transfer due to the presence of flame and hot gases is treated referring to two contributions: a non-luminous component emitted by gas, mainly given by CO_2 and H_2O, and a luminous component related to soot production.
The contribution of non-luminous radiation can be estimated starting from the dimension and shape of the gas volume and its conditions in terms of pressure, temperature, and chemical composition. The radiative heat load can be expressed:

Gas Side Radiative heat load:

$$R_1 = 0.5\sigma(1+\epsilon_w)\epsilon_g T_g^{1.5}\left(T_g^{1.5} - T_{w1}^{1.5}\right) \quad \textbf{(1.2)}$$

Where ϵ_w is wall emissivity and depends on the material, temperature, and oxidation level of the wall. Gas emissivity ϵ_g can be calculated using the expression proposed by Farag [36].

Coolant side radiation

The heat load transferred via radiation between liner and casing is significantly lower compared to the convective one. Nevertheless, it can be calculated assuming that both walls act like grey bodies. It is common practice to assume the casing temperature T_{casing} equal to coolant temperature at the entrance of the annuli T_{cool}:

Coolant Side Radiation:

$$R_2 = \sigma \frac{\epsilon_w \epsilon_c}{\epsilon_c + \epsilon_w(1-\epsilon_c)(A_w/A_c)}\left(T_w^4 - T_{cool}^4\right) \quad \textbf{(1.3)}$$

For an annular chamber A_w/A_c is equal to the ratio of the liner and casing diameters, hence < 1 for the inner liner and > 1 for the outer liner.

Gas side convection

The convection between gas and liner is certainly the most challenging from a modeling point of view. Gas is affected by rapid physical and chemical changes, as well as significant temperature and velocity gradient, due to the presence of the flame. In absence of film cooling, it is reasonable to employ a classical correlation for Nusselt number in tubes, such as:

Gas Side Convection:

$$C_1 = 0.020 \frac{k_g}{d_{h1}^{0.2}} \frac{m_g}{A_l \mu_g}\left(T_g - T_{w1}\right) \quad \textbf{(1.4)}$$

Several factors must be considered for a correct estimation of wall temperature. The presence of a swirling flow leads to the generation of a complex flow field that can differ significantly from a fully developed flow within a tube, such as a vortex breakdown phenomenon, corner recirculation zones, and a swirled component in the proximity of the wall. To take into consideration this latter effect, the gas velocity is increased by a *1/cos(β)* factor, where *β* represents the angle between velocity and the combustor axis.

Coolant side convection

To estimate the convective heat transfer between liner and coolant it is possible to rearrange Equation (1.4 using the hydraulic diameter of the annulus D_{an} and the fluid properties calculated at the air temperature T_{cool}.

Coolant Side Convection:
$$C_2 = 0.020 \frac{k_c}{d_{an}^{0.2}} \frac{m_{an}}{A_{an}\mu_c} (T_{w2} - T_{cool}) \quad \textbf{(1.5)}$$

Heat Sink

The heat removal due to convection within the hole pattern can be of particular relevance for film cooling systems, especially for effusion cooling, where it can contribute up to 60% [37] to the overall cooling of the liner. Film cooling rows are usually modeled as equivalent slot and the total heat sink can be expressed as:

Heat Skin Convection:
$$Q_{sh} = A_{slot} h (T_{cool} - T_w) \quad \textbf{(1.6)}$$

Where the heat transfer coefficient *h* could be calculated with a correlation for the Nusselt number. Due to the typical geometrical characteristics of the film cooled liners, the correlation should consider the effect related to the low *l/d* ratio, such as the expression proposed by *Gnielinski* [38].

Effusion cooling

The performance estimation of effusion cooling plates is influenced by the superposition of the coolant due to the injection through multiple locations. For this reason, the common approach is the evaluation of the film coverage provided by a single row, corrected subsequently with a criterion to manage the superposition phenomenon.

Various correlation reported in the literature are implemented inside Icons-1D. It is possible to mention some of them as *L'Ecuyer & Soechting* [39], or *Baldauf et.al* [40], or *Goldstein* [41]; the user can choose also correlations for shaped hole geometries such as *Colban et al.*[42]. An obvious problem could be that some of these correlations were developed for a single row of film cooling holes. Also, some of these correlations were developed for blade film cooling holes, and, for example, the range of some parameters such as the blowing ratio are quite lower than typical values for the combustor. It should be pointed out that outside the validity range, the code extrapolates the behaviour of the correlation.

The superposition principle proposed by *Sellers* [43] is taken into account to predict the performance of multiple film cooling rows. According to this approach, the gas temperature involving the i^{th} row is

represented by the adiabatic wall temperature of the previous row ($T_{aw,i-1}$), therefore the adiabatic effectiveness of the ith row can be expressed as:

Superposition effectiveness:
$$\eta_i' = \eta_1 + \eta_2'(1-\eta_1') + \ldots + \eta_i'(1-\eta_1')(1-\eta_2')\ldots(1-\eta_{i-1}') \quad \textbf{(1.7)}$$

in which, the generical effectiveness is expressed in the form of:

Generical effectiveness:
$$\eta_i' = \frac{T_{awi-1} - T_{awi}}{T_{awi-1} - T_{cool}} \quad \textbf{(1.8)}$$

It is important to highlight that the superposition principle was developed for *2D* slot cooling, therefore it is not able to properly take into account the increased mixing and the three-dimensional nature of coolant injection through discrete holes. Generally, this phenomenon involves lower protection in comparison with the result predicted by the superposition method. As a consequence of this interaction, the influence of injection from a row does not extend indefinitely downstream but only for a certain length. For this purpose, *Andreini et al.* [44] proposed to specify the effectiveness superposition length for each row of cooling holes.

Remarks

This section shows the methodology currently employed for the preliminary design of combustor cooling systems. This approach is highly recommended for the design phase, where several configurations have to be investigated and a rough estimation of the metal temperature is acceptable.

This methodology is not exempt from critical points. The main ones are:

- An accurate estimation of metal temperature should not ignore radiative heat loads
- The assumption of 1D conduction neglects the effect of the temperature gradients in axial and circumferential directions, resulting in 1D temperature profiles
- Classical correlations for the estimation of Nusselt number in a smooth channel are employed to estimate the heat transfer coefficient, whereas the actual flow field characteristics are far away from fully developed conditions
- Local suction/injection of coolant leads to significant heat transfer augmentation in the proximity of the holes
- Film cooling performance is assessed using flat plate correlations, which are inherently unable to consider the impact of swirling flow-liner cooling interaction
- The highly tunable inputs, that are greatly useful for the assessment of the sensitivity of the driving parameters, can be subject to variability due to user-defined criteria for their evaluation

Uncertainty Quantification

In this paragraph, the theoretical basis necessary to ensure the understanding of the analysis subsequently made will be given. For this reason, the present work should not to be considered a dissertation on this topic, as it is not the purpose of the work.

UQ techniques can be divided into two main groups: *intrusive* or *non-intrusive*. The first acts on the source code of the solver while the second imposes an input uncertainty only on the input parameters and evaluates how these propagate within the code itself.

This non-intrusive type does not require any variation of the solver, which can be considered a black box that associates each realization of the input parameters sampled to the corresponding outputs of the model. The non-intrusive analyses allow obtaining probabilistic results from already existing deterministic codes. This aspect allows to carry out UQ analysis on any numerical model, without any limitation related to its complexity. The main negative aspect of these techniques is that they require several deterministic simulations that depend on the number of uncertain variables considered and the level of approximation chosen; this aspect makes the non-intrusive analyses expensive from the computational point of view. This problem can be partially solved by performing simulations in parallel.

Since it was intended to couple a software for the uncertainty quantification with an in-house code, the work was focused on *non-intrusive* techniques. An evaluation of the uncertainty propagation between inputs and outputs of numerical codes has been carried out, without altering the source codes.

Theory

The *probability* is used to indicate the occurrence of a given event; this concept is based on empirical evidence and the theoretical justification is to be found in the theorem of J. Bernoulli on the law of large numbers [45]. The probability distribution function of a random variable $X(\omega)$, on the space of probability $(\Omega, \mathcal{B}, P)$, is defined as follows:

Probability distribution function:

$$F_x(x) = P(X(\omega) \leq x) \tag{1.9}$$

$F_x(x)$ is called Cumulative probability distribution (CDF) of $X(\omega)$ and defines the sum of the probabilities that the random variable $X(\omega)$ assumes values less than or equal to x. By definition, the cumulative probability distribution cannot assume negative values and is non-decreasing monotonous between 0 and 1.

The definition of probability presupposes the existence of an appropriate function $f(x)$, whose integral in a fixed generic range (a,b) provides the probability that the *continuous random variable X* assumes values belonging to the interval (a,b); if the integral is reduced to only one point, this is null. The probability that X is within the continuous range (a,b), where a and b are constant and with $a<b$, is defined as follows:

Continuous random variable Probability:

$$P(a < X < b) = \int_a^b f(x)dx \tag{1.10}$$

The probability distribution function of the continuous random variable X is defined through the following equation:

Continuous random variable Probability Distribution function:

$$F(x) = P(X \leq x) = \int_{-\infty}^{x} f(x)dx \tag{1.11}$$

By the definition of $F(x)$, it turns out that this is a continuous function; therefore, in all the points where $f(x)$ is continuous, the derivative of the distribution function $F(x)$ is precisely the density of probability $f(x)$.

The *normal or Gaussian distribution* is very important in manufacturing processes and measurements because it describes the distribution of random errors; this distribution is defined:

Gaussian distribution: $$f(x) = \frac{1}{\sigma\sqrt{2\pi}} e^{-\frac{1}{2}\left(\frac{x-\mu}{\sigma}\right)^2} \qquad -\infty < x < \infty \tag{1.12}$$

It can be proved that μ and σ are respectively the *mean* value and the *standard deviation* of the random variable X distributed according to distribution. $f(x)$ is defined on the whole axis of the real numbers and always assumes positive values; it is symmetrical to the straight line x=μ, that is the average value of the distribution, which also coincides with *mode* and *median*.

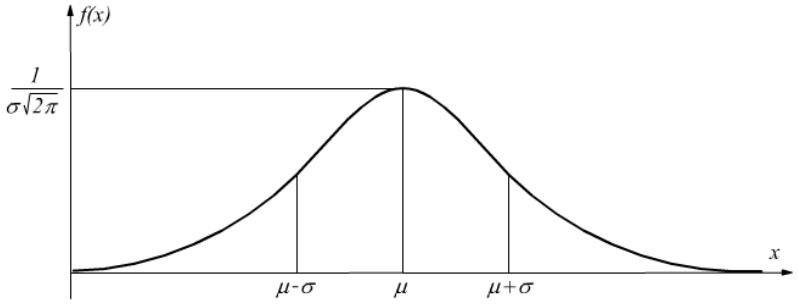

Figure 1.5 - Gaussian distribution

It is important to know that for each pair of values μ and σ, a normal distribution is uniquely defined. The variation of σ with the same average value involves a greater width of the bell, while a variation of μ with the same standard deviation, only involves a translation of the curve.

Mode and median are defined as follow:

- The *mode* is the value that occurs the most times, i.e., the one that has the highest probability to occur
- The *median* corresponds to the value that separates the underlying region from the probability distribution curve in two parts of equal area

The distribution has a bell shape, as reported in Figure 1.5. Its maximum value is inversely proportional to σ; in addition, the standard deviation defines the distance of the inflection points from the mean value as they have abscissa respectively $\mu\pm\sigma$.

The most important characteristics of a distribution associated with a random variable are the *mean value* or expected value, *variance* and moments of higher degree such as *skewness* and *kurtosis*, which characterize the form of the distribution itself.

The *mean value* is the weighted sum of the values that the random variable assumes, with the associated probabilities as weights.

The *variance* indicates how scattered are the values of the random variable regarding its average value.

The *standard deviation* σ can also be defined as the square root of the variance.

The moments centered on the mean value are often used. Since they are zero up to the third degree, they are interesting for a degree ≥ 3.

Skewness (Figure 1.6) or third-degree moment also called *asymmetry* provides an index of symmetry of the distribution. In particular, for positive asymmetry, the distribution will have a tail to the right, while for negative asymmetry the tail will be turned to the left.

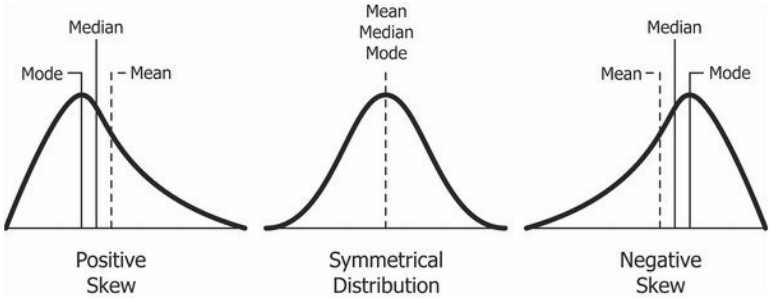

Figure 1.6 - Skewness distributions

Kurtosis (Figure 1.7) or fourth-degree moment indicates how much distribution is collected around the average value: a positive kurtosis implies a more concentrated distribution around the average and a higher mode value, while a negative kurtosis implies a flatter distribution with more marked tails.

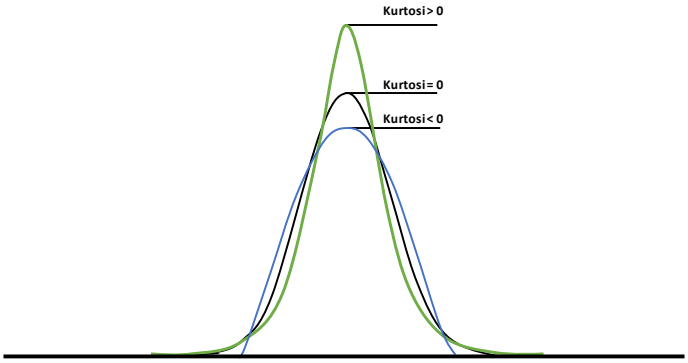

Figure 1.7 - Kurtosis distributions

Stochastic processes

In physical systems, a random variable may vary continuously or discreetly to physical space and/or time. Stochastic processes are used to study the evolution of random variables as a function of time and space. Repeated attempts of the same process obtain different trends over time. The different instant outputs give an aleatory variable *X(t)* that covers the different values assumed in that instant. It is possible to define that the random variable has an average value. Therefore, for each moment it is possible to define a random variable, Gaussian or other, which represents the most probable value of the process; it is also possible to define the *standard deviation*.

A *stochastic process* can be defined as a set of random vectors; so it is possible to extend the definitions of *mean value*, *variance,* and *covariance* for the random vector.

Covariance provides an estimation of how much the dependence of two factors influences the random variable.

Stochastic systems

Given a deterministic model that describes the physical phenomenon, it is necessary to correctly set up a stochastic model to study the effect of the uncertainty in the system inputs. The key step consists of correctly characterizing the random inputs. The critical phase for the stochastic formulation of the problem consists of correctly characterizing the space of probability defined by the random inputs of the physical system with a finite number of mutually independent random variables. It is important to understand that mathematical models of UQ require a set of random variables independent of each other. From a purely theoretical point of view, most of the software that performs UQ analysis has already implemented a procedure for the treatment of variables that are not independent from each other. This procedure allows passing from distributions of correlated variables to independent variables through a transform, which generally is non-linear [18,46–48].
This aspect is very useful for heat transfer in machinery because many factors come into play and it is even more complicated to identify two or more variables totally independent from each other.

UQ methodologies

This section describes the techniques for performing non-intrusive uncertainty quantification analyses. There are two groups of methods.

- Sampling-based methods: *Monte Carlo* (MC) and *Latin Hypercube Sampling* strategy (LHS)
- Stochastic expansion methods: *Polynomial Chaos* (PCE) and *Stochastic Collocation* (SC)

A brief digression should be made for *stochastic expansion methods* [49]. Often the systems studied are very complex; in these cases, the most used approach is to realize a simpler model, called *surrogate* model that can approximate the real starting model. These methods are based on the spectral decomposition of the stochastic process through correlation functions, more precisely a set of correlation functions to approximate the functional link between the output of the stochastic system under examination and the random variables. These methods allow obtaining the functional relation that links the output of the studied system to the incoming random variables. A distinctive feature of these methodologies is that the final solution is expressed as a functional map, not as a set of statistics; this is relevant for their use in multi-physical applications

Monte Carlo

This algorithm is simple, flexible and its convergence is not dependent on the number of input random variables of the system. The procedure of this method can be summarized as follows: generate a sample of independent input variables x using a random number generator, run the evaluations required and calculate the statistics on the outgoing quantity of interest. The estimation of the error committed is obtained directly from the application of the theorem of the central limit.

The greatest advantage of the MC method is that it has an invariant convergence rate to the size of the random space. This property makes it unique since no other methodology benefit from this property.
On the other hand, it suffers from a low convergence rate. This implies that the error made decreases with the size of the sample, therefore with the number of simulations performed. The convergence rate or the error committed is in the order of $o\left(\frac{1}{\sqrt{N}}\right)$, this means that for an increase in accuracy of a 10^{-2} factor, 10^4 additional evaluations are required. This highlights how expensive this method is in terms of computational costs.

Latin Hypercube Sampling

To accelerate the convergence rate of the Monte Carlo method, the choice of the sample can be varied. In particular, one of the most used techniques is the Latin Hypercube Sampling strategy (LHS). The input parameter sets are chosen with optimized sampling, as proposed by *Heldon* [50]. This technique (Figure 1.8) can be summarized as follows:

- Dividing the distributions of each input parameter into intervals
- The number of segments is equal to the number of samples
- Dividing the distributions into portions having all the same area, therefore all equally possible
- Finally, points are randomly selected within each area

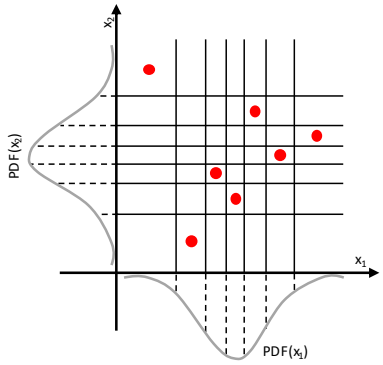

Figure 1.8 - Latin Hypercube Sampling strategy

With this sampling strategy, it is possible to exploit the advantages of the MC method but with a committed error order reduced to $o\left(\frac{1}{N}\right)$.

Polynomial Chaos

The method acts on polynomial bases. It is not based on sampling to determine the evolution of uncertainty in a dynamic system when there is probabilistic uncertainty in the parameters.
The polynomial chaos expansion of a generic response function *R* takes the following format:

Polynomial chaos expansion of a generic response function:

$$R(x,\xi) = \sum_{j=0}^{\infty} \alpha_j \psi_j(\xi) \tag{1.13}$$

where α_j are the polynomial coefficients and $\psi_j(\xi)$ are the polynomial basis functions. Equation (1.13) is always truncated with a finite number of random variables and a fixed polynomial of degree *P*.

Truncated polynomial chaos expansion of a generic response function:

$$R(x,\xi) = \sum_{j=0}^{\infty} \alpha_j \psi_j(\xi) \approx \sum_{j=0}^{P} \alpha_j \psi_j(\xi) \tag{1.14}$$

The polynomial can be truncated in two ways:

- Fixing the total order of the polynomial (*Total Order expansion*):
  - The final interpolating polynomial includes a complete polynomial base up to a specified total order
  - In this case, the number of terms N_t in an expansion with total order p involving n random variables is given by the following formula:

Truncated polynomial chaos expansion of a generic response function:

$$N_t = 1 + P = \frac{(n+p)!}{n!\,p!} \tag{1.15}$$

- Defining the maximum order of the polynomial bases (*Tensor Product expansion*):
  - Order limits are not defined on the final polynomial but on the bases of the polynomials
  - All combinations of individual one-dimensional polynomials are included
  - This technique allows imposing different polynomial orders for the various bases of the input variables; in other words, it allows to impose heterogeneous problems, property that the method of total order expansion does not have
  - In this case, the number of terms N_t in an expansion with total order p involving n random variables is given by the following formula:

Tensor Product expansion, number of terms:

$$N_t = 1 + P = \prod_{i=1}^{p} (p_i + 1) \tag{1.16}$$

The imposed total order approach overlooks a significant part of the polynomial coverage of the tensor product approach, which is why, unless a very small number of variables is involved, the fixed total order method requires fewer evaluations. *Eldred* in his work [49] proves how it is necessary to oversample the evaluations required for the total order method, at least twice the minimum number required, to obtain a more robust and accurate analysis response.

Total order expansion oversample:

$$N_t = 1 + P = \frac{(n+p)!}{n!\,p!} \Rightarrow N_{t_{eff}} \geq 2N_t \tag{1.17}$$

An indication of the required evaluation numbers for the different approaches is given in Figure 1.9.

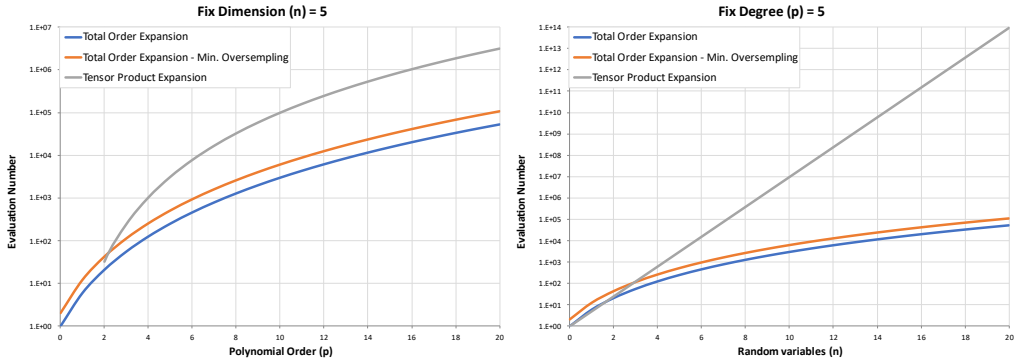

Figure 1.9 – Number of evaluations required for the two approaches

Stochastic Collocation

The stochastic collocation expansion is made by the sum of a set of multidimensional interpolating polynomials for the collocation points and a polynomial that interpolates the results on the adjacent points that can be made up of some components of the gradient of the function between the points themselves. For the evaluation of the interpolating points, Lagrange polynomials are used.

PCE vs. SC

The main difference between the polynomial chaos expansion and the stochastic collocation is that for the first method the coefficients of the interpolating polynomial must be estimated starting from known polynomial bases, while for the stochastic collocation the interpolating polynomial must be found from known coefficients. For the polynomial chaos approach, the polynomial coefficients can be found by a spectral projection method or by linear regression. The first approach implies the numerical integration with special calculation grids that optimize the procedure. The most used grids are *Gauss quadrature grids* and *Smolyak's sparse grids*.
Instead, the stochastic collocation, since it requires a structured data set for multidimensional interpolation of both point values and gradients, does not allow random sampling, but only the above-mentioned grids.

To optimize the sampling for both PCE and SC the above-mentioned grids are used. The main features for both can be reported as follows:

- *Gauss quadrature grid*: the response function is determined using one-dimensional quadrature rules; with this approach, the polynomial zeros are chosen to verify the condition of orthogonality with the weight functions. When the number of input random variables is reduced, this approach is very efficient as it requires minimal computational effort. However, as the size increases, this method presents always a lower efficiency; this is because the number of points to be evaluated increases exponentially with the number of input variables.
- *Smolyak sparse grid*: when the number of variables is moderately high it is possible to use the Smolyak grid. This approach allows to drastically reduce the collocation points while maintaining a high level of precision.

As a final remark, it should be emphasized that for problems with a reduced number of variables and limiting the polynomial order, the most efficient approach in terms of computational cost remains the one defined by the use of the Gauss tensorial grid.

Sensitivity analysis

This type of analysis allows estimating, in mathematical terms, through Sobol's indices [22], how much a particular input random variable affects the output quantity considered. This characteristic is very interesting in the field of heat transfer in turbomachinery because there are a large number of factors and physical phenomena that could affect the results.
Two different types of Sobol's indices can be defined:

- *main Sobol's index*: strictly due to the input variable considered
- *total Sobol's index*: takes into account all the effects due to the interaction between the variable considered and the others

Dakota

The number of software and libraries for uncertainty quantification is already considerable and will continue to grow over the years. This section will be used to describes the software used for the development of the workpiece.
The software used for the development of the entire work was *Dakota* [51,52], an executable capable of performing: UQ analysis, experimental test design, sensitivity analysis, reliability studies, parameter estimation, and optimization.
The software has the advantage of interfacing, potentially, with any other solver from which receives data for subsequent statistical processing; moreover, the interface with Python environments for the pre-processing of the data is directly provided. The software needs a first input, in the form of a text file, in which the type of analysis, the distributions of the input variables, the interface and the number of response functions to be analyzed are specified; at this point, the simulation cycle begins
Through the interface, for each sample input *Dakota* launches the code adopted, from which the quantities of interest are obtained. In terms of output, the software provides the four statistical moments for each point of the response functions; the discretization of the functions and the number of studied quantities must be specified in the input file
Dakota was chosen because it is open-source, easily interfaced with other software, and because it does not only perform UQ analysis but also combines it with sensitivity analysis; moreover, as already mentioned, it can also be used for optimization studies.

Therm-1D/Dakota Coupled Procedure

The main advantage of Dakota is that it processes files, so it does not have to interact directly with the code that solves the problem. Dakota and the simulation code exchange data by reading and writing short files.
In the work routine set up for this study, the required simulations are carried out in serial mode, and only at the end, the uncertainty quantification analysis is carried out. The whole procedure has been realized and

implemented during this thesis. The entire procedure has been automated through a user-defined interface script to make Therm-1D and Dakota communicate. Going into more detail, Dakota samples the uncertain variables according to the probability distributions imposed, then the values obtained are written in the inputs of the Therm-1D procedure. Once the thermal problem is solved, the solution is passed back to Dakota that stores it. This procedure is repeated until the number of simulations is equal to the required number, defined by the uncertainty quantification method used for the analysis. When all the required outputs are obtained, Dakota performs the proper UQ and sensitivity analysis. Due to the large size of the Dakota output file, a script has been written to automatize the post-processing of the data.
Figure 1.10 illustrates schematically the coupled procedure described.

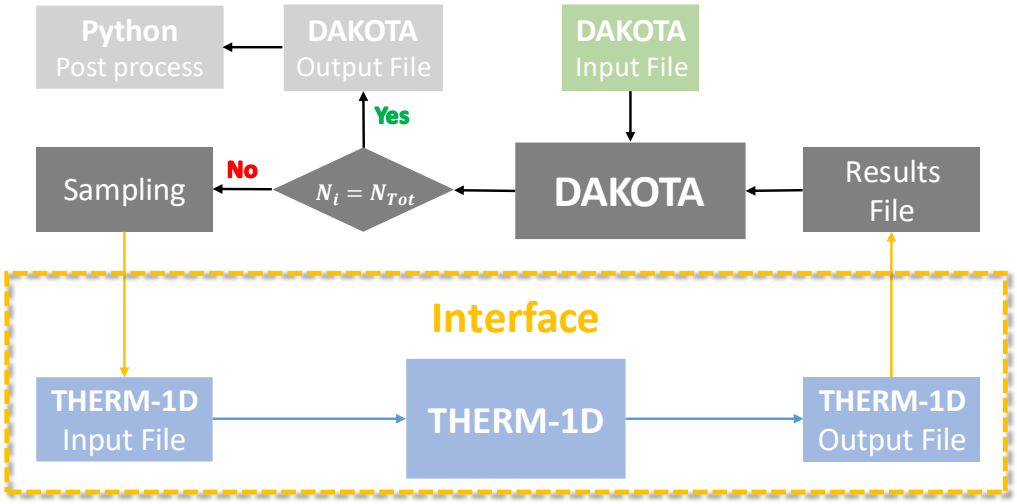

Figure 1.10 – Therm-1D/Dakota coupled procedure

It is fundamental to highlight how this coupling makes a deterministic low-order software able to give probabilistic answers by introducing uncertainties about input parameters and boundary conditions. This feature is useful in all applications and it is particularly helpful in evaluating which aspects most influence the response of the system.

The effective validity of the coupled procedure, as presented, has already been widely demonstrated in the work carried out by *Gamannossi et al.* [53]. It was also demonstrated the functionality of the coupling interface realized by *Poggiali et al.*[54]. Here the author uses the same coupled procedure, but in this case, the solver coupled with *Dakota* is different.

State of the art

The propagation of uncertainty within the numerical codes used for turbomachinery applications is relatively recent, however, there are works in the literature that deal with different aspects related to heat transfer in turbomachinery applications.
The first work regarding the comparison and validation of UQ methods was carried out by Eldred [55]; this article shows how the residuals of a CFD analysis vary with the variation of the mathematical approach used.

Regarding the applications of UQ to heat transfer in turbomachinery, there are not many works currently in literature, but they cover several problems. Many of these works are focused on the application of UQ to CFD numerical simulations. Some of these can be mentioned, as part of the research of the work carried out in this thesis. In the field of combustion, a UQ study on a CFD analysis with the LES approach was carried out by *Mueller et al.*[56]. *D'ammaro* [57] uses UQ with a simplified geometry RANS approach to study the uncertainties in the flow generated by film cooling. *Babaee* [58] evaluated the influence of the uncertainty of the blowing ratio on the film cooling effectiveness. One of the first works that evaluate the impact of uncertainties on film effectiveness is certainly the one carried out by *Montomoli et al.*[59]. On a UQ analysis on geometric parameters related to film cooling systems, important work has been carried out by *Shi et al.* [60]. Other works have been carried out by *Gamannossi et al.* [61], *Wang et al.* [62].
A general characteristic that can be found for UQ studies related to CFD numerical simulations is that they are characterized by a limited number of uncertain variables.

The studies in which a higher number of inputs are considered are related to low-fidelity codes, that allow a high amount of information to be obtained with reduced computational efforts. The study carried out by *Durocher et al.* [63] assesses the impact of atmospheric carbon compounds on the emissions of a combustor; the analysis is carried out with a one-dimensional simulator called *Cantera*. An analysis done by coupling a solver called *Genflow* with *Dakota* was done by *Zhao et al* [64] for the study of a molten salt reactor. Another research that shoud certainly be mentioned is that of *Gamannossi et al.* [65], in which an effusion cooling system for a combustor liner is analyzed. Here the author makes validation of stochastic methods applied to a one-dimensional code compared with classical MC methods. Then, a UQ analysis on many BC that are sources of uncertainty for the code is performed. Another study that combines UQ techniques with low order codes is certainly that of *Poggiali et al* [54]. This work is focused on a Civil Aero-Engine Performance Prediction where the UQ analyses take into account specific input parameters that mainly affect the modeling and, thus, the performance outputs of the engine, such as BPR, inlet mass flow, fuel mass flow, and isentropic efficiency of the components.

Chapter 2

Combustor and cooling, state of the art

Introduction

Combustors are the core component of gas turbine systems; this chapter will give a general overview of what will be the combustors or combustion systems discussed in the following chapters. This is to ease the understanding of the topics discussed later. In the same way, the main arrangements of cooling systems will be described

Gas turbine combustors are devices that operate at high energy intensity, in the order of 1 GW/m3, ensuring at the same time the operation for up to 20000 hours before undergoing significant maintenance [66]. As mentioned above, the improvement of thermal efficiency is achievable through the increase in Overall Pressure Ratio (OPR) and Turbine Inlet Temperature (TIT). The design trend is therefore moving towards the development of Ultra High-Pressure Ratio gas turbines, with OPR greater than 70 [67]. However, the high level of pressure inside the combustion chamber, in correlation with the increase of TIT, requires compromises define the optimal design not only for the burner but for the whole system. It should be considered that improving engine performance by increasing the pressure ratio results in higher coolant temperature, reducing air cooling capacity.
Even though liners are subject to low mechanical stresses, if compared to other engine components such as the turbine blades, they must survive high temperature and thermal gradients that undermine their durability. To ensure a sufficient life of such components, the metal temperature must be limited below acceptable values. The definition of an acceptable level is arbitrary and benefits from continuous evolution. According to *Lefebvre* [1], for nickel-based alloys, the maximum operating temperature should not exceed 1300 K, with flame temperatures usually above 2000 K.
With these assumptions, it is immediately clear that the design and development of more efficient cooling systems are essential to ensure further development of turbomachinery systems.

On one hand the current development trend for the *Brayton-Joule*-based system is to increase OPR and TIT. On the other hand, the changes in the basic thermodynamic cycle are one of the most important alternatives investigated in recent times. According to what asserted by *Neumann* [68], the technological

maturity of gas turbines makes every additional improvement in their performance increasingly difficult and costly to achieve. Considering what *Mcgurik* [69] said, a large number of nowadays combustors operate with constant volume combustion and this leads to a total pressure loss; it is immediately clear that the application of a system with different characteristics is becoming more and more important.

Pressure Gain Combustion (*PGC*), realized through approximations of constant volume combustion and detonative combustion, offers the possibility of the higher thermal efficiency of the respective actual gas turbine cycles [70–72]. Studies of PGC systems have also shown that a significant reduction in Specific Fuel Consumption (*SFC*) is theoretically possible. The data obtained [73] for this system has indicated that a pressure gain of ~20% is possible, and, if this could be transferred into engine operation, this would imply the impressive potential of gaining ~5% in terms of SFC. Also, *Ward & Miller* [74] have demonstrated that with some tricks to limit the intrinsic instability in this type of combustors, the PGC device allows maintaining ~70% of the pressure gain. This has only been demonstrated so far for a simple experimental system, but it is an inspiring starting point.

One of the most interesting solutions is to use sonic or supersonic combustion, also known as detonation, to increase pressure and control the entropy rise during the combustion process. Two different detonating combustor configurations were studied: Pulse Detonation Engine and Rotating Detonation Engine. The latter is preferable due to the higher stability of discharge conditions and the higher reachable energy density because of the smaller size and the absence of moving parts that could cause failures. Detonation wave spins inside an annulus, burning continuously injected fuel and air. Detonation is a phenomenon very hard to manage due to its instability and complexity of the flow field. Also, during this combustion process, a huge amount of energy at high pressure and temperature is released, considerably stressing the combustor structure.

The real challenge is the mechanical integrity of the combustor, threatened both by large pressure fluctuations and high local temperatures. The only way to guarantee a safe operation of hot gas path components is the exploitation of all possible and available cooling methods. Only by combining thermal barrier coatings, the use of temperature-resistant alloys as well as internal convective cooling, it is possible to ensure sufficient low material temperatures.

Standard Combustor

Rich-Quench-Lean Combustors

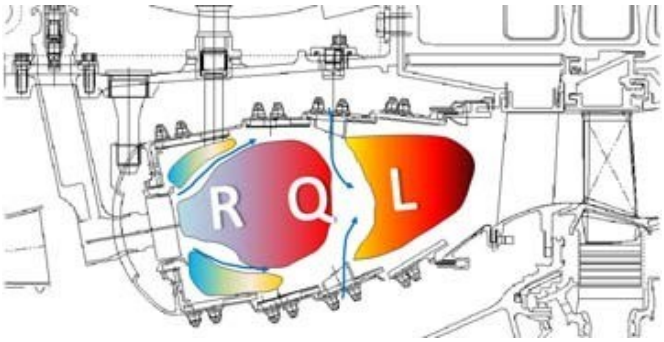

Figure 2.1 - Rich-Quench-Lean combustor scheme

The state of the art for low-NOx combustors are represented by the so-called RQL (Rich Quench Lean) scheme: in fact, this configuration allows the control of the polluting emissions and, at the same time, it guarantees an extremely wide stable operation range from idle to maximum power. A sketch of the RQL scheme is represented in Figure 2.. The fuel is injected directly into the "rich-burn" zone where it mixes through the turbulent diffusion with part of the air flow from the compressor; this results in equivalence ratios (ϕ) higher than the high power stoichiometric (ϕ=1.2÷1.6) and acceptable lower values at idle [75]. This "*primary*" zone also generates a recirculating flow that anchors the flame and provides sufficient resident time for the fuel-air mixture to carry on the combustion process. Right after this first region, there are the *dilution zones*. Here a massive amount of air is injected through wall jets (dilution holes) to favor a rapid mix with the partially burned gases, "*quenching*" the chemical reactions and creating "*lean-burn*" conditions (ϕ=0.5÷0.7) before the combustor exit section. shows the emission characteristics of RQL combustors; the critical passage to reduce NOx takes place during the switching from rich to lean combustion. The *primary* zone generates a large amount of soot which radiates heat to the walls aggravating the cooling problem; the *quench* zone requires a very fast mixing to minimize residence times near stoichiometric equivalence ratios and high temperatures.

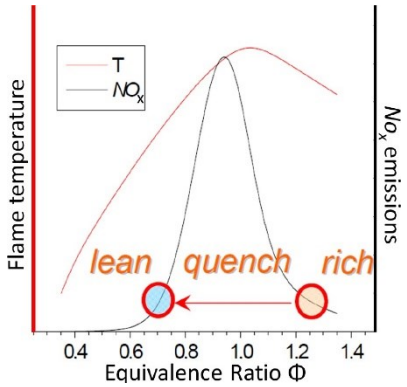

Figure 2.2 – RQL concept

The cooling of the liner is usually achieved using forced convection in the annulus and through the injection of film cooling air through holes or slots along the metal walls. Since a large amount of air is available, the design of the cooling arrangement is, paradoxically, mainly driven by other needs than cooling, such as prevention of stoichiometric regions due to the injection of film cooling air. Because of this, the application of the cooling technique based on the generation of a protective film (*effusion cooling*) requires extra care. Indeed, cooling air injections may produce locally stoichiometric conditions with high temperatures [76].

Lean Combustors

The idea of a lean-burn combustor is to operate with a high excess of air to avoid stoichiometric conditions, to keep a lower temperature level inside the combustor, and thus to inhibit the formation of NO_x. Unfortunately, moving to lean mixture, the operating range with low emissions and without occurring in flame extinction is quite narrow. The issue becomes even more critical considering that the engine is subjected to different operating regimes.

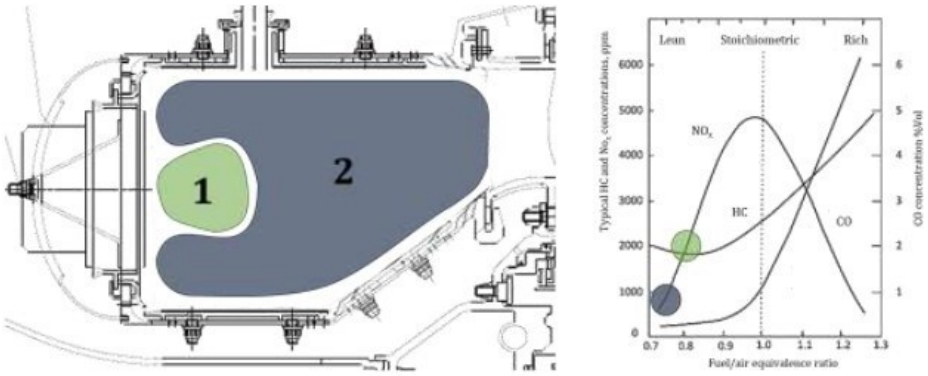

Figure 2.3 - Lean combustor

In a Lean combustor (Figure 2.3), two separated zones are designed to optimize certain aspects of combustion performance: the first zone operates at high equivalence ratios (slightly lower than stoichiometric) to achieve high combustion efficiency and to minimize pollutants production. This "*rich*" zone guarantees the stability of the combustion process, while the rest of the chamber is kept in lean conditions. To ensure the conditions listed above, the fuel must enter the chamber already completely evaporated so that the injectors play a fundamental role.

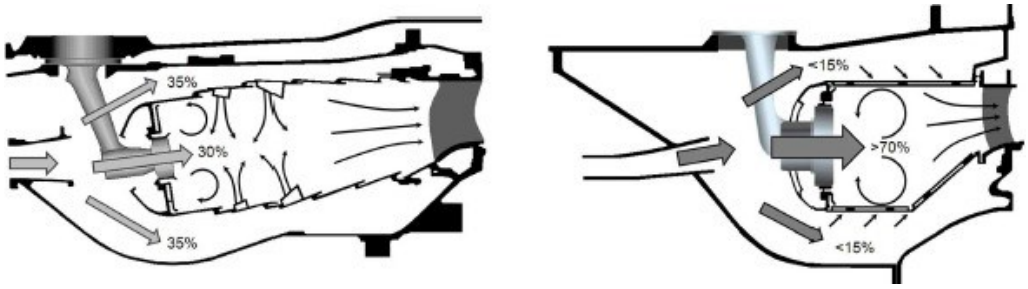

Figure 2.4 - RQL to Lean comparison [69]

Although the thermal loads on the liner walls are lower, cooling for this type of combustor is critical because the available air is limited (Figure 2.4) since most of it is used to maintain lean conditions in the chamber

[77]. Furthermore, the weight and complexity of the system are increased; also, the geometrical complexity of these combustors leads to relatively large surfaces to be cooled.

New Combustor Concept

As already mentioned, many different solutions to increase the efficiency were identified through the years, like increasing turbine inlet temperature, increasing the cycle pressure ratio, or others, but a limit seems to be reached and further improvements of this technology appear hard to get [70]. Thus, new combustion processes started to be investigated and some promising solutions seemed to be found. The most important alternative is *Pressure Gain Combustion* (PGC). As it is possible to understand from the name, during this combustion process the pressure level increases and that leads to different benefits, starting from higher cycle efficiency due to a lower entropy increase. Many different solutions were studied but two of these seems to be the most interesting alternatives to traditional combustion processes:

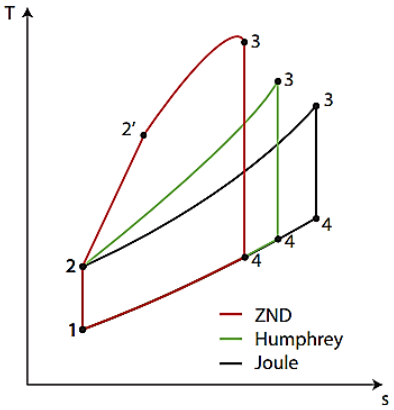

Figure 2.5 - T-s diagrams of the Joule, Humphrey and ZND cycles [78]

- *Constant Volume Combustion* (CVC): the fuel is constrained inside a constant volume, following the thermodynamic transformations of a Humphrey cycle (Figure 2.5, green). In this process, the burning wave or flame front travels along the reactants with subsonic speed, and that leads to the classification of this phenomenon as a deflagration. In CVC, the volume constraint doesn't allow this expansion, leading to an increase in total pressure after the combustion [78].
- *Detonation*: the second type of PGC that shows significant improvements is detonative combustion. A detonation is a steady-state combustion wave propagating into a combustible mixture at supersonic speed and, according to *Zel'dovich-Neumann-Doring* (ZND) theory (Figure 2.5, red), it can be described as a shock wave coupled and sustained by a chemical reaction zone. The precursory shock sharply increases both pressure and temperature levels of the reactants. After a short ignition delay time, called the induction period, the fresh mixture ignites and reacts at a rate high enough for the deflagration to propagate at the velocity of the leading shock wave (supersonic) [79].

  Analyzing the ZND cycle in detail (Figure 2.5, red), the attention is focused on the heat addition process. The normal shock wave progresses into the undisturbed fuel-air mixture, which is nearly at rest at the combustor entry condition (point 2), followed by the sensible heat release in a

constant-area region terminating at point 3. The strength of the shock wave (Mach number, pressure ratio, temperature ratio) from 2 to 2' is uniquely determined by the initial conditions and the amount of added heat. The process is entirely constrained by the CJ (Chapman-Jouguet condition) , which requires that the local Mach number at the end of the heat addition region (point 3) should be 1 (sonic or choked flow). It is important to notice that the expansion out of the combustor is assumed to be ideally isentropic, but the intermittency of the product flow at higher pressure and temperature makes hard to treat this transformation as it is [79].

Two main technologies were developed:

- *Pulse Detonation Combustors* (PDC): straight tubes with a periodic working cycle, that leads to unsteady outflows
- *Rotating Detonation Combustors* (RDC): annular vanes with a detonation that constantly spins in the combustor, producing a steadier outflow compared to the previous combustor layout

One of the most critical aspects of PGC processes is that they are fundamentally unsteady (though periodic) and this presents several challenges to their benefit analyses [80]. Regard the detonation, several problems are now under investigation, from chemical and reaction to constructive solutions.

It has emerged that RDCs seem to be the most attractive solution for PGC because of their simplicity and higher power density compared to other combustors. However, the knowledge about those systems is far to be complete. RDCs maintain a rotating detonation wave inside a concentric annulus between two cylinders and that results in an increase in pressure after the combustion process. RDCs also promise to provide a much steadier output than PDCs in a more compact package with no moving parts and a higher frequency compared to the previous one [72,81,82]. Unfortunately, the energy increase generated by the mentioned much higher frequency brings the surrounding metal to absorb more heat in a RDC than in a PDC. The heat generation is so great that RDC run time is typically measured in seconds. To run RDEs for longer periods a method for carrying this heat away from the engine walls must be devised [83,84].

One of the biggest challenges for the *Rotating Detonation Combustion* comes from the complexity of the fluid region inside the annulus where three different zones coexist simultaneously, as well as the instability and the extent of the detonation phenomenon; all these elements make the combustor thermo-fluid-dynamic

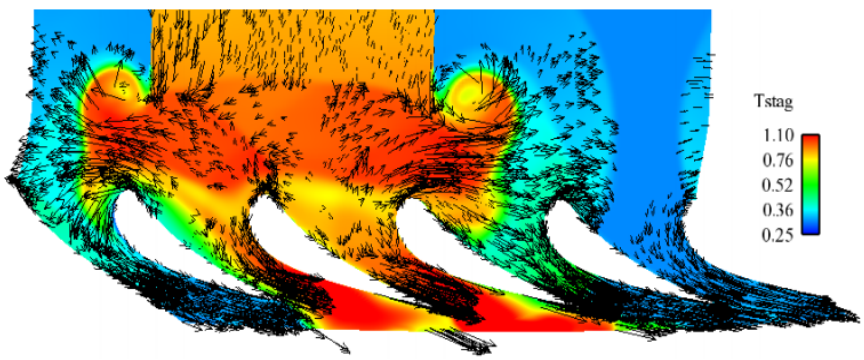

Figure 2.6 - Detonation-Stator blades interaction [87]

characterization very complex. Without this information it is not possible to have a correct estimation of the combustor thermal loads, making it hard to get long duration tests.

Furthermore, despite the lower complexity of rotating detonation engine (RDE), the problem of the periodic sonic or supersonic flow limits the possible application of these devices in a turbine cycle because of the detonation effects that comes from the RDEs to the stator blade of the first stage are still under investigation which shows the origin of reflected waves that travel back to the combustor from turbine's first nozzle [85,86]. This problem is shown in Figure 2.6 [87].

Rotating Detonation Combustion

As mentioned, RDCs operate with detonations, supersonic combustion waves across which pressure and temperature levels increase sharply. It is necessary to understand how this strong phenomenon is used to obtain high cycle efficiency. Two main aspects are crucial and have attracted the interest of researchers on detonation combustion processes: the higher efficiency due to the low entropy increase compared to the traditional CPC cycle (e.g., Brayton cycle) and the high specific thrust that can be obtained from the detonation process thanks to the expansion wave that takes place downstream the detonation itself. These reasons convinced researchers to investigate possible solutions that can involve detonation combustion engines for propulsion applications.

Anyway, detonation is not a new way of combustion. Indeed, it has been known since the fifteenth century that certain chemical compounds unusually undergo violent chemical decomposition when subjected to mechanical impact or shock. Unfortunately, until the nineteenth century, there weren't adequate diagnostic tools to observe properly this rapid combustion phenomenon. During this century, a lot of experiments were conducted by different scientists. In the late 1800s, supersonic detonation waves in gaseous explosive mixtures were conclusively demonstrated to be distinctly different from slowly propagating deflagration waves.

It is not the object of this work to make a theoretical discussion on RDC. In literature there are many works [70,88–91] that analyze RDC and its relative theory. Working principles of RDE rely on the assumption of the conservation of the rothalpy, explained as well in *Nordeen* works [86,87]. The signature of the rothalpy is the generation of swirl, which is the azimuthal velocity inflow through a rotating control volume. The rotating pressure gradient generated by a detonation performs the same function as the vanes of a turbine and does work on the flow according to the Euler turbomachinery equation and rothalpy [92].

To better understand the phenomenon, without going too deep, Figure 2.7 [93] shows the fuel is injected from the bottom, the detonation wave propagates horizontally near the inlet plane from left to right, and the detonated products expand horizontally and vertically towards the exit plane.

An oblique shock wave settled up at the top of the detonation wave and a slip line exists between the freshly detonated products and older products from previous detonation passages, as well as a weak secondary shock wave, which varies considerably depending on the inlet stagnation pressure and backpressure. The pressure immediately behind the detonation wave is high enough to completely block the micro-nozzles and no fresh mixture is therefore able to exit the nozzle immediately behind the detonation. This can also be a problem because of the potential for backflow into the premixture plenum. Further behind the detonation front, fresh reactants begin to penetrate the chamber. This region expands almost linearly away

from the detonation front. The interface between the premixture and the reacted gases is also interesting, here, the RDC shows some non-detonative combustion, which results in a loss of performance.

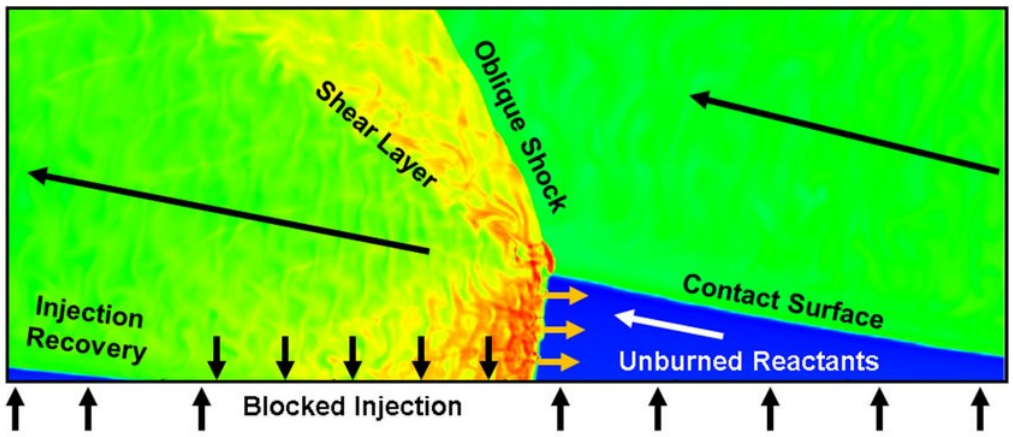

Figure 2.7 - Simulated Flowfield of an RDE [93]

The primary difference is the heat addition in the rotating frame of reference. Comparing the RDC cycle (Figure 2.8 [94]) with a Brayton cycle, the following relations can be assumed:

- The leading shock of the detonation acts as a compressor
- The reaction zone after the leading shock is the combustor
- Post detonation expansion has the thermodynamic characteristics of a turbine
- Thermal efficiency is achieved because heat is added through combustion with increasing pressure and temperature due to detonation

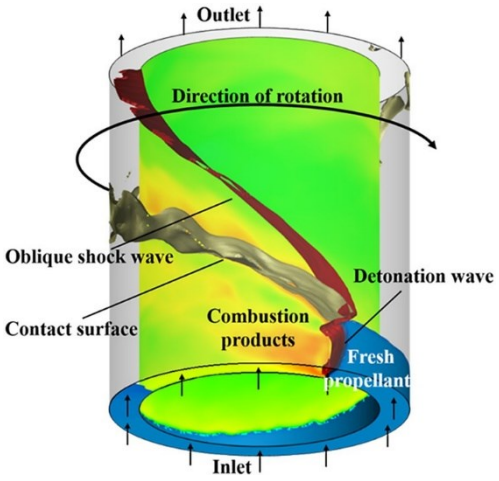

Figure 2.8 - Flowfield in a rotating detonation engine [94]

Literature review

During the years, due to the increasing interest in RDEs technology, a lot of tests were made all around the world, and different design solutions were tested and studied to understand properly the rotating detonation phenomenon. The first chamber completed by *Voitsekhovskii* realizing the continuous process of detonation

burning of premixed mixtures comprises a plane annular channel [95]. The detonation was initiated in a cylindrical channel by an electrical spark and this experiment, conducted at the Institute of the Soviet Academy of Sciences in Novosibirsk, has to be considered as the first fundamental step in developing the *Rotating Detonation Engine* [96]. As it is shown in *Bykovskii's* work [97], the annular cylinder with proper width is a suitable detonation channel for nearly all cases.

Several institutions all over the world are currently conducting studies on RDEs, to increase the knowledge on this topic and better understand the phenomenon and the behaviors of these devices, as well as the influence of different parameters of interest like mass flow and type of reactants, equivalence ratio, combustor geometry and blockage ratio of the channel.

Due to the mass flow rate and equivalence ratio variations, a lot of different operating modes of the device can be registered. Two interesting studies are those of *Anand et al.* [92] and *Voytsekhovskiy et al.* [98] that by increasing the mass flow rate, or the combustion chamber dimensions, showed that it is also possible to achieve a different number of rotating waves inside the annulus.

Despite the proper characterization of the operating mode, one of the biggest challenges regarding rotating detonation devices is the proper evaluation of heat fluxes through the walls during the combustion process. Although RDEs allow obtaining a steadier, more uniform exhaust flow compared to PDEs in a more compact package with no moving parts, the increased energy generated by these devices means the surrounding metal absorbs more heat than in a PDE. The heat generation is so great that RDEs run time is typically measured in seconds to avoid ablations in the channel. To run RDEs for practical durations the heat output must be both understood and quantified [99]. Several experiments were conducted to understand properly the heat transfer phenomenon, quantifying it and determining the parameters of interest to get a proper cooling system design. The objective is to achieve a test duration that can allow researchers to investigate properly steady state working conditions of an RDE.

The first experimental campaign was conducted by *Bykovskii and Vedernikov* [100], who have done different measurements of heat fluxes on RDE with an annular cylindrical combustor of 40 mm and obtained lower heat flux values compared to conventional combustion. They registered that the higher heat release occurs near the point of the end of the detonation front. The unsteady heating of the combustor wall (evaluated on a run time of 0.5 s) lies in the interval between 0.7÷2.7 MW/m^2. At the end, they state that the heat flux at the steady-state regime reaches values of 1.5 MW/m^2, leading to the necessity of a cooling system for long operational times. A great effort on investigating this topic was also made by *Theuerkauf et al.* [79,101–103], who successfully tested a 6-inch water-cooled RDE for about 20 seconds and a briefly investigated an uncooled RDE with the respective heat fluxes. They state that the heat flux should be no greater than 10 MW/m^2 for uncooled *RDE* and 2.2 MW/m^2 for the water-cooled one. However, they have obtained high peak heat fluxes and a detonation wave speed greater than 3000 m/s, which suggested the possibility of multiple detonation waves propagating within the combustor.

Frolov et al. [104] presented 3-D numerical simulations showing heat fluxes through the walls and their correlations from inlet temperature, concluding that the local heat fluxes values are approximately near to 16 MW/m^2 and the mean heat fluxes (evaluated as the integral-mean value between inner and outer wall surfaces) were in the order of 2.5-3.5 MW/m^2, depending on the injection pressure.

Roy et al. [105] developed 1-D and 2-D models to predict heat transfer to the combustor walls of an uncooled RDE, with different settings for each one of the models. The effort of the first one was limited to the case of a single step change in temperature, the second model used the time-varying temperature profile from a full 3-D numerical simulation. Their work shows good agreement with previous experimental works regarding heat fluxes.

Other studies were successively conducted by *Meyer et al.* [106] and *Zhou et al*. [107], converging on previous results.

Table 2.1 reports the main works, in addition to those already mentioned, for the proper evaluation of heat fluxes through the walls during the combustion process.

Author	Type	T_{max} [K]	P_{max} [bar]	Heat $Flux_{mean}$ [MW/m^2]	Wave speed [m/s]	Fuel	Coolant	Test Time [sec.]
Bykovskii & Vedernikov [100]	EXP	–	16.0	1.50	–	Acetylene Hydrogen	–	0.50
Yi et al. [108]	NUM	3000	25.0	–	1300	Hydrogen	–	1.00
Schwer & Kailasanath [109]	NUM	3000	40.0	–	1600	Hydrogen	–	0,004
Le Naour et al. [110]	EXP	–	1.0	–	3200	Hydrogen	–	2.00
Kindracki et al. [111]	EXP	–	7.0	–	2000	Methane Ethane	–	0.80
Frolov et al. [104]	NUM	3300	25.0	3.50	1500	Hydrogen	Air	0.06
Theuerkauf et al. [79]	EXP	–	1.5	2.20	3000	Hydrogen	Water	20.00
Randall et al. [112]	EXP NUM	3100	6.5	–	2000	Hydrogen	–	4.00
Roy et al. [113]	NUM	2500	12.0	3.24		Hydrogen	–	4.00
Cocks et al. [114]	EXP NUM	2400	12.5	2.00	2000	Hydrogen	–	0.80
Theuerkauf et al. [102]	EXP	–	–	10.0	3000	Hydrogen	-	0.35
Meyer et al. [106]	EXP	2200	–	1.50	–	Hydrogen	Water	0.14
Zhou et al. [107]	EXP	2100	5.0	1.00	2000	Hydrogen	–	0.20
Goto et al. [115]	EXP	1200	5.0	2.50	2500	Ethylene O_2	Water	6.00
Stevens et al. [116]	EXP	1400	–	1.60	–	Hydrogen	Water	1.00

Table 2.1 – RDE, Boundary Condition literature review

An extensive review of all works, experimental and numerical, regarding the concept of RDE can be found in the work of *Kailasanath* [117] and *Meyer* [106].

There is a lot more to know and understand about RDEs, but from actual studies it is possible to state that for further investigation, especially for stationary work conditions of an RDE, a proper cooling system is needed to allow longer running periods to study the behavior of the device itself and the variation of the most important parameters.

Cooling system arrangements

Effusion cooling

With the growing need to limit the flow of refrigerant fluid to control combustion in the chamber, the current trend is to use effusion cooling to protect the liner wall. This cooling technology allows avoiding the high quantity of air that only film/slot cooling would require and the reliability problems linked to the cooling techniques by transpiration using porous materials. It consists of a series of inclined cylindrical holes with a small diameter, similar to those of film cooling but closer together, ensuring more uniform protection (Figure 2.9). The hole has small injection angles (usually 30°), even though it is possible to achieve angles up to 10° to obtain better coolant protection in the proximity of the wall, despite increased manufacturing costs. The dense array of holes provides a uniform protecting layer, ensured by the continuous coolant injection that gradually increases due to the film superposition. Since the holes are characterized by a high length/diameter ratio, there is a high heat removal thanks to the sink effect [118–120]. The mass bleeding on the coolant side provides a significant increase in HTC, which can contribute up to 30% to total cooling effectiveness.

Effusion cooling protection only begins after the first holes, which is why the initial area of the liner is usually protected by a slot from which the cooling air escapes.

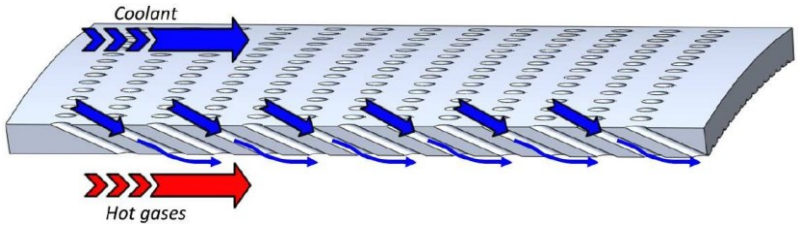

Figure 2.9 - Effusion cooled liner

This technique allows overcoming some technological issues given by classical cooling arrangements, making it very attractive for lean-burn combustors. First of all, it ensures a very efficient cooling performance with reduced coolant consumption with respect to 2D slots [28]. Moreover, effusion systems permit to avoid the protection degradation downstream of the injection point.

Geometrical parameters

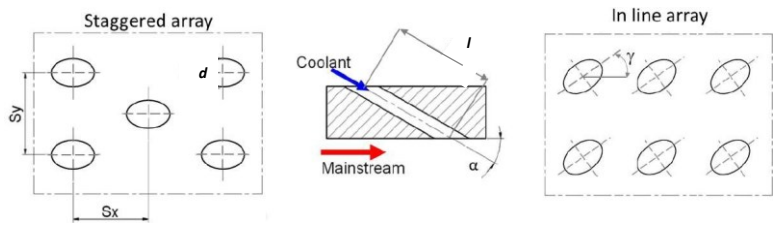

Figure 2.10 - Main geometrical parameters for effusion cooling arrangements

Literature studies on effusion cooling are usually carried out on simplified configurations representative of multi-perforated plates. Such geometries can be described, referring to Figure 2.10 in terms of hole diameter

(d) and length (l), stream-wise and span-wise pitches (Sx and Sy), inclination, and compound angle (α and γ). The selection of the effusion geometrical parameters is thus dictated by the trade-off between manufacturing costs and cooling performance.

Operating parameters

Several fluid dynamic parameters were introduced in literature to characterize the interaction between mainstream and coolant. As reported by *Acharya & Kanani* [3], the main parameters are:

Velocity Ratio:
$$VR = \frac{v_{cool}}{v_{gas}} \tag{2.1}$$

Blowing Ratio:
$$BR = \frac{(\rho v)_{cool}}{(\rho v)_{gas}} \tag{2.2}$$

Density Ratio:
$$DR = \frac{\rho_{cool}}{\rho_{gas}} \tag{2.3}$$

***Momentum Flux Ratio*:**
$$I = \frac{(\rho v^2)_{cool}}{(\rho v^2)_{gas}} \tag{2.4}$$

Another useful parameter is represented by the jet Reynolds number, which controls the heat transfer and the pressure losses within the hole:

Jet Reynolds number:
$$Re_j = \frac{(\rho v)_j d}{\mu} \tag{2.5}$$

Performance parameter

As for the operating parameters, *Acharya & Kanani* [3] reported also the main performance parameters. The first performance parameter is certainly the one introduced with Newton's law of cooling for the convective heat flux, reviewed by Goldstein [41]:

Convective Heat Flux:
$$q = HTC_{main}(T_w - T_{aw}) \tag{2.6}$$

HTC_{main} represents the heat transfer coefficient on a film cooled surface. The driving potential for convective heat transfer is the difference between wall temperature T_w and adiabatic wall temperature T_{aw}. Adiabatic wall temperature is usually presented in a non-dimensional form as the adiabatic effectiveness η_{ad}:

Adiabatic effectiveness:
$$\eta_{ad} = \frac{T_{main} - T_{aw}}{T_{main} - T_{cool}} \tag{2.7}$$

T_{main} is the mainstream total temperature and T_{cool} is the temperature of flow injected from the cooling hole.

Being the final aim of a cooling system the reduction of the heat transfer to the surface, which is dependent on both adiabatic effectiveness and heat transfer coefficient, both η_{aw} and HTC_{main} are required to determine the actual reduction of the overall heat load [121]. For this purpose, *Sen et al.* [122] suggest using the *Net Heat Flux Reduction parameter* (*NHFR*) to quantify the global heat transfer achieved on a cooled surface. It is defined as the ratio between the heat flux reduction due to film cooling and heat flux taking place without cooling (q_0):

Net Heat Flux Reduction parameter:
$$NHFR = \frac{q - q_0}{q_0} = 1 - \frac{HTC_{main}}{HTC_0}(1 - \eta_{ad}\theta) \tag{2.8}$$

θ is the non-dimensional temperature, defined as:

Non-dimensional temperature:
$$\theta = \frac{T_{main} - T_{cool}}{T_{main} - T_w} \tag{2.9}$$

The ultimate goal of a well-performing cooling system is thus to increase NHFR values: this target is achieved through a reduction in HTC rate and an enhancement in η_{aw}. It is worth to point out that increased mixing within the boundary layer due to coolant injection causes a significant increase in the mainstream heat transfer coefficient [121].

Despite the validity of the previous considerations, NHFR is not properly representative for effusion cooling systems since its definition Equation (2.8) does not explicitly take into account the heat sink within the perforation and on the backside of the plate. To overcome this aspect, the parameter overall effectiveness η_{ov} is introduced in the literature to indicate the overall cooling performance of a cooling system:

Overall effectiveness:
$$\eta_{ov} = \frac{T_{main} - T_w}{T_{main} - T_{cool}} \tag{2.10}$$

As it is possible to notice, the definition considers the actual wall temperature, hence all the contributions to wall cooling, including film protection and heat sink effects. For this reason, this parameter is the most suitable to give information about the overall performance of an effusion system.

Literature review

Effusion cooling has been the subject of attention since the ’80s [123]. In the early works, investigations have been performed to investigate the impact of geometric features and operating conditions on the thermal performance on effusion cooling plates. *Martiny et al.* [124] evaluated row-by-row adiabatic effectiveness and performed flow visualizations. Their study included also different flow patterns for the investigated blowing ratios. The same author [125] investigated the dependencies of dimensionless quantities on the overall effectiveness.

Many studies on full coverage film cooling have been focused on measuring or estimating the film effectiveness generated by coolant jets and the heat transfer of effusion cooling. One of the first works in this area and one of the most important, as it set the basis for future research, is certainly the one presented

by *Kumada et al.* [126] where a precious effort has been made in correlating the wall heat transfer coefficient variation with the jets fluid dynamics.

Scrittore et al. [127] investigated an effusion cooling scheme through flow field measurements and adiabatic wall temperatures. They studied a cooling scheme close to a real engine one and measured the adiabatic effectiveness finding the attainment of a fully developed effectiveness region at the 15th row and a very low effect of blowing ratio on cooling performance. More recently a study by *Ligrani et al.* [128] evaluated the efficiency by varying the *BR*. *Scrittore et al.* [129] performed also a flow field investigation to better understand the influence of dilution jets on effusion film development. The presence of the dilution jet caused a high increase in turbulence level, which in turn resulted in an increased spreading of the film cooling jets. Increasing dilution blowing ratio resulted in a degradation of film cooling. *Tarchi et al* [130] worked on the same topic, but employing a numerical approach.

Metzger et al. [131] studied the variation of heat transfer coefficient for full-coverage film cooling scheme with normal holes, founding an augmentation of 20÷25% in the local heat transfer with blowing ratio 0.1 and 0.2.

Martinez-Botas & Yuen [132] measured heat transfer coefficient and adiabatic effectiveness for a variety of flat plate geometries to test the influence of the injection angle. Also in *Hu*'s [133] work, the efficiency is evaluated by varying the inclination angle of the hole.

Kelly and Bogard [121] investigated an array of 90° normal holes and found that the largest values for h/h_0 occur immediately downstream of the film cooling holes and the levels of h/h_0 are similar for the first 9 rows. They explained that this could be due to an increase in the local turbulence levels immediately downstream of the holes, created by the interaction between the cooling jet and the mainstream flow.

Facchini et al. [134] estimated the heat transfer coefficient at various blowing ratios on the same real engine cooling scheme to evaluate the combined effects of the slot, effusion, and a large dilution hole. They found that an increase in *VR* makes the jets more and more penetrating in the main flow and they behave as an obstacle against film development, lowering the effectiveness values. On the contrary, they found that high *BR* values enhance the heat transfer phenomenon: in fact, the high jet velocity that draws hot gases from the mainstream flow on the liner surface alters the local boundary layer on the effusion surface causing an increase of *HTC*. The same author [135] carries out an extensive study on the influence of a recirculating area in the mainstream on the same geometry: they highlight that the presence of the recirculation impedes the creation of the film layer, leading to a general reduction of the effectiveness but without having significant effects on the heat transfer coefficient.

Andreini et al. [136] performed a numerical analysis on the same test article, simulating the behavior of the cooling system both with air and CO_2. Numerical results show that the entity of local heat transfer enhancement in the proximity of effusion holes exit is due to gas-jets interaction and that it mainly depends on effusion velocity ratio. The same author carried out an extensive study [137] in which they assess the influence of the blowing ratio (BR), the density ratio (DR) and the turbulence level (Tu) on the main stream, as well as a numerical study [138] to quantify the pressure losses associated with effusion cooling.

Gustafsson [120] in his work proposed an experiment to quantify the influence of the velocity ratio (VR) and the effect of the Reynolds number (Re) on the film cooling effectiveness.

Ligrani et al. [128] studied the effect of the blowing ratio and the influence of dense and sparse hole arrays on the thermal effectiveness, giving an extensive overview on the behavior of this system operated in several operating conditions. *Ekkad et al.* measured effectiveness and heat transfer coefficient distribution over a flat surface with one row of injection holes varying the *BR* and the compound angle; the tests were carried out using air and carbon dioxide as coolant, finding that both heat transfer and effectiveness increase with *BR*. *Lin et al.* [139,140] investigated both experimentally and numerically adiabatic film cooling effectiveness varying the hole geometrical parameters and the blowing ratio on film cooling
Krewinkel [141] and *Yellu-Kumar et al.* [142] reported a comprehensive review of the main studies carried out on this cooling procedure.
Not all the works have been included in the literature review, but for an in-depth analysis in Table 2.2 are reported a series of numerical and experimental setups on multi-perforated plates.

Author	M	I	Rows	α	Regions	Analyzed data
Experimental Setup						
Leger et al. [143]	1-3	7-12	9-35	60	Injection	T, η
Andreini et al. [144]	7.2	16	21	60	Injection	V, T, η
Miron et al. [145]	3.6	13	12	30	Injection	V
Michel et al. [146]	8.8	77.4	9	60	Injection	V
Scrittore et al. [127]	3.2-5	12.27	30	60	Injection	V, η_{ad}
Zhong and Brown [147]	0.4	1	12	90	All	V, T, η, η_{ad}
Andreini et al. [137]	0.5-5	0.2-25	14-22	30, 90	Injection	η, η_{ad}
Jonhson et al. [148]	0.4-1.7	0.17-0.94	3	30	Injection	η, η_{ad}
Kakade et al. [149]	0.47-2	0.15-4.12	6	20	Injection	V_{hot}, η, η_{ad}
Martiny et al. [124]	0.5-3	0.14-5.3	8	17	Injection	η, η_{ad}
Andreini et al. [150]	0.8-4.5	0.6-20	23	20, 30, 90	Injection	η_{ad}
Andreini et al. [151]	1.5-7	1.3-49	29	30	Injection	η, η_{ad}
Numerical Setup						
Most [152]	1.3-2.3	1.8-4.6	12	60	Injection	V
Harrington et al. [153]	0.4	0.8	10	90	Injection	T_{ad}, V, η_{ad}
Errera and Chemin [154]	1.2	0.5	12	45	All	T
Mendez and Nicoud [155]	1.5	2.25	1	30	All	V
Zhong and Brown [156]	0.1	0.1	12	90	All	T, η, η_{ad}
Cottin [157]	3.2-8.5	3.1-21.7	15	30	All	T, η
Florenciano and Bruel [158]	8.0	29	12	30	All	T, η, η_{ad}
Andrei et al. [159]	1-3	0.6-9	18	30, 90	Injection	η_{ad}

Table 2.2 - Review of the experimental and numerical multi-perforated plate setup

Convective cooling system arrangements

The convective heat transfer mode is sustained both by random molecular motion (diffusion, which dominates near the surface where the velocity is low) and by the bulk motion of the fluid (because the boundary layer grows as the flow progresses along the streamwise) within the boundary layer [160]. Appreciation of boundary layer phenomena is essential to understand the convective heat transfer process. Convective heat transfer may be classified according to the nature of the flow in:

- Forced convection when the flow is caused by external means
- Free (or natural) convection when the flow is induced by buoyancy forces

The important thing to understand is the connection between velocity and thermal boundary layer. Convection is strongly dependent on the boundary layers that develop on the surface and the convective coefficient depends on the surface geometry and flow conditions. Indeed, an essential step in the treatment of any convection problem is to determine whether the boundary layer is laminar or turbulent. Surface friction and convection transfer rates depend strongly on boundary layer characteristics.
The thermal boundary layer grows in the streamwise direction, and the temperature gradient decreases in the same direction as the heat transfer coefficient. As it induces large velocity gradients, turbulent mixing promotes large temperature and species concentration gradients adjacent to the solid surface as well as a corresponding increase in the heat transfer coefficient across the transition region. Turbulence induces mixing, which reduces the importance of conduction and diffusion in determining the thermal boundary layer thickness. Differences in the thicknesses of the velocity and thermal boundary layers tend to be much smaller in turbulent flow than in laminar flow [160].

According to all these considerations it is clear that having a turbulent flow allows obtaining a higher heat transfer coefficient to the wall, due to the higher mixing that allows to quickly and continuously feed the zone near to the solid surface with lower temperature fluid and move the hotter fluid in the bulk zone where is located the fluid at a lower temperature. An important thing to keep in mind is that turbulent flow can increase the heat transfer coefficient, but it leads to considerably higher-pressure losses due to the friction factor enhancement compared with the laminar flow.

For very high heat fluxes it is necessary to adopt different solutions that allow improving the heat transfer coefficient:

- Maintain turbulent conditions instead of letting the boundary layer develop completely using turbulators
- Directly injected coolant jets using a buffer on the surface that needs to be cooled

Dimples

Dimples are arrays of indentations along internal surfaces (Figure 2.11). These are most commonly spherical in shape, although a variety of other shapes have also been employed, including triangular and tear drop shape. Arrays of dimples are a beneficial method for internal cooling because they produce multiple vortex pairs which augment local Nusselt number distributions as they move downstream. . They are notable for the low-pressure drop penalties which they produce thanks to the fact that they do not

protrude into the flow to produce significant amounts of form drag. With this benefit, dimples offer advantages for cooling later turbine stages where lower pressure cooling air is employed. They are also advantageous because the pressure drop that they produce through an airfoil passage is relatively low, which allows favorable pressure margins to be maintained in some interior parts of the airfoil that are further downstream [161,162].

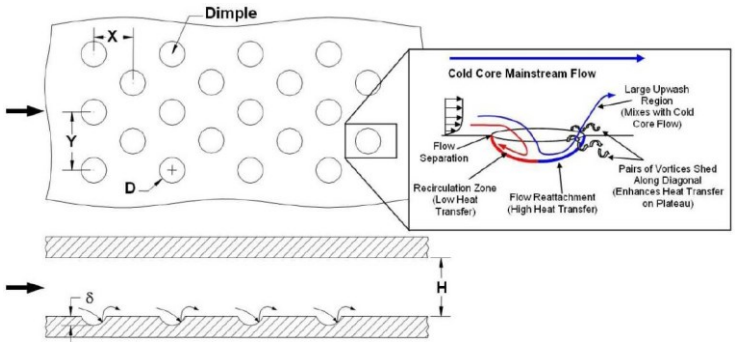

Figure 2.11 - A typical test model for dimple cooling studies with a conceptual view of dimple induced secondary flow [168]

Another benefit is that dimple manufacture removes material from internal cooling passage components, in contrast to rib turbulators and pin fins, which require the addition of extra material and weight [161]. Heat transfer in a dimpled channel is typically 2÷2.5 times greater than the heat transfer in a smooth channel with a pressure loss penalty of 2 to 4 times that of a smooth channel [161]. The ribbed surface can have higher heat transfer augmentation but only with higher friction factor augmentation [161]. Dimpled surface performances show little dependence on Reynolds number and channel aspect ratio, but dimple size (D), depth (δ), distribution, shape, and pitch (streamwise (X), spanwise (Y)) can strongly affect heat transfer distribution in the channel [163].

Dimples, literature review

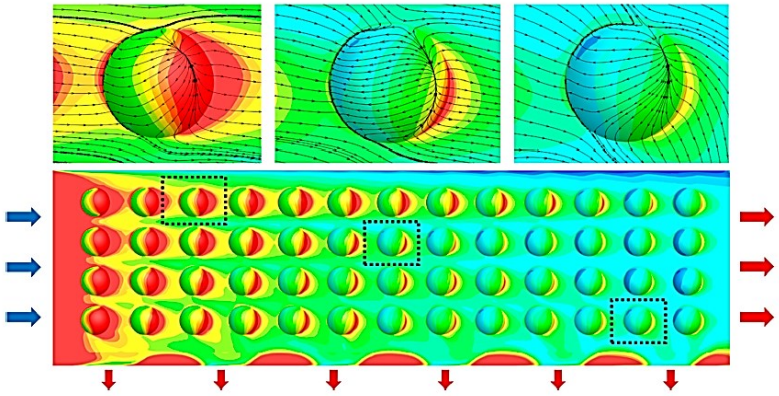

Figure 2.12 - Nusselt Number distribution in a dimple in line arrangement [168]

One of the first studies on the effects of hemispherical dimples on flow structure and heat transfer is described by *Gromov et al.* [164] with symmetric and nonsymmetric streamlines and flow patterns produced by hemispherical cavities with a variety of sizes. *Kesarev & Kozlov* [165] presented distributions of local heat transfer coefficients inside a single hemispherical cavity, and indicate that the convective heat

transfer from the cavity is higher, especially on the downstream portion. *Afanasyev et al*. [166] described the heat transfer enhancement mechanism for flows over walls indented with regular arrays of spherical pits with several different shapes. They found Enhancements of *30÷40 %*, with pressure losses that are not increased appreciably relative to a smooth surface. *Kimura & Tsutahara* [167] found the geometry of the dimples corresponding to the optimum concavity depth by for minimum drag on cylinders. At high Reynolds numbers, significantly lower drag coefficients are present with arrays of dimples compared to smooth surfaces.

Chyu et al. [168] showed the effects of Reynolds number on local heat transfer coefficient distributions with staggered arrays of two different shapes of concavities.

Gortyshov et al. [169], employs spherically shaped dimples placed at different relative positions on the opposite sides of a narrow channel. They observed that an increase in relative dimple depth increases the heat transfer rates, as well as streamwise pressure loss. *Moon et al*. [170] illustrate the effects of channel height on a surface with a staggered pattern of dimples. According to *Isaev et al.* [171], the flow inside of a spherical indentation dimple is also quite complex, with occasional nonsymmetric flow patterns, even though the dimple is symmetric.

Kithcart and Klett [172] compare heat transfer and skin friction of flows over surfaces on one wall of a rectangular channel with hemispherical dimples, hemispherical protrusions, and rectangular protrusions. The authors conclude that all three geometries produce similar levels of heat transfer augmentation.

Pin-fins

Pin-fins are prismatic support, generally having circular cross sections, widely used in gas turbine trailing edge cooling. They are placed orthogonally to the flow direction to maximize forced convection cooling; the main advantage consists of increasing the heat transfer coefficient without increasing the thickness of the wall surface.

Flow around the pin fin behaves in the same way as around a single cylinder: the coolant separates and wakes are shed downstream, whereas a horseshoe vortex forms upstream the base of the pin, wrapping it and creating additional mixing. In addition to flow disturbances, pins conduct thermal energy away from the heat transfer surface and long pins can increase the effective heat transfer area. Pin spacing (in both streamwise (*X*) and spanwise (*Y*) direction), size, shape, or fillet radii dimensions (*d*) are all factors that can influence heat transfer performance (Figure 2.13).

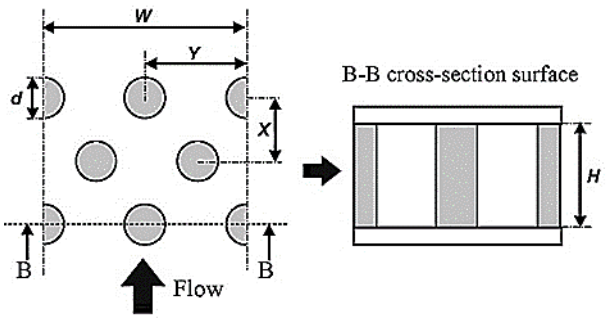

Figure 2.13 - Pin-fins main geometrical parameters

Pin-fins, literature review

Most existing pin fin investigations only focus on heat or mass transfer. The most important parameters are the influences of pin geometry, pin materials, pin fin array configuration, channel geometry, Reynolds numbers, and other [173–175]. *Brigham & VanFossen* [176] reported large overall heat transfer and mass transfer augmentations for circular pin fins arranged in in-line and staggered arrays. *Chyu & Goldstein* [177], and *Chyu et al.* [178] reported local and spatially averaged mass transfer coefficients for different pin fin arrays, which provide evidence of large overall mass transfer augmentations for certain inline and staggered circular arrays.

A variety of pin fin shapes are investigated, including circular [179–182], diamond [178,179,181], three-dimensional protruding elements [178], cubic [178,179], and elliptical [182].

According to *Won et al.* [183] (Figure 2.14), the most important features downstream of an individual pin are two large vortex pairs, which are formed by the blockage effects of the pin fins.

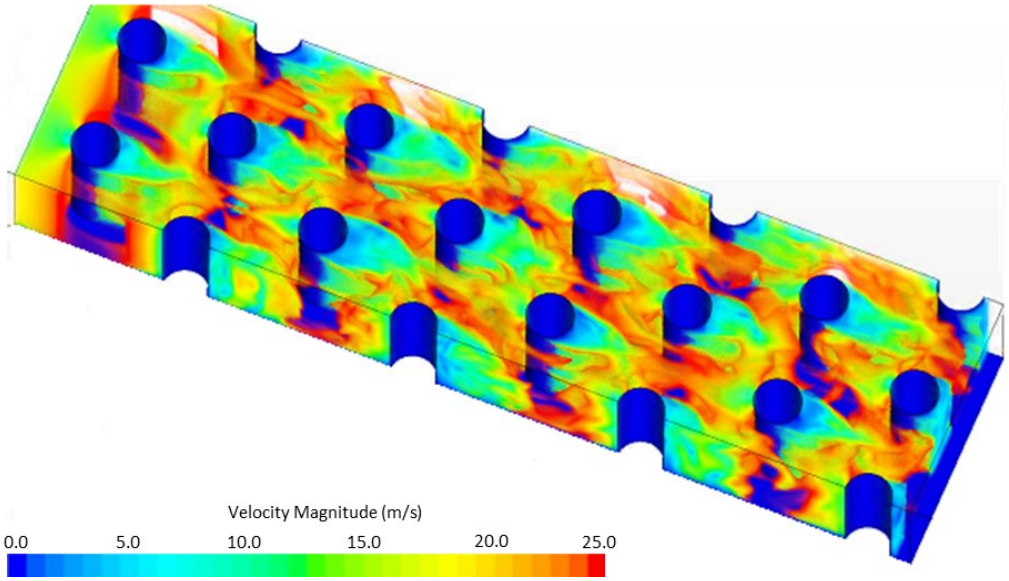

Figure 2.14 – Flow features in a Pin-fins channel [183]

The secondary flows within and around these vortices are especially intense relative to other secondary flows that are present. Additional description of the different flow structures which develop near one end wall junction of one pin fin (as it is contained within a pin array) is provided by *Ligrani et al.* [162], including a typical surface Nusselt number ratio distribution, produced on the end wall by these flow structures [184].

Ribs

The main effect of ribs is to increase the heat transfer coefficient and the surface through which the transfer takes place. These elements promote turbulence inside the duct and break the coolant boundary layer, allowing an effective mixing of the flow; this results in a more uniform temperature distribution and a heat transfer augmentation in cooled airfoils. This geometric condition disturbs the boundary layer, leading to greater turbulence, which in return allows better mixing of the hot flow near the wall with the cooler one, that flows at the center. This turns into a continuous fluctuation of the heat transfer coefficient due to the

separation and reattachment of the flow, but also in a generalized increase of the coefficient itself. This behavior is accentuated on the sides that present this design solution. In the first analysis, however, it can also be affirmed that the presence of ribs implies a benefit also on the smooth side of the duct. It is possible to measure an increase in heat transfer ranging from 20 to 60% [185] compared to the smooth duct.
On the other hand, with the presence of these turbulators, there is a pressure loss increase inside the cooling fluid network.

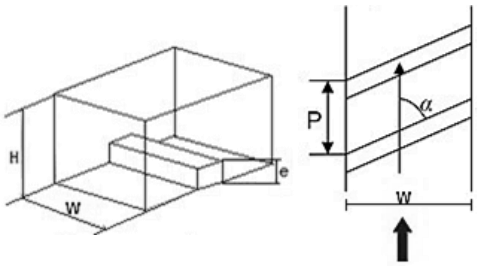

Figure 2.15 - Ribs main geometrical parameters

The main geometric parameters that must be considered when studying the changes introduced to the flow motion in the presence of a ribbed surface are the *Aspect ratio* given by the ratio between duct width and height (*W/H*), the height of the rib (*e*), ribs pitch (*P*), and the inclination angle (α) (all described in Figure 2.15).

Ribs, literature review

A significant number of experimental and numerical studies address the effects of rib turbulators on heat transfer in internal channels. Single pass and multipass channels, square and rectangular channels, and channels with and without rotation are considered. *Casarsa et al.* [186] characterized the velocity and heat transfer fields in an internal cooling channel with 90° ribs which produce 30% blockage. Heat transfer enhancement magnitudes, time-averaged distributions of mean velocity components, and time-averaged distributions of normalized root-mean-square velocity fluctuations are included. *Ligrani et al.* [187] proved that spatially resolved local Nusselt numbers are higher on top of the rib turbulators, with lower magnitudes on flat surfaces between the ribs, where regions of flow separation and shear layer reattachment have pronounced influences on local surface heat transfer behavior. Intense, highly unsteady secondary flows and vortex pairs are also important as they increase secondary advection and turbulent transport over the entire channel cross-section. *Cho et al.* [188] verified that discrete ribs with gaps in between produce more uniform heat transfer coefficient distributions than continuous ribs. According to these authors, remarkable enhancements of local and spatially averaged surface heat transfer rates are possible with rib turbulators, despite lowered local Nusselt numbers at certain locations along ribbed surfaces.
Computational studies of flows and heat transfer in ducts with rib turbulators consider straight single-pass ducts [189–192], two-pass ducts [193], two-pass ducts with U-shaped channels in between [192,194], 90° orthogonal ribs [190,191,194], 45° angled ribs [189,192,193], 45° V-shaped ribs [191], and rotation [189,190,193,194].

Regarding the flow structure, flow recirculation patterns around a single rib are positioned just downstream of each rib and cover a considerable portion of the ribbed wall. Each of these recirculation zones is often considered to be a potential hot spot because it is associated with locally lower surface Nusselt numbers [187]. Downstream of the flow recirculation zone, downstream of each rib, is a line across the surface where streamlines reattach. With angled ribs, additional secondary flows are induced by flow skewing [186].
Casarsa et al. [186] also provide quantitative detail on the recirculation zone which forms just above a rib, the recirculation zone near the corner just upstream of a rib, the large recirculation zone present downstream of a rib, and the spanwise vortex, or second smaller separation zone, present in the vicinity of the downstream bottom corner of a rib. According to the authors, the shear layer reattachment line exhibits a particular shape near the lateral wall because sidewall boundary layers are altered by the presence of the rib. When the boundary layer is deviated by the rib, new streamwise vorticity is generated inside of it. The flow then rolls upon itself. The result is local deformation of the reattachment line from a straight line.
The main geometric parameters that must be considered when studying the changes introduced to the flow motion in the presence of impingement cooling are jet hole diameter, impingement channel height, streamwise pitch, spanwise pitch, buffer thickness.

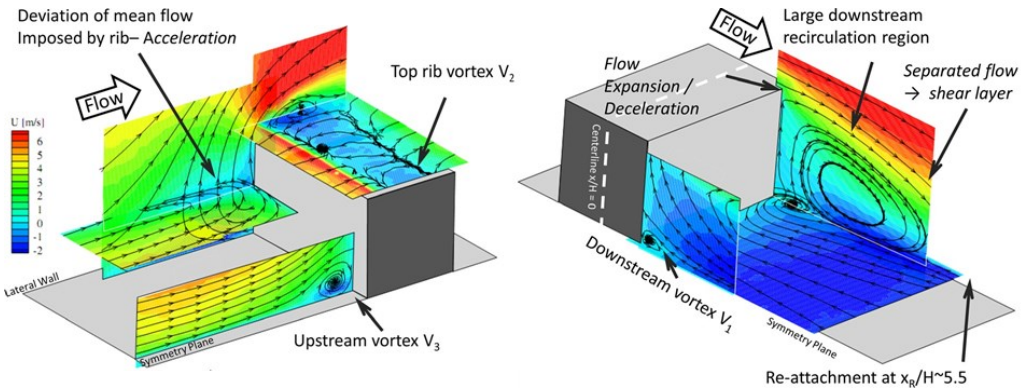

Figure 2.16 - Visualization of the ribbed channel flow field [186]

Impingement

Impingement systems are widely used in many cooling applications. Usually, these systems consist of a target plate, for example, a combustor liner, that is cooled by multiple impingement rows of orthogonal jets. The cooling air is forced to impinge cold side surfaces of the liner, and the increased level of turbulence that is generated increases the heat transfer considerably. Single jet impingement cooling is the application of a high-velocity coolant mass flow ejected from a hole (or slot) and directed to the target surface.
The impingement configuration can be characterized by non-dimensional parameters, like Sx/d_d, Sy/d_d, and Z/d_d, where Sx/d_d and Sy/d_d represent the jet-to-jet spacing in streamwise and spanwise direction respectively, and Z/d_d gives the jet-to-target plate spacing, all normalized with the diameter d_d (Figure 2.17).

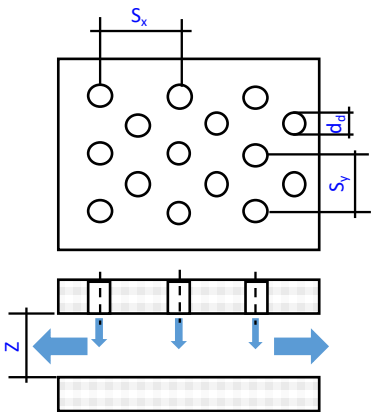

Figure 2.17 – Jet impingement main geometrical parameters

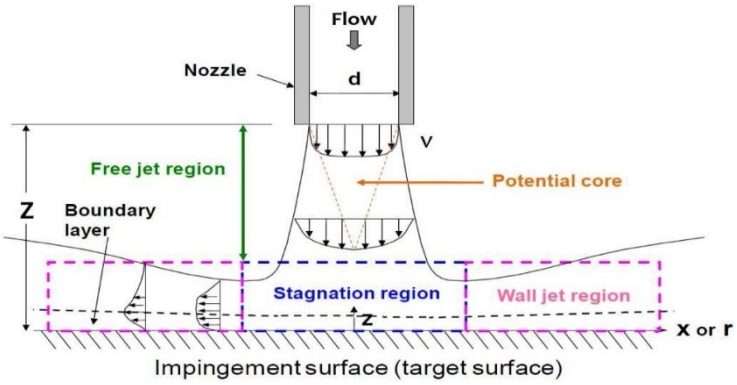

Figure 2.18 - Scheme of flow regions in an impingement jet [200]

Impingement, literature review

A lot of research publications are available about impingement cooling: many works are based on studies performed on a single impinging jet, like the one of *Martin* [195] or *Bradbury* [196], that studied the details of fluid mechanics in a free jet. *Goldstein et al.* [41] provided variations in single jet heat transfer with considerations of Reynolds number and again by changing jet-to-target plate spacing.

Goldstein & Seol [197] compared the heat transfer between a row of circular jet and a slot jet, while an analysis of the crossflow impact on the jet structure was performed in [198] by *Goldstein & Behbahani*. The accumulation of the impinged exhaust fluid in large arrays of impingement jets creates a significant crossflow that interacts detrimentally, as shown by *Florschuetz et al.* [199]. The authors stated that accumulating crossflow decreases the peak heat transfer coefficient of the impinging jets.

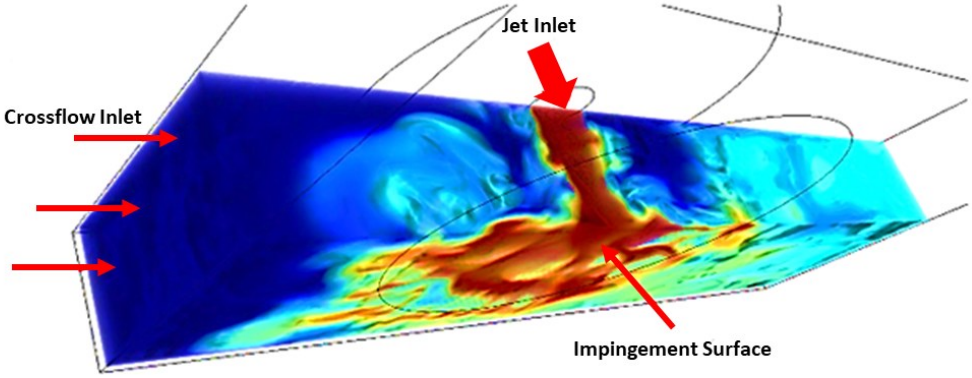

Figure 2.19 - Impinging jet in crossflow

Depending on the geometric configurations and flow rate, the crossflow effect can decrease the row averaged heat transfer coefficient by more than 20% [200].

The effects of non-dimensional geometrical parameters (all the described parameters are normalized to the jet diameter) on the Nusselt number evaluation have been studied by *Florschuetz et al*. [199]. As expected, increasing jet-to-jet spacing in streamwise or spanwise direction will lead to a decrease in heat transfer coefficient and a larger jet-to-wall spacing also produces lower heat transfer

.

Chapter 3

Therm-1D/Dakota coupled procedure validation

Introduction

In this chapter, the first application of the coupled procedure described above will be presented. This application was performed with a triple purpose. The first aim was to increase the level of experience in the use of UQ techniques applied to one-dimensional codes. The second purpose was to verify the accuracy of the uncertainty propagation methods and the relative sampling grids, comparing the spectral methods with the Monte Carlo method. The third purpose was to carry out a critical analysis of the Therm-1D procedure, analyzing the main input or tuning parameters, those that introduce the greatest uncertainties in the system response.

A total of four types of macro-analysis were carried out. In the first one, the influence of the uncertainty of two geometric parameters was evaluated. Another was conducted for the three heat transfer tuning factors of the code and in the third one, the uncertainties of the quantities defining the boundary conditions inside the machine were considered. The last and final analysis contains all the previous random variables (seven) and was performed to assess the behavior of the Smolyak sparse grids.

The first analysis of uncertain geometric factors was used to verify the correct number of samples to ensure the convergence of the Monte Carlo method, the sensitivity of the final interpolating polynomial to the various polynomial orders, and the relative sampling methods.

It has been verified that the stochastic collocation method provides the same results as the polynomial chaos expansion with the tensor product, which is why this method was carried out only for geometric analysis.

For all the analyses mentioned, a Monte Carlo simulation was also carried out to validate the results obtained by stochastic expansion methods.

The liner wall temperature was evaluated as the output variable.

The fluid network realized for this application is the one related to the inner liner of the combustor developed during the European project LEMCOTEC (Low EMission COre-engine TEChnologies). The validation of the analysis was performed by comparison with experimental tests carried out at CIAM (Central Institute of Aviation Motors); the working conditions were simulated by *Bertini et al.* [77,201].

The conditions analyzed during the experimental tests are shown in Table 3.1. Here P_{30} and T_{30} are referred to the plane 30 (compressor outlet), while P/T describes the Pilot-to-total fuel split.

Only approach conditions were analyzed as they are the most suitable for this application, as both the experimental data and those obtained by numerical methods are available.

Test Point	P_{30} [bar]	T_{30} [K]	FAR %	P/T %	Active Injectors
Idle (ICAO 7)	5.4	518	14.5	100	9
Approach (ICAO 30)	13.5	655	17.2	70	18
Cruise (ICAO 85)	13.5	655	28.3	10	18
Take-Off (ICAO 100)	19.0	840	28.3	10	18

Table 3.1 - Tested Conditions at CIAM [201]

Test case

The combustor considered for the UQ analysis was the one developed for the European project LEMCOTEC. The main objectives were focused on the development of a new engine with greater thermal efficiency with a high overall pressure ratio (OPR) up to 70, which results in a reduction of the CO_2 emitted. The increase in TIT due to the higher OPR inevitably leads to an increase in NO_x emissions; therefore, research focused on the development of new lean combustion techniques to compensate for this phenomenon.

The combustor has an annular structure and it develops combustion in lean mixture conditions guaranteed by a particular injection system, in which the stability of the flame is ensured by staging the fuel with a pilot injection through an atomizer. Part of the primary air is used for the cooling of the swirler and the dome, which is cooled by jets of impingement. The remaining air feed the annuli cooling the liner walls, protected in the first part with a slot and for the majority by effusion cooling.

The LEMCOTEC combustor has an optimized structure and cooling system to minimize pollutant emissions and improve the life of the components.

The fluid network realized for this application is the one related to the inner liner of the combustor supplied by *GE Avio Aero*. The network under examination has only two regions, one for the main flow and one affected by the cooling fluid between the liner and the casing (Figure 3.).

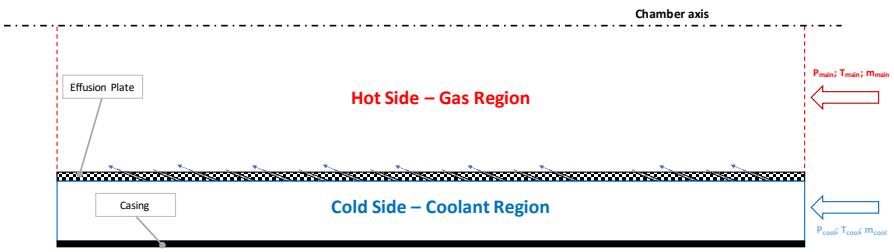

Figure 3.1 - Fluid network modelling - LEMCOTEC

The network has been supplied without slot cooling modeling, whose effect is simulated by imposing a lower hot gas temperature than the real ones in the initial part of the liner. As can be seen from the results

section, this modeling will have a great impact in terms of liner wall temperature for this part of the liner. It was decided to analyze the Approach conditions because both the experimental data and those obtained by numerical simulation are available.

The conditions imposed on the various planes of the model were obtained from the experimental tests carried out at CIAM, performed under different operating conditions. For the cooling system, the output flow rate has been set, as the bleeding flow rate is fixed in actual operation; in other words, the effusion cooling has been modeled as operating with the measured pressure drop.

Random variables setting

In this paragraph, all the setting parameters of the variables chosen as uncertain would be reported. These are classified according to the type of analysis performed.

Geometric analysis

Two uncertain variables have been considered: the inclination angle α and the discharge coefficient C_d. The distributions have been hypothesized basing the choices on the works currently present in literature and according to the industrial partner preferences. For the distribution limits of α, the work of *Bunker* [7] has been taken as reference, where a tolerance of ±5° on the inclination angle is considered for a film cooling hole concerning a mean value of 30°. The assumed tolerance (±5°) has a confidence interval of 95.45%. Although the cooling system is not the same, it was decided to use this parameter because of the high affinity between film and effusion cooling. With no direct information on the variation of the C_d, it has been decided by analogy. The uncertainty was modeled as reported in Table 3.2.

	μ	σ	Upper Limit	Lower Limit	Distribution
Angle	30°	2.5°	35°	25°	Normal
Discharge coeff.	0.7	0.05	0.8	0.6	Normal

Table 3.2 - Geometric variables probability distribution

Heat transfer tuning factors analysis

Three heat transfer tuning factors were considered as uncertain variables: hot gas side (HTC_{hot}), coolant side (HTC_{cold}), and the one inside the hole related to the sink effect (HS_{factor}).

	Upper Limit	Lower Limit	Distribution
HTC_{cold}	1.2	0.8	Uniform
HS factor	1.2	0.8	Uniform
HTC_{hot}	1.3	0.7	Uniform

Table 3.3 - Heat transfer tuning factors probability distributions

The purpose was to assess how much these uncertainties affect the result. It should be highlighted that these are tuning parameters that are imposed to achieve the correct heat transfer value, obtained from experimental tests or more accurate numerical simulations.
These parameters play a key role especially in the early stages of design, where most of the quantities involved are not yet investigated. Therefore, a correct evaluation of how much these parameters impact the response function can lead to the definition of a reasonable range in which to vary the heat transfer coefficients and accelerate the whole procedure.
Following *Durocher et al.* [63], it has been defined as a variable with uniform distribution for each of the three parameters. The three variables have been assumed as multiplicative factors, which increase or reduce the relative nominal heat transfer factor supplied by *GE Avio Aero*. The uncertainty was modeled as reported in Table 3.3.

Boundary conditions analysis

The analysis has the objective to study the impact of the conditions that occur inside the combustion chamber on the considered response function. The uncertain quantities taken into consideration are the temperature of the gas, the radiative temperature with which the radiation is modeled, the type of mixture through *FAR* (Fuel-Air ratio), and the kinetic conditions of the gas. The random variables considered were only two: one for the thermal conditions (including *FAR*) and another factor for gas velocity. This type of approach has allowed avoiding non-physical conditions by placing a multiplicative factor for each quantity.
Two normal distributions have been assumed and since in literature there are no works analogous to the cases analyzed, a Gaussian distribution was chosen to be able to give greater probabilistic value to the nominal working conditions. The uncertainty was modeled as reported in Table 3.4, defining the factor that multiplies the temperatures and the *FAR* with *BC-1* and the factor affecting the velocity with *BC-2*.

	μ	σ	*Upper Limit*	*Lower Limit*	*Distribution*
BC-1	1	0.05	1.1	0.9	Normal
BC-2	1	0.25	0.5	1.5	Normal

Table 3.4 - Probability distribution for boundary conditions variables

Results

This section will provide and describe all the results obtained from the study of uncertainty quantification on the *Therm-1D* procedure. It is necessary to make a preface on the type of approach used and on the results obtained. The one-dimensional approach is greatly influenced by the imposed internal temperature range. As already mentioned, the temperature range has been defined according to *GE Avio Areo*'s best practices. The temperature distribution of the gas inside the chamber has been imposed to model the effect of the slot cooling since it is not present in the fluid network supplied; this involves an initial trend of the liner wall temperature which does not depend on the behavior of the solver itself but is attributable to the temperature range of the hot gases imposed.

To provide a precise comparison among the methods, when the surrogate model was used, a further LHS sampling of 1000 points was performed to get the same sample size obtained with the MC method. The results obtained were used to make the comparison among the various methods.

In agreement with *Silverman* [202], to obtain a probabilistic estimate linked to the temperature range provided by the UQ methods, a further procedure that exploits the non-parametric estimate of the probability density based on sampled data on the surrogate model was carried out. In this way, it was possible to obtain an estimation of the continuous probability starting from the results of the metal temperature obtained.

The magnitude used as reference was the liner wall temperature: mean value, maximum and minimum values, and standard deviation are calculated both for the results obtained from the simulations carried out with Therm-1D and for those obtained from the surrogate model.

Geometric analysis results

The sample size for the Monte Carlo method has been defined to be able to evaluate the convergence. All samples were taken with the LHS method to speed up convergence. The tests were carried out for three sample sizes: 10, 100, and 1000 samples.

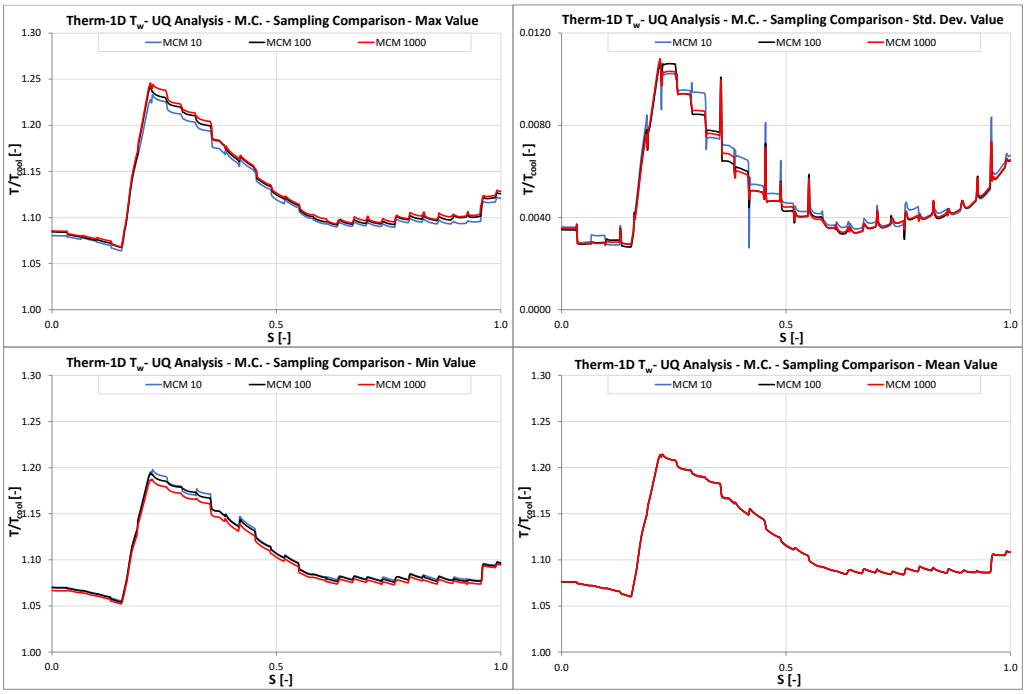

Figure 3.2 - Monte Carlo method analysis

It is possible to observe in Figure 3.2 (Graphs show non-dimensional temperature trend as a function of non-dimensional curvilinear abscissa) that the Monte Carlo method is not affected by the sample size regarding the mean value, but the same cannot be said for the extreme values and the standard deviation. The main differences between the sample sizes can be seen from the graph relative to the standard deviations. As the sample size increases, the gap between the minimum and maximum values increases: this phenomenon is explained by the type of sampling carried out. The LHS technique divides the initial distribution into areas of equal probability and then randomly samples a point within each area; this causes

many more points to be considered in the analysis at the far end of the distribution, leading to an increase in the dispersion of the results. It can be seen also the plots segmentation shown in Figure 3.2. This happens because each point has a probability of occurrence that does not depend on the others. The same analysis can be done for all following plots.

The first comparison carried out for the spectral expansion methods is the one between the polynomial chaos expansion method based on the tensor product of the bases and the stochastic collocation method. In Figure 3.3 the change in liner temperature as the polynomial order increases for both methods is shown.

The results obtained are following *Montomoli et al.* [203], which declared a variation between the two methods of 0.6%. Since the two methods provide the same result, both in terms of average and interval, the stochastic collocation method was not considered for the subsequent analyses and comparisons.

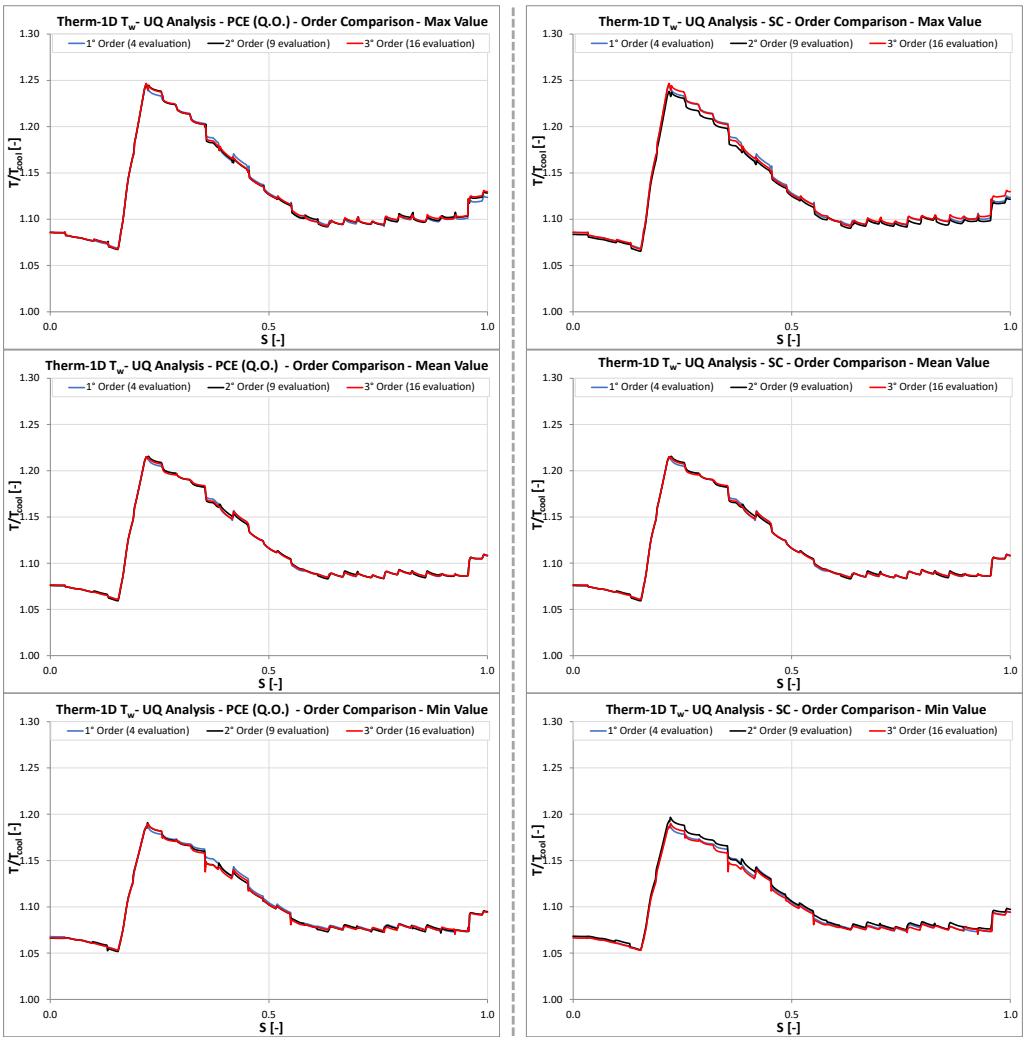

Figure 3.3 - Comparison PCE (Q.O) and S.C.

The last stochastic expansion methodology to be shown is that one of the PCE with total order imposed; in this case, the polynomial order coincides with the degree of the final interpolating polynomial. As already asserted by *Eldered et al.* [55], an over-sampling is mandatory to obtain results comparable with the previous methods. For all subsequent analyses, carried out with this expansion technique, an over-sampling of a factor of two was carried out (*collocation ratio* = 2).

Comparing the results obtained with the Monte Carlo method and those obtained with stochastic methods (Figure 3.4), the latter are much more efficient; in fact, a surrogate model obtained with only 4 simulations (*PCE Q.O.*) can predict both the average trend and the limit values of the metal temperature.
Subsequently, it will be shown that these will be able to predict the probabilistic distribution with excellent results. For a limited number of variables, the need to ensure over-sampling for the fixed-order PCE (*PCE T.O.*) results in a higher computational cost (12 evaluation) than with the tensor-product method (*PCE Q.O.*), which achieves the same result with only 4 evaluations.

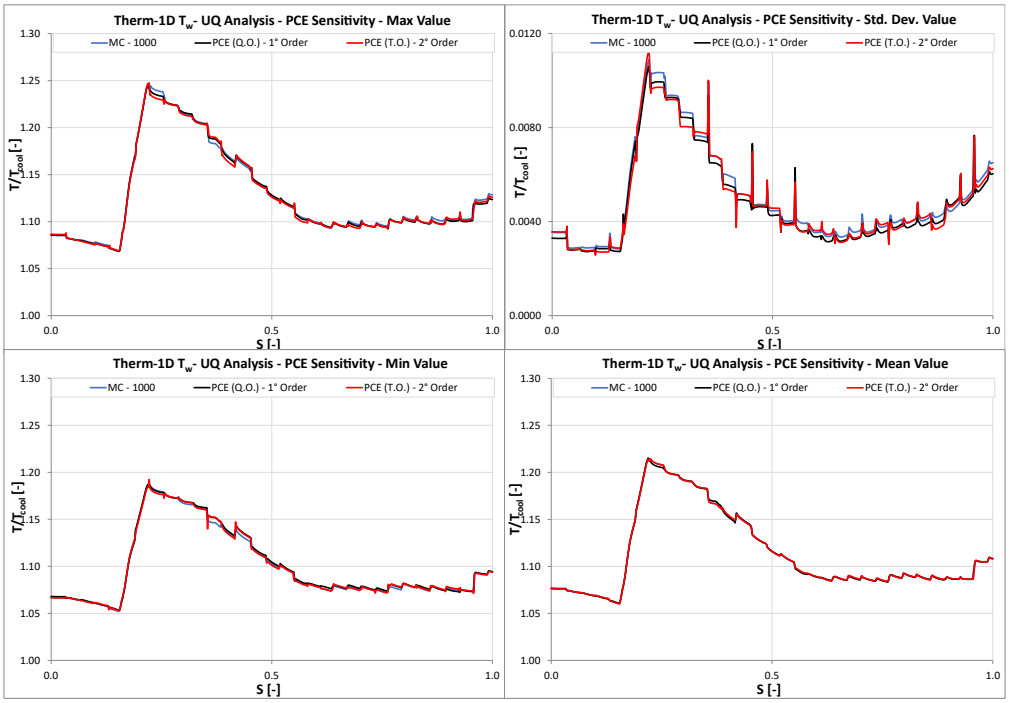

Figure 3.4 - Comparison between MC and PCE

In Figure 3.5 the sensitivity study is reported as a histogram. It revealed that the discharge coefficient has a generally greater influence on the liner temperature than the angle of inclination of the effusion hole. Sobol's indices are reported in a cumulative graph, the sum will always give 100%. The presence of the peaks seems to be dictated by the presence of the effusion hole rows.
The estimation of the probability density obtained with the Monte Carlo method (1000 samples) and those obtained by sampling on the surrogate models of the two PCE methods are reported in Figure 3.6. The first one is based on the Gauss grid and the other has a fixed total order, which require respectively 4 and 12 simulations. The result obtained with the stochastic collocation is also reported (4 simulations). In this way, it is possible to observe the variation of the PDF of the wall temperature as a function of the non-dimensional abscissa of the liner. The 3Ds give a better view of the PDF variability by visually relating it to the wall temperature trend along the liner. It should be noted that these graphs are based on independent points, each point has a probability of occurrence that does not depend on the others. The correct use of this type of graph is to fix a coordinate of the liner and assess the probability to get a certain wall temperature because at each point of the liner there is a certain probability distribution that is independent of the previous and following one. Overall, the methods agree with themselves in probabilistic terms. In all the liner regions there is a zone with a greater probability, associable to the modal value of the probability distribution.

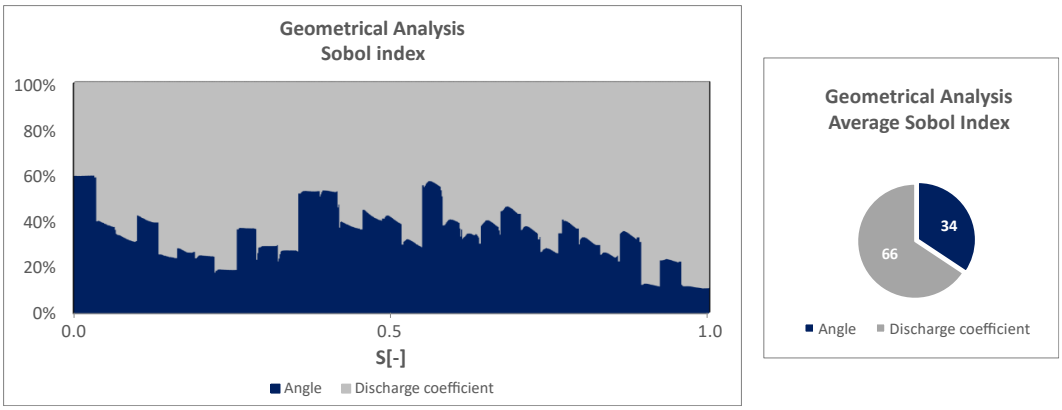

Figure 3.5 - Sensitivity analysis for geometric parameters

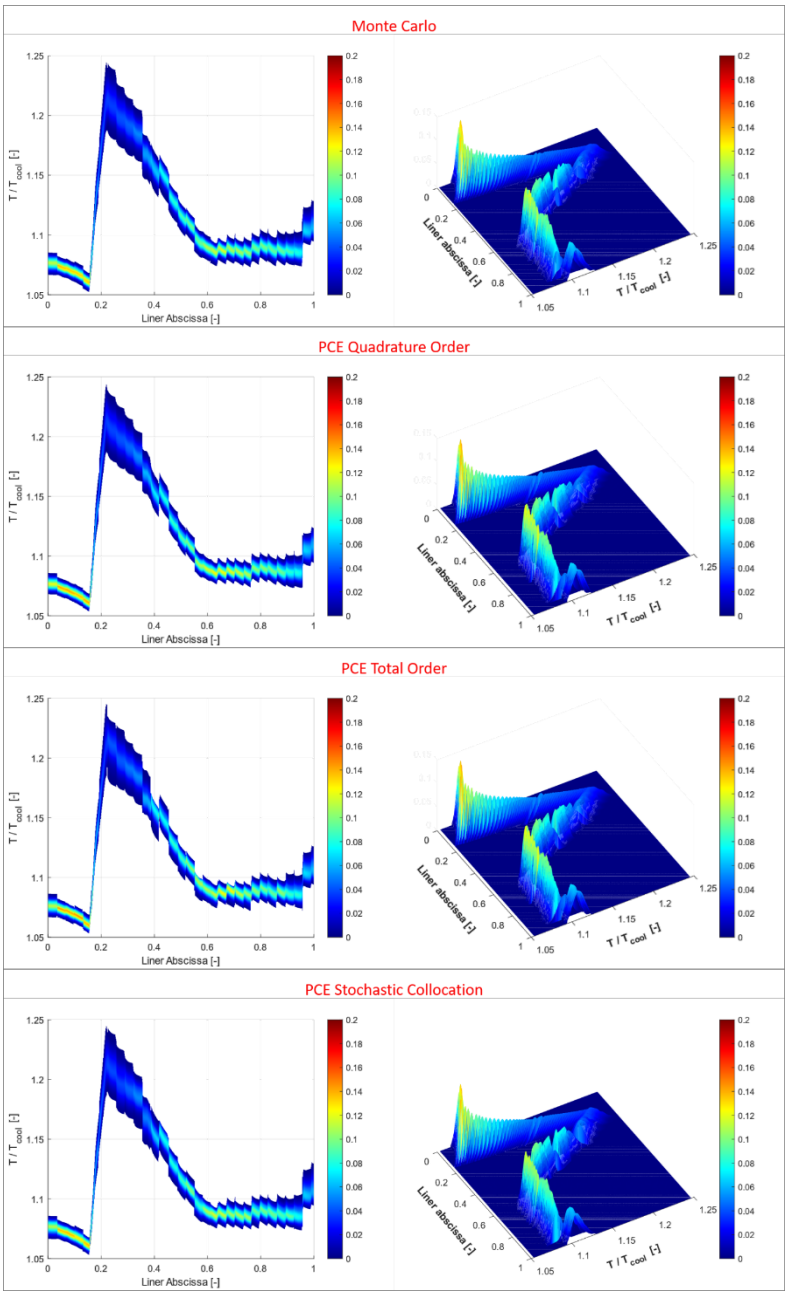

Figure 3.6 - Geometric analysis output probability

The study has shown that spectral expansion methods are in good agreement with the Monte Carlo method for reduced polynomial orders; this has allowed to conduct the UQ remaining analysis with minimum polynomial orders and therefore, ensuring the lowest computational cost. For the remaining analyses, only comparisons among methods will be provided.

Heat transfer factor analysis results

The purpose of this analysis is to quantify how and which heat transfer tuning factor most influences the response function. The study shows a perfect agreement between the stochastic expansion methods with the Monte Carlo method, both in terms of temperature trend and standard deviation (Figure 3.7).

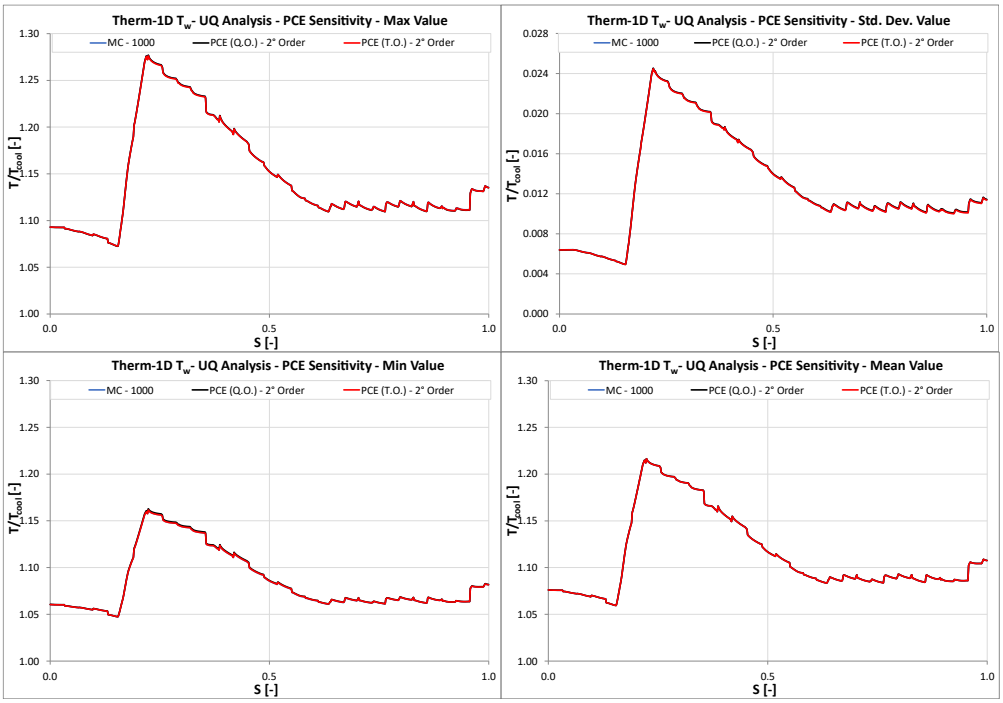

Figure 3.7 - Comparison HTC analysis

From the comparison of the figure below it can be seen that the analysis of the HTC tuning factors has led to a greater range of variability for the liner temperature. This is easily recognizable by comparing Figure 3.8, realized for the M.C. method, with Figure 3.2 for the geometric analysis.

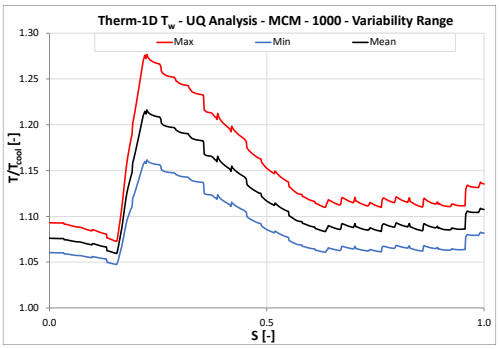

Figure 3.8 – M.C. variability range for HTC tuning factors evaluations

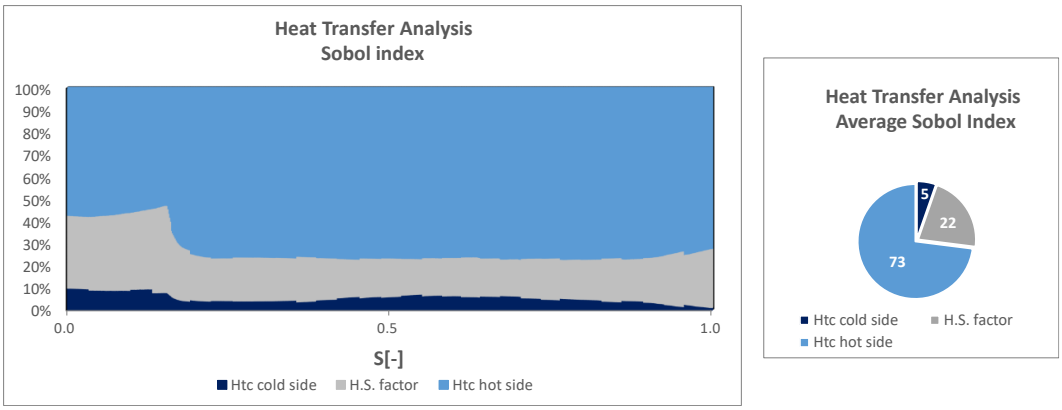

Figure 3.9 - Sensitivity analysis for heat transfer tuning factors analysis

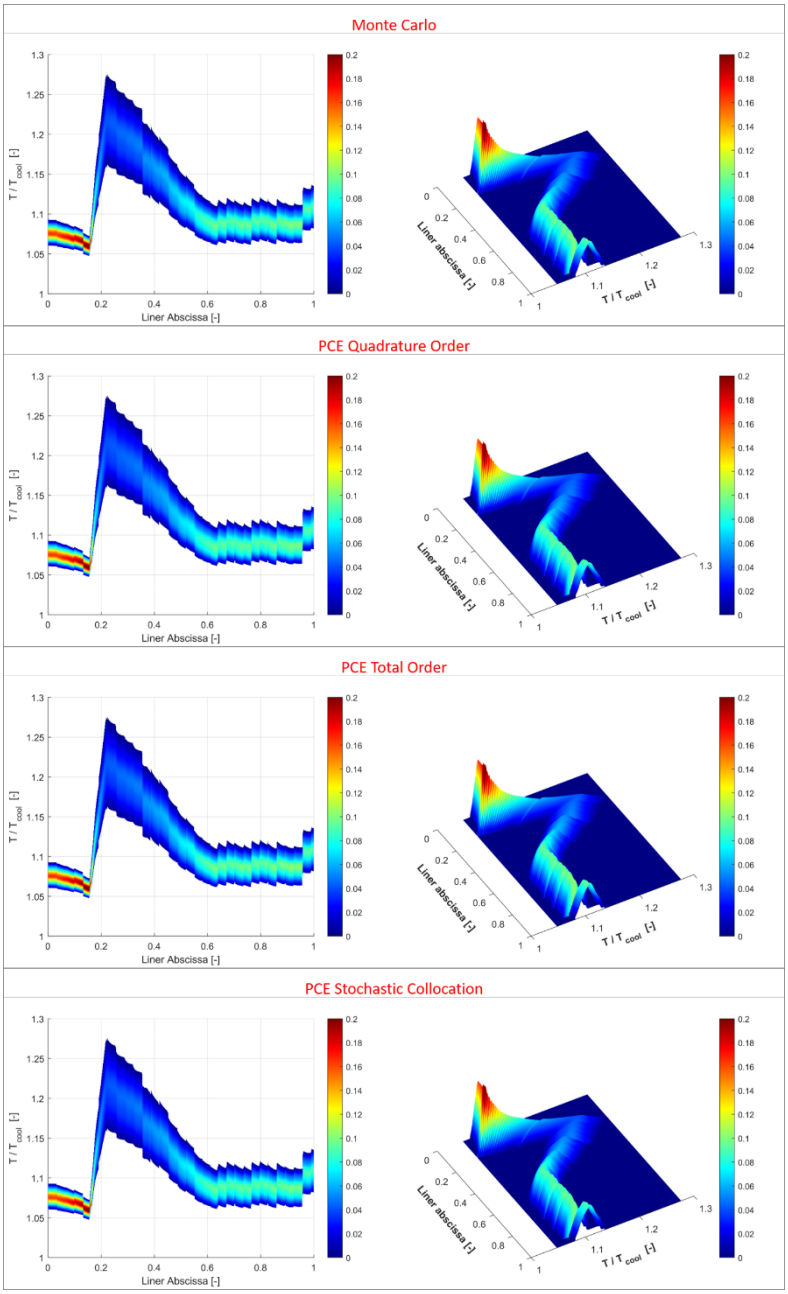

Figure 3.10 – HTC tuning factor analysis output probability

From the sensitivity analysis proposed in Figure 3.9 and carried out by the Sobol indices, it appears that the heat transfer coefficient on the gas side has a predominant effect on the liner temperature. The second major contribution is represented by the factor that acts on the heat transfer coefficient linked to the sink effect. The cold side heat transfer tuning factor has a limited influence on the liner wall temperature.

The probability maps obtained for the four methods are provided below in Figure 3.10. The results are analogous to those already described for the geometric analysis; the graphical visualization of the data obtained highlights the greater variability associated with the temperature range of the liner.

Boundary conditions analysis results

For this application two multiplicative factors have been considered. One working on the temperature of the hot gas, on the FAR, and on the temperature at which the radiation occurs, while the other acts on the velocity of the gas inside the chamber, influencing both the gas velocity and the density-velocity product. The different UQ methods are compared in Figure 3.11.

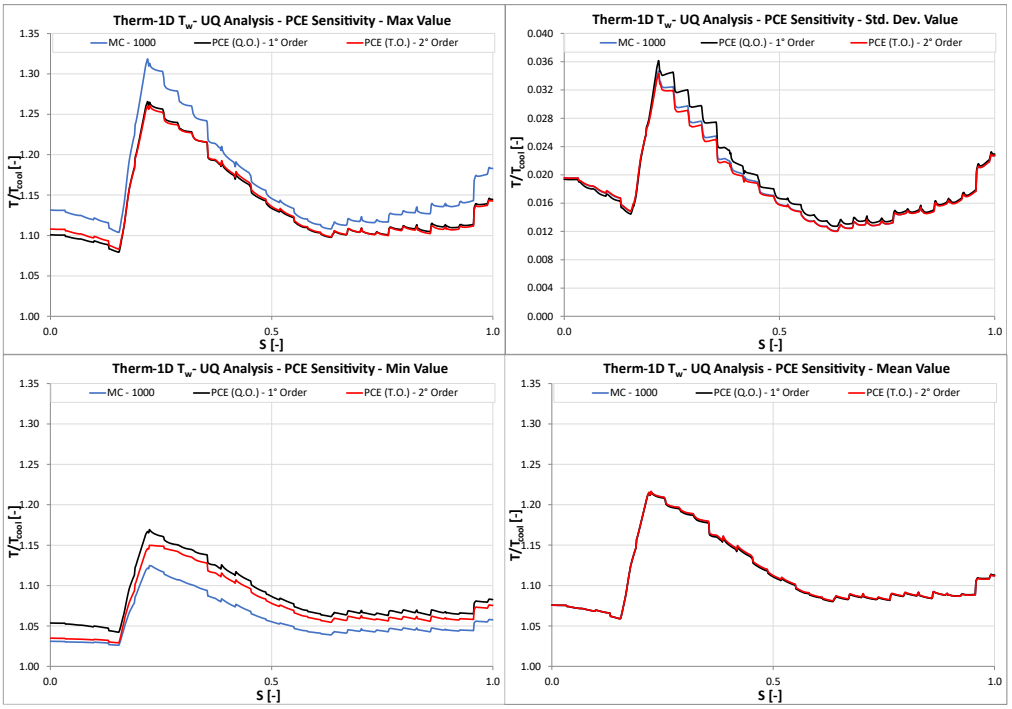

Figure 3.11 - Boundary condition analysis comparison

In average terms, both stochastic expansion methods present good agreement with the Monte Carlo method; the method based on the Gauss grid tends to differ from the other two in terms of standard deviation.

Sensitivity analysis using Sobol's indices (Figure 3.12) shows how the factor acting on thermal parameters has a greater impact in the first zone of the liner wall temperature compared to the kinetic variable, while the factor acting on kinetic terms takes on greater weight in the final region of the combustor. In the middle of the liner, the situation is well balanced. This study confirms that the solution obtained by the fluid network solver is extremely dependent on the conditions that are imposed as input. It can be concluded that acting on the temperature of the internal gas to model the effect of the film cooling with the fluid network supplied by *GE Avio Aero* is equivalent to impose a priori the temperature of the liner wall.

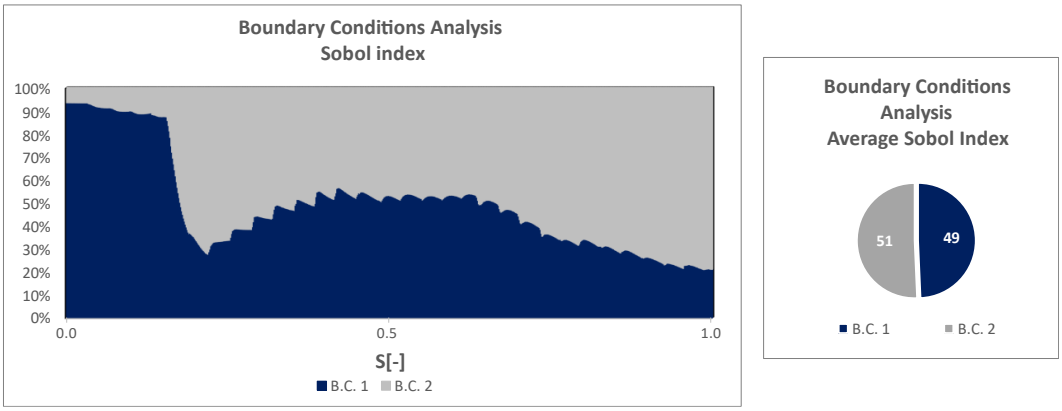

Figure 3.12 - Boundary conditions sensitivity analysis

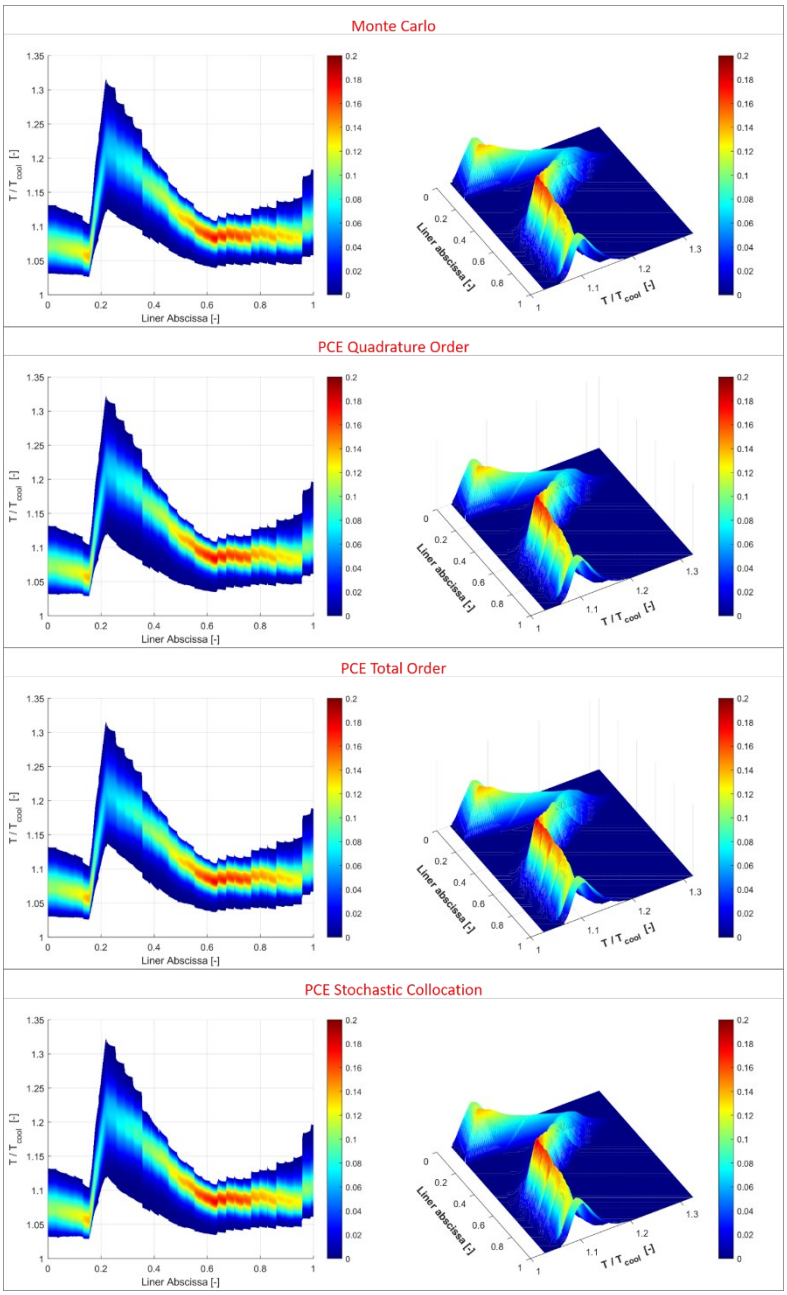

Figure 3.13 - Boundary conditions analysis output probability

All four probabilistic approaches (Figure 3.13) provide qualitatively the same result. This type of analysis involves the largest amplitude in terms of liner wall temperature.

Smolyak grid validation and Overall analysis

Additional analysis has been conducted for the validation of the Smolyak grid, which has an excellent efficiency as the number of variables increase. This is useful since it is not always possible to perform studies with a small number of variables in heat transfer analysis on high temperature components in turbomachinery applications. The analyses carried out have been combined in a macro-study; this has been used not only for the validation of the Smolyak grids but also to evaluate which are the magnitudes that influence the response function obtained by the fluid network solver.

For this analysis, the first level for the Smolyak grid has been chosen to have an extremely reduced number of simulations. This choice has been made in agreement with *Avila et al.* [204], who shows how the grid level does not affect the medium term and that the difference between this level and the others is estimated around 5%.

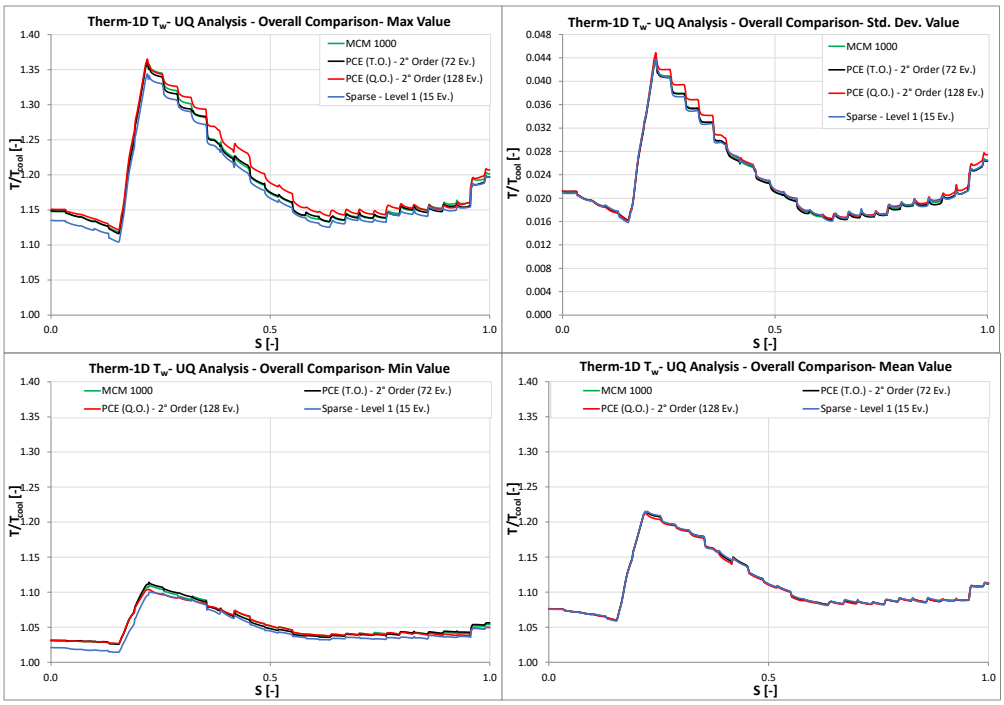

Figure 3.14 - Overall analysis comparison

For a more detailed comparison, the methods of polynomial chaos expansion with Gauss grid and fixed order, respectively of order one and two, have also been evaluated. Figure 3.14 reports the methods comparisons.

The polynomial chaos expansion based on the Smolyak grid slightly underestimates both the maximum and minimum trends, but given the extremely low computational cost, it can be an important tool for applications where simulation requires more computational resources.

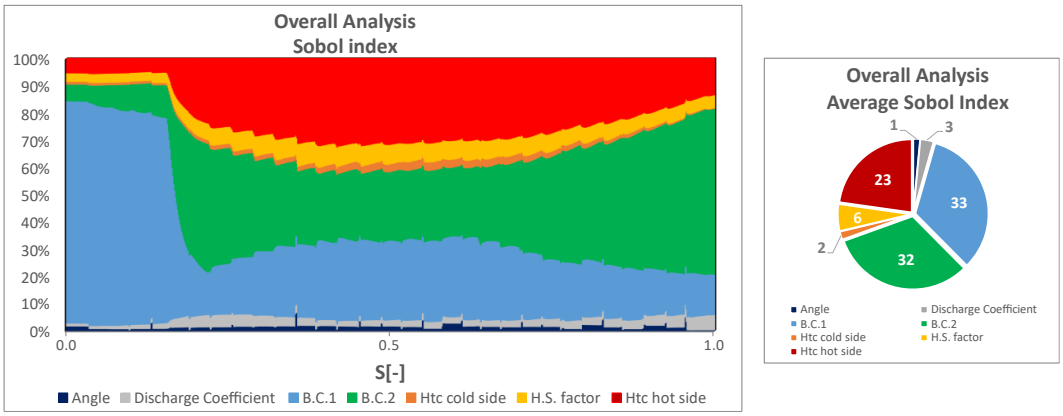

Figure 3.15 – Sensitivity analysis for overall comparison

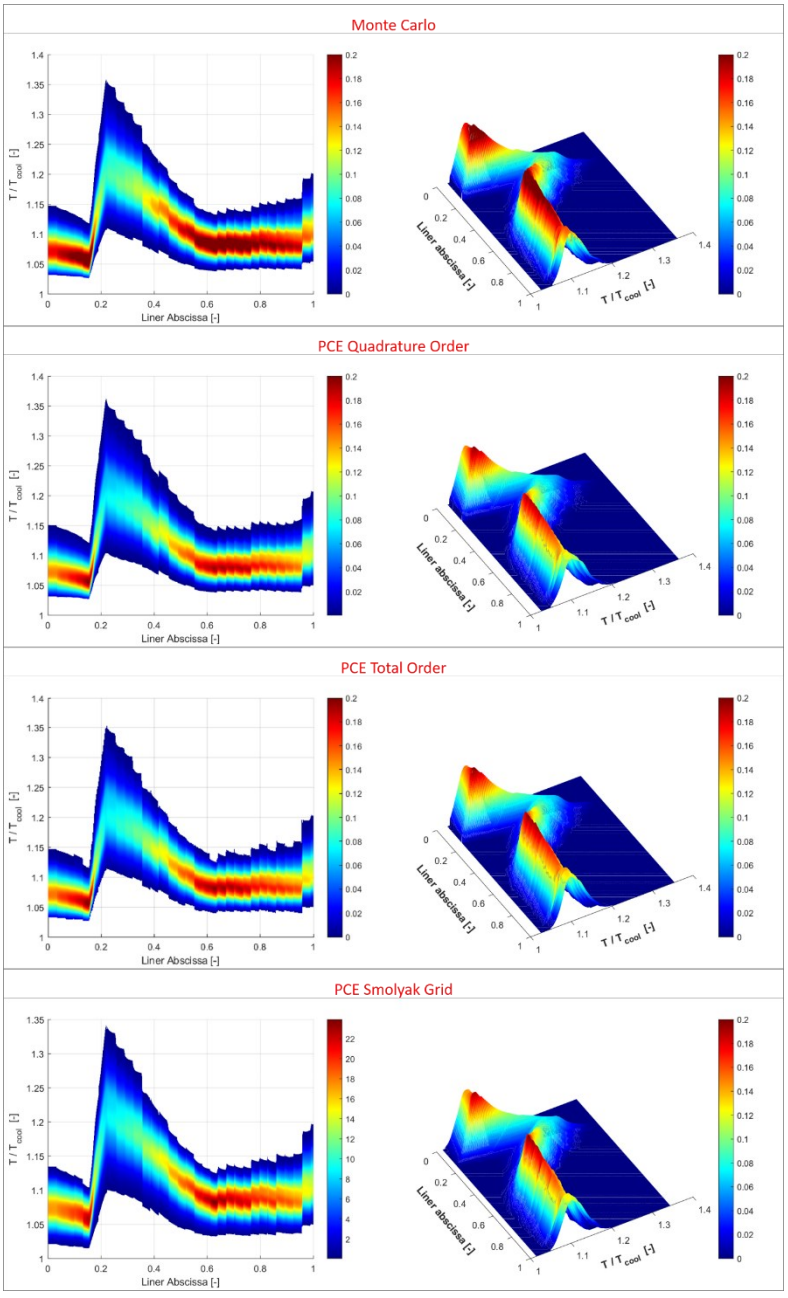

Figure 3.16 - Overall analysis output probability

The sensitivity analysis results are shown in Figure 3.15. Excluding the initial part in which the results strongly depend on the temperature distribution of the gas set, in the central zone the variable that acts on the heat transfer coefficient inside the combustor assumes an importance approximately equal to the variables related to the boundary conditions. Overall, these three quantities have the greatest weight on the response function.

In the last part of the component, the variable that has the greatest impact on the T_w is the one related to the temperature field. The terms related to the geometry of the holes have a cumulative Sobol's index of less than *5%* over almost the entire development of the liner, excluding the last part. Regarding heat transfer it can be concluded that the current modeling of the geometrical effects of the fluid network does not affect the response function; this behavior is following what is reported in the study of Bunker [7].

In Figure 3.16 the probabilistic maps of the Monte Carlo method and the three cases for the polynomial chaos expansion are reported. It is possible to notice more clearly the slight underestimation of the T_w provided by the method based on the Smolyak grid.

Effusion cooling adiabatic effectiveness evaluation

Figure 3.17 shows the adiabatic effectiveness distribution along liner abscissa, including the minimum and maximum limits obtained by the UQ analysis. The predicted adiabatic film effectiveness in the central region is not significantly influenced by the investigated uncertainties. An additional source of uncertainty, not included in the present investigation, could be ascribed to the criteria adopted to model film superposition. The classical criteria proposed by Sellers is here used [43], which assumes a perfect overlapping of consecutive film layers produced by effusion jets. The presence of a highly three-dimensional flow field produced by the swirling jet issued by the burner may greatly affect the flow field in the near-wall region, with local flow structures impinging on the film layer and therefore significantly limit the superposition process [150].

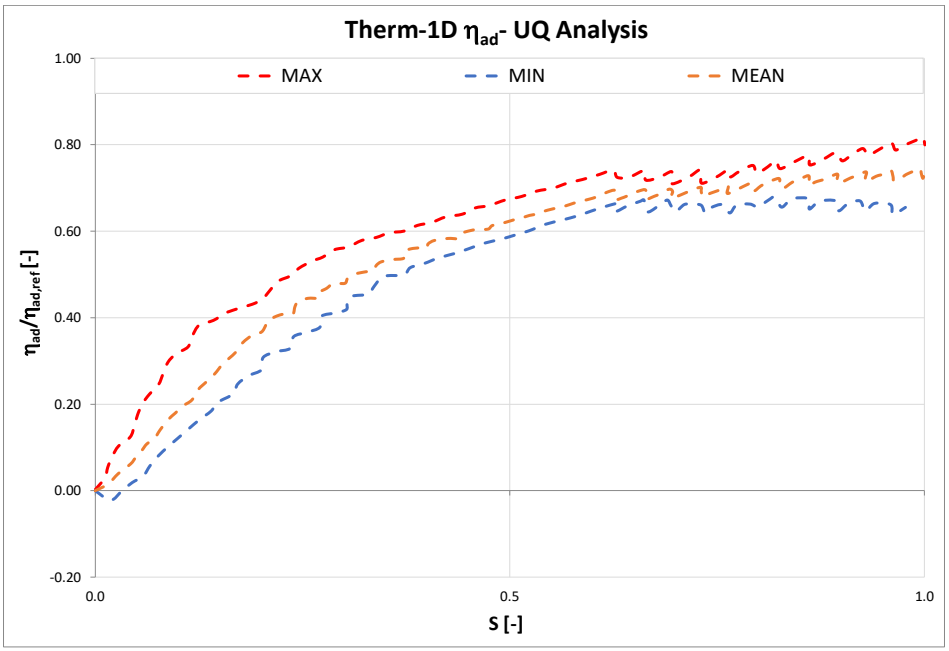

Figure 3.17 – Normalized adiabatic effectiveness trends with UQ evaluations

Specific sensitivity to the uncertainty related to the superposition criteria may point out this problem but such detailed analysis is out of the scope of the present work.

Results Comparison

Figure 3.18 shows the deterministic results obtained by applying the Therm-1D only procedure. As expected, the trend of the liner wall temperature obtained by CFD (*U-Therm3D*) simulation from *Bertini et al.* [77] has a greater agreement with experimental data than the one-dimensional approach. From the results shown it can be seen how the maximum excursion between the two approaches is found in the initial section of the combustor and in the temperature rise ramp, which can be attributed to the slot cooling modeling.

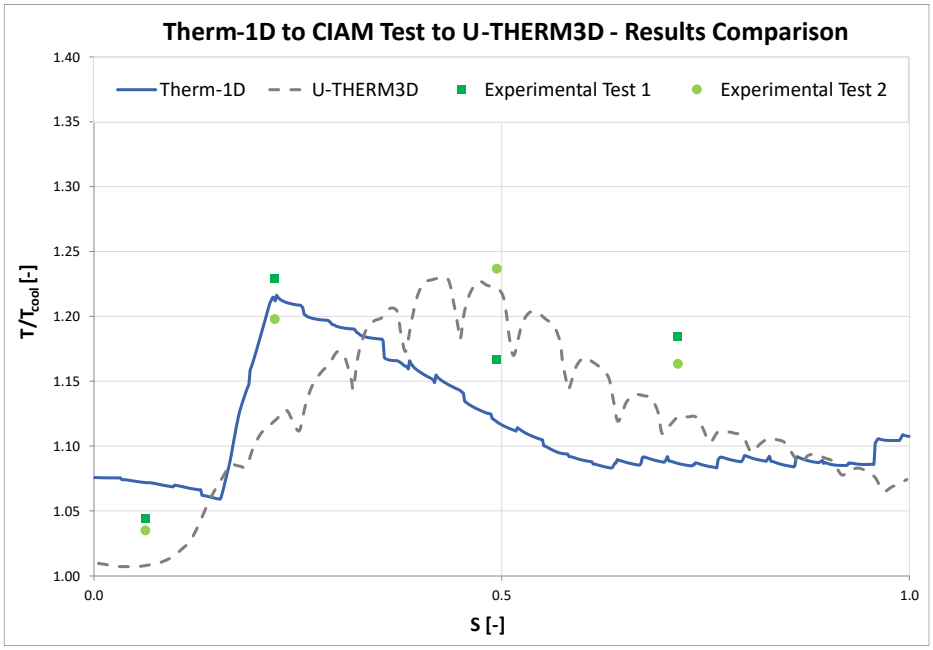

Figure 3.18 - Comparison among results: Therm-1D, Experimental test at CIAM, and Numerical Simulation [77]

With this consideration and the analysis shown in Figure 3.19, it is possible to better understand the result provided by the fluid network solver and proceed to the description of the results obtained with the uncertainty quantification analysis.

Figure 3.19 includes some experimental data, whose scattering highlights the variability of the liner temperature on the centreline of different sectors of the combustor. The range of the calculated PDF, for the boundary conditions analyses, is quite representative of the experimental uncertainty. The zone $0.5<S<0.8$ suggests that the underestimation is probably due to an overestimation of the adiabatic film effectiveness produced by the effusion cooling system. This is also motivated by the reduced effect on the predicted metal temperature due to the uncertainty of the investigated parameters. It is visible the potentiality of the UQ analysis and the results can now properly be assumed reasonable. However, the methodology used is not capable of justifying the gap with the experimental data measured.

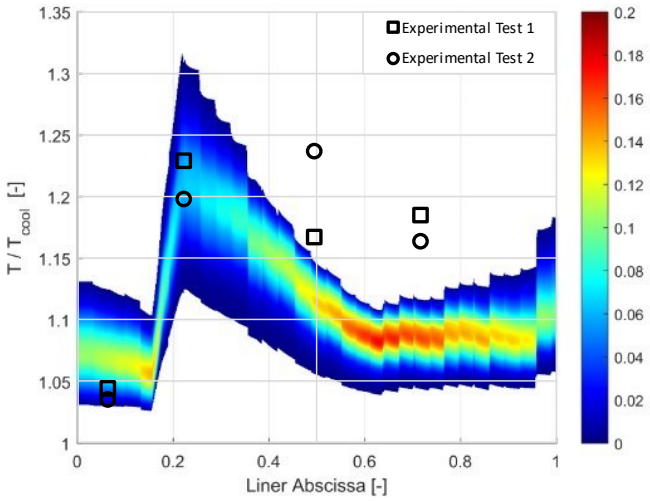

Figure 3.19 - Probabilistic map including experimental data

Final Remarks

Several UQ methods of analysis have been studied and tested to define the main factors of uncertainty in input to the Therm-1D solver. To carry out this analysis the combined *Therm-1D/Dakota* procedure has been used, which allows a one-dimensional deterministic type solver to obtain probabilistic results. In Table 3.5 are reported all the methods applied to the case-studies and the number of simulations needed.

	Geometry	*HTC factors*	*BC*	*Total*
Monte Carlo	10 – 100 – 1000	1000	1000	100 – 500 – 1000
Q.O. 1	4	8	4	128
Q.O. 2	9	-	-	-
Q.O. 3	16	-	-	-
T.O. 2 (cr=2)	12	20	12	72
T.O. 3 (cr=2)	20	-	-	-
T.O. 4 (cr=2)	30	-	-	-
S.C. 1	4	-	-	-
S.C. 2	9	-	-	-
S.C. 3	16	-	-	-
Smolyak Lev. 1	-	-	-	15
Smolyak Lev. 2	-	-	-	128
Smolyak Lev. 3	-	-	-	807

Table 3.5 - Different analyses carried out

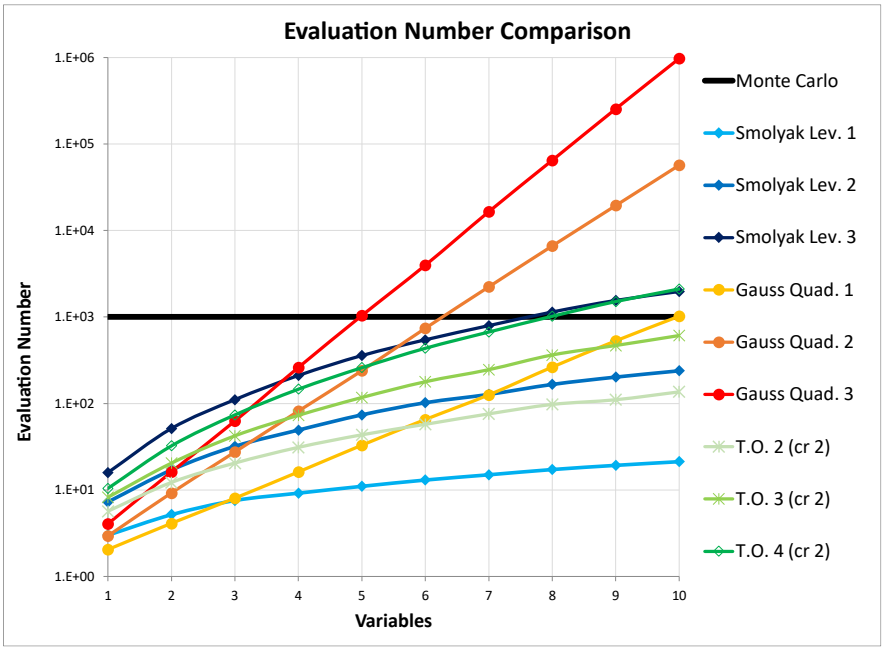

Figure 3.20 - Number of evaluations required by each method

Figure 3.20 above also shows the number of evaluations required for each method tested.
Generally, the lowest computational cost would be guaranteed by the total order polynomial chaos expansion, but since this methodology requires sampling at least twice the minimum value required, the condition that requires the least number of evaluations is the one based on the Smolyak grid.
It should be emphasized that the agreement between the results obtained from the Monte Carlo method and the stochastic expansion is not generalizable in absolute sense; the extreme efficiency that the polynomial chaos expansion presents is attributable also to the system studied.
Most likely, with a model having a response function with a highly non-linear trend, to obtain a good level of prediction it would have been necessary to have a higher polynomial order and, therefore, a higher computational cost linked to the uncertainty quantification analysis.

The *Therm-1D/Dakota* procedure was used to perform a UQ analysis of the combustor preliminary design. Dakota has proven to be a very versatile software. The test case analyzed is the LEMCOTEC combustor. The results achieved are presented in terms of liner wall temperature. To do this evaluation, four different simulations were carried out estimating for each one the liner wall temperature, the probability associated with each zone, and the sensitivity analysis. In the first three analyses, the effusion cooling holes geometry, the heat transfer tuning factors and the boundary conditions have been respectively evaluated. In the last simulation, all the variables have been considered at the same time.
The main objective was to investigate different analyses with different methods: Monte Carlo classical approach, stochastic expansion methods, Smolyak grid.
The spectral methods were extremely efficient compared to the Monte Carlo method: for a small number of variables the method based on tensor quadrature is the most efficient. Only 4 evaluations are required for 2 uncertainty variables and 8 evaluations for 3 variables, against 1000 requested by the Monte Carlo method. The problem related to the number of parameters to vary, which involves the exponential increase

of the evaluation number, is partially solved using the Smolyak grid. The method requires only 15 simulations for 7 uncertain variables.

In quantitative terms, the maximum difference between the results obtained with spectral methods and those obtained with the Monte Carlo method is in the order of 1%, proving the efficiency of the stochastic expansion methods. Regarding the sensitivity, when all variables have been analyzed together, the results obtained show that:

- The geometric variables have a limited impact on the liner wall temperature
- The range is 25% for the geometric analysis and 54% for the boundary conditions
- The maximum uncertain zone is the one close to the temperature peak. Here, the maximum excursion is recorded, and the probability associated with this zone has a wider PDF
- The analysis on Sobol's indices has determined that the variable that acts on the heat transfer coefficient inside the combustor assumes an importance approximately equal to the variables related to the boundary conditions; overall, these three quantities have the greatest weight on the response function. The terms related to the geometry of the holes have a cumulative Sobol's index of less than 5% over almost the entire development of the liner.

It can be concluded that the application of UQ methods with sensitivity analysis to low order deterministic codes can be used for optimization and preliminary robust design applications.

Chapter 4

Non-reactive RQL combustor

Introduction

As already mentioned, in modern aeroengine combustors, one of the most effective cooling techniques is the effusion cooling [67,205], where a uniform film protection of the wall is combined with a significant heat sink effect by coolant convection inside a large number of small holes through the use of multi-perforated liners. The most common modern aeroengine combustor strategies are the Rich-Quench-Lean (RQL) and the Lean Burn that are characterized by highly swirling flows and a strongly three-dimensional flow field to ensure the stability of the combustion process and the containment of pollutant emissions [69]. These complex fluid dynamics features consist in a large flow recirculation due to vortex breakdown, which may result in a not trivial interaction with liner cooling flows close to combustor walls. Therefore, a reliable prediction of the coupling between the gas flow field and the cooling system is of primary importance to properly determine the thermal conditions of the liners. This problem should be addressed since the very beginning of the design process, during the preliminary analysis or concept design carried out using low order codes.

In the last years, the study of heat transfer in realistic combustion chamber configurations is becoming a topic of growing interest in literature. A comprehensive study was performed by *Patil et al.* [206,207], on both can and annular combustors employing numerical simulations and experiments, to investigate the effects of the swirling flow on the convective heat transfer without involving chemical reaction and without film cooling. The impingement on the liner surface of the swirling flow leads to a substantial enhancement of the heat transfer coefficient, decreasing the performance of the liner cooling system. Further experiment analyses have been made by *Wurm et al.* [208] and *Andreini et al.* [150,209,210]. Both research groups carried out several measurement campaigns on atmospheric enlarged-scale test rigs with a three-sector combustion chamber.

The test rig considered for this analysis is part of the European project SOPRANO (SOot Processes and Radiation in Aeronautical inNOvative combustors) and is carried out in collaboration with the industrial partner GE Avio Aero. The SOPRANO project aims to provide a deeper understanding, analysis, and better design tools, opening the way for alternative combustion system projects for future aircraft capable of simultaneously reducing pollutants and particles and improving the durability of the liners. SOPRANO

aims to develop clean and efficient combustion technologies for aeroengines capable of simultaneously meeting the following challenges:

- Meeting the ambitious objectives of ACARE NO_X and CO_2
- Increases the life of the combustor liner
- Check the PM emitted in terms of mass, number, and morphology

The expected contribution of SOPRANO is to apply these developments to determine the new main promising combustor concepts.

The analyzed test rig consists of a non-reactive linear sector with five engine-scale swirlers equipped with outer/inner dilution ports and with a simple inner liner cooling scheme composed of an effusion plate and a slot system. The related experimental tests, used in this work, were carried out with the following techniques:

- InfraRed (IR) thermography, to measure the wall temperature on the plate
- Pressure-Sensitive Paint (PSP), to measure the adiabatic effectiveness on the plate [137]

The tests were performed at different pressure drops across the swirlers and varying the mass flows of the slot and through the inner/outer liners.
Numerical simulations have been realized using a strongly coupled RANS CHT method on the same test rig configuration adopted for the experimental campaign in order to investigate the cooling performances and to obtain some distributions that represent a necessary input for the Therm-1D tool.

Before analyzing the test rig, it is important to highlight that the main source of uncertainty (mainly due to inaccuracy related to simplified modeling), for a tool like Therm-1D [24], consists of the one-dimensional approach with which the fluid dynamics of the system and the heat transfer are solved. This approach assumes that the flow develops in only one direction: it is therefore not possible to evaluate the effects of gradients in the two directions to the main one. These hypotheses were not excessively reductive for the design of the old combustor's generation, where the high aspect ratio ensured a predominantly axial flow development. In modern combustors, the design of the structure and the adoption of elements such as swirlers are functional to the generation of turbulent flow and recirculation zones, which can promote an efficient mixing between reactants and exhaust gases and ensure a stable and complete combustion in small areas. Therefore, while in older combustors a highly three-dimensional flow structure was typical only of edge effects, in recent combustion chambers it extends for almost the entire length. The simplifying assumptions do not allow to include in the evaluation of the heat transfer all the phenomena that influence it, such as the strong local gradients of temperature, velocity, and the recirculation zones downstream of the swirlers. Therefore, the one-dimensional approach can provide very approximate results if no particular measures are taken for the correct description of the thermo-fluid dynamics phenomena that occur in the combustion chamber and that are directly involved in the heat transfer process to the liners.

In practice, the tool requires one-dimensional distributions of the main quantities (e.g., temperature, pressure, velocity, density) of the hot gases in the combustion chamber. These quantities are then used to

determine the heat transferred through the liner thickness along the liner. Such distributions are of fundamental importance for the correct representation of the thermo-fluid-dynamic phenomena present in the combustion chamber near the liner zone, even if simplified.

Since the test case is not reactive, this confines the analysis only to the problems of convective heat transfer. It is useful to analyze the problems related to the hot gas side uncertainties. Since they are introduced as a one-dimensional distribution, these parameters are affected by uncertainties and can only partially account for the three-dimensional aspects of the phenomena that are created in the combustion.
The analysis process will be developed by testing the behavior of Therm-1D by interpolating hot gas side quantities from larger and smaller zones around the effusion plate, to obtain temperature distributions as close as possible to the experimental test results.
The aim is to determine a general guideline to try to minimize what are the uncertainties due to these inputs and optimize code setting time. Currently, this procedure is carried out through a Trial-and-Error process; this involves a considerable amount of time for the setting phase.
The inner liner will be the object of the measurements. The *Therm-1D/Dakota* coupled procedure will then be used for a sensitivity analysis.

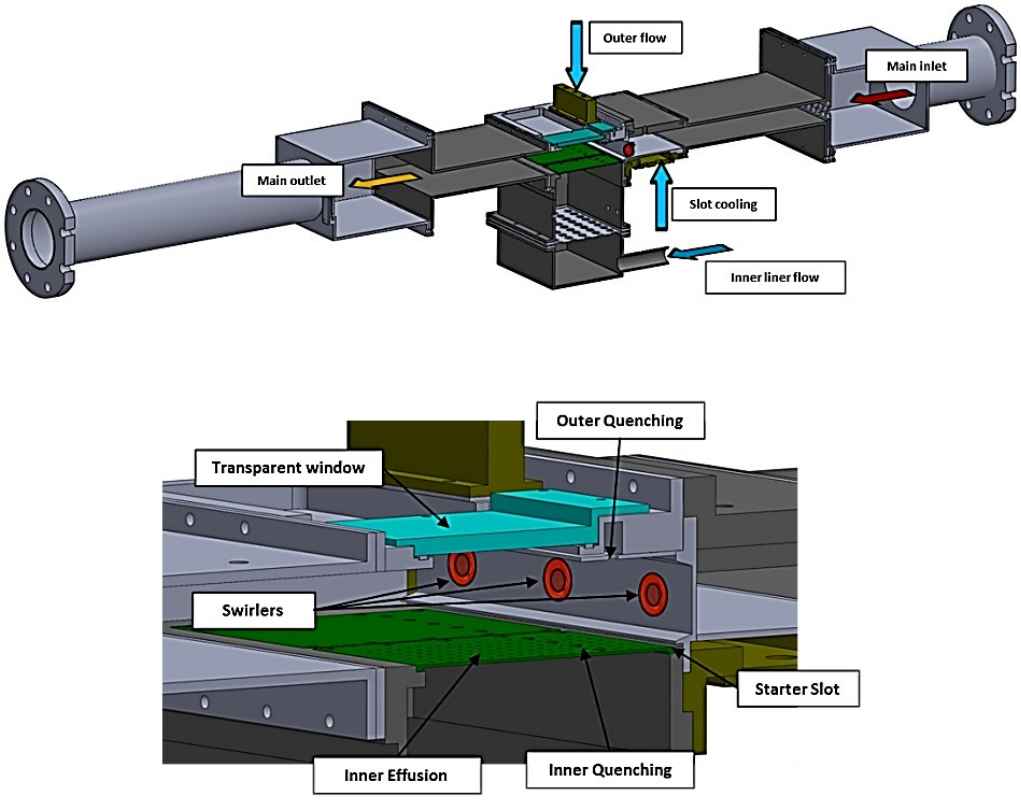

Figure 4.1 - Sketch of the experimental apparatus [211]

Experimental investigation

The experimental apparatus consists of a linear non-reactive five injectors combustion chamber simulator operating in warm condition. The measurements were carried out in the *THT Lab* research laboratory of the Department of Industrial Engineering of Florence (*DIEF*).

The model reproduces in a 1:1 scale of five sectors of a typical RQL combustor architecture where the multiple-injector configuration allows the replication of the periodicity conditions in the primary zone also reported in *Picchi et al.* [211]. The swirlers are fixed at the dome in a linear arrangement with the fuel lines plugged since only non-reactive tests have been done, to accurately reproduce the flow behavior. Figure 4. shows a cross-sectional view of the test rig highlighting the different involved flows. The main flow passes through the injectors, arrives in the chamber, and is subsequently expelled to the outlet. The component of greatest interest for the study is the inner plate that represents a part of a multiperforated liner. Under the inner liner, a large plenum is equipped with a grid to ensure a uniform coolant flow. The plate is composed of two lateral panels with only the dilution holes while the central one presents an effusion cooling geometry with a pattern of inclined cylindrical holes. Before the inner plate, a slot system generates the film cooling in the initial part of the liner (distant from the first effusion row 18 times the effusion hole diameter). At the top, there is an inlet for the outer dilution flow to guarantee a realistic flow field within the test section. The inner and outer dilution holes are four per sector and they have a diameter of 9 times the effusion holes diameter.

The effusion plate is manufactured using metal additive technologies with effusion holes realized employing the laser drilling process. An example of a classic and general arrangement is shown in Figure 4.2. The analyzed plate presents a constant hole streamwise/spanwise pitch to diameter ratio equal to S/d=12, a length to diameter ratio, equal to l/d=6, and an effusion holes angle equal to 20°. As schematized in Figure 4.3, the test rig is integrated into a dedicated hot wind tunnel, with compressed air delivered by two screw compressors accounting for a maximum total mass flow rate of 1 kg/s at the maximum pressure of 10 bar.

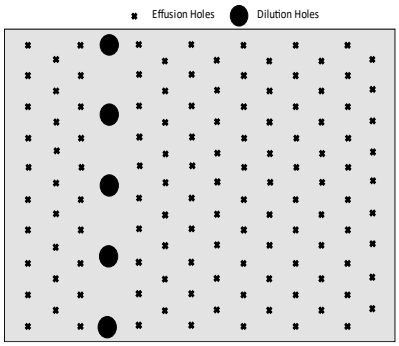

Figure 4.2 - Typical scheme of a Multi perforated plate

The air flows through a drier that removes the humidity, then it goes to an air tank to dump pressure fluctuation, and to a set of filters that eliminate potential impurities from the flow. The air is split into four mass flows rates: one for the outer dilution, one to the inner liner, one to the inner slot, and one to the swirlers. The last one represents the main flow, which is preheated up to a temperature of 520 K through

an electrical heater. All the lines are equipped with dedicated calibrated orifice flowmeters and regulating valves to separate the control of each mass flow rate.

The inner flows can be fed with carbon dioxide to perform PSP tests. Finally, the pressure drop inside the test rig is regulated with a counter-pressure valve between the test rig outlet and the stack.

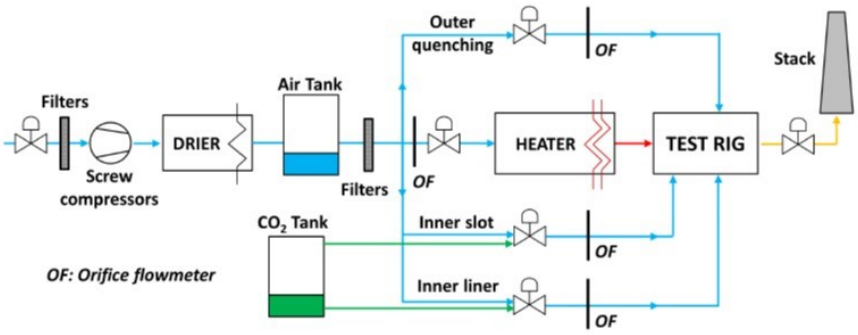

Figure 4.3 - Test Facility Diagram [211]

Inside the test rig, several thermocouples and static pressure taps are installed to monitor and control the operating conditions. Three optical accesses are installed to evaluate:

- Flow field with PIV
- Temperature with InfraRed thermography
- Adiabatic effectiveness with PSP.

The first stage in the combustor analysis consisted of evaluating the internal aerodynamics, to understand the flow interactions between the central swirler and dilution holes jets. A standard 2D PIV technique has been chosen for carrying out average flow field measurements on the rig median plane. This investigation comes from previous activities conducted on the same test rig.

For liner thermal investigations an Infrared thermography is utilized to obtain high-resolution temperature distributions on the central region of the test article. The IR camera used in this activity is a *FLIR SC6700*, working in the medium wavelength range (l = 3÷5 μm) and able to provide thermal images with a spatial resolution of 640x512. The camera incorporates a cooled Indium Antimonide (*InSb*) detector with a 15 μm pixel-pitch. To cover the entire temperature span, the camera operates employing four active pre-set operating modes, providing adjustable integration times. The optical access to the effusion coupon is guaranteed by installing a Sapphire window within a dedicated housing on the top side of the chamber. For high-resolution temperature distributions, internal surfaces of the chamber and the effusion plate are sprayed with opaque black paint to avoid reflections and to enhance the emissivity of the walls. To correctly adjust the raw signal values of the IR detector, the calibration approach proposed by *Martiny et al.* [124] is employed. For this reason, on the effusion coupon are incorporated six thermocouples. Implementation of this fitting procedure has led to an average error of about 5% for thermocouples reading values. The surface temperature distributions on the plate (T_w) are then used to estimate the overall cooling effectiveness:

$$\eta_{OV} = \frac{T_{main} - T_w}{T_{main} - T_{cool}} \tag{4.1}$$

where T_{main} represents the mainstream temperature upstream the set of swirlers and T_{cool} the coolant temperature inside the feeding plenum.

To examine the liner behavior in terms of film covering a Pressure Sensitive Paint technique is employed to achieve bidimensional distributions of adiabatic effectiveness. PSP is an organic substance composed of oxygen-sensitive molecules embedded in a polymeric binder. Due to the luminescence behavior of these molecules, it is possible to detect oxygen partial pressure in the surroundings of the painted wall, which in turn can be linked to local oxygen concentration. Using as coolant a tracer gas without free oxygen and considering valid the temperature and mass transfer analogy, the definition of adiabatic film cooling effectiveness can so be formulated as reported below:

$$\eta_{ad} = \frac{T_{main} - T_{aw}}{T_{main} - T_{cool}} = \frac{C_{main} - C_w}{C_{main}} = 1 - \frac{1}{\left[1 + \left(\frac{\frac{P_{O2_{main}}}{P_{O2_{ref}}}}{\frac{P_{O2_{cool}}}{P_{O2_{ref}}}} - 1\right)\frac{M_{cool}}{M_{main}}\right]} \tag{4.2}$$

where T_{aw} is the adiabatic wall temperature, $C_{main,}$ and C_w are the oxygen concentration in the main flow and the proximity of the wall respectively. The correct excitation to the target surface is provided by a high-performance UV LED Illuminator system *IL104* (Figure 4.4) and image acquisition is carried out exploiting a 1600x1200 resolution 14-bit CCD camera (*PCO.1600*) equipped with a 610 nm red filter. Carbon dioxide is used as foreign gas, for this reason during this campaign the inner slot and inner liner feeding lines are switched through a system of control valves from the compressed air line to a CO2 pressure tank. Since PSP tests are conducted at nearly atmospheric conditions a PMMA window is used as optical access on the top side of the test section.
More details on the PSP technique and the adopted procedure can be found in [212]. PSP employed in the present activity is an *UniFIB* formulation supplied by Innovative Scientific Solutions Inc.

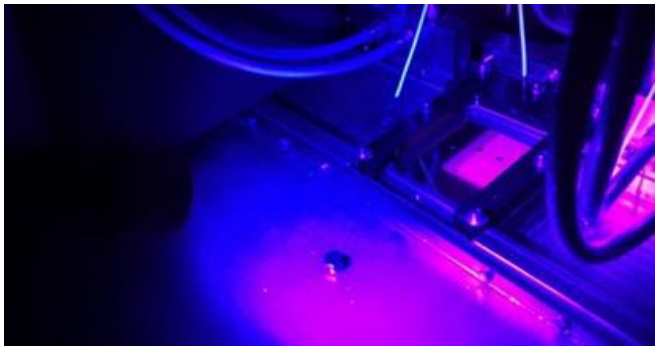

Figure 4.4 - PSP Experimental Test [211]

In the experimental study of the combustor, tests were carried out under different operating conditions. The test points analyzed in this work are reported in Table 4.1.

TP	ΔP/P Swirler	T_{main}/T_{cool} [-]	ΔP/P Coolant / ΔP/P Swirler	T_{cool} [-]	Re (sim.)	M (sim.)	Slot	ΔP/P Slot / ΔP/P Swirler	T_{slot}/T_{cool} [-]
A	P_{ref-1}	1.85	64.0%	T_{cool-1}	V	V	Yes	64.0%	1.06
B	P_{ref-1}	1.83	61.5%	T_{cool-1}	V	V	No	-	-
C	P_{ref-2}	1.74	77.0%	T_{cool-2}	X	V	Yes	68.5%	1.07
D	P_{ref-2}	1.70	80.0%	T_{cool-2}	X	V	No	-	-

Table 4.1 - Test points and Normalized operating conditions

As shown in Table 4.1 (sim. is short for similitude), pairs of test points with the same *ΔP/P* conditions for the swirler and the coolant were taken for the analysis. The only difference is the slot presence or absence. In this way, the TP-B is equal to TP-A without slot, as well as TP-D with TP-C.
Reference pressures and coolant temperatures are reported in that format due to non-disclosure agreements with the industrial partner.

Experimental results

Figure 4.5 shows the experimental tests analyzed area. This zone will also be the addressed zone for the comparison of the results produced with Therm-1D and for some numerical post-process. For PSP tests it reaches up to $x/Sx = 7$, while for I.R. tests it reaches up to $x/Sx = 9$.
As for the rig test, also for the numerical simulations and the Therm-1D procedure, the effusion/dilution plate has been modeled.

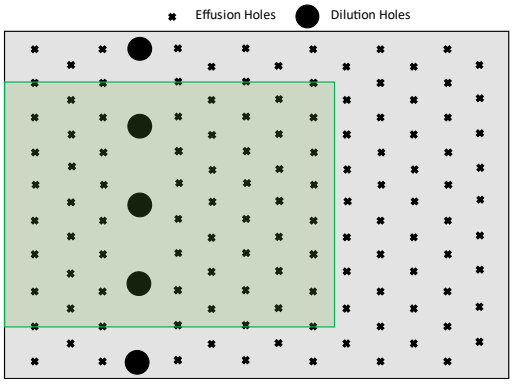

Figure 4.5 – Experimental tests analyzed area

Overall Effectiveness

For all the geometries the test matrix reported in Table 4.1 has been followed to replicate engine main parameters and to assess the impact of slot cooling.

Results are reported from Figure 4.6 to Figure 4.9, where η_{ov} is normalized with the same procedure reported in [211]. The area of the dilution holes has been covered with a gray band due to non-disclosure agreements with the industrial partner. The images show two-dimensional distributions and laterally averaged profiles.

For TP-A, a high-temperature zone is highlighted in the very first part of the liner, due to the swirler behavior.

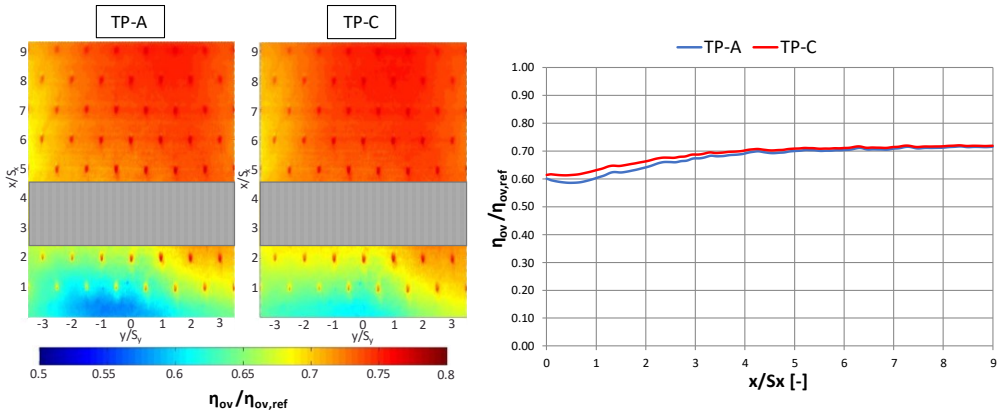

Figure 4.6 - η_{ov} distributions: the impact of mainstream pressure drops (TP-A vs. TP-C)

Downstream of the dilution holes, high effectiveness values are recognized because of the high amount of cold air injected that leads to strong mixing phenomena and at the same time due to the effusion film superposition effect, which becomes more intense. The slight asymmetry of the map can be ascribed to the injector geometry. The result is indeed coherent with the swirler channels rotating direction.

Moving the attention to the impact of varying swirler pressure drop, results from the comparison of TP-A and TP-C are reported in Figure 4.6. The two test points are performed at the same Coolant/Mainstream mass flow ratio and with slot cooling enabled. Maps and 1D curves highlight an almost negligible effect in terms of thermal performance, with some discrepancies only in the first part of the liner, where the reduced momentum of the swirling jet for TP-C reasonably leads to a decreased heat transfer coefficient.

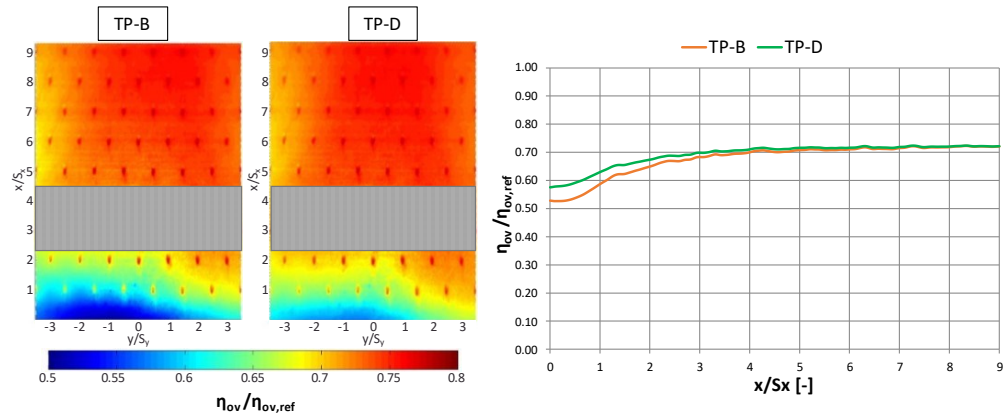

Figure 4.7 - η_{ov} distributions: the impact of mainstream pressure drops (TP-B vs. TP-D)

Remaining on the analysis of the impact of varying swirler pressure drop, Figure 4.7 shows the distributions for TP-B and TP-D. As already described, both test points are run without slot cooling. Analyzing the maps and the one-dimensional curves it is possible to achieve the same conclusions already expressed for TP-A and TP-C.

Another aspect considered in the investigation has been the evaluation of slot cooling impact; for all the test points, the imposed pressure drop across the line is the same as the one across the inner liner. Results showed in Figure 4.8 and Figure 4.9 reports a comparison for both the ΔP/P studied.

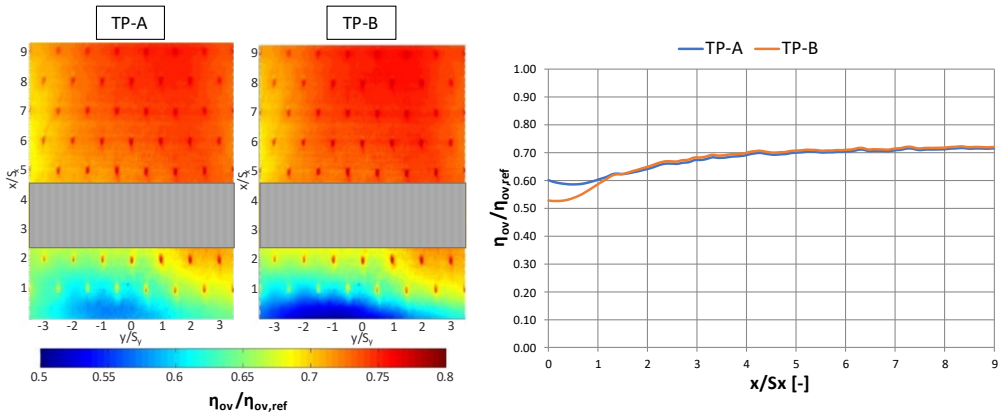

Figure 4.8 - η_{ov} distributions: the impact of slot cooling (TP-A vs. TP-B)

For TP-A versus TP-B (Figure 4.8), it is possible to see a decay in overall effectiveness. However, for TP-B is observed only in the very first part of the liner, where it suffers from the absence of the slot, while downstream of the first row of effusion holes the two curves look very similar. This behavior suggests a deep interaction with swirler and dilution flows which inhibits the slot protection development.

The same analysis can be repeated for the comparison between TP-C and TP-D (Figure 4.9), where however there is a lower decay of the overall effectiveness in the first part of the liner for the slotless case. This is due to the impact of a lower main pressure drop.

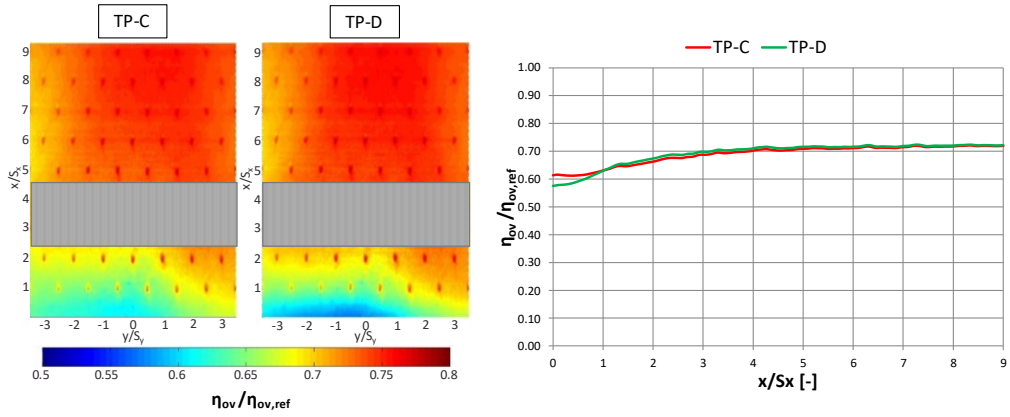

Figure 4.9 - η_{ov} distributions: the impact of slot cooling (TP-C vs. TP-D)

Adiabatic Effectiveness

For this campaign, all the cooling features are fed with Carbon dioxide. Test point numbers identify the corresponding hot tests performed during the Infrared investigation.

For all the geometries the test matrix reported in Table 4.1 has been followed to replicate engine main parameters and to assess the impact of slot cooling.

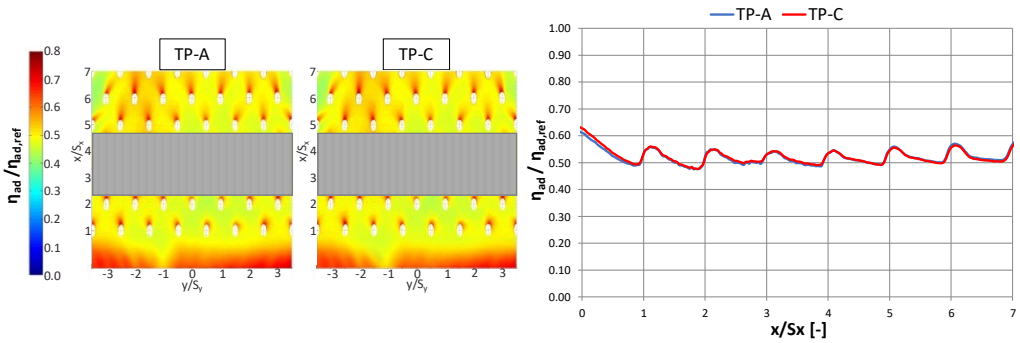

Figure 4.10 - η_{ad} distributions: the impact of mainstream pressure drops (TP-A vs. TP-C)

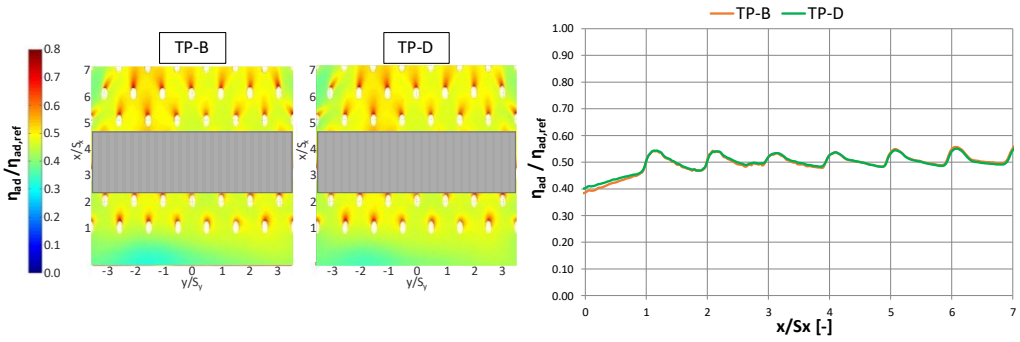

Figure 4.11 - η_{ad} distributions: the impact of mainstream pressure drops (TP-B vs. TP-D)

As shown for overall effectiveness, results are reported in Figure 4.10-Figure 4.13, where η_{ad} is normalized with the same procedure reported in [211]. The images show bi-dimensional distributions and laterally averaged trends.

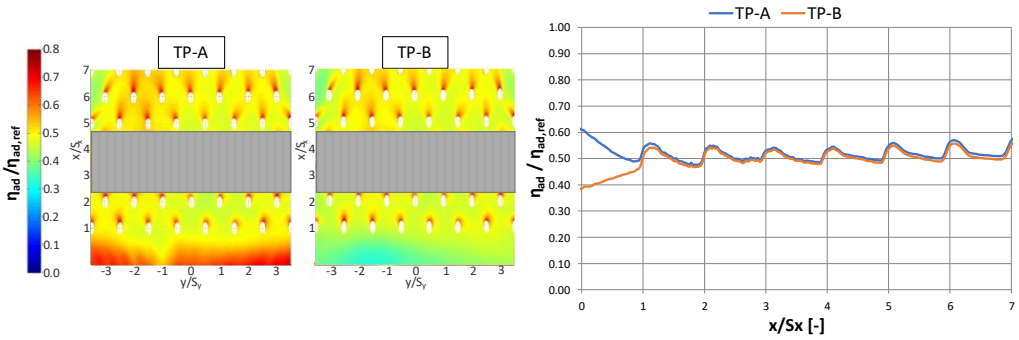

Figure 4.12 - η_{ad} distributions: the impact of slot cooling (TP-A vs. TP-B)

Moving the attention to the impact of varying swirler pressure drop, Figure 4.10 and Figure 4.11 highlights the almost negligible effect on the adiabatic film cooling effectiveness profiles along the entire length of

the plate. Besides, they confirm the possibility of comparing properly warm and cold test points preserving chamber pressure drop and mass flow ratio.

The impact of slot cooling is shown in Figure 4.12 comparing TP-A and TP-B, and in Figure 4.13 comparing TP-C and TP-D. Slot coolant is relegated only very close to the exit plane. Downstream of the first row of holes the two curves tend to overlap.

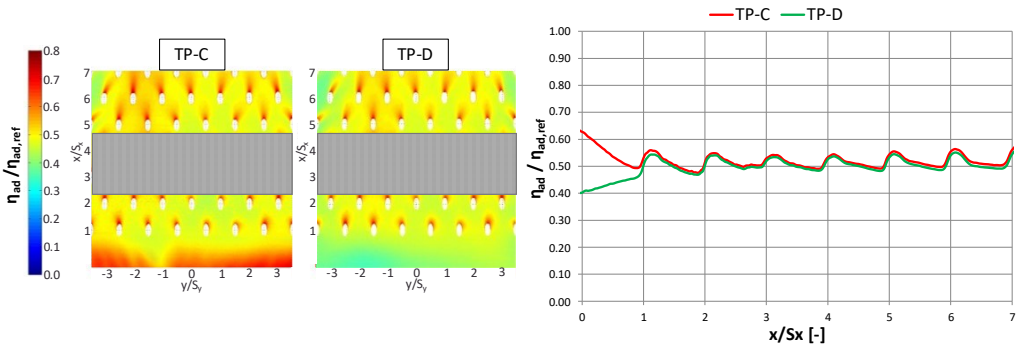

Figure 4.13 - η_{ad} distributions: the impact of slot cooling (TP-C vs. TP-D)

Numerical Simulations

Liner thermal study is fundamental and CFD models can be used to predict the 3D heat load distribution on the wall. Nowadays, steady simulations with the RANS (Reynolds Averaged Navier-Stokes equations) approach are the standard in industrial applications for the preliminary design of the combustor due to its performances in a reasonable computational time. In this context, the CHT (Conjugate Heat Transfer) simulations with RANS approach represent one of the most used approaches in the preliminary design of aeroengine.

The heat transfer occurs in three different ways (conduction, convection, and radiation) in two distinct domains: the main flow (the reactive flow and the air of the cooling system) and the solid (the walls of the combustor). The involved phenomena require a continuity of quantities going from one domain to the other. The region that divides the two different physical domains is the coupling interface, and the two domains exchange information at this surface.

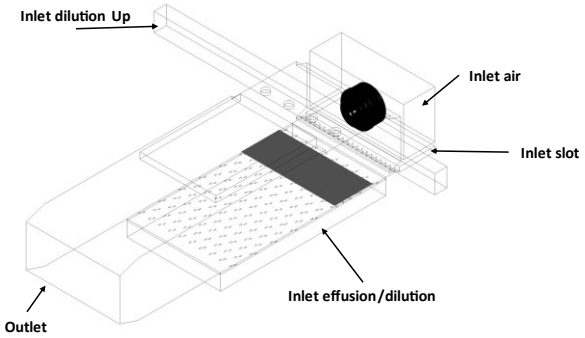

Figure 4.14 - Computational combustor domain with effusion plate

For this work, steady RANS CHT simulations with a strongly coupled method were performed to understand the interaction of the swirling flow with the cooling system, how the cooling performances are affected by the main flow and how these phenomena can influence the results obtained by Therm-1D, once interpolated the one-dimensional input magnitudes distributions.

Figure 4.14 represents the coupled domain employed for these analyses. As shown, the employed computational domain includes the entire combustion chamber, the burner, and the plenums upstream of the dilution jets, the slot, and the swirler.

Regarding the CHT simulation, the geometry includes the fluid and the solid domains. The grid employed in the preliminary simulation is composed of tetrahedral elements and 5 prism layers are employed for near-wall modelling. In the near dome region, the mesh is finer to accurately compute the velocity gradients generated by the swirling flow exiting from the burner. The resulting mesh is composed of $8x10^7$ elements. The coarse mesh has the same sizing as the previous one, but it is composed of $4x10^7$ elements, decreasing the whole computational cost of the sensitivity, but also reducing the reliability of results.

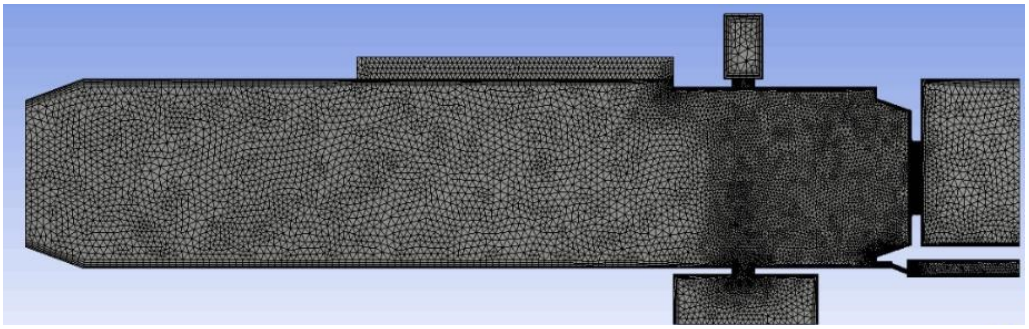

Figure 4.15 - Full domain mesh without effusion plate

The best grid resultant from sensitivity analysis has the same sizing as the previous but it is composed of $5.1x10^7$ elements (Figure 4.15). In all the simulations carried out, the mass flow rates are imposed on the upper dilution, slot, and effusion inlets because they provided better performances from a point of view of the stabilization of the calculation. Boundary conditions are not reported explicitly due to non-disclosure agreements with the industrial partner.

Navier-Stokes equations are solved with a RANS approach and a Realizable k-ε turbulence model is employed [213], due to its capability in the prediction of the main features of swirling flow fields and for its stability. As far as the near-wall treatment is concerned, the scalable wall function is adopted [214]. Air property is modeled employing polynomial functions of temperatures for the calculation of the specific heat, thermal conductivity, and viscosity whereas the ideal gas model is adopted for the calculation of the density. The solutions are obtained employing a spatial discretization of the first order for the turbulent parameters equations and a second order for pressure, density, momentum, and energy equations to obtain a more accurate solution [214]. Pressure-velocity coupling is solved by the coupled algorithm [214]. A periodic condition is imposed on the lateral faces of the chamber and of the plenum before the injector to simulate the presence of near burners as in the real test rig.

To distinguish the various effects associated with the slot, the dilutions, and the effusion a numerical analysis has been performed on the coverage provided to the wall defining four additional transport

equations for four different passive scalars (representing the experimental CO_2 coming from the different secondary inlets). The scalar variable diffusivity set equal to the effective turbulent thermal diffusivity to replicate the mixing behavior of the thermal field. Its value is 1 for the flow coming from the source points and 0 at the other inlets of the domain. The employed scalars represent:

- the effusion flows (later defined as *scalar-E*)
- the slot flows
- the inner dilution flows
- the outer dilution flows
- the effusion, the slot, and the inner dilution flows

This evaluation is used to better understand the covering effect of the several coolant inlets.

Flow Field Analyses

For these analyses, the magnitudes distributions are reported in two planes, as highlighted in Figure 4.16, and named Midplane XZ and Midplane YZ. The first is realized with a plane passing through the axis of the burner and parallel to plane XZ, whereas the second is realized in the same way but parallel to the plane YZ.

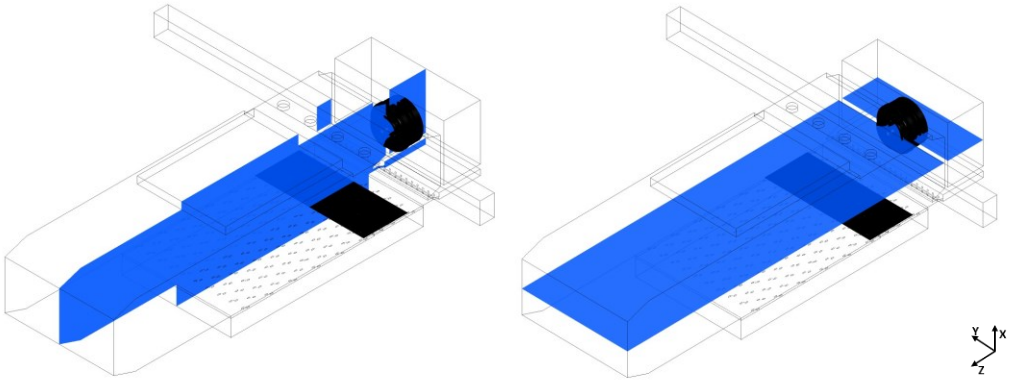

Figure 4.16 - Midplane XZ (left) and Midplane YZ (right)

The swirler is composed of two concentric ducts that supply the fluid with opposing tangential components, generating two counter-rotating vortices, one internal and one external.

First of all, the flow field is analyzed particularly in the area immediately downstream of the swirler, since the velocity structures of the swirling flow have a significant impact on heat transfer as widely demonstrated in the literature [215,216].

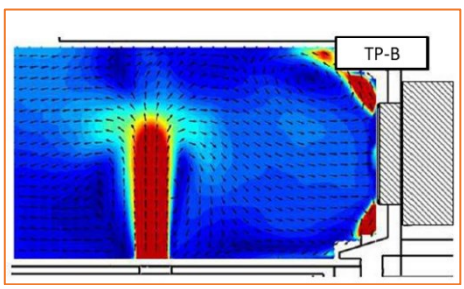

Figure 4.17 - Average velocity maps measurements [211]

All the test points examined showed the averaged flow field map displayed in Figure 4.17. Typical main flow structures of swirl stabilized flames are highlighted [217], the jet exiting from the burner is spread by the large central recirculation zone induced by the vortex breakdown.

The quenching hole jet presents a significant penetration in the main flow and a large amount of air from the dilution flow tends to recirculate in the first part of the swirling flow thanks to the vortex breakdown, contributing to widening the swirling jet expansion.

The velocity distributions on the Midplane XZ (Figure 4.18) and Midplane YZ (Figure 4.19) present the typical characteristics of the swirling flows described by Gupta [218] and similar as observed in the experimental campaign. The jet exiting from the burner is spread by the tangential velocity component given to the air by the swirler. This causes the formation of a large inner recirculating region, due to the vortex breakdown, and of the corner vortices. The inner recirculating region widens through all the opening angle of the swirling flow that impacts on the outer and inner liners. Regarding the dilution jets, the exiting air from the visible hole penetrates the main flow preserving a coherent structure and only in the last part of the jet is lightly deviated downstream.

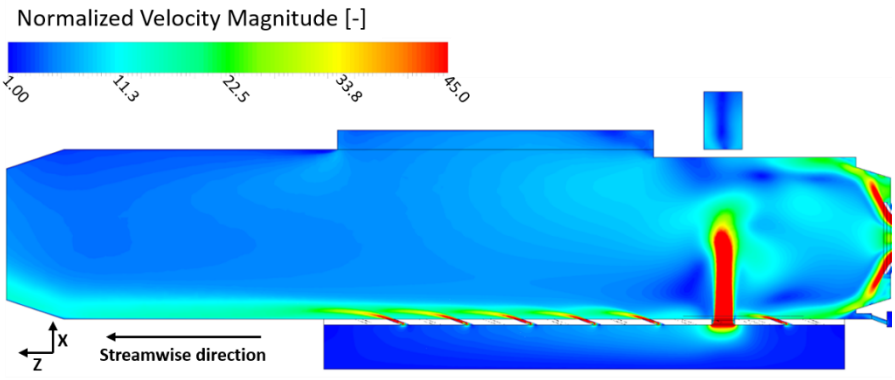

Figure 4.18 - Normalized velocity magnitude distribution Midplane XZ

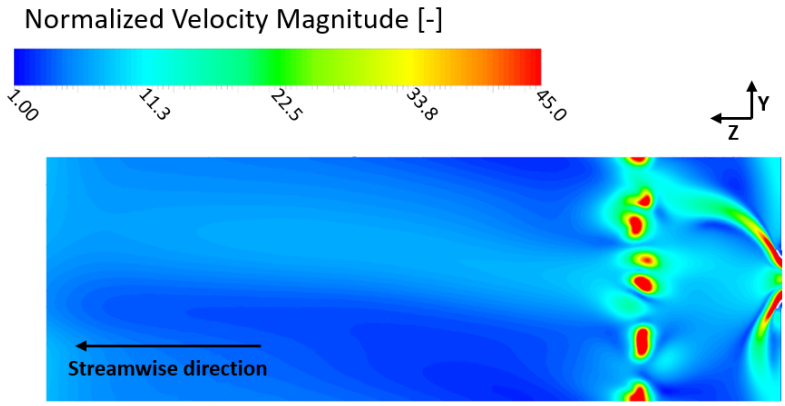

Figure 4.19- Normalized velocity magnitude distribution Midplane YZ

In a real combustor, the dilution jets separate the primary and secondary zone with quenching of the flame decreasing the temperature in the downstream region, as shown in Figure 4.20.

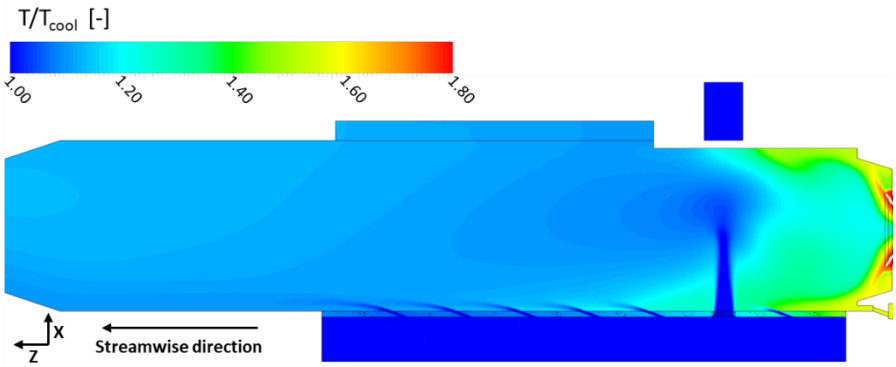

Figure 4.20 – Normalized temperature distribution Midplane ZX

Concerning the velocity distribution on the Midplane YZ (Figure 4.19), an asymmetry to the axis of the burner is clearly notable between the two arms of the swirling flow. The right jet remains adjacent to the dome, while the left part remains detached from the wall. In this region, the flow is probably strongly unstable.

In the streamwise velocity profile (Figure 4.21), the trend is symmetrical to the axis of the burner. The central zone, before the dilution, presents a low-speed region according to a typical swirling flow ensuring efficient combustion in case of reaction flow. Moreover, the profile presents a central zone with very low values of velocity, due to the inner recirculating region that partially penetrates the injection system. Instead, the tangential velocity is asymmetrical for the presence of the eddies in the corner of the combustion chamber, which presents an opposed direction. The velocity component decreases going downstream, presenting a drop in their absolute value due to the sudden expansion and mixing with the non-swirling environment.

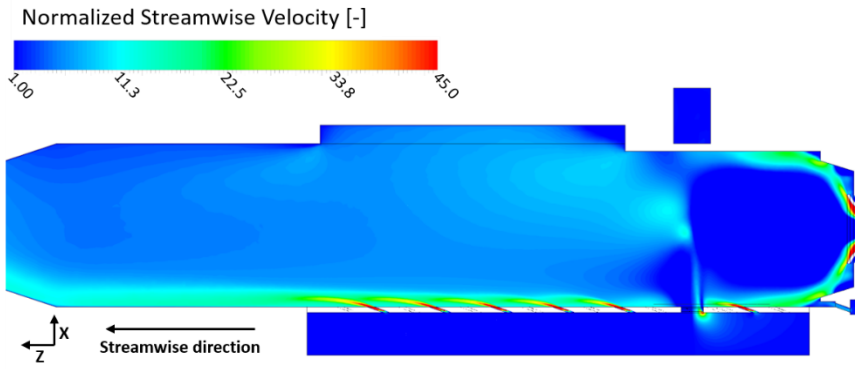

Figure 4.21 – Normalized streamwise velocity Midplane – XZ

Scalars Analyses

η_{ov} is a fundamental parameter in the evaluation of the cooling system performances but does not allow to distinguish the various effects associated with the slot, the dilutions, and the effusion. For this reason,

further numerical analysis has been performed on the coverage provided to the wall defining four additional transport equations for four different passive scalars.

In this sense, Figure 4.22 and Figure 4.23 show the distribution of the adopted passive scalars for TP-A in order to qualitatively understand the covering effect of the several coolant inlets. In the first part of the plate, the slot provides high coverage, but the swirling jet coming from the burner impinges the plate and blows away a good part of the coolant due to the rotational component, reducing the adiabatic effectiveness. The dilution flows distributions (C in Figure 4.22 and Figure 4.23) show a uniform diffusion on the plate, due to their mutual interaction, with slight peaks of protection downstream of the holes. The last part of the plate is mainly covered by the effusion system which increases its performance moving towards the outlet of the chamber.

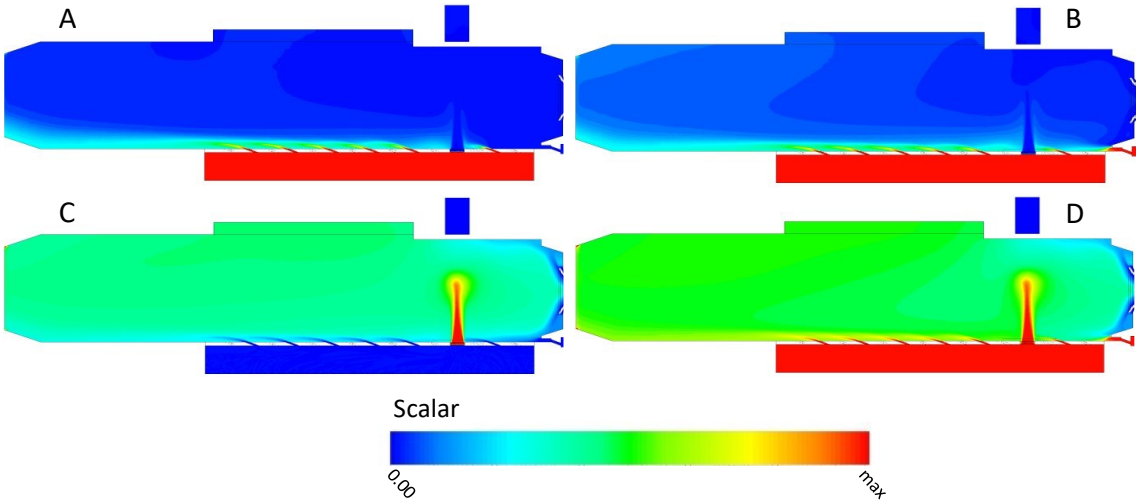

Figure 4.22 - Covering effect provided by effusion (a), effusion and slot (b), inner dilution (c) and for effusion, slot, and inner dilution (d) scalars for TP-A on Midplane XZ

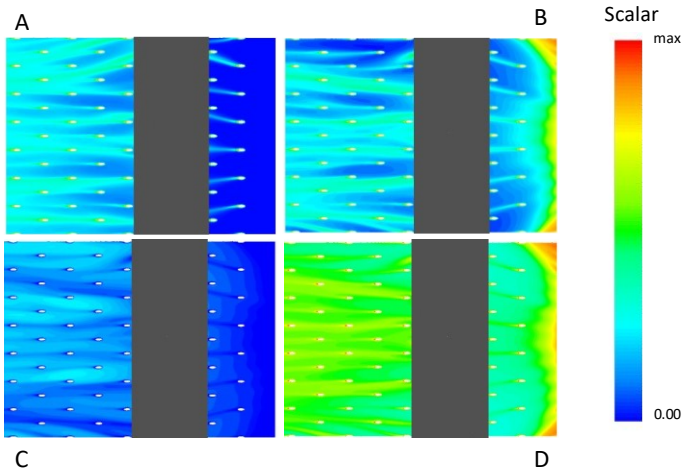

Figure 4.23 - Covering effect provided by effusion (a), effusion and slot (b), inner dilution (c) and for effusion, slot, and inner dilution (d) scalars for TP-A on the plate

Analyzing the results of the scalars analysis, it is possible to notice that the slot coverage (Figure 4.23-B) provides high protection in the first part of the plate, while it is uncovered with only the effusion holes

contribution (Figure 4.23-A). The effusion and the slot provide the typical covering trend due to their combination (Figure 4.23-B), as widely seen in the literature. In the first part of the plate, thanks to the slot, the adiabatic effectiveness is close to one (Figure 4.23-B), but the coverage steeply decreases because the film is blown away by the swirling flow. Instead, the effusion cooling ensures a progressive increase in coverage towards the final part of the plate, thanks to uniform protection. The dilution flows to protect the wall with a sort of bottom threshold that is almost uniform for the whole plate (Figure 4.23-C).

Interpolation zone for Therm-1D

To determine the interaction between the hot gas region and the Therm-1D response (liner metal temperature), the one-dimensional hot side magnitudes trends will be discretized with 200 planes normal to the flow direction, equally spaced and distributed along the entire plate. Figure 4.24 shows an example of a plane used for the discretization of the region. Here Therm-1D hot side input quantities are averaged over the mass flow.

For each evaluation, the height (*H* in Figure 4.24) will be varied, starting from 5% of the chamber height up to full chamber height. The runs performed will have the following scan: 5, 10, 25, 50, 100 %.

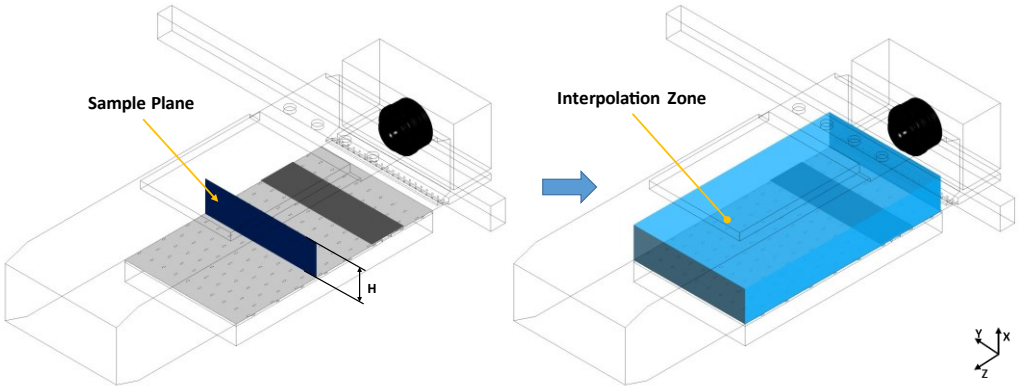

Figure 4.24 - Sample XY plane used for hot side magnitudes zone discretization

Therm-1D – Evaluation Procedure

As previously introduced, for the Therm-1D tool, gas side heat loads are evaluated from a given description of the hot side conditions in terms of *FAR*, temperature, velocity, density, and pressure.

The interpolation of these quantities from the results of the preliminary numerical simulations leads to describe purely three-dimensional trends with one-dimensional averages. The height of this zone (Figure 4.24) is crucial for the correct description of the phenomena that occur in the combustion chamber and around the liners. Especially in presence of an effusion cooling system, it is necessary to consider the continuous coolant injection that protects the thermally exposed side of the liner and how the injected coolant interacts with the hot flow near the wall. Also, it is important to consider that the effect of the swirler is not negligible.

In this application of the code, a feature will be used that allows the imposition of the one-dimensional streamwise distribution of adiabatic effectiveness as input. It will be used the one obtained from

experimental tests with PSP for the various test points, averaged in the spanwise direction. In this way, the cooling system modeled by the tool will work with the same performance as the one tested in the laboratory. The interpolation zone, as previously described, defines how convective heat transfer should be determined. Considering that the convective heat transfer to the wall is affected by the presence and performance of the effusion jets, it can be assumed for this zone that when the jet mixing process develops the convective heat transfer and the momentum of the jet stream is depleted.

In the first part of the work the networks representing the cooling systems will be created. These networks will reproduce the geometric, fluid-dynamics, and thermal characteristics for the relative Test Points. The conditions described above for the adiabatic effectiveness of the cooling system will be applied.

The results of the tool will be compared with the data obtained from the thermography one-dimensional mediated trend. The aim is to determine the region in which the hot gas side flow field gives the tool the best one-dimensional distributions.

The analysis procedure can be outlined as follows:

- TP-A and TP-B will be the two test points. An analysis will be carried out at various zone heights. It will be determined an optimal value for the two TPs, verified the accuracy in a deeper range
- Determined a possible relationship with the hot gases flow field.
- TP-C and TP-D will be used for a verification procedure
- For TP-B and TP-D will be used Therm-1D without imposing the adiabatic effectiveness, and to ask the tool to calculate it. This is to verify the robustness of the introduced guideline.
- A sensitivity analysis will be conducted using the *Therm-1D/Dakota* coupled procedure to determine how much the choices made on the gas side parameters discretization affect the output magnitudes.

Tool Setup

As previously defined, the main inputs of the tool are related to the geometrical discretization of the combustor chamber, the definition of cooling systems, and the thermo-fluid dynamics of the hot gas. All these elements define the operating conditions of the combustor. The geometry of the combustion chamber is representative of the test rig central sector.

In terms of the cooling system, the analyzed rig has a slot, which feeds the coolant on the first part of the plate (not fed for TP-B and TP-C), and an effusion system made by rows of holes uniformly distributed along the plate. As demonstrated by *Bunker* [219], a uniform distribution of holes helps to obtain a very high level of effectiveness. Moreover, as described by *Gustafsson* [220] the most interesting aspect is the significant effect of wall cooling due to the heat removed by the passage of the coolant inside the holes. A larger number of small holes, uniformly distributed over the entire surface, allows a significant improvement in the lowering of the wall temperature. Dilution holes are included in the model. The plate thickness to effusion hole diameter ratio is equal to t/d=2.

For the modeling of the effusion/dilution cooling system, we use a model that represents a smooth channel, corresponding to the meatus between the liner (effusion plate) and the casing of the combustion chamber (the outer wall of the cooling plenum). This model can be inserted inside a more complex fluid network but, if used individually, it allows to completely describe a cooling system made with several rows of small

holes and dilution holes. The air coming from the cooling system is fed tangentially, through a slot, in the direction of the hot liner wall to create a protective film able to avoid direct contact with hot gases. The representative model is a duct consisting of an inlet port, coinciding with the beginning of the liner, and an outlet port. The effect of the superposition of the coolant for the slot is assumed to be effective until about the beginning of the dilution holes. Using these two models it was possible to represent the cooling system with similar characteristics to the one tested on the Rig.

The scheme of the cooling network is represented in Figure 4.25.

The effusion and dilution holes are described in the model row by row. For each of them can be defined:

- Number of rows of effusion and dilution holes
- Number of holes for each row
- Row positioning in cylindrical coordinates
- I/O Diameter and Area
- Inclination Angle
- Discharge coefficient
- Bleeding coefficient (the model simulates losses due to bleeding, in addition to losses of momentum due to warming and friction)

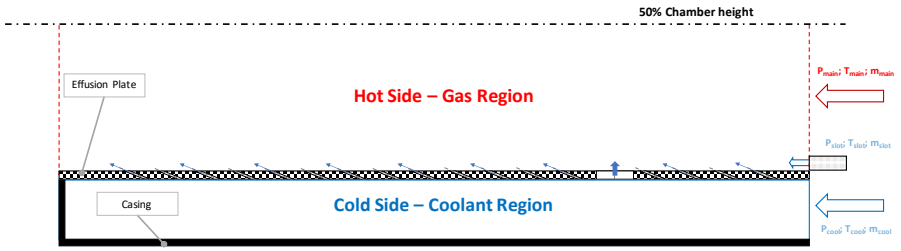

Figure 4.25 - Fluid network modelling - SOPRANO

As regards the model representing the cooling slot, the following parameters can be specified:

- Cross-section
- Wet Perimeter
- Lip Slot Height

In each of the four cases analyzed the coolant flow rates are those related to the central zone, where the plate is present.

I/O cooling network pressures and temperatures are those detected and/or imposed during the experimental measurements. For the several test points, the cooling network BCs refer to Table 4.1.

As already explained (*Flow Field Analyses* and *Interpolation zone for Therm-1D* paragraphs), the hot gas thermo-fluid-dynamic conditions are imposed as one-dimensional distribution extracted from numerical simulations. These distributions are determined for the heights already discussed in *Interpolation zone for Therm-1D.* Figure 4.26 shows the normalized trends of pressure, density, streamwise velocity, velocity magnitude, velocity consisting of streamwise, and spanwise components. Velocity, density, and pressure are the main parameters for the definition of convective heat transfer in the cases where the cooling system's

adiabatic effectiveness is imposed. The interaction zone of the dilution holes is highlighted and it is clearly recognizable due to the sudden variations in the magnitude's trends.

These quantities have been normalized according to some parameters:

- Total pressure to the static pressure exiting from the chamber
- Velocity to the average streamwise velocity on the plane normal to the streamwise at $x/Sx = 0$
- Density to the air density under ISO conditions.

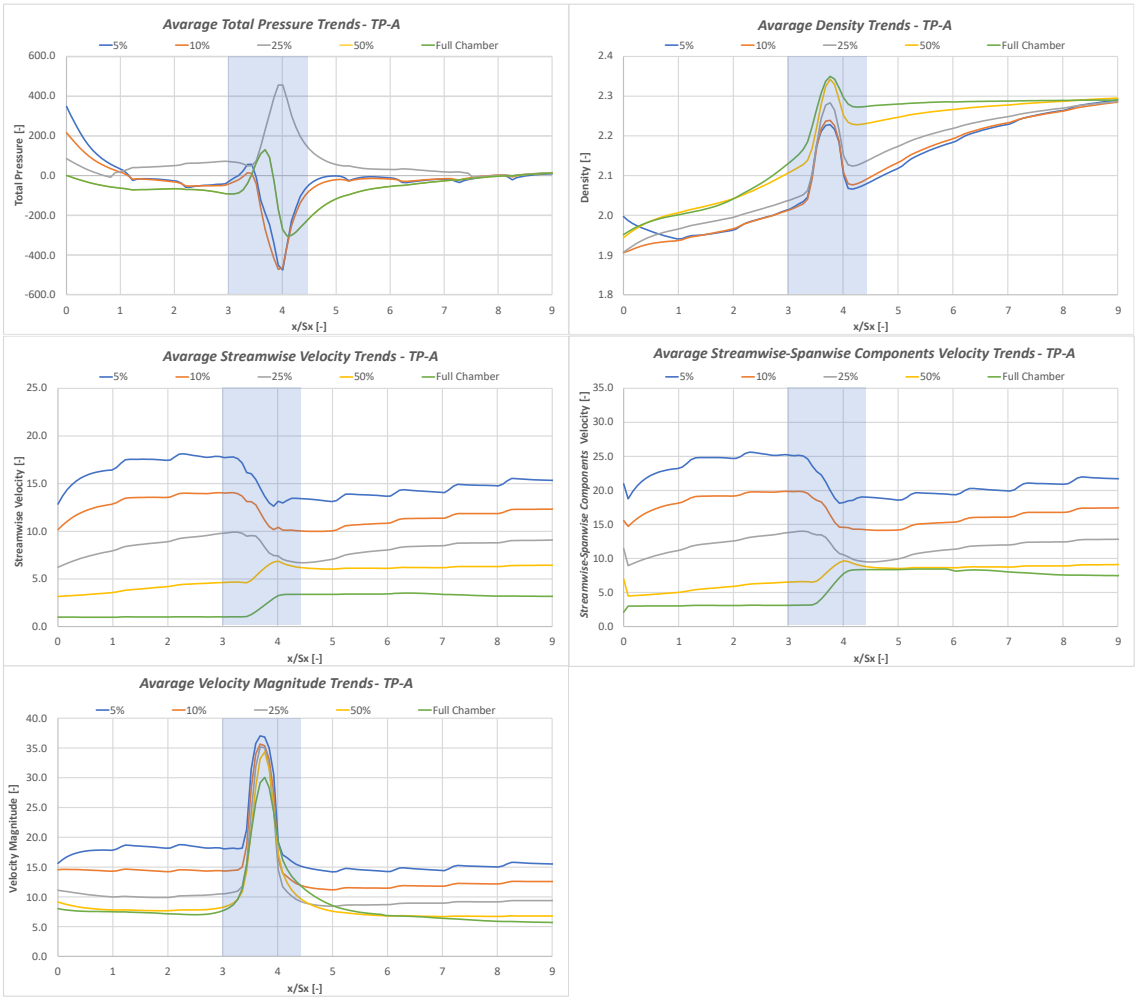

Figure 4.26 – Normalized Average Magnitude, Hot Side Trends for TP-A

Also, the choice to impose η_{ad} involves the need to take a constant one-dimensional trend of the temperature of hot gases. This finds its explanation in the fact that the experimental adiabatic effectiveness also takes into account the contribution of dilution holes. Therefore, to not consider a double effect should be used a temperature equal to the main one and not the one interpolated by numerical post-processing.

The reference value is T_{main} shown in Table 4.1 In this way, it is avoided to consider the cooling system effectiveness twice.

For a better understanding, the steps taken for the tool setup are summarized:

- Create the chamber's geometry
- Impose hot flow conditions as one-dimensional distributions

- Create the effusion/dilution plate and slot geometries
- Impose the BCs for the cooling system
- Impose the effective areas determined by cold test

For the cooling networks representing the four TPs studied, both total pressures in input and static pressures in output are imposed. The check will be done by comparing the flow rates.

As can be seen from Table 4.2 below, the one-dimensional network gives results in agreement with the results obtained during the experimental tests.

The values shown in Table 4.2 are normalized to the input values for the effusion plate supply system.

The four cases analyzed are reported. The normalized values of flow rate, total input pressure, total input temperature, and static output pressure obtained from the experimental tests are reported for each case. In the last two lines are reported the relative percentage errors for the results obtained by Therm-1D compared to the experimental data.

Regarding the thermal assessment for the Therm-1D simulations, once they have reached convergence, a comparison will be made between the tool predicted trend of the metal temperature along the streamwise direction and the temperature distribution results of the experimental thermography.

TP-A - Aero Check				
	Exp Flow Rate	Exp Input Tot. Pres.	Exp Input Tot. Temp.	Exp Output Stat. Pres.
	[-]	[-]	[-]	[-]
Plate	0.403	1.000	1.000	0.922
Slot	0.053	1.001	1.061	0.922
Comparison with the results of the tool - Percentage Relative Error				
	Flow Rate	In. Tot. Press.	In. Tot. Temp.	Out. Stat. Press.
Plate Model	0.32%	0.00%	0.02%	0.00%
Slot Model	0.04%	0.00%	0.00%	0.00%

TP-B - Aero Check				
	Exp Flow Rate	Exp Input Tot. Pres.	Exp Input Tot. Temp.	Exp Output Stat. Pres.
	[-]	[-]	[-]	[-]
Plate	0.403	1.000	1.000	0.924
Slot	-	-	-	-
Comparison with the results of the tool - Percentage Relative Error				
	Flow Rate	In. Tot. Press.	In. Tot. Temp.	Out. Stat. Press.
Plate Model	0.48%	0.00%	0.00%	0.00%
Slot Model	-	-	-	-

TP-C - Aero Check				
	Exp Flow Rate	Exp Input Tot. Pres.	Exp Input Tot. Temp.	Exp Output Stat. Pres.
	[-]	[-]	[-]	[-]
Plate	0.403	1.000	1.000	0.973
Slot	0.051	0.997	1.064	0.973
Comparison with the results of the tool - Percentage Relative Error				
	Flow Rate	In. Tot. Press.	In. Tot. Temp.	Out. Stat. Press.
Plate Model	0.45%	0.00%	0.00%	0.00%
Slot Model	0.00%	0.00%	0.00%	0.00%

TP-D - Aero Check				
	Exp Flow Rate	Exp Input Tot. Pres.	Exp Input Tot. Temp.	Exp Output Stat. Pres.
	[-]	[-]	[-]	[-]
Plate	0.403	1.000	1.000	0.908
Slot	-	-	-	-
Comparison with the results of the tool - Percentage Relative Error				
	Flow Rate	In. Tot. Press.	In. Tot. Temp.	Out. Stat. Press.
Plate Model	0.84%	0.00%	0.00%	0.00%
Slot Model	-	-	-	-

Table 4.2 - Aero Check - Comparison with the tool results

In this way, it will be possible to compare two one-dimensional trends. Also, the values recorded by the thermocouples placed from *x/Sx*=1 to *x/Sx*=9, near the plate centerline will be used.

The one-dimensional trends derived from thermography are shown in Figure 4.27 comparing the cases with the same $\Delta P/P$. The data have been normalized with the T_{cool} of the Test Point (Table 4.1).

The graphs in Figure 4.27 show that the only differences are for the initial zone of the plate, which is the one affected by the slot cooling effect (if present). After the first row of effusion holes, the two trends (TP-A and TP-B, TP-C and TP-D) are almost identical. This result agrees with what was previously seen for the effectiveness trends. It can be emphasized that the slot effect decreases when the $\Delta P/P$ is reduced.

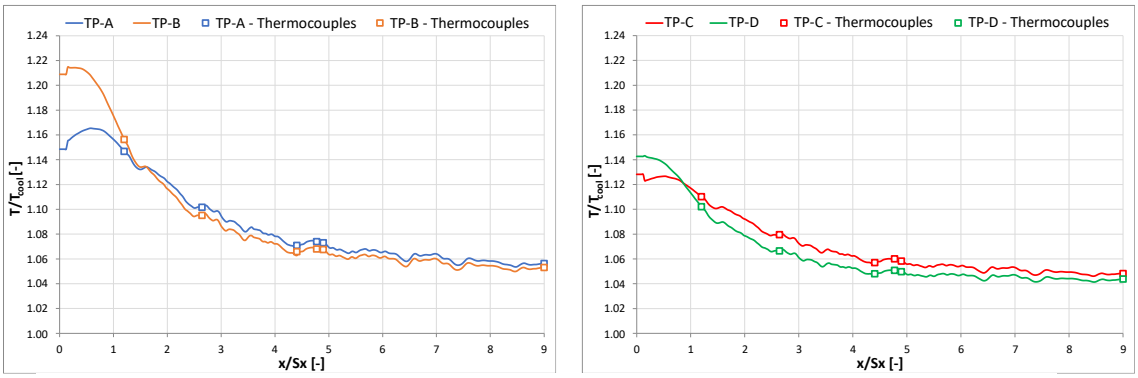

Figure 4.27 - One-Dimensional Trends of the Experimental Thermography Temperature

Thermal Analyses

In the first part of the work, the two test points TP-A and TP-B will be considered. The networks representing the cooling systems will be created. The conditions described above for the adiabatic effectiveness of the cooling system will be applied. As already described in the *Interpolation zone for Therm-1D*, the hot gas side magnitudes will be discretized. For each evaluation, the height will be varied, starting from 5% of the chamber height up to full chamber height. The runs performed will have the following scan: 5, 10, 25, 50, 100 %.

The region that will produce the results closest to the experimental ones, in terms of temperature distribution along the plate wall, will then be subject to further analysis, moving around (± 5%) to check if there is a close value that achieves better results. After this, a numerical post-process will be used to verify if this region presents distinctive characteristics for the description of the heat transfer phenomena.

Once this correlation has been determined, the verification process will be carried out for TP-C and TP-D to verify the results and deductions consistency.

First Analyses results

For TP-A and TP-B the trends obtained with Therm-1D are reported in comparison with those obtained by thermography. To determine the region height that allows the best results, a relative percentage are determined.

The trends will be those obtained using the gas side velocity, both the streamwise component and the magnitude. As can be seen from Figure 4.26, the main differences between the streamwise and magnitude velocity trends are in the interaction zone of the dilution jets. The magnitude considers this aspect, while it is not possible to visualize it with only the axial component.

Comparing the trends (Figure 4.26), the analysis of the velocity distribution determined considering the streamwise and spanwise components can be neglected since it does not differ much from the streamwise one.

Figure 4.28 shows the metal temperature trends for the two runs made. The main difference can be immediately seen: the temperature increases in the dilutions influence zone (graph on the right). This zone has a velocity peak in case the magnitude is considered for the hot gas side (visible in Figure 4.26). For the type of simulation chosen, the code uses velocity, density, and pressure to determine the convective heat transfer.

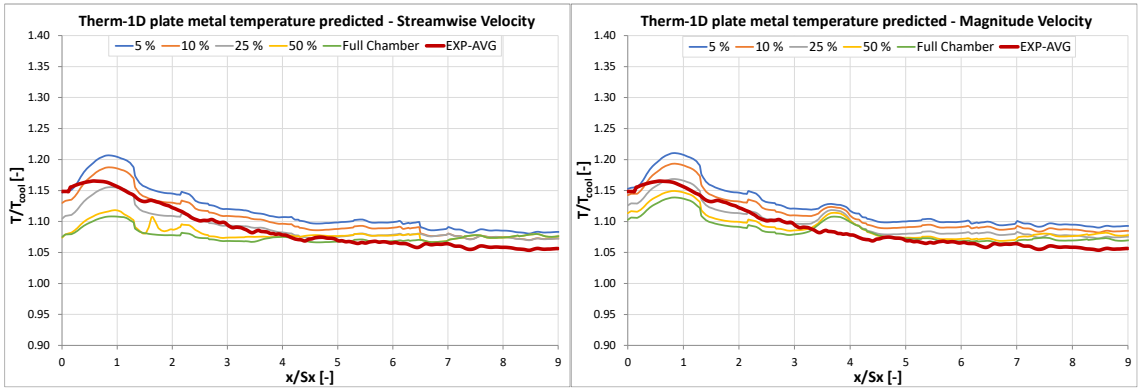

Figure 4.28 – TP-A - Therm-1D plate metal temperature predicted vs. Thermography

Plate T_w AVG. Error vs. Thermography (Streamwise velocity)				
5%	10%	25%	50%	Full Chamber
ΔT	ΔT	ΔT	ΔT	ΔT
Rel. %	Rel. %	Rel. %	Rel. %	Rel. %
2.59%	1.59%	1.10%	1.95%	2.08%

Table 4.3 - TP-A - Average Error vs. Thermography (Streamwise Velocity)

Plate T_w AVG. Error vs. Thermography (velocity Magnitude)				
5%	10%	25%	50%	Full Chamber
ΔT	ΔT	ΔT	ΔT	ΔT
Rel. %	Rel. %	Rel. %	Rel. %	Rel. %
3.04%	2.16%	1.33%	1.43%	1.46%

Table 4.4 - TP-A - Average Error vs. Thermography (Velocity Magnitude)

The simplifications introduced by a correlative and one-dimensional approach must be kept into consideration; also, the correlation used for the determination of convective heat transfer is that of *Lefevbre* [1]. With this substantially it is assumed that what happens in the chamber can be treated as a duct in which the flow is completely developed. With the efficiency of the cooling system imposed, an increase of gas side velocity can carry as consequence only an increase of the liner metal temperature.

It should also be observed the temperature increase in the first part of the plate ($0<x/Sx<1$). This is mainly due to the decrease of the applied η_{ad} for this range.

Due to the application of the plenum model, are also visible: the trends constancy after $x/Sx = 7$ and a general tendency to overestimate the T_w after this coordinate. The two aspects do not arise any concerns because the trend from the thermography is constant. Also, the simplified approach with the plenum model will be affected by the coolant low speed in the final region. On the other hand, this will put the analysis in a conservative situation.

Analyzing Table 4.3 and Table 4.4, the best accuracy is obtained with 25% of the chamber height.

To be sure that this solution is the most suitable, the gas-side magnitudes can be interpolated varying the height of the region by ± 5% with respect to the best result obtained. The runs performed will have the following scan: 20, 22.5, 25, 27.5, 30 %.

Plate T_w AVG. Error vs. Thermography (Streamwise velocity)				
20%	22.5%	25%	27.5%	30%
ΔT	ΔT	ΔT	ΔT	ΔT
Rel. %	Rel. %	Rel. %	Rel. %	Rel. %
1.25%	1.17%	1.10%	1.12%	1.16%

Table 4.5 - TP-A - Average Error vs. Thermography (Streamwise Velocity) - ± 5% to the 25% chamber height

As it is possible to see from Table 4.5 and Table 4.6, the results of the scan around the best solution found previously confirm the precedent outcome. Differences in terms of average error are in the order of one degree for all evaluations. Even if the deviation is minimal, the analysis is still relevant. This allows defining the region in which presumably the whole mixing process of effusion cooling jets takes place and therefore the phenomena of convective heat transfer occur.

Plate T_w AVG. Error vs. Thermography (velocity Magnitude)				
20%	22.5%	25%	27.5%	30%
ΔT	ΔT	ΔT	ΔT	ΔT
Rel. %	Rel. %	Rel. %	Rel. %	Rel. %
1.51%	1.42%	1.21%	1.27%	1.33%

Table 4.6 - TP-A - Average Error vs. Thermography (Velocity Magnitude) - ± 5% to the 25% chamber height

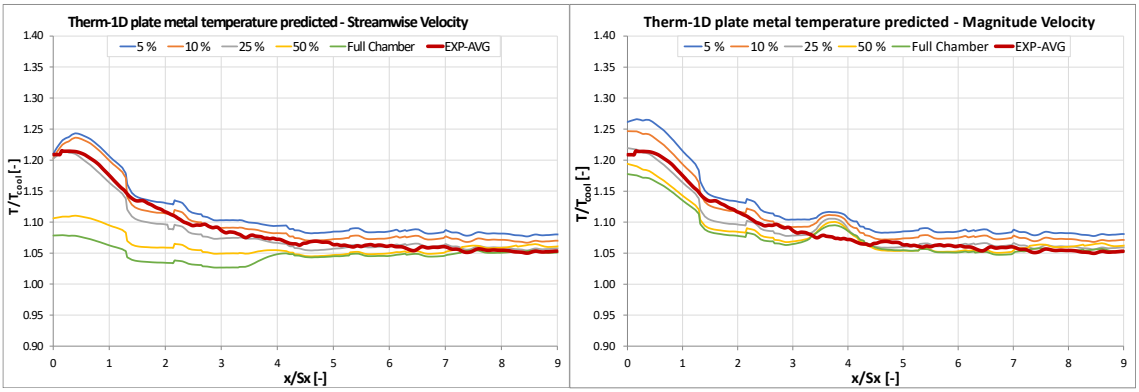

Figure 4.29 - TP-B - Therm-1D plate metal temperature predicted vs. Thermography

In conclusion for that TP, the best interpolation zone of the quantities that describe the hot gas side phenomena is the one at 25% of the chamber height.

Switching to TP-B (same conditions of the TP-A without slot cooling), the same analyses made for the previous TP are reported, starting from the metal temperature trends for the two runs made.

The temperature in the first zone is higher than in the previous case, due to the absence of the slot that protects the initial zone of the plate. It is also absent the sudden increase in temperature that there was in the zone $x/Sx<1$ because the imposed η_{ad} trend does not present the same characteristics as the previous one.

It is important to note that for TP-A and TP-B, the distribution trends derived from thermography are comparable from the position *x/Sx*=3, and after the dilution holes they become almost identical.
Analyzing the trends in Figure 4.29 it is possible to deduce the conclusions already reported for the TP-A

Plate T_w AVG. Error vs. Thermography (Streamwise velocity)				
5%	10%	25%	50%	Full Chamber
ΔT	ΔT	ΔT	ΔT	ΔT
Rel. %	Rel. %	Rel. %	Rel. %	Rel. %
2.08%	1.95%	0.78%	2.86%	3.85%

Table 4.7 - TP-B - Average Error vs. Thermography (Streamwise Velocity)

Plate T_w AVG. Error vs. Thermography (velocity Magnitude)				
5%	10%	25%	50%	Full Chamber
ΔT	ΔT	ΔT	ΔT	ΔT
Rel. %	Rel. %	Rel. %	Rel. %	Rel. %
2.50%	1.46%	0.84%	1.44%	1.56%

Table 4.8 - TP-B - Average Error vs. Thermography (Velocity Magnitude)

Analyzing Table 4.7 and Table 4.8, the best accuracy is obtained with 25% of the chamber height, also for this TP for all the comparisons made.
The conclusions do not change performing a more accurate analysis around the best solution obtained (Table 4.9 and Table 4.10), as already done for the TP-A.
In conclusion, also for this TP, the best interpolation zone of the quantities that describe the gas side phenomena is the one at 25% of the chamber height.

Plate T_w AVG. Error vs. Thermography (Streamwise velocity)				
20%	22.5%	25%	27.5%	30%
ΔT	ΔT	ΔT	ΔT	ΔT
Rel. %	Rel. %	Rel. %	Rel. %	Rel. %
0.89%	1.16%	0.78%	1.30%	1.45%

Table 4.9 - TP-B - Average Error vs. Thermography (Streamwise Velocity) - ± 5% to the 25% chamber height

Plate T_w AVG. Error vs. Thermography (velocity Magnitude)				
20%	22.5%	25%	27.5%	30%
ΔT	ΔT	ΔT	ΔT	ΔT
Rel. %	Rel. %	Rel. %	Rel. %	Rel. %
0.85%	0.86%	0.84%	0.88%	0.91%

Table 4.10 - TP-B - Average Error vs. Thermography (Velocity Magnitude) - ± 5% to the 25% chamber height

First Analyses Remarks

For the two TPs studied, having the same BCs, the conclusion is that the best agreement between the values predicted by the tool and the thermography trend is achieved by taking, on the hot gas side, a region above the effusion plate that has a 25% of the total chamber height.

The slot presence or absence seems to have little influence on the Therm-1D trends. This is mainly due to the limited effect that the slot has in these conditions; its effect tends to decline after the first row of effusion holes. However, remains significant the difference in the zone with coordinates $0 \leq x/Sx \leq 1$, where the two test points have different trends due to the presence of the slot. For the setup with which these two analyses have been conducted, the slot effect is considered through the imposition of adiabatic effectiveness.

The thermography trends are similar for $x/Sx \geq 3$ and identical after the dilution holes. Also, in this case, the behavior is dictated by the effectiveness developments, which are to be considered almost identical for this sector. This condition also affects the results predicted by the tool.
Finally, for Therm-1D there is a substantial tendency to overestimate the T_w after $x/Sx=7$, which implies a maximum deviation from the expected result of 3%. Such results are mainly due to the choice of the model used for the cooling meatus simulation. Since this is a closed plenum, in the final part a low-velocity stagnation zone is generated; this leads to a reduction of the convective heat transfer coefficient through the plate thickness.

Hot gas side flow field analysis

The purpose of this study is to determine a correlation, if any, between the optimal gas side region height obtained from Therm-1D runs and the characteristics of the flow field in the chamber. This analysis is complicated by several elements that have a relevant effect on the interaction that effusion holes have with the mainstream. These factors also influence the performance of the cooling system. Table 4.11 shows some of the main factors.
Ideally, the coolant blown out from the effusion hole should remain attached to the surface of the plate, in this way it would provide complete coverage of the liner surface bringing it to a temperature equal to that

Coolant/mainstream conditions	Hole geometry and configuration
Mass flux ratio Momentum flux ratio	Shape of the hole Injection angle Compound angle
Mainstream turbulence Coolant density ratio Approach boundary layer	Spacing between holes Length of the hole Spacing between rows
Unsteady mainstream flow Swirl	

Table 4.11 - Factors affecting film-cooling performance

of the coolant and consequently minimizing heat transfer. This would result in a film effectiveness of 1.
As explained by *Bogard et al.* [221], in reality, this might not happen in certain conditions, because the coolant mixes very quickly with the mainstream. Figure 4.30 shows the coolant dispersion after exiting from a film-cooling hole where temperature measurements along the centerline are shown. The temperature contours are normalized as defined by the equation below [221]:

$$\theta = \frac{T_{gas} - T}{T_{gas} - T_{cool}} \tag{4.1}$$

As described by *Bogard et al.* [221], the definition of θ is equivalent to that of η. Therefore, it is possible to affirm that such contours also show the distribution of η. According to the authors, the values of θ represent a measure of the coolant jet mixing with the mainstream, i.e. a θ value of 0.2 indicates a mixture with 20% of coolant and 80% of fluid from the mainstream (Figure 4.30).

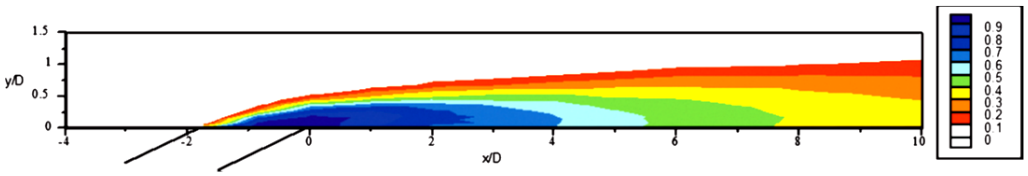

Figure 4.30 - Thermal profiles of coolant jet, decay of the normalized temperature θ downstream of hole [221]

Another interesting work for this analysis is the one proposed by *Thole et al.* [222]. Here the temperature profiles are measured for a film cooling hole row normalized as described in Equation (4.1). The study is carried out under different conditions of density ratio, mass, velocity, and momentum flux of the jets to the mainstream. The chosen intervals allow studying the jets in three configurations, when remaining attached to the surface, detached and then reattach, or completely detached. These three scenarios were also used to study the vertical penetration of the jet in the mainstream. The author concludes by pointing out the difficulty of determining appropriate scale parameters to univocally describe the thermal field.
The results of the study by *Scrittore et al.* [129] indicate that the cooling effectiveness for a realistic combustor wall is dependent on multiple flow mechanisms. It was important in this study to quantify the effect of the dilution jets and effusion jets to understand the behavior of the cooling flow. The flow and thermal fields that these fluxes produce give an idea of how the coolant was transported from the film-cooling jets to the freestream. The study was then completed by *Scrittore et al.* [127] where the development of the film-cooling effectiveness was compared to the developing flow field. Here the author asserted that a prediction of the cooling effectiveness based on the behavior of the film cooling flow allows identifying where a full coverage cooling scheme becomes fully developed.

Based on the analysis exposed during the above-mentioned works, it is possible to conclude that the characterization of the interaction between coolant flow and mainstream for effusion/film cooling systems is complex and influenced by multiple parameters. In the same way, it has been demonstrated that the process of heat transfer between coolant flow and mainstream decays following the decay of θ. At the same time, as already stated in [221], this parameter also identifies the percentage of coolant flow inside the mixing in the zone under analysis.
With this approach, the scalar for the coolant is coming from the pattern of the effusion holes is taken into account. In this way, in analogy with what has been said before (*Numerical Simulations paragraph*), by controlling the decrease of this quantity it is possible to suppose a region where the mixing with the mainstream is achieved. it can be assumed that in this region the momentum of the jets will be completely

dissipated. In the same way, it is possible to consider that the convective heat transfer process has completely developed.

This choice is supported by works in the literature that include the use of a passive scalar to predict the mixing of the coolant with hot gases. In the work of *Yusop et al.* [223], it is asserted that the surface distribution of the tracer is a direct prediction of the effectiveness of cooling. The mixing between coolant and traditional gases has been studied. The boundary layer and mixing temperature profiles have been predicted. *Thomas et al.* [224], give an example of the usefulness of this method to study the contributions of individual film cooling holes to the overall cooling efficiency on a highly film-cooled component. Another analysis always on the same topic is realized by *Walton* [225].

So, assuming to take the region above the plate in which the decay of the *scalar-E* (identifying the mass fraction of coolant originating from the effusion holes) is very high, this guarantees to have taken into account the whole mixing region. Here, the convective heat transfer process between coolant and hot gas is completed. It is correct to assume that averaging the Therm-1D hot gas side input values in this region allows considering all those thermo-fluid-dynamic phenomena for the proper one-dimensional characterization of the flow field.
With such deductions, it is necessary to determine whether there are analogies between the Therm-1D results showed before and the behavior of *scalar-E*.

Evaluation process

For the analysis (Figure 4.31), a zone is taken normal to the direction of the flux (Figure 4.32). This one will always have 1% of the chamber height. In the area created, the concentration mass flow average of the *scalar-E* is determined. Once this average value has been determined, the area will move away from the plate by 1% in the X direction (with reference to Figure 4.32).

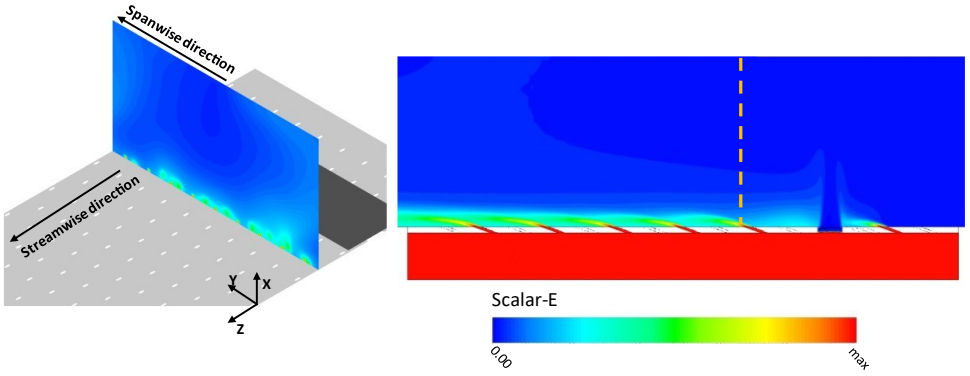

Figure 4.31 - Scalar-E trend visualization for x/Sx = 5 (TP-B)

The process will be repeated for the entire chamber height and all the 200 planes chosen for the one-dimensional trend's representation along the plate (Figure 4.24). This determines the variation of the mass fraction of the *scalar-E* along the entire chamber height.

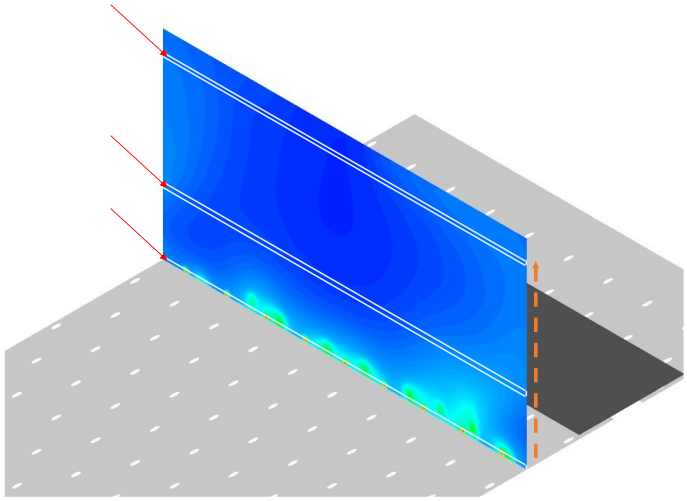

Figure 4.32 - Sketch of the Scalar-E evaluation process of

Applying this procedure by post-processing the RANS-CHT simulations of TP A and B, the resulting trends are shown in Figure 4.33 below.
Each color/line represents the scalar trend for a certain position. Each point of the graph represents the average value obtained on the previously described plane.

The tracer profiles decrease rapidly in the zone just above the effusion plate and then remain almost constant. Such phenomenology is found for both TPs as it is possible to see from Figure 4.33. By reporting the height for which Therm-1D obtains the closest T_w average trend to the thermography one (red dotted line), it is appreciable how all the curves settle around the same value. Such result is valid for both TPs shown in Figure 4.33.

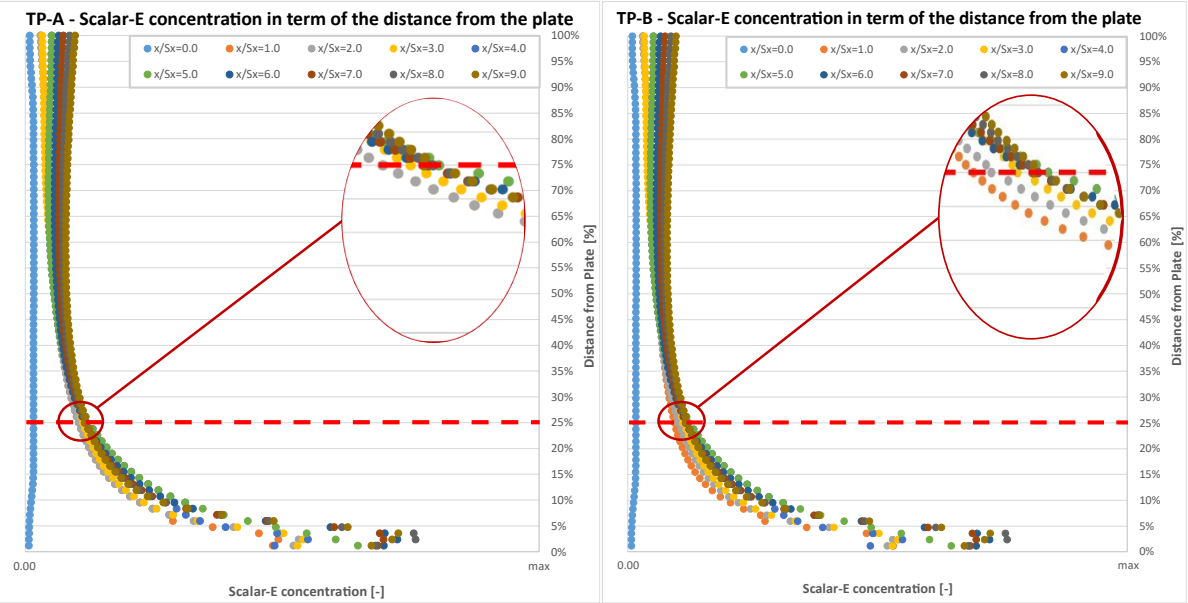

Figure 4.33 - Scalar-E concentration - distance from the plate (TP-A and TP-B)

TP-A Scalar-E concentration 25%		TP-B Scalar-E concentration 25%	
x/Sx [-]	% from max	x/Sx [-]	% from max
0.0	0.83%	0.0	0.83%
1.0	5.22%	1.0	4.69%
2.0	5.22%	2.0	5.02%
3.0	5.62%	3.0	5.52%
4.0	6.02%	4.0	6.10%
5.0	6.02%	5.0	6.10%
6.0	5.87%	6.0	5.81%
7.0	5.86%	7.0	5.83%
8.0	5.94%	8.0	5.91%
9.0	5.80%	9.0	5.80%

Table 4.12 - Scalar-E concentration at 25% height (TP-A and TP-B)

Focusing the analysis around this area, it is possible to define that the *scalar-E* decays by 95% for the boundary height of the optimal region determined by Therm-1D analyses. More precisely, as shown in Table 4.12, there is decay between 94 and 95%. This means that a coolant fraction of 5.5% will still be detectable, with a possible oscillation of ±0.5%.

On the left of Figure 4.34 is shown the velocity magnitude distribution for some planes normal to the stream direction. The yellow axis delimits the area defined by the 95% decay of the Scalar-E.

On the left of Figure 4.34 the velocity magnitude contour for the ZY (*streamwise*/*spanwise*) plane at 25% of the chamber height.

Analyzing the contours shown in Figure 4.34, it can be concluded that it is in the defined zone that the mixing of the jets is completed. The velocity magnitude above this zone can be considered comparable to that of the undisturbed flow. This confirms the validity of the analysis previously done.

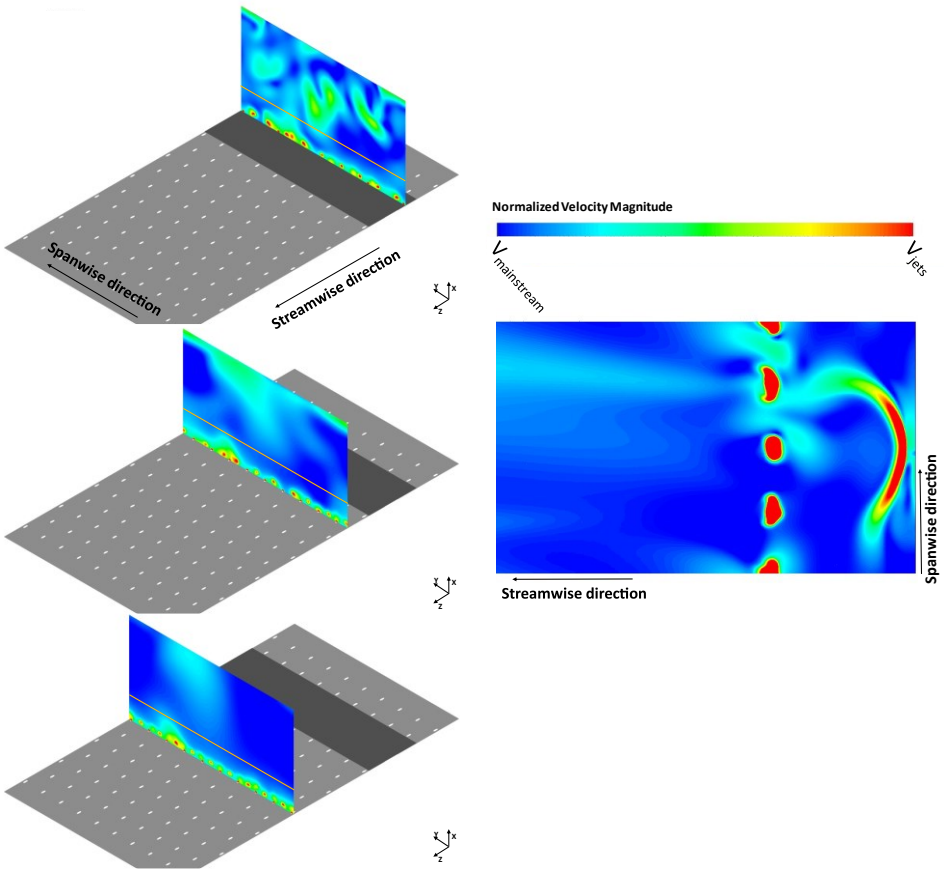

Figure 4.34 – Scalar-E decay zone – magnitude velocity contours

Applying the same analysis to TP-C and TP-D, which have different BCs compared to the two previous ones (see Table 4.1), the scalar trends have similar characteristics to those previously seen. The tracer trends decrease rapidly in the zone just above the effusion plate and then remain almost constant. In these second test points, the scalar decay of 95% is obtained at 15% of the chamber height.

This can be seen in Table 4.13 and Figure 4.35.

Figure 4.33 and Figure 4.35 are reported in that format due to non-disclosure agreements with the industrial partner.

TP-C Scalar-E concentration 15%		TP-D Scalar-E concentration 15%	
x/Sx [-]	% from max	x/Sx [-]	% from max
0.0	0.81%	0.0	0.78%
1.0	3.41%	1.0	3.18%
2.0	4.91%	2.0	5.18%
3.0	5.11%	3.0	5.38%
4.0	5.31%	4.0	5.58%
5.0	5.97%	5.0	5.97%
6.0	5.63%	6.0	5.63%
7.0	5.67%	7.0	5.67%
8.0	5.91%	8.0	5.91%
9.0	5.83%	9.0	5.83%

Table 4.13 - Scalar-E concentration at 15% height (TP-C and TP-D)

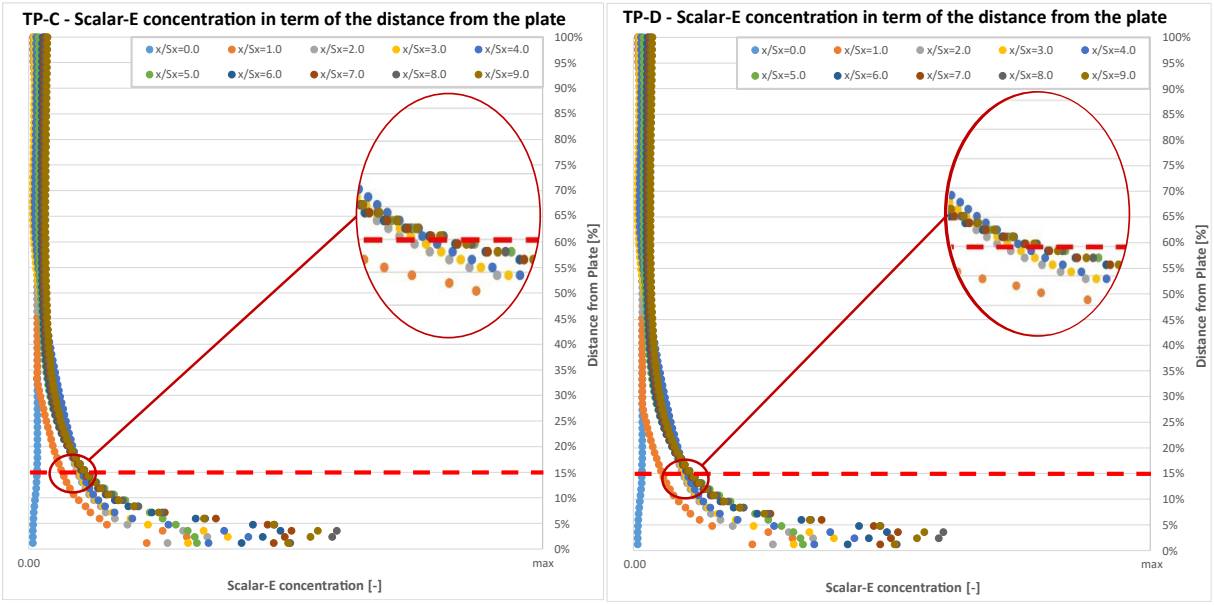

Figure 4.35- Scalar-E concentration - distance from the plate (TP-C and TP-D)

Remarks

Some further analysis can be done. The first is that the value of the scalar-E is not zero at $x/Sx = 0$, but this is easily explained because of the recirculation that is created in the primary zone caused by the dilution.
In the case of TP-C and TP-D, it is noted that there is a deviation from the trend for $x/Sx = 1$. However, the problem is visible only for this abscissa.

Thermal Analyses – verification process

With the results obtained from the analysis carried out in the previous paragraph, the verification process for TP-C and TP-D will be applied. In other words, the gas side input quantities for Therm-1D will be mediated in the 15% chamber height region. This height is the one for which we obtain a 95% reduction of the scalar that represents the mass fraction of the coolant coming from the effusion holes that is still present in the hot side stream.
Again, the tool will be used imposing the experimentally determined η_{ad}, and determining the distribution of T_w, which will be compared with that obtained with thermography. The runs performed will have the following scan: 5, 10, 15, 22.5, 25 %.
The analyses proposed here are the same as those already discussed for TPs A and B in paragraph *First Analyses results.*
The results are proposed for the two TPs as the predicted metal temperature trends (Figure 4.36 for TP-C and Figure 4.37 for TP-D) and the average error (Table 4.14 and Table 4.15 for TP-C, Table 4.16 and Table 4.17 for TP-D). All Therm-1D results are compared to thermography.

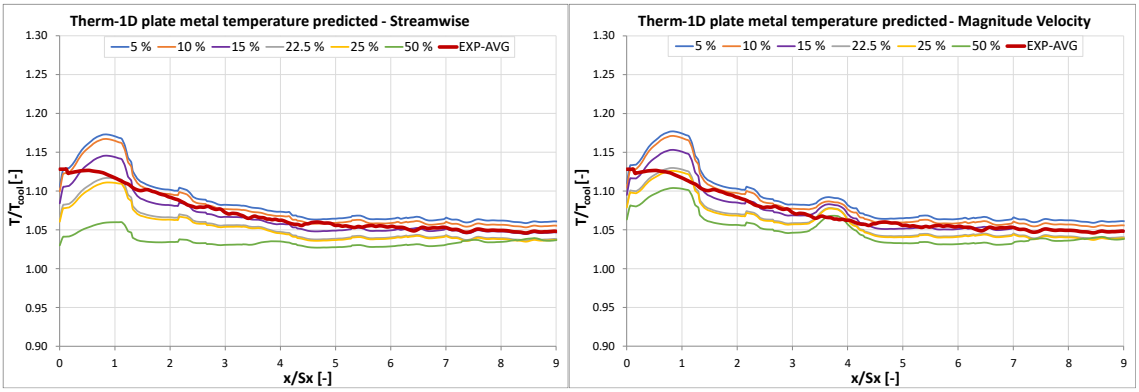

Figure 4.36 - TP-C - Therm-1D plate metal temperature predicted vs. Thermography

Plate T_w AVG. Error vs. Thermography (Streamwise velocity)				
5%	10%	15%	22.5%	25%
ΔT	ΔT	ΔT	ΔT	ΔT
Rel. %	Rel. %	Rel. %	Rel. %	Rel. %
1.33%	0.84%	0.60%	1.45%	1.67%

Plate T_w AVG. Error vs. Thermocouples (Streamwise velocity)				
5%	10%	15%	22.5%	25%
ΔT	ΔT	ΔT	ΔT	ΔT
Rel. %	Rel. %	Rel. %	Rel. %	Rel. %
1.52%	0.99%	0.87%	1.20%	1.37%

Table 4.14 - TP-C - Average Error vs. Thermography or Thermocouples (Streamwise Velocity)

Plate T_w AVG. Error vs. Thermography (velocity Magnitude)				
5%	10%	15%	22.5%	25%
ΔT	ΔT	ΔT	ΔT	ΔT
Rel. %	Rel. %	Rel. %	Rel. %	Rel. %
1.51%	1.01%	0.59%	1.09%	1.21%

Plate T_w AVG. Error vs. Thermocouples (velocity Magnitude)				
5%	10%	15%	22.5%	25%
ΔT	ΔT	ΔT	ΔT	ΔT
Rel. %	Rel. %	Rel. %	Rel. %	Rel. %
1.68%	1.01%	0.78%	0.87%	0.97%

Table 4.15 - TP-C - Average Error vs. Thermography or Thermocouples (Velocity Magnitude)

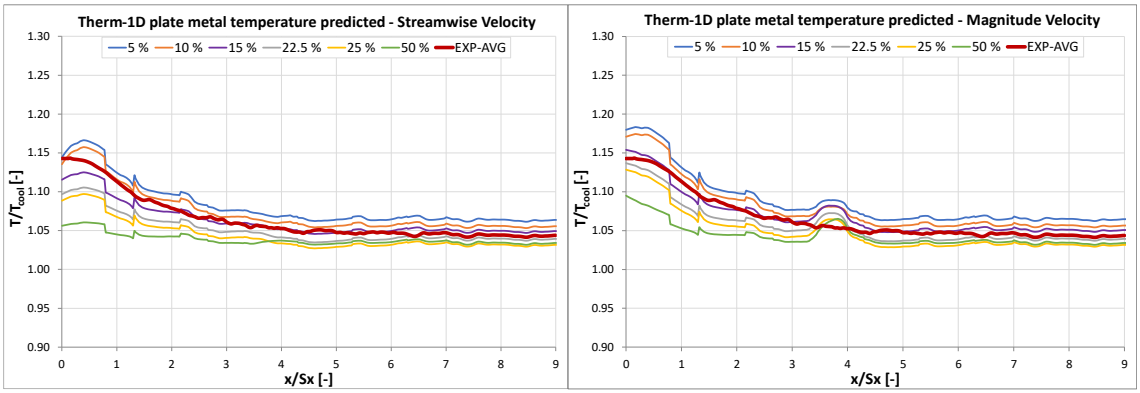

Figure 4.37 - TP-D - Therm-1D plate metal temperature predicted vs. Thermography

Plate T_w AVG. Error vs. Thermography (Streamwise velocity)				
5%	10%	15%	22.5%	25%
ΔT	ΔT	ΔT	ΔT	ΔT
Rel. %	Rel. %	Rel. %	Rel. %	Rel. %
1.69%	0.94%	0.58%	1.21%	1.95%

Plate T_w AVG. Error vs. Thermocouples (Streamwise velocity)				
5%	10%	15%	22.5%	25%
ΔT	ΔT	ΔT	ΔT	ΔT
Rel. %	Rel. %	Rel. %	Rel. %	Rel. %
2.01%	1.10%	0.71%	1.28%	1.43%

Table 4.16 - TP-D - Average Error vs. Thermography or Thermocouples (Streamwise Velocity)

Plate T_w AVG. Error vs. Thermography (velocity Magnitude)				
5%	10%	15%	22.5%	25%
ΔT	ΔT	ΔT	ΔT	ΔT
Rel. %	Rel. %	Rel. %	Rel. %	Rel. %
2.06%	1.29%	0.65%	0.94%	1.58%

Plate T_w AVG. Error vs. Thermocouples (velocity Magnitude)				
5%	10%	15%	22.5%	25%
ΔT	ΔT	ΔT	ΔT	ΔT
Rel. %	Rel. %	Rel. %	Rel. %	Rel. %
2.19%	1.37%	0.65%	0.98%	1.04%

Table 4.17 - TP-D - Average Error vs. Thermography or Thermocouples (Velocity Magnitude)

For the two TPs studied having the same BCs, the conclusion is that the best agreement between the values predicted by the tool and the thermography trend is achieved by taking, on the hot gas side, a region above the effusion plate that has a 15% of the total chamber height. This is in accordance with what was previously assumed during the study done on scalar-E.

The slot presence or absence seems to have little influence on the Therm-1D trends. However, it remains significant the difference in the zone with coordinates $0 \leq x/Sx \leq 1$, where the two test points have different behaviors. For the setup with which these two analyses have been conducted, the slot effect is considered through the imposition of adiabatic effectiveness.

The thermography trends are similar for $x/Sx \geq 3$ and identical after the dilution holes. Also, in this case, the behavior is dictated by the effectiveness developments, that are to be considered almost identical for this area. This condition also affects the tool results.

Thermal Analyses Final Remarks

It has been determined a relationship that allows taking the coolant mass fraction tracer coming from the effusion holes as a fundamental parameter. This is for the definition of the reference region for the Therm-1D hot gas side one-dimensional trend inputs set up.

The 95% reduction of the scalar representing this trace is the target value. This value is directly related to the limit height of the region where velocity, density, and pressure are mediated. According to what asserted by *Bogard et al.*[221] and what was reported by *Yusop et al.* [223] and *Thomas et al.* [224], the chosen region is the one where the mixing between effusion coolant and mainstream is completed and therefore the whole process of convective heat transfer over the plate is done. The relationship defined in this way leads to having regions with different heights from time to time depending on the thermo-fluid-dynamic conditions in the chamber.

For TP A and B, the analysis determined that the optimal height for the region was 25%. This allowed determining the relationship between this and the target value of the *scalar-E*.

TP C and D were used for the verification process, first determining the height as a function of the target value of the scalar, and then going to check if this was the optimal height for the analysis with Therm-1D. The results of the plate metal temperature trends predicted by the tool have confirmed the reliability of the assumptions made.

Therm-1D – Adiabatic effectiveness analyses

The methodology used during the whole analysis is to apply the experimentally determined adiabatic effectiveness to the tool, forcing the cooling system to work in analogy to the tested one.
However, this condition may cause some problems:

- Consider realizing a test rig each time, which cannot always be done
- PSP measurements for adiabatic effectiveness. These measurements are almost always economically feasible, but some test rigs maybe not be properly equipped for such measurements

To avoid using experimental data, the η_{ad} trend to be imposed on the tool could be determined using the results of RANS-CHT simulations performed on the test case. This can only be a solution when the design is in a preliminary phase, but it is not applicable in cases where the conceptual design phase is the main objective. In this scenario, a screening of as many solutions as possible is done to find the most promising one. Usually in this situation, a low-cost numerical simulation, often RANS, allows to determine a mixing history between coolant and mainstream, and that gives basic information to characterize the hot gas flow field.

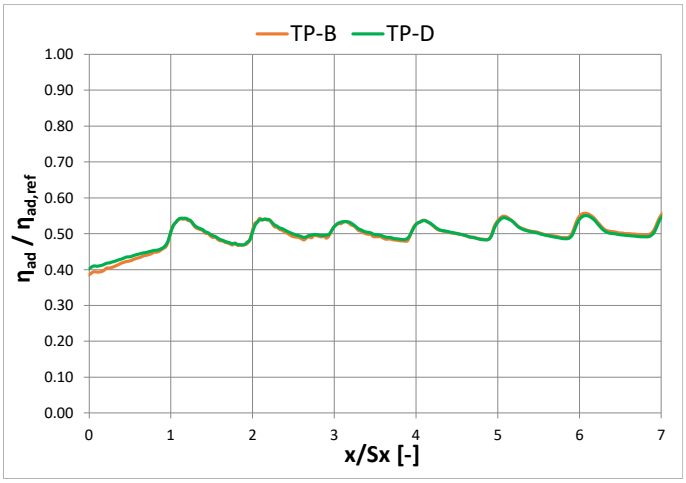

Figure 4.38 - η_{ad} distributions (TP-B vs. TP-D)

With these considerations, the idea is to use the tool with the gas side magnitudes previously obtained to verify if it can determine cooling system effectiveness that is comparable to that measured experimentally.

As is visible from the graphs the normalized η_{ad} shown in Figure 4.38 are for TP-B and D, where the initial value of adiabatic effectiveness is already high, about 0.4. With further experimental tests (Figure 4.39), it has been shown that this value is dependent on the dilutions effect, which for this test rig takes about 85% of the coolant flow rate for the plate supply. A plausible explanation is that the barrier created by the coolant coming out of the dilutions involves a very high recirculation in the primary zone. This means that the plate area, that should not be covered by the film, is also cooled.

Investigations have been conducted to determine the effective contribution of the dilution holes to the experimentally determined effectiveness.
Two PSP tests are performed for the same test point (TP-H), as described in Figure 4.39 below:

- One with all the holes fed, effusion and dilution (purple line)
- One with only the dilution holes fed (grey line)

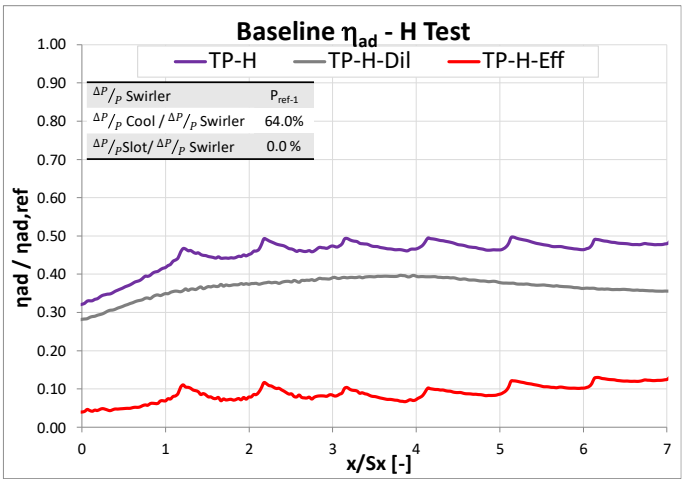

Figure 4.39 - η_{ad} contributions assessment (TP-H)

The boundary conditions for the TP-H are included in the figure above.

In this way, a baseline value can be determined by evaluating the second measurement (with the only Dilution fed).

It is visible from the TP-H-EFF curve in Figure 4.39 (red line) the experimental adiabatic effectiveness representative of the contribution given only by the effusion cooling. This one-dimensional trend is obtained from the one with all the holes fed reduced by the contribution made by the dilution cooling effect. This background level obtained should be considered during the Therm-1D effectiveness evaluation, and the one-dimensional trends obtained experimentally will be reduced to this contribution.

The TPs evaluated are B and D, as the experimental analysis for the dilution baseline assessment was conducted in the absence of slots, so it is not possible to deduce the contribution in cases where this protection system is enabled.

Film Effectiveness evaluation

As seen in *Therm-1D Procedure*, the tool iteratively calls a series of codes to solve the fluid-wall conjugate computing. At equilibrium, the liner metal temperature is sufficient to equilibrate the heat fluxes inside and outside. The evaluation of the adiabatic effectiveness is performed within the code (Icons-1D) that solves the coolant side fluid network and evaluates the internal convective thermal loads. Once the convergence of the cycle is reached, Icons-1D evaluates the film cooling, using correlations like the one proposed by *L'Ecuyer* [39]; a correlation for holes placed on a flat plate which allows evaluating the adiabatic effectiveness, developed in the mid-eighties following extensive literature research. Based on some geometric and fluid dynamic parameters (blowing ratio, velocity ratio, etc.), the correlation allows analyzing the efficiency for each row of holes. For the determination of the superimposition film efficiency, it is referred to the hypotheses proposed by *Sellers* [43] stated in *Effusion cooling*.paragraph

Once the resolution of the cooling network is complete, some quantities are stored:

- The coolant fluid-dynamic parameters

- The flow rate distribution in the effusion cooling rows
- The adiabatic effectiveness trends
- The heat transfer coefficient and the convective thermal load on the liner cold side
- The adiabatic wall temperature.

These quantities are used for both the estimation of the other thermal loads to which the liner is subjected and for the conductive evaluation through the thickness.

Results

The simulation results for TP B and D are shown in the figures below in terms of normalized η_{ad}. These are compared with one-dimensional trends obtained experimentally reduced by the contribution made by the dilution cooling effect. In this way, the experimental adiabatic effectiveness obtained will be representative of the contribution given only by the effusion cooling.

The one-dimensional trends for the hot gas side boundary conditions (combustion chamber) are those chosen from the previous analyses. In this case, the temperature trend applied as hot side boundary condition should be the interpolated one and not the constant one as assumed in *Therm-1D – Evaluation Procedure*. This is because it is necessary to take into account the contribution of wall cooling given by the dilution, which cannot be done by the correlation used for estimation proposed by *L'Ecuyer* [39]. Before this was done by imposing the adiabatic effectiveness that included the two effects (effusion/dilution).

It is possible to see in Figure 4.40 and Figure 4.41 the trends predicted by Therm-1D for the adiabatic effectiveness. Keeping in mind the simplification of the correlative one-dimensional approach, it is possible to conclude that the tool can predict the trend of the η_{ad} with good accuracy.

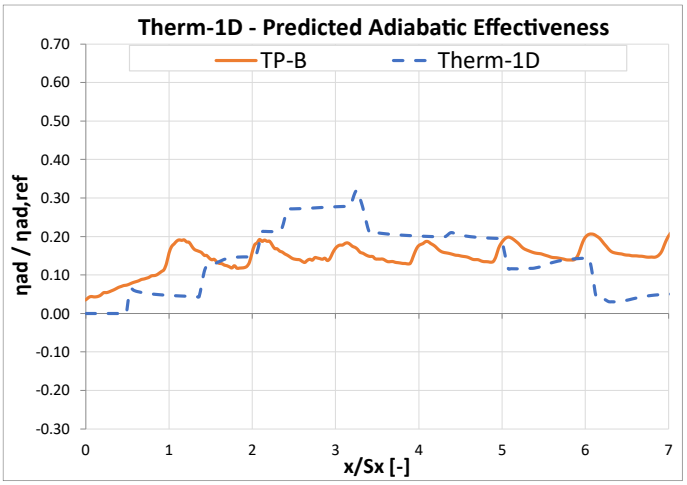

Figure 4.40 - normalized η_{ad} trend result for film effectiveness evaluation (TP-B)

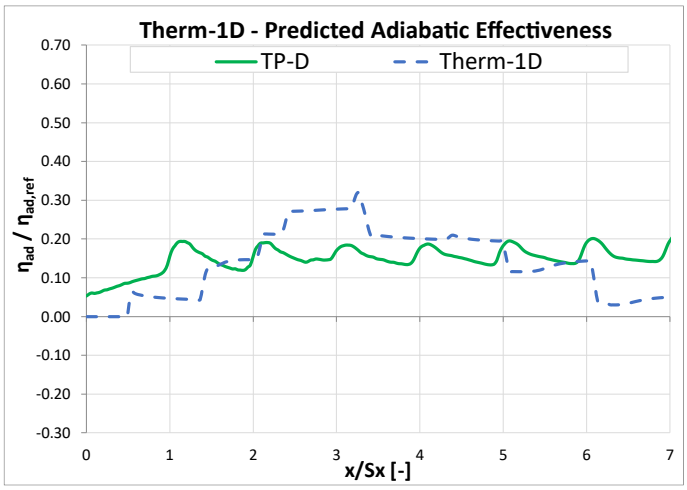

Figure 4.41 - normalized η_{ad} trend result for film effectiveness evaluation (TP-D)

Sensitivity analysis on the gas side discretization parameters

This last paragraph will analyze how the discretization used for the Therm-1D gas side one-dimensional trends can affect the predicted metal temperatures. The two parameters that have been analyzed are the investigation region height and the number of points (and therefore the planes normal to the streamwise direction).

This investigation has allowed a better understanding of how these two parameters influence the behavior of the tool and, through the Sobol indexes, what is their real influence on the T_w predicted along the effusion plate.

As a result, there will be a consistency assessment of the assumptions and a guideline on the most correct choices in presence of a cooling system based on effusion and dilution holes.

Uncertainty quantification analysis was performed for TP-B.

Setup

The *Therm-1D/Dakota* coupled procedure, already introduced, was used for the evaluation. Two uncertain variables have been considered (previously described in the paragraph *Interpolation zone for Therm-1D*):

- The number of planes normal to the streamwise direction
- The height scan interval

The distributions characteristics imposed for the variables are summarized in Table 4.18.

	Upper Lim.	*Lower Lim.*	*Distrib.*
Height	100%	5%	Uniform
N. Planes	500	50	Uniform

Table 4.18 - UQ Variables probability distributions

How these two quantities affect the tool response directly affects the importance of the appropriate zone selection for the definition of convective heat transfer. At the same time, it will have an impact on how this

should be discretized in the direction of the flow for the definition of the one-dimensional distributions to be imposed in Therm-1D.

For the two parameters, a uniform distribution has been chosen, because none of the values should be associated with a higher probability, as also proposed by *Durocher et al.* [63]. Additionally, this was done to avoid influences on the sampling performed by the Dakota tool. For the uniform distributions,

The surrogate model has been utilized, obtained with a number of evaluations reduced by stochastic expansion, to perform an additional LHS sampling of 1000 points, to obtain the same sample size that would be possible with the MC method.

The obtained Sobol indices were analyzed. These indices define the incidence of each uncertain contribution to the studied output magnitude [226]. For this analysis, the Total Sobol indices have been used, because they define how much the variability of an uncertain parameter affects the response of the system, but also how this affects the other uncertain variables. This choice is necessary to have a clearer understanding of the results obtained.

Sensitivity Results

The evaluation required nine samples. Figure 4.42 shows the maximum, minimum, and mean trends determined by the Stochastic evaluation. It also shows the best temperature distribution determined in the previous analysis for TP-B (25% chamber height), indicates in the graph as *TP-B/25%*.

The *TP-B/25%* trend is entirely contained in the range of variability calculated for the T_w. It should be emphasized that this trend can be considered comparable to the average distribution determined by Dakota.

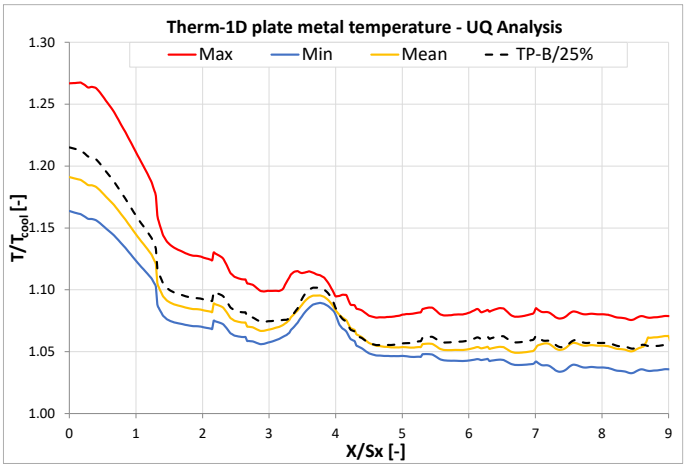

Figure 4.42 - TP-B - Therm-1D plate metal temperature - Sensitivity Analysis (Max, Min, Mean trends)

This result should enhance the reliability of the choices made for the definition of the inputs.

Figure 4.43 shows the sensitivity analysis in histogram format. This allows defining Sobol indexes trend along the plate.

The behavior is recognizable in 3 main zones:

- *x/Sx* < 3 (primary zone): upstream of the dilutions, here there is a substantial balance between the two variables

- $3 \leq x/Sx \leq 5$ (dilution interaction zone): the most important parameter is the number of planes used for the discretization
- $x/Sx > 5$ (downstream the dilution holes): here prevails the plane heigh parameter

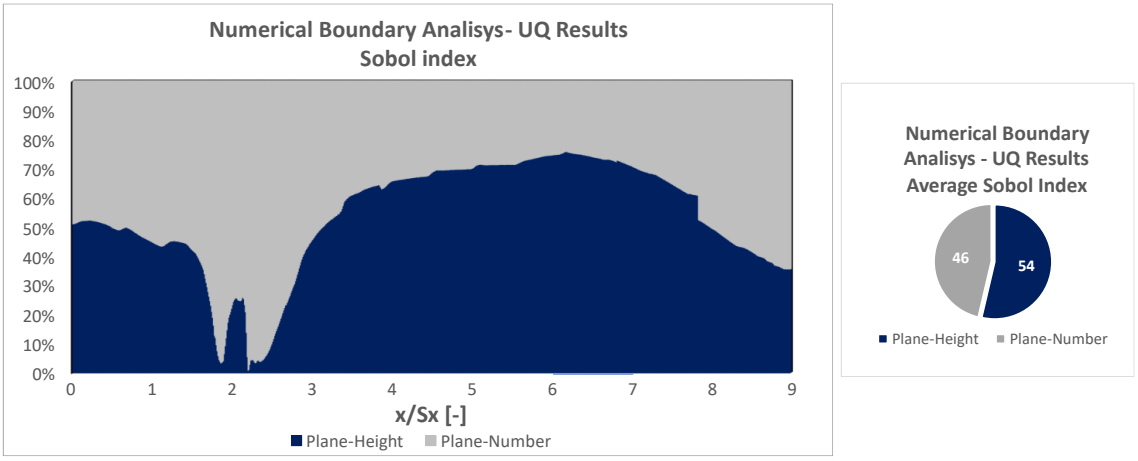

Figure 4.43 - TP-B - Sobol Index Distribution and Average Values

Analyzing more closely the results obtained, two further considerations can be made:

- The result obtained for the dilutions interaction area makes it clear how to properly describe the phenomena that operate here. The number of points that will represent the zone is the main parameter. Such result is also supported by the effective dilution height extension across the chamber, as is shown in Figure 4.18.
- The trends obtained for $x/Sx > 5$ highlights how fundamental is the choice of the height for an accurate definition of the mixing zone for the effusion cooling system

Finally, evaluating the average Sobol indices values obtained for the two uncertain variables, it is concluded that there is a slight predominance in the effect of the region height.

Remarks

The UQ analysis has shown the reliability of the choices made for the definition of the hot gas side input magnitudes region. This is confirmed by the distribution reported for TP-B (*TP-B/25%*), which is the optimum.

The average Sobol indexes showed that there is a slight prevalence of the parameter that defines the region height. However, three zones can be identified. The most important result is obtained for the dilutions interaction zone. Here the discretization accuracy has more importance (with 95% peaks) than paying attention to where the mixing process is completed. The experience matured with this analysis could then be applied to future evaluations.

Final Remarks

The test rig considered for this analysis is part of the European project SOPRANO. The model reproduces in a 1:1 scale five sectors of a typical RQL combustor architecture where the multiple-injector configuration

allows the reproduction of the periodicity conditions in the primary zone. The component of greatest interest for the study was the inner plate that represents a part of a multiperforated liner. Before the inner plate, a slot system was equipped to generate film cooling in the initial part of the liner. The effusion plate presents a constant hole streamwise/spanwise pitch to diameter and it was manufactured using metal additive technologies, with effusion holes realized employing the laser drilling process.

The related experimental tests used in this work were carried out with InfraRed thermography and Pressure-Sensitive Paint (PSP). The tests were performed at different pressure drops across the swirlers and varying the mass flows of the slot and through the inner/outer liners. Since the test case is not reactive, this confines the analysis made only to the convective heat transfer phenomena.

RANS CHT simulations with a strongly coupled method were performed to understand the interaction of the swirling flow with the cooling system, and how the cooling performances are affected by the main flow. To distinguish the various effects associated with the slot, the dilutions, and the effusion, a numerical analysis has been performed introducing four additional transport equations for four different passive scalars (representing the experimental CO_2 coming from the different secondary inlets).

In this Therm-1D application, a feature was used that allows imposing as input the one-dimensional streamwise distribution of adiabatic effectiveness. It was used the one obtained for the various test points from PSP, mediated in the spanwise direction. In this way, the cooling system modeled by the tool worked with the same performance as the one tested in the laboratory. Under these conditions, the present study has made possible to define the region on which the Therm-1D gas side input quantities are averaged from RANS results. Considering that the convective heat transfer to the wall is conditioned by the presence and performance of the effusion jets, it has been assumed to determine the region, near the plate, where the process of mixing and the convective heat transfer develops.

For the first two TPs studied, having the same BCs, the conclusion was that the best agreement between the values predicted by the tool and the thermography trend was achieved by taking, on the hot gas side, a region above the effusion plate corresponding to 25% of the total chamber height.

Based on what *Bogard* [221] said, the Normalize Temperature definition was equivalent to that of η, but also this value represents a measure of the coolant jet mixing with the mainstream. So, it has been assumed to consider the region above the plate in which the decay of the *scalar-E* (identifies the mass fraction of coolant originating from the effusion holes) was very high. This allows taking into account the whole mixing region. Here, the Therm-1D hot gas side input magnitudes have been averaged from numerical simulation post process. This allowed considering all those thermo-fluid-dynamic phenomena necessary for a proper one-dimensional characterization of the combustor chamber flow field. This relationship has been assumed and verified with two other TPs with different BCs. It has been determined a relationship that allowed taking as a fundamental parameter the coolant mass fraction tracer coming from the effusion holes. This relationship led to the definition of the reference region for the determination of the gas side one-dimensional trends for the Therm-1D inputs.

The 95% reduction of the scalar represents the target.

To avoid using experimental data as input, the idea was to use the tool with the chamber side quantities previously obtained to verify if it could determine the cooling system effectiveness that was comparable to

that obtained experimentally. The results showed that the tool can predict the trend of the η_{ad} with reasonable accuracy.

Finally, a UQ analysis for the discretization parameters has been carried out. The sensitivity analysis has shown the reliability of the choices made for the definition of the zone. The Sobol indices highlighted the importance of the two parameters studied. This has allowed a better understanding of the importance of both the width of the region and the plane's number used for discretization.

Chapter 5

Air-Cooling Feasibility Assessment for Rotating Detonation Combustor

Introduction

In the continuous search for a technology to overcome the efficiency limitations found by conventional constant pressure combustion systems, rotating detonation combustors (RDCs) have emerged as one of the most promising pressure gain combustion (PGC) devices available. In an RDC, a self-sustaining, continuous detonation wave propagates around a closed-loop combustion chamber (typically an annulus), which is constantly supplied with reactants. The pressure gains through the leading shock of the detonation wave more than compensates for the pressure drop through the reaction front, leading to a net increase in pressure. This creates less entropy than isobaric combustion and leading to a substantial theoretical gain in thermal efficiency [227]. There is the potential to increase further the substantial performance gains made by the pulsed detonation engine concept over the traditional constant-pressure cycle-based propulsion engines by moving from “pulsed” or “periodic” detonations to a more “continuous” mode of operation with detonations [97]. Therefore, the RDE concept [97,228–230] can lead to several advantages for propulsion providing a much steadier output than previous pulse detonation engines and in a more compact package than axial combustors [106]. Moreover, the RDE can provide an almost steady source of thrust, without having to start a detonation at very high frequencies.

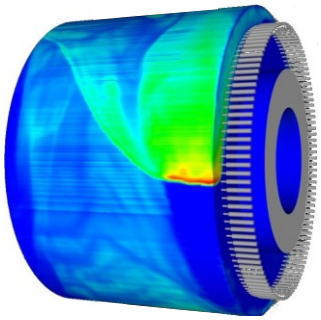

Figure 5.1 – RDC Detonation spin wave [*95*]

On the other hand, the RDE has its own challenges. As stated by *Kailasanath* [95], due to the detonable mixture is injected axially and the detonation wave runs circumferentially around the combustion chamber, the flow field within an RDE has both very strong axial and azimuthal components, which makes the analysis of the engine more complex and an efficient design potentially more difficult to develop.
The most important issues in RDCs comes from the complexity and high frequency of the flow field inside the combustion annulus, as well as the continuous presence of a detonation wave in the combustion chamber. These are further complicated by the current lack of bypass flow and the large area to volume ratio. These issues cause the surrounding structures to absorb more heat than an axial combustor. As a result, most laboratory RDEs operate for only a few seconds.
This means that control of this thermal load is necessary to allow this innovative type of combustor to operate for longer times (currently within 0.5 to 3 seconds). These aspects lead to the problem of heat fluxes to the combustor walls, how to measure them, and how to ensure a proper cooling layout to prevent system failures during experimental runs.

Unfortunately, the peculiar operating conditions of RDCs make the development of an effective cooling system challenging. The main factors behind these issues are as follows:

- Pressure of cooling air (usually blown from the compressor) lower than the one of the gases in the combustion chamber. Due to this fact, it not feasible to use solutions with film cooling or effusion cooling
- Detonation can only be initiated and sustained by using stoichiometric mixtures and therefore with the highest values of laminar flame speed. This results in very high flame temperatures
- If hydrogen is used as fuel, temperature peaks approach 3000K

With these conditions and limitations, the only cooling systems that can be used for the purpose are convective cooling systems. These cooling systems have already been examined in the section *Convective cooling system arrangements*.

Since this is still in the early stages of studying air cooling systems for RDCs, the design parameters were assumed or approximated, making the use of advanced investigation solutions (such as CFD simulations) not very useful. There is a need for a simplified tool to easily and quickly investigate different design solutions to identify the best layout.

In this work, an heat transfer problem analysis and an assessment of air cooling feasibility for Rotating Detonation Combustors have been done. Starting from boundary conditions assumed from the literature review, heat fluxes per surface unit relative to the detonation zone were evaluated with a one-dimensional model using conduction and convection relationships.
Due to these results from the first analysis, once a maximum temperature limit has been imposed according to the material used for the construction of the combustor at the *energy laboratory of the department of fluid dynamic at Berlin Technische Universitat*, it has been possible to identify a working region in terms

of heat transfer coefficient in which it is necessary to work to cool properly the operating combustor (Figure 5.2).

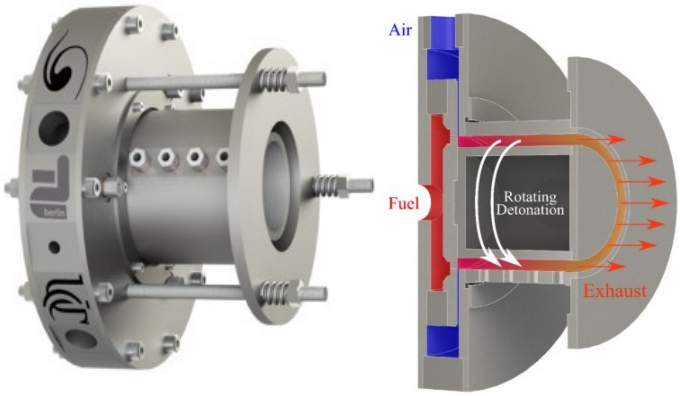

Figure 5.2 - TU Berlin's RDC Test Rig [231]

Thus, with *Therm-1D/Dakota* procedure, different air-cooling system fluid network layouts were modeled and their performances have been evaluated varying the characteristic parameters of every solution adopted, to highlight what are the main influencing aspects relative to each heat transfer augmentation solution.

Once that these parameters have been found, an Uncertainty Quantification and Sensitivity Analysis has been performed to evaluate how the variation of each one of them, singularly and overall, could affect cooling system performances. From these analyses it has been possible to build several operational maps that show the behavior of the different tested layouts, giving a guideline to possible improvements in the cooling system design operations.

So, it has been possible to study different layouts behavior, giving useful guidelines to keep eventually in mind for further study, design, and implementing phases of an air-cooling system for this new and promising technology.

Test Rig

The test rig used in this work is the 90 mm outer diameter combustor developed at TU Berlin [231] based on the one used by the *US Air Force Research Lab* (AFRL) [232]. This combustor, shown in cross-section in Figure 5.3, utilizes a radial-inward configuration for the combustion air, injecting into the combustion annulus through an injection slot 1 mm in height. Fuel (F) is injected through 100 discrete fuel injection holes with a diameter of 0.5 mm. These fuel injection holes are evenly distributed around the perimeter of the outer wall of the combustion annulus, oriented tangentially to the outer. The oxidizer (O) is injected radially inward through a continuous slot at the base of the annulus with an outer diameter of D = 90 mm, as indicated by the blue arrows. Here are used compressed air as oxidizer and hydrogen as fuel.

Reactant injection pressures are variable, up to approximately 12 bar and 25 bar for the air and fuel injection, respectively. Two electronic pilot regulators together with dome-loaded pressure regulators allow for fast and reproducible control of the reactant mass flows. After injection, fuel and oxidizer mix in a jet-in-crossflow situation, as sketched in the zoomed view to the left of the RDC cross section in Figure 5.3. In the standard configuration the fuel injection holes are oriented tangentially to the annulus outer wall. Depending on the local blowing ratio, impingement of the fuel jets on the oxidizer slot wall is expected to change the mixing scheme.

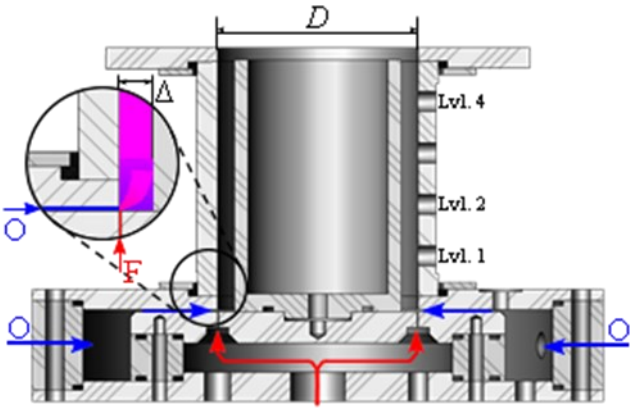

Figure 5.3 - Cross section of the RDC at TU Berlin [231]

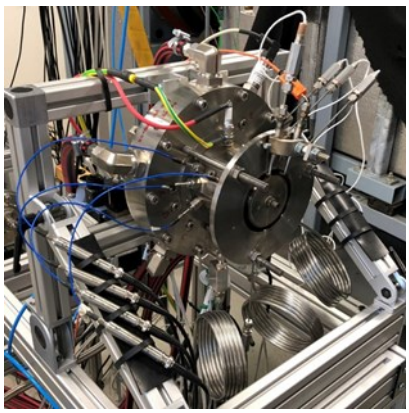

Figure 5.4 - instrumented test rig at TU Berlin [233]

Since the RDC is uncooled, tests are limited to short duration (usually around 150 ms [233]) and purge air flow allows for cooling of the combustor between runs. At the start of each test run, first the oxidizer flow rate is ramped up to a target value. Shortly afterwards ($\Delta t < 1$ s), the fuel flow rate is ramped up to a corresponding target value, simultaneously opening the solenoid ball valve upstream of the RDC fuel plenum. Following reactant flow rate stabilization ($\Delta t < 1$ s), the RDC is ignited using an automotive spark plug flush-mounted in the annulus outer wall close to the base of the annulus.

The outer body of the RDC is equipped with multiple instrumentation ports distributed both circumferentially and axially that can host a variety of sensors, as showed in Figure 5.4.

Boundary condition evaluation

As already mentioned, the first step, in agreement with the cited works about heat fluxes estimations [79,101–105] (reported in *Rotating Detonation Combustion*), was to realize a simple one-dimensional model, that was created to predict the heat fluxes from the combustion annulus to the combustor walls according to applied boundary conditions. It will be useful for the assessment of an air-cooling system needed to remove heat from RDC walls and keep it cooled to achieve longer test durations.

The model has been realized starting from the actual combustor geometry in the *Laboratories at TU Berlin* (Figure 5.2). The device is composed of a central body and an outer body that create the combustion annulus. The outer body presents several longitudinal features for instrumentations. Both the bodies are fixed on the injection plate, in which the plenum spaces are located for both fuel and oxidizer. The detonation is initiated by a pre-detonator.

The model is built to identify a proper operating condition zone for heat transfer coefficient on the cold side in which it could be possible to work without the risk of mechanical or thermal failures, mainly caused by the uncontrolled heat fluxes from the reaction zone to the combustion annulus, preventing damages to the walls subject to a long exposition to high thermal fluxes.

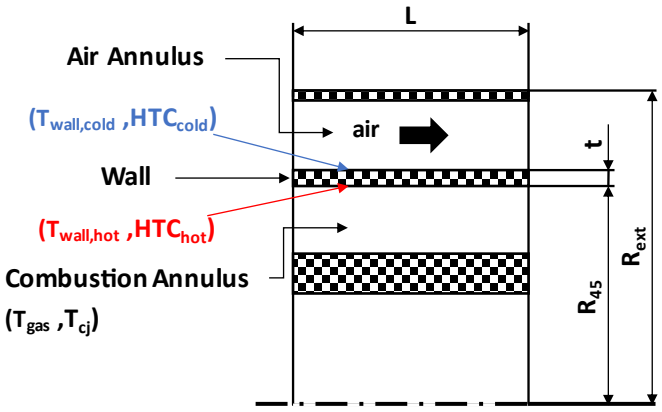

Figure 5.5 - RDC geometry scheme with the main interest parameters

According to the test facility geometry, a simple scheme with the main interesting parameters has been created, including a second annulus, for the coolant passage (Figure 5.5).

The simple 1-D model is based on the heat transfer relationships for convection and conduction:

- The convective heat transfer for the gas side (hot side)
- The convective heat transfer for the coolant side (cold side)
- The heat conduction through the outer wall, which is the main heat transfer process

The three unknowns of the system are $T_{wall,hot}$, $T_{wall,cold}$ and $\dot{Q}$. $T_{wall,hot}$ represents the temperature of the inner wall of the outer body, which is directly exposed to the flame front. $T_{wall,cold}$ stands for the temperature of the outer wall of the outer body, wetted by the coolant. The system is assumed to be at thermal equilibrium, so the three heat fluxes values must be coincident. $\dot{Q}$ is the heat flux.

To build the model it was necessary to make some assumptions and to set some boundary conditions. According to a literature review, some values were imposed and used for the realization of the numerical model:

- λ_{wall} , the thermal conductivity of the wall, assumed initially constant, equal to 16.2 W/mK for the used material (AISI 316L)
- $T_{in,coolant}$, coolant inlet temperature, assumed equal to 300 K
- $T_{wall,HOT}$ established less than 1200 K which is the AISI 316 structural limit, as reported in [234]
- t, wall thickness, assumed equal to *3 mm* to obtain a more feasible range of HTC_{COLD} from the evaluation
- HTC_{HOT}, heat transfer coefficient of the hot side (the inner side of the outer body), assumed within a range of 500-2000 W/m^{2}K, according to the works of *Roy et al.* [105] and *Randall et al.* [235]
- HTC_{COLD} limited to a maximum value of 10000 W/m^{2}K, according to a more realistic value that is possible to obtain with an air-cooling system.
- T_{gas} assumed as a portion of T_{CJ}[1], according to Randall et al. [235], with a range between 2000÷2500 K
- $\dot{Q}$ assumed in a range within 1,0 ÷2,0 MW/m^2, according to mean heat flux values from the literature

The most important within these assumptions are those for T_{gas} derived from the observation of the rotating detonation phenomena. Considering detonation high spin frequency, a wall measuring point is exposed at T_{CJ} only for a short time. The remaining time in which the detonation travels around inside the annulus, the same point is exposed to several other conditions: the burned products, which are at a sensible lower temperature compared to the *CJ* temperature, and the injection of fresh reactants, which even act as coolant according to the considerably low injection temperature compared with the higher temperatures that the annulus can reach. According to these assumptions, the cited gas temperature range was set.

Results

The first run of the model was done to estimate potential upper limits to heat transfer coefficient and heat fluxes reached in the detonation zone, giving a first evaluation of them. Imposing a value for *t*, λ_{wall}, a given range for $HTC_{HOT}$and investigating a wide range for HTC_{COLD}, the first run of the model has been conducted. As it can be seen from the results reported in Figure 5.6, a map of heat flux as a function of the heat transfer coefficient variation on both the hot and cold sides was created for an assumed starting value of the gas temperature in the detonation zone. Figure 5.6 shows the same heat flux diagram from different angles. As can be seen from the view on the right, different heat flux curves are reported, one for every considered gas temperature within the range of 0.5÷1 T_{CJ} equal to 3887 K according to CEA software by NASA.

[1] *Chapman-Jouguet Temperature, temperature reached in the detonation front, which is at Chapman-Jouguet conditions. T_{CJ} is evaluated thanks to CEA software by NASA, assuming a H_2O_2 stoichiometric mixture, at injection conditions of T=300 K and p=3 bar),* ***https://www.grc.nasa.gov/WWW/CEAWeb/***

Results show good agreement with literature for heat flux maximum up to 6 MW/m^2 and mean values around 2 MW/m^2, reaching peaks comparable with those registered from other researches with experimental tests and advanced numerical simulations [79,99,104,106–111,113–116,235]

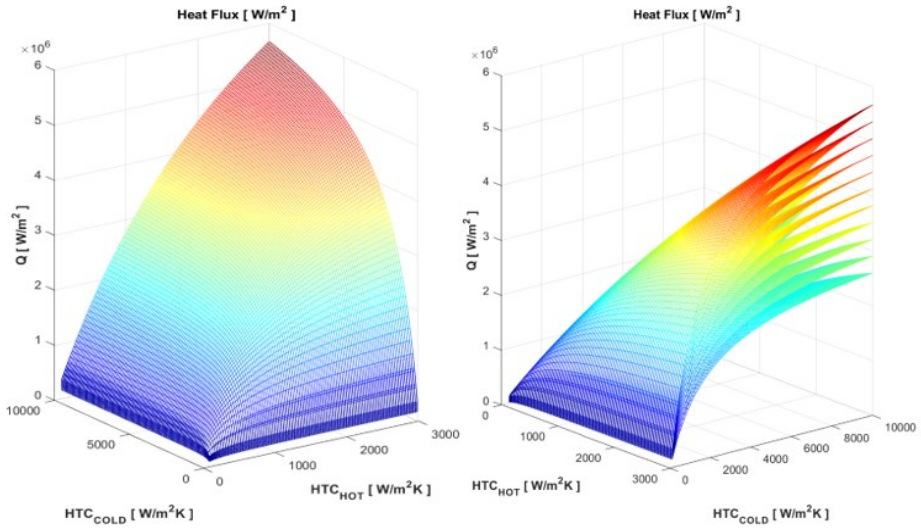

Figure 5.6 - Heat fluxes curves from the first evaluation

Due to the large gas temperature range (approximately 2000 K wide), some restrictions were necessary to refine the focus and reduce the range of values:

- To prevent the material from reaching the limit temperature and causes device failures, a limit value for the wall temperature was imposed to 1200 K
- Gas temperature was scaled down to a restricted range within 2000 and 2500 K
- Heat flux considered within 1.0 and 2.0 MW/m^2

With these assumptions, another evaluation with the model for heat fluxes was performed, looking for a restricted range of values to be investigated to evaluate the feasibility of an air-cooling system. This time the considered heat fluxes limits were reported too, as shown in Figure 5.7. As in the previous case, different curves were obtained, one for every considered gas temperature.

Examining the intersection between the heat flux curves and the planes that represent the heat flux considered limits, it is possible to identify the region for heat transfer coefficient for the hot side and cold side where it is recommended to operate in order to remove the desired amount of heat. In this way, the heat flux curve and heat transfer coefficient region were identified.

From the model, it is possible to evaluate the curve of $T_{wall,HOT}$ limit as a function of the considered ranges for HTC_{HOT} and HTC_{COLD}, for a given T_{gas}. Thus, it has been possible to identify the operative region located between the two considered heat fluxes and, from that, the heat transfer coefficients combination needed to respect wall temperature and heat flux limit conditions imposed.

As shown in Figure 5.8, assuming a heat transfer coefficient of 1500 W/m^{2}K, to keep the liner properly cooled it is recommended to operate with a heat transfer coefficient on the cold side higher than 3000 W/m^{2}K, a value not impossible to obtain with convective air-cooling systems, but a proper fluid network layout needs to be built and evaluated.

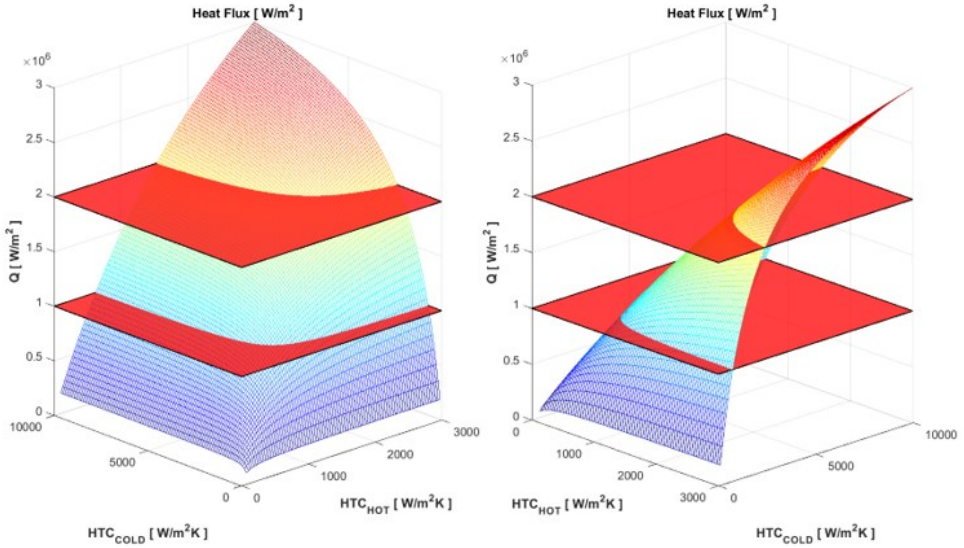

Figure 5.7 - Heat fluxes curves from the second evaluation

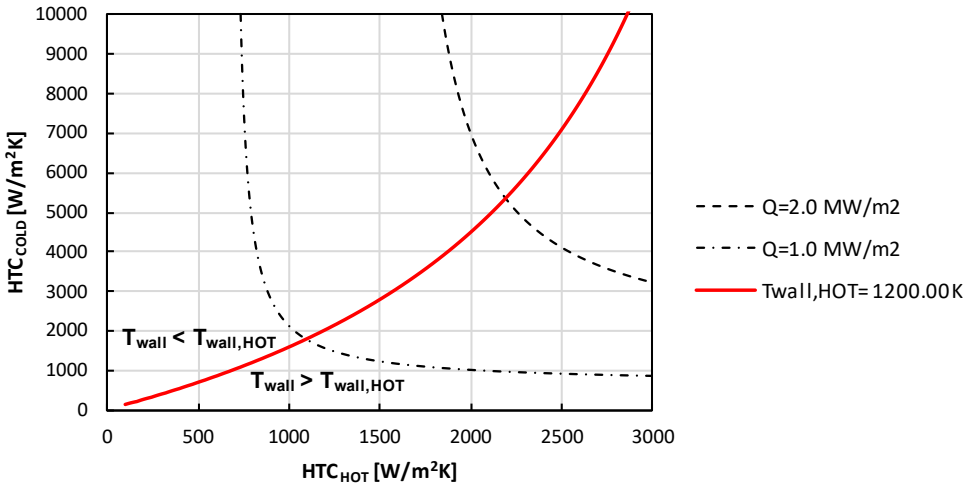

Figure 5.8 - Operative region

Cooling system assessment

The design of a proper cooling system that can allow longer test durations, facilitating studies of the combustor's steady state working conditions. According to the previous assumptions, a high value of the convective heat transfer coefficient is required on the external wall of the combustor's outer body to keep it properly cooled. In this work, internal cooling methods should be adopted according to the annular layout proposed and the thermo-fluid dynamic conditions of a rotating detonating combustor.

The main cooling configurations that will be used are those already introduced in the paragraph *Convective cooling system arrangements* of the ***chapter 2***: impingement and turbulence promoters such as Rib, Pin-fin, Dimple.

Boundary conditions for Therm-1D

In addition to those previously determined, some other boundary conditions need to be specified to make the analysis as realistic as possible even keeping in mind the low order analysis limitations. The most important ones are the hot gas heat transfer coefficient and temperature distribution. Some values have been assumed to evaluate heat transfer problems under supposed *medium-high* stressing operating conditions due to the ranges considered from the literature [79,99,104,106–111,113–116,235].

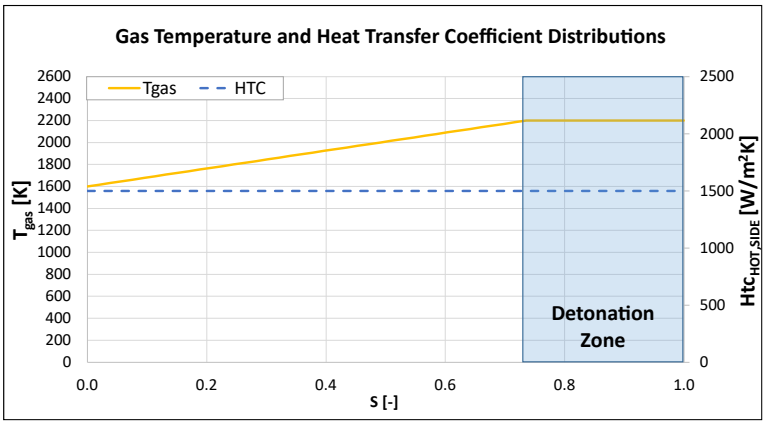

Figure 5.9 - Hot side T_{gas} and HTC distributions

In the Therm-1D hot gas side input parameters, a temperature profile has been set, according to the rotating detonation phenomenon. Referring to *Schwer & Kailasanath* [236], the detonation wave height was assumed equal to 30 mm and a constant temperature was imposed for the whole height. The chosen values are T=2200 K for the detonation region and a linear decreasing temperature distribution down to T=1600 K as discharge temperature, according to *Nordeen* [237] and *Braun et al.* [238] works. For the heat transfer coefficient, a value of 1500 W/m^{2}K was assumed for the whole gas region. The two trends are shown in Figure 5.9.

Another important aspect was to set the conductivity of AISI 316, to properly consider its changes with increasing temperature. A correlation for the desired range can be found in [239]. Air annulus outer liner, or casing, was assumed adiabatic to eliminate its contribution to heat transfer. In this way, it was possible to quantify the amount of heat transferred only from the outer wall of the combustion annulus.

As already defined Therm-1D procedure also requires the definition of coolant inlet conditions to evaluate cooling system thermal performances. Starting from the real conditions of the actual combustor in the *Laboratories at TU Berlin*, the following coolant parameters were set:

- Inlet pressure = 8 bar
- Inlet temperature = 543.3 K (evaluated from compressor outlet conditions assuming η_{is} = 0.95, P_{air} = 1 bar and T_{air} = 293.15 K).

Other important layout parameters for the fluid network are the geometry of the liner and the coolant channel:

- Liner inner radius = 48 mm
- Liner thickness = 3 mm

- Liner length = 110 mm
- Coolant channel height = 4mm

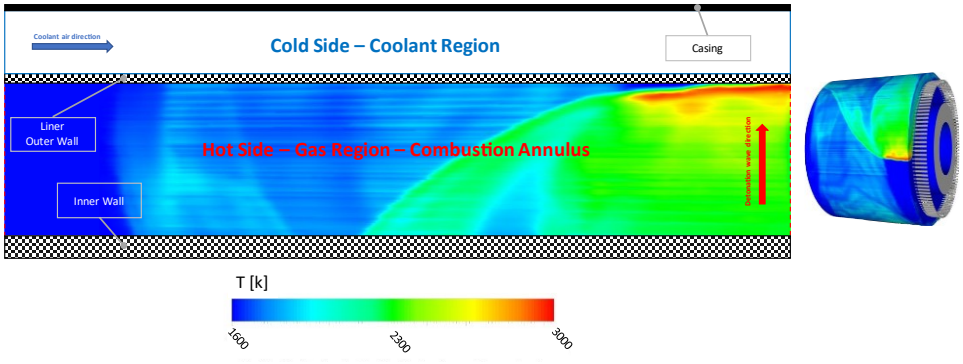

Figure 5.10 - Fluid network modelling *RDC*

Different channel heights were investigated with the Therm-1D procedure to finally establish the value of 4 mm, which grants a flow section large enough to allow reasonable pressure losses and at the same time small enough to get sensible heat transfer coefficient enhancement thanks to the presence of turbulence promoter.

Figure 5.10 shows that the analysis was conducted on a reverse flow layout. In this layout, cooling air flows from the combustor outlet to the injection plate and it can be used as mixing fluid to prepare the mixture once that it has been injected inside the combustion chamber with incoming fuel, which comes from a separate injection plate.

Single Configuration

After heat fluxes evaluation, once that a restricted operating condition zone has been identified, the next step is to verify if a single configuration cooling system layout could be able to cool properly the combustor liner. Cooling system performances have been evaluated varying the geometric parameters of every solution adopted. This in order to highlight what are the best configurations and the main influencing aspects relative to each heat transfer augmentation solution. The analyzed parameters were chosen according to *Bunker* [7]. Once these parameters have been evaluated a Sensitivity Analysis has been performed, to determine how the variation of each one of them could affect cooling system performances.

In this phase, a *DOE* has been realized for the main geometrical parameters of each cooling configuration to understand how these variations influenced the output magnitudes and therefore the performances of the cooling system.

Moreover, the Reynolds number has been investigated for every single configuration in the DOE. Its range of variation goes from 20000 to 130000. From the DOE results, it has been possible to build several operational maps that show the behavior of the different tested configuration.

As different types of heat transfer augmentation systems have been investigated, for the comparison the Reynolds number was defined based on the hydraulic diameter of the cooling duct and considering the air

velocity at the outlet of the cooling system. This is in order to have a univocal and valid definition regardless of the cooling scheme.

More than *25000* simulations with Therm-1D were required to complete the *DOE* on single cooling system configurations. This fact highlights that in the preliminary design phases, when a very deep design space needs to be explored, the use of low order tools and/or coupled procedures such as *Therm-1D/Dakota* is necessary.

Used layouts

For the performance estimation of the cooling system the used cooling configurations are:

- Smooth cylindrical tube
- Ribbed cylindrical tube
- Dimpled cylindrical tube
- Pin-finned cylindrical tube
- Jet impingement

Performances of every one of them have been investigated singularly to obtain the most efficient solution in terms of hot wall temperature profile, according to relative pressure drop.

The correlations used by Therm-1D for the layouts under investigation are reported in *Appendix A*.

Smooth

This layout was the baseline for the comparison. The Reynolds number was the only parameter evaluated, as reported in Table 5.1. The heat transfer coefficient is derived from the Nusselt number, estimated from the used correlation. The most used is the *Dittus-Boelter* [240] equation, where the Nusselt number depends on the Reynolds and Prandtl number, and it's typical for smooth cylindrical tube layouts. For the pressure drop, it was used the one proposed by *Blasius* [241].

Reynolds Number										
20000	30000	40000	50000	60000	75000	90000	100000	110000	120000	130000

Table 5.1 - Reynolds number test matrix

Ribbed

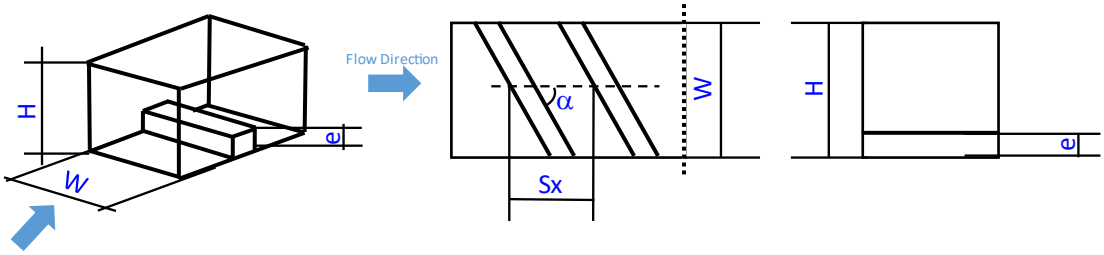

Figure 5.11 - Rib main geometric parameters

In this case, in addition to the variation of Reynolds, the main geometric parameters (reported in Figure 5.11) have also been studied:

- Rib inclination angle (α)
- Rib eight to Hydraulic diameter ratio (e/D_h)

Ribs		
e/D_h	S_x/e	α
0.0125	5.0	30
0.0375	6.5	45
0.0625	10.0	60
0.0875	12.0	75
0.1125	15.0	90
0.1375	18.0	-
0.1625	20	-
0.1875	-	-

Table 5.2 – Ribbed configuration test matrix

- Streamwise rib pitch to rib eight ratio (S_x/e)

The test Matrix is shown in Table 5.2.

All possible geometric combinations have been realized with this set of parameters.

In this case, the used correlations for the heat transfer coefficient and pressure drop evaluation are those of *Han* [242–244].

Dimpled

The main geometric parameters (shown in Figure 5.12) studied are (Table 5.3):

- Dimple depth to dimple diameter ratio (e/d_d)
- Streamwise dimple pitch to dimple diameter ratio (S_x/d_d)
- Spanwise dimple pitch to dimple diameter ratio (S_y/d_d)

Dimple		
e/d_d	S_x/d_d	S_y/d_d
0.1	5.0	5.0
0.3	10.0	10.0
0.5	15.0	15.0
0.7	20.0	20.0
0.9	25.0	25.0
1.0	30.0	30.0
1.1	35.0	35.0
1.3	40.0	40.0
1.5	-	-

Table 5.3 - Dimpled configuration test matrix

In this case, the used correlation for the heat transfer coefficient and pressure drop evaluation is the one proposed by *Kumar* [245] corrected by *Maithani* [246].

All possible geometric combinations have been realized with this set of parameters, and the variation of Reynolds was taken into account.

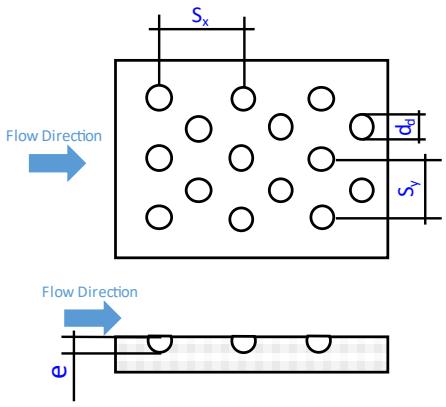

Figure 5.12 – Dimple main geometric parameters

Pin-finned

Pin-fin		
Z/d_d	S_x/d_d	S_y/d_d
2.00	1.5	2.0
1.60	2.0	3.0
1.33	2.5	4.0
1.14	3.0	-
1.00	3.5	-
0.89	4.0	-
0.80	4.5	-
0.73	5.0	-

Table 5.4 – Pin-finned configuration test matrix

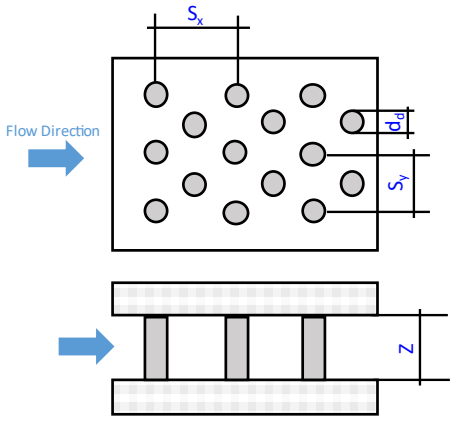

Figure 5.13 – Pin-fin main geometric parameters

The main geometric parameters studied are (Table 5.4):

- Channel height to pin-fin diameter ratio (Z/d_d)
- Streamwise pin-fin pitch to pin-fin diameter ratio (S_x/d_d)
- Spanwise pin-fin pitch to pin-fin diameter ratio (S_y/d_d)

All these are shown in Figure 5.13.

In this case, the used correlations for the heat transfer coefficient and pressure drop evaluation are those proposed by *Metzger* [247] and *Faulkner* [248]. The analysis was conducted in the same way as for the other layouts.

Jets impingement

The main geometric parameters studied are (Table 5.5):

- Channel height to jet hole diameter ratio (Z/d_d)
- Streamwise pitch to jet hole diameter ratio (S_x/d_d)
- Spanwise pitch to jet hole diameter ratio (S_y/d_d)

Impingement		
Z/d_d	S_x/d_d	S_y/d_d
1.0	5.0	4.0
2.0	6.0	5.0
3.0	7.0	6.0
4.0	8.0	7.0
5.0	9.0	8.0
6.0	10.0	-
-	11.0	-
-	12.0	-
-	13.0	-
-	14.0	-
-	15.0	-

Table 5.5 – Jets impingement configuration test matrix

All these are shown in Figure 5.14.

In this case, the used correlation for the heat transfer coefficient and pressure drop evaluation is the one proposed by *Florschuetz* [199]. The analysis was conducted in the same way as for the other layouts.

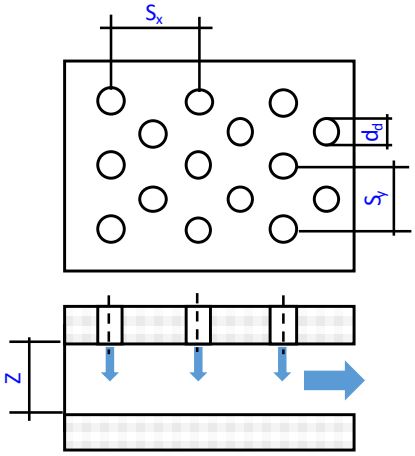

Figure 5.14 – Jets impingement main geometric parameters

Performance Parameters

Before proceeding to the analysis, some performance parameters are defined in this paragraph. This was done in order to be able to compare the efficiencies of the single layouts and determine, as a function of Reynolds, which are the best configurations for the aim.

$$\bar{\eta} = \frac{\left(\overline{T_{gas}} - \overline{T_w}\right)}{\left(\overline{T_{gas}} - \overline{T_{cool}}\right)} \tag{5.1}$$

The parameters chosen for the comparisons were: average metal temperature, average heat transfer coefficient, and averaged heat flux along the entire length of the liner. The same three parameters but this time evaluated only in the already defined detonation zone. An average thermal effectiveness is defined in Equation (**5.1**), while the relative pressure drops are defined in Equation (**5.2**).

$$\Delta p_R = \frac{P_{in,coolant} - P_{out,coolant}}{P_{in,coolant}} \tag{5.2}$$

These two parameters are in agreement with what Bunker reported in two of his papers [249,250]. It might be convenient to multiply the previously defined thermal effectiveness by the ratio between outlet pressure and inlet pressure from the cooling system, to take into account simultaneously both thermal efficiency and pressure drops. An additional parameter, global efficiency (η_{Global}) has been defined according to Equation (**5.3**).

$$\eta_{Global} = \frac{\left(\overline{T_{gas}} - \overline{T_w}\right)}{\left(\overline{T_{gas}} - \overline{T_{cool}}\right)} \cdot \frac{P_{out,coolant}}{P_{in,coolant}} \tag{5.3}$$

In this way, the global effectiveness would tend to unit value only for a cooling system that does not present pressure losses and in case $T_W = T_{cool}$. In the same way, the global effectiveness would tend to zero in case of high-pressure losses or if the T_W tends to T_{gas}.

Therefore, through this parameter, it was possible to check if the studied system is effective under both aspects: heat transfer and pressure losses.

Results

After the needed operating region for the heat transfer coefficient on the cold side has been identified according to input assumptions and after the definition of performance parameters, several fluid network investigations have been done to assess the performances and feasibility of a first-try single configuration air cooling system. Due to the preliminary phase of the assessment for RDCs air cooling, no proper guidelines were available. This results in a wide range of possible layouts that can be evaluated during the *DOE*. Using the *Therm-1D/Dakota* procedure, it has been possible to obtain a one-dimensional analysis of the heat transfer problem and an evaluation of performance variation.

The results obtained for each layout as a function of Reynolds are reported below, in various tables and graphs. This analysis aimed to define an optimal geometry for each cooling configuration.

The purpose was to determine if there was a layout for which these occur:

- $T_{wall} \leq 1200$ K
- $\Delta P/P_{in} \leq 10\%$

Comparisons were made primarily as a function of the η_{Global} defined in Equation (**5.3)**.

Smooth								
Re [-]	Q_{mean} [MW/m²]	HTC_{mean} [W/m²K]	T_{wall_mean} Detonation [K]	Q_{mean} Detonation [MW/m²]	HTC_{mean} Detonation [W/m²K]	η_{Ovr} [-]	$\Delta P/P_{in}$ [%]	η_{Global} [-]
20000	0.51	523.04	1810.87	0.58	544.01	0.252	0.17%	0.252
30000	0.63	701.10	1716.88	0.72	730.29	0.308	0.35%	0.307
40000	0.73	860.43	1645.26	0.83	896.77	0.350	0.59%	0.348
50000	0.80	1007.31	1589.07	0.92	1050.06	0.383	0.90%	0.379
60000	0.86	1145.01	1541.95	0.99	1193.58	0.410	1.26%	0.405
75000	0.91	1275.76	1501.94	1.05	1329.59	0.433	1.69%	0.426
90000	0.95	1400.87	1467.34	1.10	1459.70	0.453	2.18%	0.443
100000	0.99	1521.12	1436.71	1.14	1584.52	0.471	2.74%	0.458
110000	1.03	1637.71	1409.86	1.18	1705.43	0.486	3.36%	0.470
120000	1.06	1750.99	1385.82	1.22	1822.79	0.500	4.06%	0.480
130000	1.09	1861.83	1364.57	1.25	1937.59	0.513	4.83%	0.488

Table 5.6 - Results for smooth configuration

For the smooth layout (Table 5.6), it is visible that the heat fluxes, the heat transfer coefficients, such as η, as well as the pressure drops increase as the *Re* increases. On the contrary, the liner wall temperature decreases. These results depend on the increase of the coolant turbulence with the rise of the Reynolds number.

For the ribbed configuration (Table 5.7), all the best geometric layouts have two constant parameters. These

Rib											
Re [-]	e/D_h [-]	S_x/e [-]	α [deg]	Q_{mean} [MW/m²]	HTC_{mean} [W/m²K]	T_{wall_mean} Detonation [K]	Q_{mean} Detonation [MW/m²]	HTC_{mean} Detonation [W/m²K]	η_{Ovr} [-]	$\Delta P/P_{in}$ [%]	η_{Global} [-]
20000	0.19	5	75	0.89	1371.40	1389.51	0.99	1485.50	0.454	2.23%	0.444
30000	0.19	5	75	1.01	1761.75	1305.97	1.14	1877.48	0.505	4.82%	0.481
40000	0.19	5	75	1.10	2107.20	1248.64	1.24	2222.23	0.541	8.47%	0.495
50000	0.14	5	75	1.10	2057.12	1247.67	1.25	2147.57	0.535	6.30%	0.501
60000	0.11	5	75	1.12	2157.62	1230.26	1.28	2238.57	0.543	6.47%	0.508
75000	0.09	5	75	1.15	2240.04	1216.82	1.31	2312.83	0.550	6.37%	0.515
90000	0.06	5	75	1.16	2307.84	1206.25	1.33	2373.20	0.556	6.04%	0.522
100000	0.04	5	75	1.17	2354.62	1198.84	1.34	2412.13	0.559	5.48%	0.528
110000	0.04	5	75	1.20	2530.60	1178.37	1.38	2587.84	0.572	6.77%	0.534
120000	0.04	5	75	1.23	2700.63	1160.35	1.41	2757.44	0.584	8.24%	0.536
130000	0.01	5	75	1.22	3072.03	1166.12	1.40	3197.02	0.579	6.61%	0.540

Table 5.7 - Results for ribbed configuration

are $S_x/x=5$ and α=75°. The e/D_h parameter, also called *blockage ratio*, must decrease as the Reynold increases. In this way, the cooling system efficiency does not decay. This behavior minimizes the pressure drops. All heat transfer parameters are affected by this. This behavior is evidenced in the Reynolds transition from 120000 to 130000. Here there is a general reduction of the heat transfer capacity of the cooling system, and the metal liner temperature increases in the detonation zone. In this case, the overall effectiveness improvement is mainly due to the reduction of pressure drops by 1.5 percentage points.

In the dimpled configuration case (Table 5.8) there is total agreement on what is the best geometric layout to maximize global effectiveness. Indeed, all thermal parameters improve as *Re* increases. At the same time, there is an increase in pressure drops.

In general, it can be concluded that as *Re* increases, global effectiveness also increases.

In agreement with *Metzger* [247] and *Faulkner* [248], for the configuration with pin-fins as turbulence promoters (Table 5.9), as Re increases, the optimal geometric layout sees a reduction in the Z/d_d ratio and an increase in S_x/d_d ratio. There will be larger diameter pins, but more distant rows in the streamwise direction. In this case, the geometric layout prioritizes heat transfer rather than pressure drop control. It is found instead that $S_y/d_d = 2$ maximizes the global effectiveness for all flow conditions.

Dimple											
Re [-]	S_x/d_d [-]	S_y/d_d [-]	e/d_d [-]	Q_{mean} [MW/m²]	HTC_{mean} [W/m²K]	T_{wall_mean} Detonation [K]	Q_{mean} Detonation [MW/m²]	HTC_{mean} Detonation [W/m²K]	η_{Ovr} [-]	$\Delta P/P_{in}$ [%]	η_{Global} [-]
20000	5	15	1.3	0.49	871.46	1835.31	0.53	881.65	0.240	1.18%	0.238
30000	5	15	1.3	0.68	1274.77	1693.36	0.74	1280.39	0.330	1.79%	0.324
40000	5	15	1.3	0.82	1663.93	1580.61	0.91	1665.42	0.400	1.82%	0.393
50000	5	15	1.3	0.94	2036.53	1490.07	1.05	2046.54	0.455	3.11%	0.441
60000	5	15	1.3	1.04	2400.76	1416.46	1.16	2419.83	0.499	3.83%	0.480
75000	5	15	1.3	1.11	2758.47	1355.23	1.25	2786.75	0.535	4.60%	0.510
90000	5	15	1.3	1.18	3111.25	1304.68	1.33	3126.48	0.564	5.42%	0.534
100000	5	15	1.3	1.23	3459.87	1261.97	1.39	3484.56	0.589	6.29%	0.552
110000	5	15	1.3	1.28	3805.20	1225.51	1.45	3839.31	0.610	7.22%	0.566
120000	5	15	1.3	1.32	4147.01	1194.06	1.50	4190.44	0.628	8.22%	0.576
130000	5	15	1.3	1.35	4487.30	1166.71	1.54	4539.72	0.644	9.29%	0.584

Table 5.8 - Results for dimpled configuration

Pin-fin											
Re [-]	Z/d_d [-]	S_x/d_d [-]	S_y/d_d [-]	Q_{mean} [MW/m²]	HTC_{mean} [W/m²K]	T_{wall_mean} Detonation [K]	Q_{mean} Detonation [MW/m²]	HTC_{mean} Detonation [W/m²K]	η_{Ovr} [-]	$\Delta P/P_{in}$ [%]	η_{Global} [-]
20000	2.0	1.5	2.0	1.02	1255.35	1607.71	0.88	1304.52	0.569	6.35%	0.533
30000	1.6	1.5	2.0	1.13	1635.72	1500.28	1.08	1695.24	0.597	9.12%	0.542
40000	1.3	1.5	2.0	1.19	1973.12	1425.24	1.19	2040.88	0.611	11.14%	0.543
50000	1.1	2.0	2.0	1.19	2282.20	1368.65	1.26	2357.31	0.598	9.31%	0.542
60000	1.0	2.0	2.0	1.22	2571.35	1324.31	1.32	2653.25	0.604	10.42%	0.541
75000	0.9	2.5	2.0	1.21	2841.92	1287.15	1.36	2928.58	0.592	8.89%	0.539
90000	0.8	2.5	2.0	1.23	3101.19	1256.95	1.39	3193.63	0.596	9.62%	0.539
100000	0.8	2.5	2.0	1.26	3349.59	1231.23	1.43	3447.42	0.609	11.84%	0.537
110000	0.9	3.5	2.0	1.25	3589.41	1209.08	1.45	3692.31	0.601	10.85%	0.536
120000	0.7	3.5	2.0	1.24	3818.26	1189.39	1.45	3924.01	0.593	10.00%	0.534
130000	0.7	3.5	2.0	1.26	4041.61	1172.11	1.47	4150.93	0.602	11.76%	0.531

Table 5.9 - Results for pin-finned configuration

Table 5.10 shows the results for the jet impingement configuration. To maximize the overall efficiency, as the Reynolds in the duct increases, larger diameter impingement holes are required, with more holes per row and more rows. There is an improvement in thermal parameters as *Re* increases. At the same time, there is an increase in pressure drops.

These results are also shown in the graphs below (Figure 5.15) to compare all five configurations and the best layouts obtained as a function of the Reynolds number.

Jet Impingement											
Re [-]	Z/d_d [-]	S_x/d_d [-]	S_y/d_d [-]	Q_{mean} [MW/m²]	HTC_{mean} [W/m²K]	T_{wall_mean} Detonation [K]	Q_{mean} Detonation [MW/m²]	HTC_{mean} Detonation [W/m²K]	η_{Ovr} [-]	$\Delta P/P_{in}$ [%]	η_{Global} [-]
20000	6	15	8	0.94	868.58	1697.44	0.97	908.48	0.535	5.00%	0.508
30000	6	15	7	1.04	1111.97	1608.56	1.04	1147.18	0.561	8.86%	0.511
40000	4	9	8	1.07	1327.57	1542.84	1.08	1356.90	0.558	7.93%	0.513
50000	3	6	8	1.07	1524.61	1491.33	1.06	1550.19	0.546	6.35%	0.511
60000	3	6	8	1.13	1709.39	1448.43	1.12	1730.44	0.567	9.38%	0.514
75000	3	5	8	1.13	1884.17	1412.78	1.10	1899.81	0.565	8.68%	0.516
90000	3	5	8	1.17	2051.43	1382.32	1.15	2060.32	0.580	11.65%	0.513
100000	2	5	6	1.14	2212.44	1355.93	1.26	2212.91	0.560	9.09%	0.509
110000	2	5	6	1.17	2368.36	1332.85	1.29	2358.37	0.572	11.42%	0.507
120000	2	5	5	1.16	2520.04	1312.50	1.29	2497.16	0.566	10.86%	0.504
130000	2	5	5	1.19	2667.11	1293.96	1.32	2633.74	0.576	13.18%	0.500

Table 5.10 - Results for jet impingement configuration

The graphs in Figure 5.15 show that only the rib and dimple geometric layouts can achieve T_w lower than the chosen limit (1200 K). This happens, however, only for high *Re* (above 110000).
For all layouts, pressure drops are maintained below, or around, 10% (maximum limit value). Of course, it should be emphasized that this result is mainly due to changes in geometric layouts as *Re* varies. A worse result is obtained by impingement and pin-fin.

Thermal and global effectiveness differences are more significant at low Reynolds, while they tend to disappear at high values, probably because the flow turbulence becomes the main factor for the thermal heat transfer. Also, to avoid high pressure drops, the contribution given by the turbulence promoters geometry is reduced. One example is surely the reduction of the *blockage ratio* with the increase of the *Re* obtained for the ribbed configuration.

For the heat flux analysis, it turns out that the best systems are always the rib and pin-fin configurations. Dimple configurations recover the gap as the Reynolds increase, probably due to the effects already described.
It should be noted that the analyzed behaviors are closely related to the heat transfer correlations implemented in the Therm-1D procedure and already described. All the correlations are dependent on Reynolds and the analyzed geometric parameters. It is intended that by varying the correlation used the results obtained may be different. It is necessary to specify that some of the used correlations have a *Re* validity range lower than the one investigated.

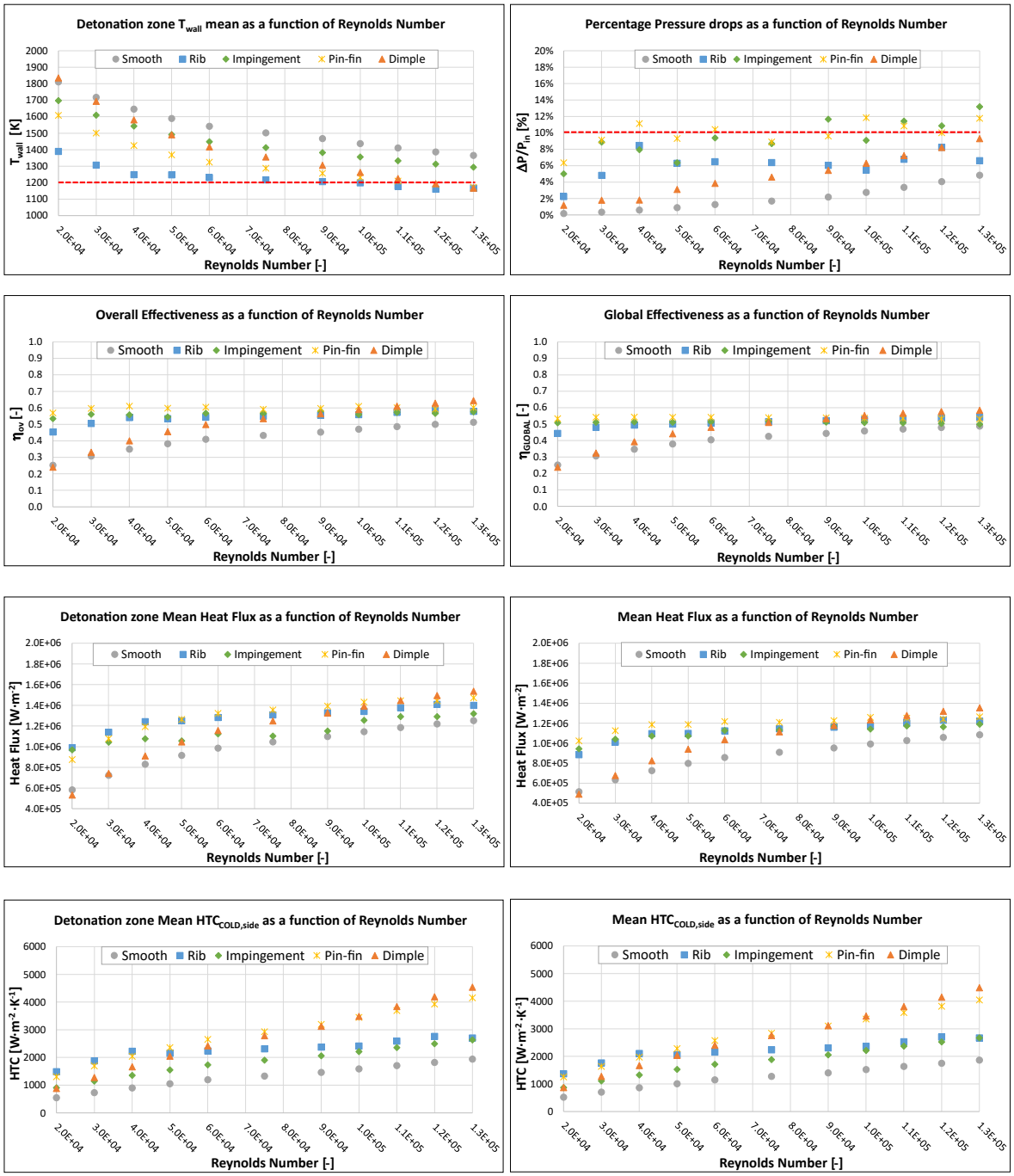

Figure 5.15 – Cooling system single best configurations comparison in terms of *Re*

Operational maps

From the *DOE* obtained results it has been possible to build an operational map, reporting the results from the different layouts investigation. The map shows global effectiveness as a function of the main geometric parameter and Reynolds number. This was done to make an easy and first quick evaluation of what could be the operative region relative to each one of the considered layouts. That will be useful for further studies in which an effective air cooling system for RDCs could be examined and properly designed.

Ribbed configuration

The contour of Figure 5.16 and Figure 5.17 show the operational maps for the cooling system in the ribbed layout. On the contour axes there are the blockage ratio (e/D_h) and the rib inclination angle to the flow direction (α). In Figure 5.16 the comparison was made with the same Reynolds (30000). While in Figure 5.17 with the same streamwise pitch to rib height ratio (the best one from *DOE*).

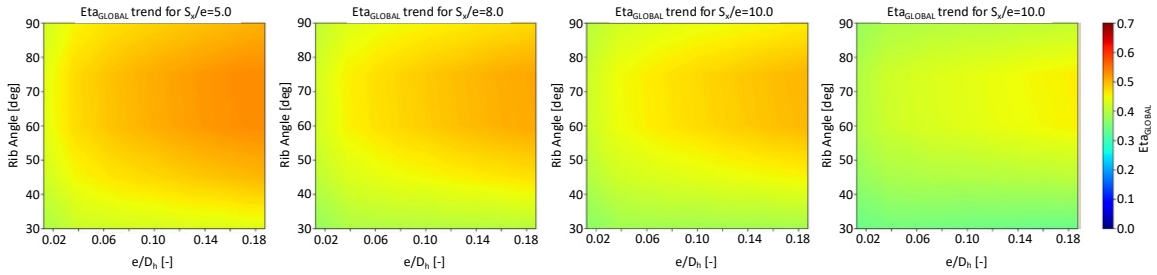

Figure 5.16 - η_{Global} in terms of S_x/x – Ribbed configuration

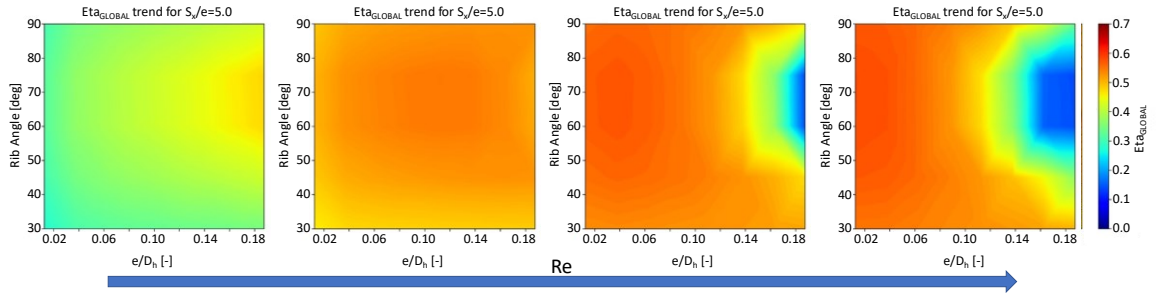

Figure 5.17 - η_{Global} in terms of *Re* – Ribbed configuration

The analysis in Figure 5.16 shows that the overall effectiveness declines as rib pitch increases. It is also visible how the -η_{Global} is maximized for alpha values close to 75°.

Figure 5.17 shows the effect of increasing Reynolds, but also the effect of *blockage ratio*. It is evident that as the turbulence increases (contour from left to right, from 20000 to 130000), global effectiveness improves. The combined effect of the e/D_h ratio and *Re* is also evident. Even at low turbulence levels, the increase in *blockage ratio* improves the cooling system, whereas moving to higher *Re* the behavior is reversed. In fact, for the last contour on the right (*Re*=130000) it is visible an area where η_{Global} decays. In Figure 5.17 it is also noticeable how the effect on the effectiveness of the ratio e/D_h is reversed with an increase in *Re*.

Dimpled configuration

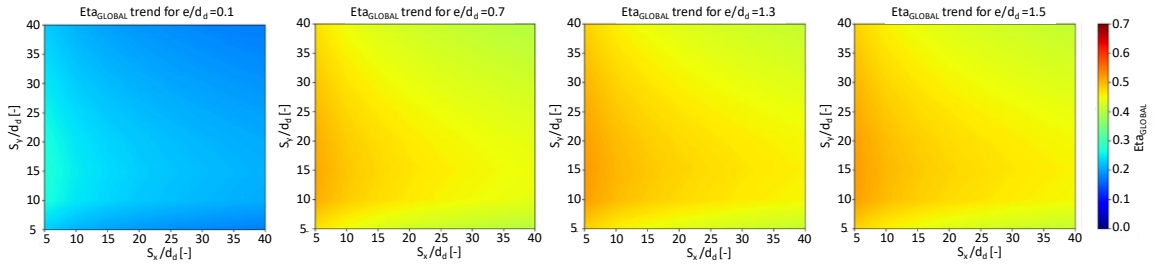

Figure 5.18 - η_{Global} in terms of e/d$_d$ – Dimpled configuration

Figure 5.18 shows the overall effectiveness as a function of e/d_d. where the streamwise and spanwise pitches are normalized to the dimple diameter. It is visible that η_{Global} increases as e/d_d increases. The previous analysis (Table 5.8) showed that the effectiveness is maximized for e/d_d = 1.3. The four contours clearly show that the cooling system's best performances are obtained for low S_x/d_d and $S_y/d_d \approx 15$.

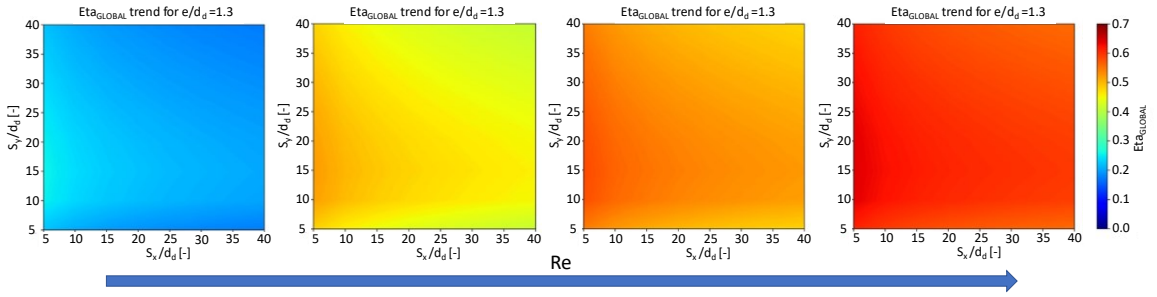

Figure 5.19 - η_{Global} in terms of *Re* – Dimpled configuration

Figure 5.19 shows the effect of increasing Reynolds. The comparison was made with the same dimple depth to dimple diameter ratio (the best one from *DOE*). Effectiveness improves globally as turbulence increases.

Pin-finned configuration

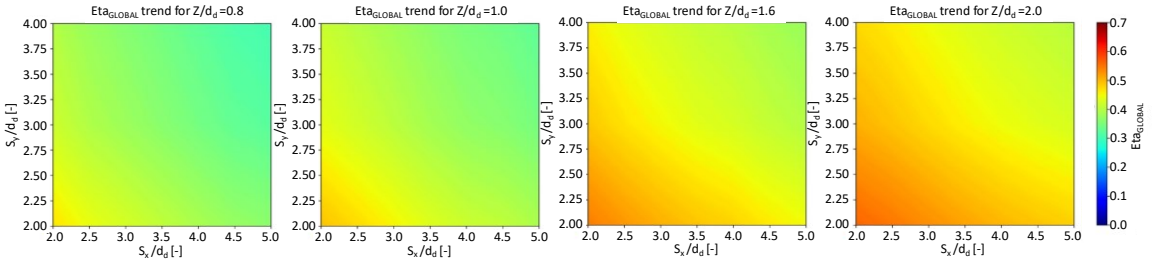

Figure 5.20 - η_{Global} in terms of Z/d$_d$ (Low Reynolds - 20000) – Pin-finned configuration

Figure 5.20 and Figure 5.21 show the behavior of η_{Global} as Z/d_d varies. Figure 5.20 shows low Reynolds numbers, while in Figure 5.21 the behavior for high ones is analyzed. On the contour axes, the streamwise and spanwise pitches are normalized to the pin diameter. For the first case, it is visible how higher Z/d_d ratios are necessary to obtain better effectiveness while keeping constant the remaining geometrical

parameters. A completely different behavior can be seen in the second case (high *Re* values at the cooling system output). Here, to maximize η_{Global} it is necessary to opt for lower Z/d_d ratios.

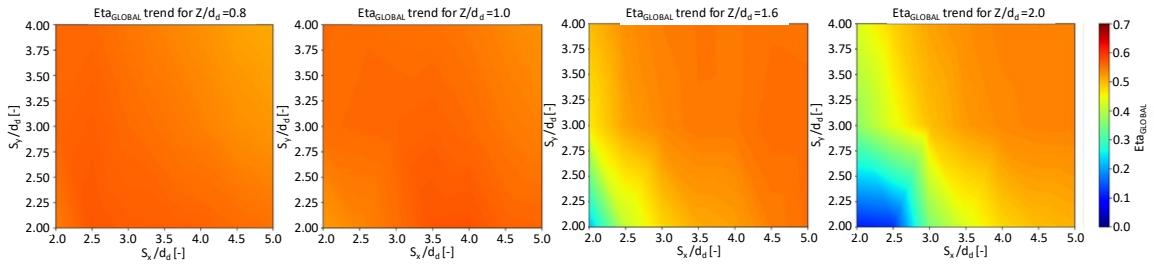

Figure 5.21 - η_{Global} in terms of Z/d_d (High Reynolds - 120000) – Pin-finned configuration

Another important aspect to be analyzed is certainly the behavior of the effectiveness when varying not only Z/d_d but also the two pitches. For low turbulence, the performance parameter is maximized for low S_x/d_d and S_y/d_d ratios. This happens independently from the value of the channel height to pin diameter ratio. For high *Re*, this behavior is confirmed only at low Z/d_d ratios. In fact, as this parameter increases, the global effectiveness is maximized for geometric layouts with high pitch spacing.

In conclusion, for low Reynolds number, the geometric layouts maximize effectiveness when it maximizes heat transfer. At high levels of turbulence, it is necessary to minimize pressure drops to maximize the performance parameter.

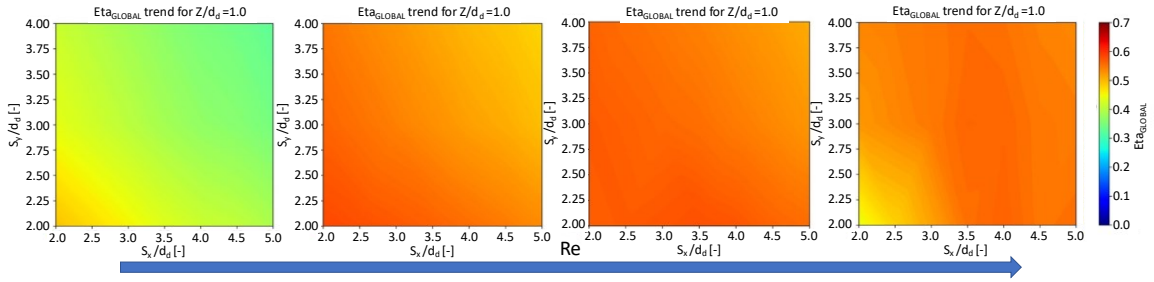

Figure 5.22 - η_{Global} in terms of *Re* – Pin-finned configuration

Figure 5.22 shows the effect of increasing Reynolds. The comparison was made with the same channel height to pin diameter ratio. Effectiveness improves globally as turbulence increases. It is also visible how the best geometrical setup is reached for higher values of the S_x/d_d and S_y/d_d ratios. This supports previous observations.

Jets impingement configuration

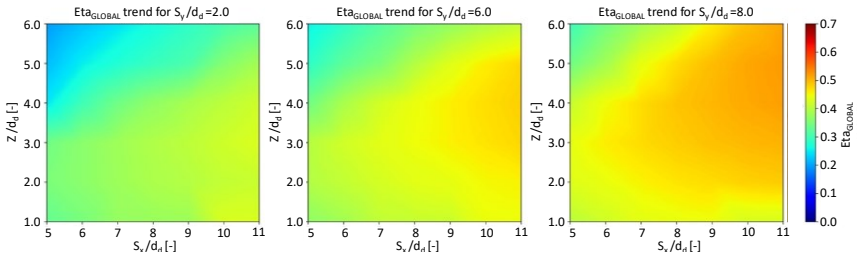

Figure 5.23 - η_{Global} in terms of S_y/ d_d – (Low Reynolds - 20000) - Jets impingement configuration

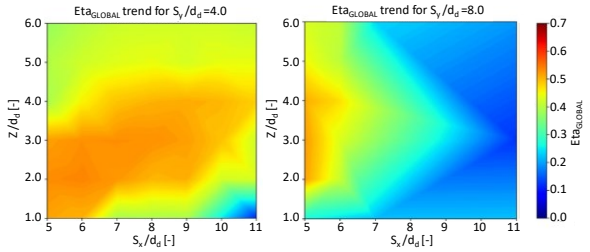

Figure 5.24 -η_{Global} in terms of S_y/ d_d – (High Reynolds - 120000) - Jets impingement configuration

Figure 5.23, Figure 5.24 and Figure 5.25 show the contour of the operational maps for the cooling system in the jets impingement configuration. The S_x /d_d ratio and the Z /d_d ratio are reported on the contour axes. In Figure 5.23 the comparison was made with the same Reynolds (20000), while Figure 5.24 shows the comparison for high *Re*. In Figure 5.25, the contours are shown with the same streamwise pitch to jet hole diameter ratio.

Figure 5.23 shows that global effectiveness increases as S_y /d_d ratio increases. While this is valid for a cooling channel with low turbulence flows, the opposite behavior is recorded for high *Re*.

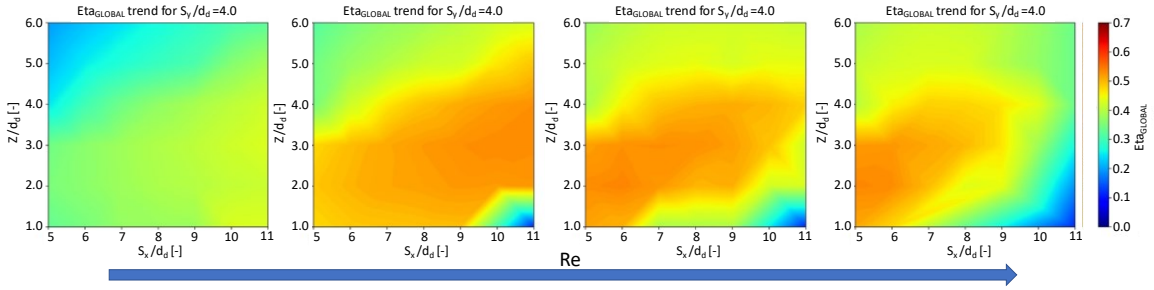

Figure 5.25 - η_{Global} in terms of *Re* – Jets impingement configuration

Figure 5.25 shows that an increase in Reynolds number leads to an increase in the η_{Global} peak value. Also, it shows how this behavior reduces the medium/high zone of global effectiveness. More in general the turbulence increase causes the high η_{Global} zone to move towards lower ratios. This means that in the geometric layout a higher number of impingement jets is required to better oppose the cooling channel transverse flow.

Sensitivity Analyses

Thanks to the *Therm-1D/Dakota* procedure, it has been possible to simulate the behavior of the cooling system as a function of the variation of the most important geometrical parameters. These analyses have been done to estimate which parameters could affect single cooling system layout performances more than others.

The liner metal temperature (T_w) and the pressure drops were evaluated as output variables.

Sobol indexes are calculated for every input value to quantify how much the result is affected by its variation. This information is extremely important for a solid design and eventually for optimization because they allow focusing the design process on those parameters that mostly influence the desired response functions [22].

The method applied was the *PCE* (Polynomial Chaos Expansion) fixing the total order of the polynomial. Using a 3rd order interpolating polynomial, for three random input variables, the number of evaluations required is *27*. To realize these evaluations, the surrogate model, obtained with a number of evaluations reduced by the stochastic expansion, has been used. This provides a sample size equal to that which would be obtained with a Monte Carlo method, as already reported in *chapter 3*.

Random variables setting

In this paragraph, all the settings of the variables chosen as uncertain would be reported. These are classified according to the type of analysis performed. Normal distributions have been assumed because in literature there are no works analogous to the cases analyzed. The uncertainty variables were modeled as reported in Table 5.11.

Rib			
	Upper Limit	Lower Limit	Distribution
e/D_h	0.0125	0.01875	Uniform
S_x/e	5.0	20.0	Uniform
α	30	90	Uniform

Dimple			
	Upper Limit	Lower Limit	Distribution
e/d_d	0.1	1.5	Uniform
S_x/d_d	5.0	40.0	Uniform
S_y/d_d	5.0	40.0	Uniform

Pin-fin			
	Upper Limit	Lower Limit	Distribution
Z/d_d	2.00	0.73	Uniform
S_x/d_d	1.5	5.0	Uniform
S_y/d_d	2.0	4.0	Uniform

Impingement			
	Upper Limit	Lower Limit	Distribution
Z/d_d	1.0	6.0	Uniform
S_x/d_d	5.0	15.0	Uniform
S_y/d_d	4.0	8.0	Uniform

Table 5.11 - Probability distribution for single configuration variables

Sensitivity analysis results

Figure 5.26 shows the sensitivity analysis expressed as pie charts for every single configuration used. The first row represents the metal temperature of the liner and in the second row, the pressure drops.

For the rib cooling system, the parameter with the greatest influence on heat transfer is the angle of inclination, while the parameter that most influences the pressure drops is the *blockage ratio*.

For this reason, with the presence of dimples, there is an agreement between the two evaluations which identify the e/d_d ratio as the most important parameter.

For the system with pin-fin, the main parameter is Z/d_d, even if there is no strong prevalence as in the previous cases. For pressure drops, the e/D_h ratio has a value of 80%.

The same can be said for the evaluation of the impingement cooling system. Heat transfer is mainly influenced by the S_x/d_d ratio, but the other parameters also have values that cannot be neglected. A different situation can be found in the result obtained from the pressure drops analysis, where the same geometric parameter weights 73%.

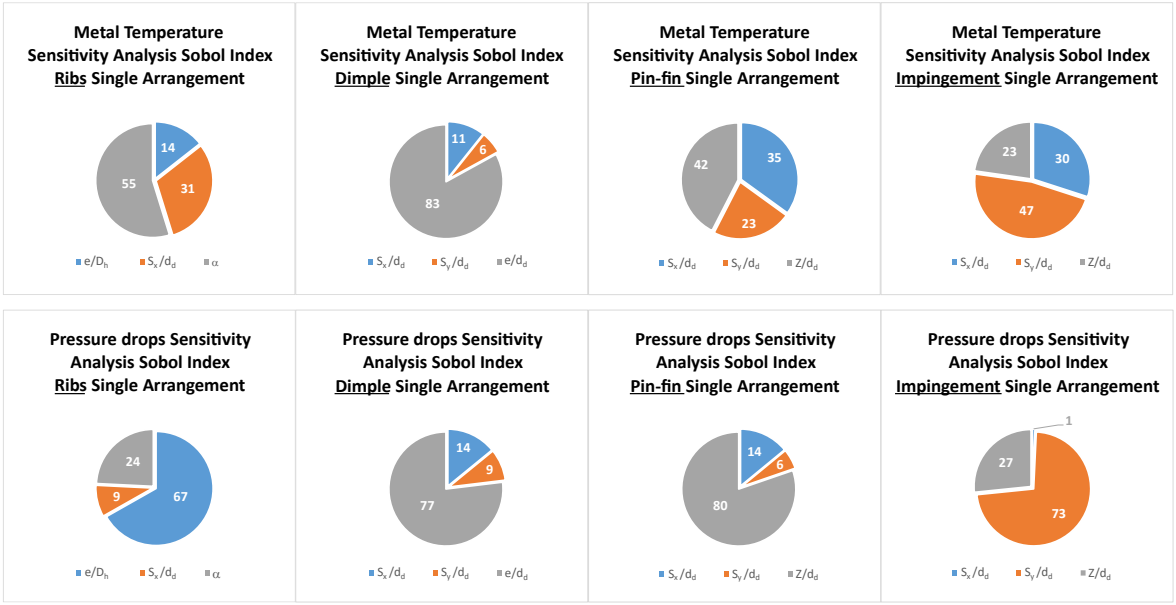

Figure 5.26 - Single configuration sensitivity analysis results

Remarks

It has been realized a DOE due to the preliminary phase of the assessment for RDCs air cooling because no proper guidelines were available. This results in a wide range of possible layouts that can be evaluated. Several fluid networks have investigated, to assess the performances and feasibility of a first-try air single layout cooling system. In this study, the most common cooling solutions were investigated identifying a possible reasonable layout for the air-cooling system. Performances were evaluated changing the most important geometric features of every respective heat transfer enhancement method adopted.

For each turbulence level and each cooling configuration, the geometric layout that allows the best overall effectiveness has been determined.

The results showed that none of the geometries tested for the different cooling configurations were able to achieve the targets set, if not in the case of high Reynolds numbers. All the best geometrical layouts can keep the pressure losses in the range of 10%.

The configurations with ribs, pin-fins, and dimples are those that achieve the best balance between thermal performance and pressure drops. In general, for low values of Re number layouts that favor the heat transfer are adopted, while for high *Re* the pressure drops must be limited.

Operational maps have been created. These highlights the overall effectiveness once the geometric layout of the cooling configuration has been determined. These were made for each level of turbulence investigated in order to allow a first quick evaluation of what could be the operative region relative to each one of the considered configurations. This will be useful for further studies in which an effective air-cooling system for *RDCs* could be examined and properly designed.

A sensitivity analysis was performed using the *Therm-1D/Dakota* coupled procedure. The method applied was the PCE fixing the total order of the polynomial. Normal distributions have been assumed. The surrogate model has been used to provides a sample size equal to the one that would be obtained with a Monte Carlo method. The sensitivity analysis defines which geometric parameters are most relevant for each cooling configuration. The results were shown in relation to both heat transfer augmentation and pressure drops.

In conclusion, the data collected defines the impossibility of achieving the targets using the cooling system in a single configuration. Only with the dimple configuration and only for the highest *Re* tested, it was possible to achieve all three aims in order to prevent combustor from failure caused by the exposition to high temperature.

However, comparing the values, it has been possible to obtain some important information about potential cooling system layouts that could be preferable.

It is clear that to achieve the desired aims, it is necessary to investigate a double cooling system configuration.

Double configuration

Since it is very difficult to achieve the aims for metal temperature and pressure drops using a single cooling system configuration, a double configuration was tested.

In this case, the cooling system will be divided into two different zones as shown in Figure 5.27. A first one where there is no detonation inside the combustion chamber; where a cooling configuration that allows low pressure drops will be used. For the other zone, where there are the detonation phenomena, a cooling configuration that promotes heat transfer will be preferred.

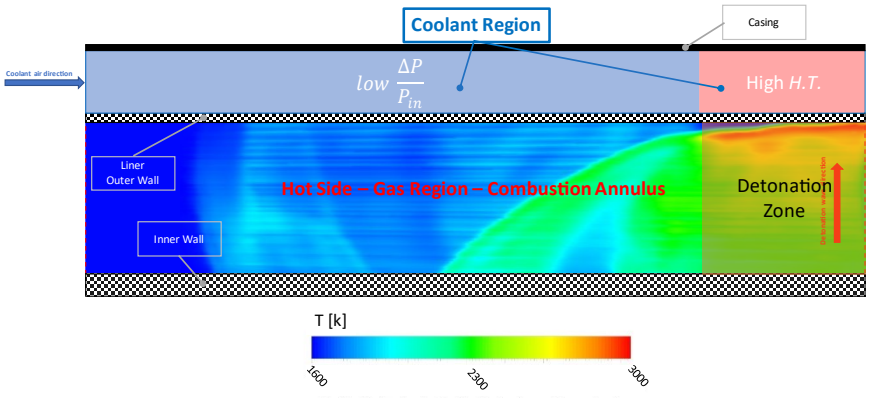

Figure 5.27 – Double cooling system configuration

So, the experience acquired with the *DOE* made on the single configuration cooling system will be applied here.

The analyses have been carried out for three Reynolds values: *Low* (20000), *Mid* (60000), *High* (130000).

Tested Configurations	
Low Pressure drop zone	**High Heat Transfer Zone**
Ribbed	Jets Impingement
Ribbed	Dimpled
Ribbed	Pin-finned
Pin-finned	Jets Impingement
Pin-finned	Dimpled
Pin-finned	Ribbed
Dimpled	Ribbed
Dimpled	Pin-finned
Dimpled	Jets Impingement
Jets Impingement	Ribbed
Jets Impingement	Pin-finned
Jets Impingement	Dimpled
Smooth	Jets Impingement
Smooth	Ribbed
Smooth	Pin-finned
Smooth	Dimpled

Table 5.12 – Double configuration

All possible combinations were used according to the geometries seen in Table 5.12. Depending on the location (low pressure drops zone or high heat transfer zone) the geometric configurations were chosen to maximize the required effect. The two cooling layouts were fed sequentially. This is particularly relevant in case the impingement jets are in the detonation zone. Here the jets are fed with the air exiting from the first coolant layout. This ensures that the simulation conditions are equivalent (*Re*, flow rate) between the tested configurations. The smooth configuration has been proposed only in the zone at low pressure losses. The analysis results are provided by examining the average values of metal temperature in the detonation zone. The overall effectiveness is also reported, as well as and the pressure drops of the cooling system. The decision to report the thermal analyses results only for the detonation zone is due to the fact that this zone is more exposed to thermal stress and therefore the imposed target conditions are more difficult to obtain.

Results

The results in presence of a cooling system with *low* Reynolds (Figure 5.28) show that no configuration studied allows to stay below 1200 K for the liner metal temperature. On the other hand, the pressure drops remain below the limit (10%).

The overall efficiency does not exceed 40%, mainly due to the lack of thermal performance.

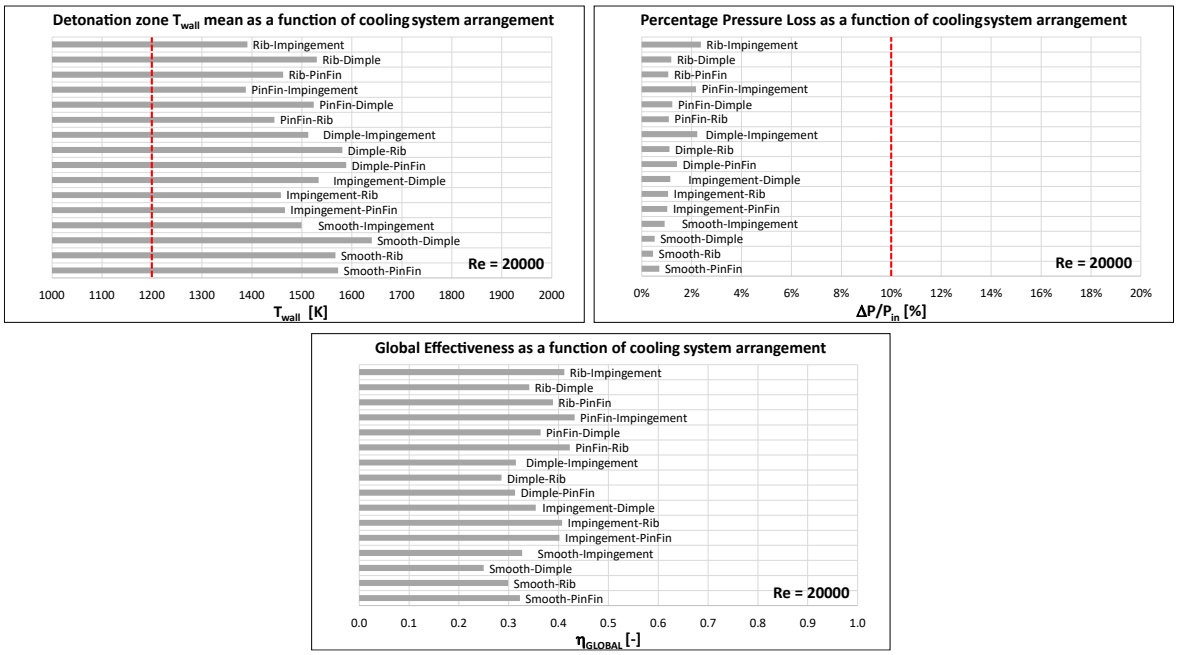

Figure 5.28 - Double configurations - Results (Re = 20000)

So even with the double configuration, it is impossible to reach the targets in case of low Reynolds numbers. Figure 5.29 shows the results for *Mid* Reynolds value. Some double configurations allow to get close to the aims and in some cases to reach all two. For cooling systems that have the smooth configuration in the initial zone (*low pressure drop zone*), it is visible that none of the thermal targets are reached.

Overall efficiency is higher, with peaks over *50%*, because thermal performance has improved. This result is also due to the higher turbulence of the cooling flow, which leads to better efficiency of the turbulence promoters especially in the area where they have to face the thermal shock due to detonation.

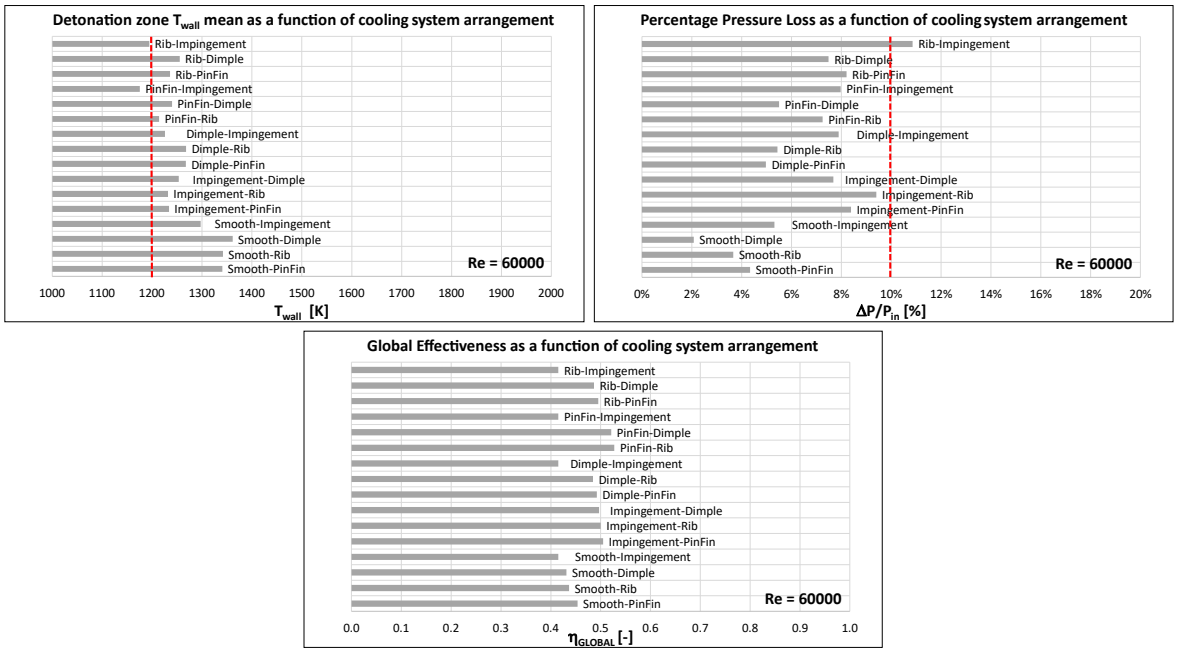

Figure 5.29 - Double configurations - Results (Re = 60000)

These results already show how with a configuration involving pin-fin in the first zone and jets impingement in the second zone it is possible to achieve all two tasks. So, it is important to show this geometric configuration (Table 5.13).

Pin-fin			*Impingement*		
Z/d_d	S_x/d_d	S_y/d_d	Z/d_d	S_x/d_d	S_y/d_d
0.89	3.5	3.0	2.0	7.0	8.0

Table 5.13 – Best Double Configuration (Re = 60000)

Figure 5.30 shows the results for *Mid* Reynolds value. In this case, all configurations result in a mean metal temperature in the detonation zone below the imposed limit. However, it is impossible to use any of these configurations due to the high pressure drops. In some cases, these are more than twice the maximum imposed limit.

So even with the double configuration, it is impossible to reach the targets in case of high Reynolds numbers.

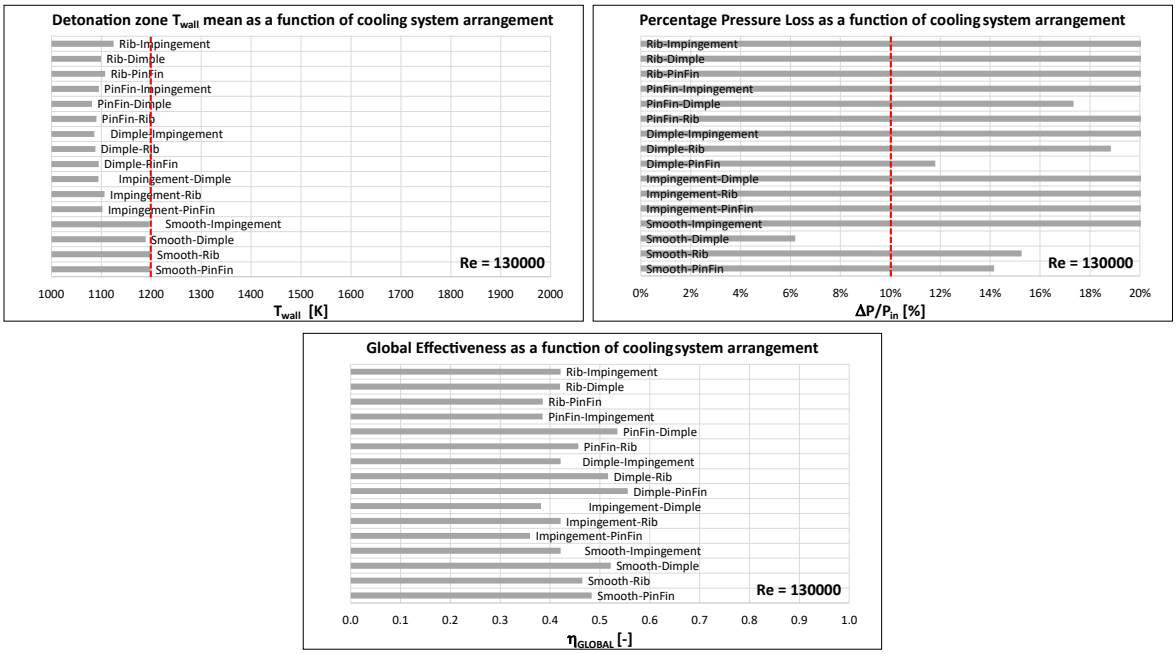

Figure 5.30 - Double configurations - Results (Re = 130000)

Additional Double configurations, UQ and sensitivity analyses

To avoid limiting the results of the investigation to only one possible configuration, the mid-level Reynolds analysis has been deepened. It has been chosen to modify the limits of the metal temperature. The limit temperature has been increased by 3% (about 40 K). This variation is motivated by the order of uncertainty from the simplified one-dimensional analysis performed.

Thus, other interesting configurations may exist (Figure 5.31). Although these did not achieve all two original aims simultaneously, they were subject to a further optimization analysis using the *Therm-1D/Dakota* coupled procedure. This is to determine if there is a possible configuration that allows a better result than the one obtained.

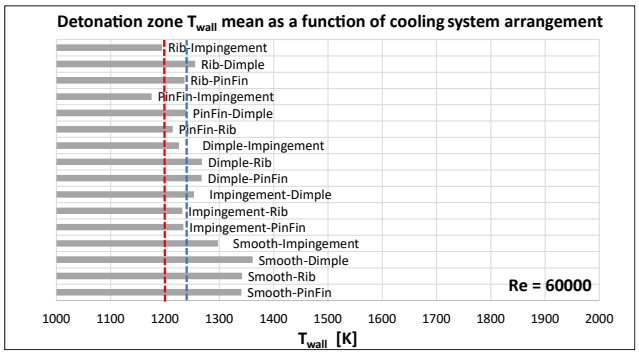

Figure 5.31 - Double configurations - Results (Re = 60000) – New T_W limit

Figure 5.31 shows the new limits imposed on the analysis of more configurations. The red dashed lines represent the original limit, and the blue dashed ones represent the new limits.

With this new assumption, it is possible to consider six additional double configurations. Referring to Figure 5.31, Table 5.14 shows the ones that will be the object of further analysis.

New Limits - Tested Configurations	
Low Pressure drop zone	**High Heat Transfer Zone**
Ribbed	Jets Impingement
Pin-finned	Ribbed
Pin-finned	Dimpled
Dimpled	Jets Impingement
Jets Impingement	Ribbed
Jets Impingement	Pin-finned

Table 5.14 - Double configuration - Re = 60000 – Additional tested configurations

Although the *DOE* was performed with a wide range for the single configuration geometric parameters, it was not possible to explore all feasible arrangement. This most probably limited the definition of efficient configurations in the proposed analysis for double cooling systems.

It has been imposed the probability distributions of the six geometric parameters that characterize each double configuration equal to those seen for the analysis of single cooling system configurations (Table 5.11). Due to the coupled procedure cited in *Therm-1D/Dakota Coupled Procedure* paragraph, it has been possible to evaluate system performances with the variation of those parameters.

The method applied was the *PCE* (Polynomial Chaos Expansion) fixing the total order of the polynomial. Using a 3rd order interpolating polynomial, for six random input variables, the number of evaluations required is 729. To realize these evaluations, the surrogate model, obtained with several evaluations reduced by the stochastic expansion, has been used.

Due to the UQ and sensitivity analyses and comparing the results from every configuration subcase (729 for every double configuration), it has been possible to estimate the fluid network behavior as a function of the geometrical layout for the considered cooling solutions. Furthermore, it has been possible to evaluate the mean T_w and pressure drops for every subcase to determine if any feasible solutions would achieve the limits originally imposed.

The results are shown, also for this analysis, according to global effectiveness in order to find the best compromise between heat transfer promotion and pressure drops minimization.

Results

For each double cooling system configuration additionally tested, the geometric layouts with the best overall performance are reported here. The mean parameters T_w as well as pressure drops and η_{Global} define the performance.

The results will be shown referring to Table 5.14. The following tables show the determined geometric layout on the left and the thermal and performance parameters on the right.

Ribs and Jets Impingement - Configuration					
Low Pressure drop zone			High Heat Transfer Zone		
Rib			Jets Impingement		
e/D_h	S_x/e	α	Z/d_d	S_x/d_d	S_y/d_d
0.10	12.50	75	1.5	10.0	6.0

Ribs and Jets Impingement - Results		
$\overline{T}_{w,det}$ [K]	$\Delta P - \%$ [-]	η_{Global} [-]
1155	16.0	0.475

Table 5.15 - Ribs and Jets Impingement configuration results

The configuration that uses ribs for the first zone and jets impingement for the detonation zone (Table 5.15) does not achieve to keep the pressure drop below 10%. Although the other parameters would ensure a good performance of this system, it cannot be considered as a cooling solution.

The configuration with pin-fins for the first zone and ribs for the detonation zone (Table 5.16) does not achieve any of the two aims. So even this configuration is not feasible as a cooling solution.

Pin-fins and Ribs - Configuration					
Low Pressure drop zone			High Heat Transfer Zone		
Pin-fin			Rib		
Z/d_d	S_x/d_d	S_y/d_d	e/D_h	S_x/e	α
1.05	3.25	3.5	0.25	10.0	75

Pin-fins and Ribs - Results		
$\overline{T}_{w,det}$ [K]	$\Delta P - \%$ [-]	η_{Global} [-]
1330	12.2	0.527

Table 5.16 – Pin-fins and Ribs configuration results

Pin-fins and Dimples - Configuration					
Low Pressure drop zone			High Heat Transfer Zone		
Pin-fin			Dimple		
Z/d_d	S_x/d_d	S_y/d_d	e/d_d	S_x/d_d	S_y/d_d
1.00	3.25	3.0	0.8	5.0	15.0

Pin-fins and Jets Impingement - Results		
$\overline{T}_{w,det}$ [K]	$\Delta P - \%$ [-]	η_{Global} [-]
1198	6.7	0.603

Table 5.17 - Pin-fins and Dimples configuration results

In the case of Table 5.17 a cooling system configured with pin-fins in the first zone and dimples in the detonation zone was tested. The values on the right show how this configuration is able to achieve all two goals. The mean detonation zone T_w is just below the limit. The most interesting data concerns the pressure drop at 6.7%. This configuration allows having overall effectiveness among the highest seen during this work.

The case in Table 5.18 (*Dimples and Jets impingement*) can also be considered as a feasible solution for a cooling system. Only the average metal temperature in the detonation zone is just above the imposed limit, while the other two values are within the feasibility range.

Dimples and Jets Impingement - Configuration					
Low Pressure drop zone			High Heat Transfer Zone		
Dimple			Jets Impingement		
e/d_d	S_x/d_d	S_y/d_d	Z/d_d	S_x/d_d	S_y/d_d
0.8	9.0	22.5	1.14	10.0	6.0

Dimples and Jets Impingement - Results		
$\overline{T}_{w,det}$ [K]	$\Delta P - \%$ [-]	η_{Global} [-]
1217	9.5	0.545

Table 5.18 - Dimples and Jets impingement configuration results

The configurations using jets impingements for the first zone and ribs or pin-fins for the detonation zone (Table 5.19 and Table 5.20) do not achieve thermal targets. Even if pressure losses are maintained below 10%, these configurations are not feasible as cooling solutions.

Jets Impingement and Ribs - Configuration					
Low Pressure drop zone			High Heat Transfer Zone		
Jets Impingement			Rib		
Z/d_d	S_x/d_d	S_y/d_d	e/D_h	S_x/e	α
1.5	10.0	6.0	0.26	12.5	75

Jets Impingement and Ribs - Results		
$\overline{T}_{w,det}$ [K]	$\Delta P - \%$ [-]	η_{Global} [-]
1231	9.4	0.500

Table 5.19 - Jets impingement and Ribs configuration results

Jets Impingement and Pin-fins - Configuration					
Low Pressure drop zone			High Heat Transfer Zone		
Jets Impingement			Pin-fin		
Z/d_d	S_x/d_d	S_y/d_d	Z/d_d	S_x/d_d	S_y/d_d
1.14	14	6.0	1.0	3.50	3.50

Jets Impingement and Pin -fins - Results		
$\overline{T}_{w,det}$ [K]	$\Delta P - \%$ [-]	η_{Global} [-]
1233	8.4	0.504

Table 5.20 - Jets impingement and Pin-fins configuration results

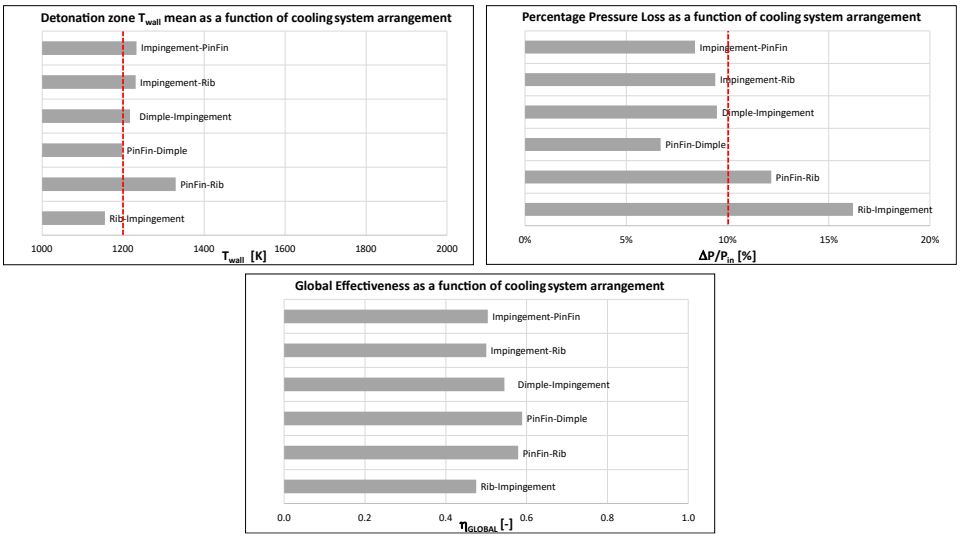

Figure 5.32 - Additional Double configurations analyses – Overall comparison

Figure 5.32 shows graphically all the results obtained in this additional analysis.

Sensitivity analysis results

Figure 5. shows the sensitivity analysis expressed as pie charts for every additional double configuration that achieves the analysis aims. The first row represents the metal temperature of the liner and the second row the pressure drops.

For the configuration using pin-fins for the first zone and jets impingement for the detonation zone, the parameter with the greatest influence on heat transfer is the jets impingement zone parameter S_x/d_d. Also, the Z/d_d parameter of the same cooling scheme is not negligible. While the pressure drops is mostly influenced by the normalized streamwise pitch for the pin-fins zone and the Z/d_d ratio for the jets impingement zone

With the presence of pin-fins and dimples, the pin-fins Z/d_d ratio has a high incidence in both assessments. This is even more evident for pressure drops evaluation (63%), while in the case of metal temperature the pin-fins S_x/d_d ratio is also influential.

For the system with the presence of dimples and jets impingement, the main parameter is the jets impingement S_x/d_d ratio for both the metal temperature and the pressure drops.

Figure 5.33 - Additional Double configuration sensitivity analysis results

Remarks

Since it is very difficult to achieve the targets for metal temperature and pressure drops simultaneously using a single cooling system configuration, a double configuration was tested.

In this case, the cooling system was divided into two different areas. A first one without detonation where a cooling configuration that allowed low pressure drops was used. For the second zone, where there were the detonation phenomena, a cooling configuration that promoted heat transfer was adopted. The analyses have been carried out for three Reynolds values. The results have shown that only for *Mid-level* Reynolds and only the configuration that involved pin-fin in the first zone and jets impingement in the second zone was able to achieve all the two aims ($T_w<1200\ K$, $\Delta P/P_{in}<10\%$).

To avoid limiting the investigation results to only one possible configuration, the mid-level Reynolds analysis has been deepened. Six additional dual cooling configurations were chosen. These were close to the aims of the previous analysis. The *Therm-1D/Dakota* coupled procedure was here employed to evaluate system performances. The method applied was the *PCE* fixing the total order of the polynomial. A 3rd order interpolating polynomial was used. For six random input variables, the number of evaluations required was 729. Due to the UQ and sensitivity, it has been possible to evaluate the mean T_w, and pressure drops from every configuration subcase. This was done in order to determine if any feasible solutions would achieve the limits originally imposed.

In conclusion, a total of three double cooling configurations have been determined:

- Pin-fins and Jets impingement
- Pin-fins and Dimples
- Dimples and Jets impingement

A sensitivity analysis was performed on the geometric parameter of these configurations in order to understand which ones of them are the most relevant for each cooling configuration.

Final Remarks

The work has been conducted to investigate the thermal problem relative to RDCs. Starting from assumed boundary conditions, the heat fluxes estimation model gives a good approximation of the heat fluxes relative to the detonation zone, according to literature values. Therefore, it could be possible to identify an operating region in terms of heat transfer coefficient for a given T_{gas} and once assumed T_w and $\dot{Q}$ limits. The region identifies the value of heat transfer coefficient that a cooling system needs to obtain to maintain an equal or lower wall temperature than T_w. First, a *1-D* model using a simple heat transfer correlation was built, with the aim of quantifying the amount of heat to be removed from the rotating detonation region in order to prevent combustor failure from the extended exposition to high temperature. Once that the heat flux has been estimated, it has been possible to evaluate a proper heat transfer coefficient working region for a hypothetical cooling system.

After that, thanks to a DOE, it has been possible to investigate different single cooling system configurations to explore the design space and get some guidelines for further studies. The Reynolds number at the outlet of the cooling system was varied between 20000 and 130000. Several simulations with different layouts were conducted, starting from some reference geometry and varying the main geometric

parameters of every modeled solution adopted to create the fluid network. From simulation results, it has been possible to build an operational map to show the region in which every tested layout was collocated, according to the assumptions made. To compare results from the heat fluxes model and simulations, the liner metal temperature, the percentage pressure drops and a global effectiveness were plotted for each investigated combination of considered input values. Comparing the values, it has been possible to obtain some important information about potential cooling system layouts that could be preferable and their feasibility. Operational maps were built, identifying the global performance of every single configuration geometric layouts. The map reports the global effectiveness of every investigated case as a function of the relative geometric parameter.

A sensitivity analysis was performed using the *Therm-1D/Dakota* coupled procedure. The method applied was the PCE fixing the total order of the polynomial. Normal distributions have been assumed. The surrogate model has been used to provides a sample size equal to the one that would be obtained with a Monte Carlo method. The sensitivity analysis defines which geometric parameters are most relevant for each cooling configuration. The results were shown in relation to both heat transfer augmentation and pressure drops.

In conclusion, the data collected defines the impossibility of achieving the targets using the cooling system in a single configuration.

After the results of this initial feasibility study, a double arrangement cooling system was considered. In this case, the cooling system was divided into two different areas. In the first one there was no detonation and a low pressure drop cooling configuration was used. The other zone is identified by the presence of the detonation phenomena, where a cooling configuration that promoted heat transfer was preferred. The analyses have been carried out for three Reynolds values. The results have shown that only for *Mid-level* Reynolds and only the configuration that involved pin-fin in the first zone and jets impingement in the second zone it was possible to achieve all the two aims.

To avoid limiting the results to one configuration, the mid-level Reynolds analysis has been deepened. Six additional dual cooling configurations were chosen, which were able to provide close results to the aims set in the previous analysis. Thanks to the *Therm-1D/Dakota* coupled procedure; it has been possible to evaluate system performances, while the UQ and sensitivity were employed to evaluate the mean T_w and pressure drops for every subcase. In four cooling configurations have been determined:

- Pin-fins and Jets impingement
- Pin-fins and Dimples
- Dimples and Jets impingement

A sensitivity analysis was performed to understand which geometric parameters are most relevant for each cooling configuration.

This work has been conducted starting from several assumptions due to the complexity of the detonation phenomenon and difficulties in managing unsteady heat fluxes and high pressures relative to the detonation zone, which make the study of this type of combustion very complex. More investigations are needed to characterize correctly rotating detonation parameters, such as heat transfer coefficient, temperature and

pressure profiles along the combustor to better define boundary conditions for a more detailed thermal analysis.

Due to the preliminary phase of RDEs technology, the test rig taken as reference needs to be made by simply machining material because of the necessity of positioning sensors and instrumentation for measurements during the experimental tests. That is the reason why no thermal barrier coating effects were investigated in this work. The application of a thermal barrier coating could help the realization of a combustion annulus that can withstand high thermal stresses better than the modeled one, requiring less extreme cooling system conditions and a lower heat transfer coefficient. This could reduce pressure drops, increasing the efficiency of the whole system.

The present work gives some guidelines for further improvement in the assessment of air-cooling system feasibility and design, which could be helpful to advanced research that could lead to a proper cooling system design necessary for steady-state operating conditions of rotating detonation combustors.

Conclusion

In an attempt to further improve turbogas systems performance, two factors are mainly involved: increased operating pressures and increased turbine inlet temperature. In the same context, one of the most important alternatives investigated in recent times is the possibility of changing the thermodynamic cycle at the base of the system. Therefore, it is evident that the need to develop more powerful and efficient gas turbine systems leads all the components of the hot path, combustor and turbine, to undergo stronger thermal stresses that could lead to dangerous damages and failures. For these reasons, the design of efficient cooling systems becomes mandatory and the definition of the most appropriate cooling scheme represents one of the most challenging tasks in the combustor and turbine design since it directly determines the component's life. For this reason, it is immediately comprehensible that from the early stages of design it is necessary to have the most powerful and flexible tool to rely on.

The research activity presented in this dissertation developed a novel numerical procedure for the preliminary thermal design of combustor liners (*Therm-1D/Dakota*). This procedure is based on the coupling of a one-dimensional tool that solves the radial heat transfer inside the combustor and obtains the liner wall temperature (*Therm-1D*) and a software that allows uncertainty quantifications analyses (*Dakota*). The UQ methodologies can evaluate the effect of uncertainties of one or more variables on selected output quantities; in particular, it allows to estimate the propagation of an error within a numerical code. These methodologies, if correctly used, can lead to a complete understanding of how the mathematical model approximates and solves the real physical problem; then, through the sensitivity analysis, it is possible to quantify, in mathematical terms, which quantities mostly affect the response functions considered.
This has allowed the development of an innovative, faster, and more reliable procedure for the preliminary design and optimization of combustor cooling systems. The proposed procedure has been successfully tested and validated.

The first application was performed with a triple purpose. the first aim was to increase the level of experience in the use of UQ techniques applied to one-dimensional codes. The second purpose was to verify the accuracy of the uncertainty propagation methods and the relative sampling grids, comparing the spectral methods with the Monte Carlo method. The third purpose was to carry out a critical analysis of the Therm-1D procedure, analyzing the main input or tuning parameters, those that introduce the greatest uncertainties in the system response. The fluid network under examination was provided by the industrial partner *GE*

Avio Aero and simulates the behavior of a combustor operating under lean flame conditions, developed and tested at CIAM during the European project *LEMCOTEC*. The procedure established has allowed comparing both the average trend and the maximum and minimum value for the different methods used. Furthermore, probability distribution maps were also obtained: in this case, a probability of occurrence was associated with each temperature of the liner and, spatially, for a specific non-dimensional abscissa. Different types of analyses were carried out, specifically focusing on some key quantities of the one-dimensional code. Regarding the UQ methodology, from this first application, it was evident how efficient the spectral expansion methods are. These methods can create a surrogate model with a reduced number of evaluations able to approximate the response function considered. For each analysis, the classical Monte Carlo analysis was compared with four stochastic expansion processes: Gauss quadrature, stochastic collocation, total order with LHS sampling, and Smolyak. It was demonstrated how the first two methods are the most effective when the number of variables considered is reduced. During this first activity, the Smolyak grid was also validated, which is extremely effective when the number of random variables considered increases because other models (except for the Monte Carlo Simulation) suffer from the curse of dimensionality.
So, it can be concluded that the application of UQ methods with sensitivity analysis to low order deterministic codes can be used for optimization and preliminary robust design applications.

A more relevant assessment has been performed on a non-reactive combustor simulator rig equipped with an effusion cooled plate where a representative swirling main flow interacts with the effusion jets. This analysis is part of the European project *SOPRANO*. The model reproduces in a 1:1 scale five sectors of a typical RQL combustor architecture. The component of greatest interest for the study was the inner plate that represents a part of a multiperforated liner. The related experimental tests used in this work were carried out at the *THT LAB* of the University of Florence in association with the industrial partner *GE Avio Aero*. The tests were performed at different pressure drops across the swirlers and varying the mass flows of the slot and through the inner/outer liners. Since the test case is not reactive, the analysis made is only confined to the convective heat transfer phenomena, which is useful for investigating problems related to hot gas side uncertainties. Therm-1D input data such as temperature, pressure and velocity distributions are extracted from numerical simulations. These parameters are affected by uncertainties since they are introduced as input to the code as a one-dimensional distribution and can only partially take into account the strongly three-dimensional aspects of the phenomena created in the combustion chamber. RANS CHT simulations with a strongly coupled method were performed to understand the interaction of the swirling flow with the cooling system, and how the cooling performances are affected by the main flow. To distinguish the various effects associated with the slot, the dilutions, and the effusion, a numerical analysis has been performed introducing four additional transport equations for four different passive scalars (representing the experimental CO_2 coming from the different secondary inlets). In this Therm-1D application, a feature was used that allows imposing the one-dimensional streamwise distribution of adiabatic effectiveness as input. The distribution obtained for the various test points from *PSP*, mediated in the spanwise direction, was employed. In this way, the cooling system modeled by the tool worked with the same performance as the one tested in the laboratory. Under these conditions, the present study has

made possible to define the region on which the Therm-1D hot side input quantities are mediated. Considering that the convective heat transfer to the wall is conditioned by the presence and performance of the effusion jets, it has been assumed to determine the region, near the plate, where the process of mixing and the convective heat transfer develops. Finally, it has been determined a relationship that allowed taking as fundamental parameter the coolant mass fraction tracer coming from the effusion holes. This relationship led to the definition of the reference region for the determination of the hot side one-dimensional trends for the Therm-1D inputs. A sensitivity analysis for the hot side discretization parameters has been carried out. The analysis has shown the reliability of the choices made for the definition of the hot gas side input magnitudes region. The Sobol indices highlighted the importance of the two magnitudes studied. This has allowed a better understanding of the importance of both the width of the region and the precision of discretization. Also, it gives a general character and makes it applicable subsequently in the presence of effusion/dilution cooling.

In the last part of this work, a heat transfer problem analysis and an assessment of air-cooling feasibility for *Rotating Detonation Combustors* have been done. Starting from boundary conditions assumed from the literature review, heat fluxes per surface unit relative to the detonation zone were evaluated with a one-dimensional model using conduction and convection relationships. Due to these results from the first analysis once a maximum temperature limit has been imposed it has been possible to identify a working region in terms of heat transfer coefficient in which it is necessary to work to cool properly the operating combustor. After that, thanks to a DOE, it has been possible to investigate different single cooling system configurations, to explore the design space to get some guidelines for further studies. The Reynolds number at the outlet of the cooling system was varied between 20000 and 130000. Operational maps were built, identifying the global performance of every single configuration geometric layouts. The map reports the global effectiveness of every investigated case as a function of the relative geometric parameter. A sensitivity analysis was performed using the *Therm-1D/Dakota* coupled procedure that highlighted which geometric parameters were most relevant for each layout. After the results of this initial feasibility study, a double arrangement cooling system was considered. Thanks to the *Therm-1D/Dakota* coupled procedure, it has been possible to evaluate the system performances. In conclusion, a total of three dual cooling configurations, that could appropriately cool the combustor liner under study, were determined. A sensitivity analysis was performed on the geometric parameter of these configurations to understand which ones are the most relevant for each cooling configuration. The present work gives some guidelines for further improvement in the assessment of air-cooling system feasibility and design. In advanced research, this could be helpful in the definition of a proper cooling system design which will be useful for steady-state operating conditions studies of rotating detonation combustors.

The integrated tool *Therm-1D/Dakota* was necessary to obtain a robust design, i.e., within the limits of the capabilities of the code, having the output quantities as independent as possible from uncertainties. Thus, the result has been made independent from what are the uncertainties related to the behavior of the code and those dependent on the input data.

These methodologies, if correctly used, can lead to a complete understanding of how the mathematical model approximates and solves the real physical problem. The output is no longer a deterministic distribution, but it is a range and above all, it is a statistical evaluation of occurrence, which is an essential aspect for a one-dimensional code. Finally, it was possible to realize a sensitivity analysis to determine which uncertain input parameter has the greatest impact on the output investigated. The tool has been tested on different types of cooling systems, with different applications and aims. This has allowed to develop and validate an innovative, faster and more reliable procedure for the preliminary design or optimization of cooling systems for combustors.

As for future perspectives, it is possible to hypothesize the addition of further functionalities to the procedure, one of all the machine learning, to make it even more independent from possible uncertainties. It is also expected the possibility of application in new and different fields, thanks to the versatility of the tool, as already demonstrated in this work.

Appendix A

Here are the correlations used by the code to estimate heat transfer and pressure losses for the convective cooling system arrangements shown in this dissertation.

Smooth

Dittus-Boelter

$$Nu = 0.0243 \cdot Re^{4/5} \cdot Pr^{n} \qquad \textbf{(A.1)}$$

$$n \begin{cases} 0.3 & warming\ flux \\ 0.4 & cooling\ flux \end{cases}$$

Blasius

$$f = 0.046 \cdot Re^{-0,2} \qquad \textbf{(A.2)}$$

Rib

Han et al. 1978

Validity ranges: Han et al. 1978
$2000 < Re < 30000$
$12 < A_r < 25$
$5 < S_x/e < 10$
$0,07 < e/D_h < 0,1$
$20° < \alpha < 90°$

Table A.1 Han et al.1978 [242] validity ranges

Friction Roughness Function:

$$R(e^+) = 4.9\left(\frac{45}{\alpha}\right)^{0.57}\left(\frac{S_x/e}{10}\right)^{n}$$

$$n\begin{cases} -0.13 & if\ \dfrac{S_x}{e} < 10 \\ 0.53\left(\dfrac{\alpha}{90}\right)^{0.71} & if\ \dfrac{S_x}{e} \geq 10 \end{cases} \quad \textbf{(A.3)}$$

Friction Factor for two opposite ribbed walls:

$$f_{r2} = \frac{2}{\left(R(e^+) - 2{,}5ln\left(2\frac{e}{D_h}\right) - 3{,}75\right)^2} \quad \textbf{(A.4)}$$

Roughness Reynolds Number:

$$e^+ = \frac{e}{D_h} Re \left(\frac{f_{r2}}{2}\right)^{0{,}5} \quad \textbf{(A.5)}$$

Heat Transfer Roughness Function:

$$H(e^+) = \frac{10\left(\dfrac{e^+}{35}\right)^{0{,}28}}{\left(\dfrac{\alpha}{45}\right)^{j}} \quad \textbf{(A.6)}$$

$$j\begin{cases} 0.5 & se\ \alpha < 45 \\ -0.45 & se\ \alpha \geq 45 \end{cases}$$

Stanton number for two opposite ribbed walls:

$$St_{r2} = \frac{f_{r2}}{[H(e^+) - R(e^+)] \cdot (2f_{r2})^{0.5} + 2} \quad \textbf{(A.7)}$$

Han et al. 1985

Validity ranges: Han et al. 1985
$5000 < Re < 90000$
$A_r = 1$
$10 < S_x/e < 20$
$e/D_h = 0.06$
$30° < \alpha < 90°$

Table A.2 Han et al.1985 [243] validity ranges

Friction Roughness Function:

$$R(e^+) = \left[15.6 - 31.6\left(\frac{\alpha}{90}\right) + 21.1\left(\frac{\alpha}{90}\right)^2\right] \cdot \left(\frac{S_x/e}{10}\right)^{0.35} \cdot (0.003 \cdot e^+)^n \quad \textbf{(A.8)}$$

$$n\begin{cases} 0.17 & if\ \alpha < 45° \\ 0 & if\ \alpha \geq 45° \end{cases}$$

Friction Factor for two opposite ribbed walls:

$$f_{r2} = \frac{2}{\left(R(e^+) - 2{,}5ln\left(2\frac{e}{D_h}\right) - 3{,}75\right)^2} \quad \textbf{(A.9)}$$

Friction Factor for four opposite ribbed walls:

$$f_{r4} = \frac{2}{\left(R(e^+) - 2{,}5ln\left(2\frac{e}{D_h}\right) - 3{,}75\right)^2} \quad \textbf{(A.10)}$$

Roughness Reynolds Number:

$$e^+ = \frac{e}{D_h} Re \left(\frac{f_{r2}}{2}\right)^{0{,}5} \quad \textbf{(A.11)}$$

Heat Transfer Roughness Function:

$$H(e^+) = 2.83\left(\frac{\alpha}{90}\right)^{0{,}3} \cdot e^{+0.28} \cdot \left(\frac{S_x/e}{10}\right)^{0.14} \quad \textbf{(A.12)}$$

Average Heat Transfer Roughness Function:

$$\bar{H}(e^+) = 3.74\left(\frac{\alpha}{90}\right)^{0,3} \cdot e^{+0.28} \tag{A.13}$$

Stanton number on ribbed side, for two opposite ribbed walls:

$$St_{r2} = \frac{f_{r2}}{2 \cdot \left\{[H(e^+) - R(e^+)] \cdot \left(\frac{f_{r2}}{2}\right)^{0.5} + 1\right\}} \tag{A.14}$$

Average Stanton number in the center of the duct with two opposite ribbed walls:

$$St_m = \frac{f_{r4}}{2 \cdot \left\{[\bar{H}(e^+) - R(e^+)] \cdot \left(\frac{f_{r4}}{2}\right)^{0.5} + 1\right\}} \tag{A.15}$$

Stanton number on the smooth side, for two opposite ribbed walls:

$$St_s = St_m + \frac{W}{H}(St_m - St_{r2}) \tag{A.16}$$

Han & Park 1988

Validity ranges: Han & Park 1988
$5000 < Re < 80000$
$1 < A_r < 4$
$10 < S_x/e < 20$
$0,02 < e/D_h < 0,08$
$30° < \alpha < 90°$

Table A.3 Han & Park 1988 [244] validity ranges

Friction Roughness Function:

$$R(e^+) = \left[12.31 - 27.07\left(\frac{\alpha}{90}\right) + 17.86\left(\frac{\alpha}{90}\right)^2\right] \cdot \left(\frac{S_x/e}{10}\right)^{0.35} \cdot (A_r)^m \tag{A.17}$$

$$m\begin{cases}0.35 & if\ \alpha < 90° \\ 0 & if\ \alpha = 90°\end{cases}$$

$$if\ A_r > 2\ \ let\ \ A_r = 2$$

Friction Factor for two opposite ribbed walls:

$$f_{r2} = \left(f_{r4} + \frac{W}{H} f_{FD}\right)\left(\frac{W}{W+H}\right) \tag{A.18}$$

Friction Factor for four opposite ribbed walls:

$$f_{r4} = \frac{2}{\left(R(e^+) - 2{,}5ln\left(2\frac{e}{D_h}\cdot\frac{2W}{W+H}\right) - 2{,}5\right)^2} \tag{A.19}$$

Roughness Reynolds Number:

$$e^+ = \frac{e}{D_h} Re \left(\frac{f_{r4}}{2}\right)^{0{,}5} \tag{A.20}$$

Heat Transfer Roughness Function:

$$G(e^+) = 2.24\left(\frac{\alpha}{90}\right)^y \cdot e^{+^{0.28}} \cdot \left(\frac{p/e}{10}\right)^n \cdot \left(\frac{W}{H}\right)^{0.1}$$

$$y\begin{cases} 0 & se\ \frac{W}{H} > 1 \\ 0.35 & se\ \frac{W}{H} = 1 \end{cases} \tag{A.21}$$

$$n\begin{cases} 0 & se\ \frac{W}{H} > 1 \\ 0.10 & se\ \frac{W}{H} = 1 \end{cases}$$

Stanton number on ribbed side, for two opposite ribbed walls:

$$St_{r2} = \frac{f_{r2}}{2\cdot\left\{[G(e^+) - R(e^+)]\cdot\left(\frac{f_{r2}}{2}\right)^{0.5} + 1\right\}} \tag{A.22}$$

Average Stanton number in the center of the duct with two opposite ribbed walls:

$$St_m = \frac{f_{r4}}{2 \cdot \left\{ [1.2 \cdot G(e^+) - R(e^+)] \cdot \left(\frac{f_{r4}}{2}\right)^{0.5} + 1 \right\}} \quad \textbf{(A.23)}$$

Stanton number on the smooth side, for two opposite ribbed walls:

$$St_s = St_m + \frac{W}{H}(St_m - St_{r2}) \quad \textbf{(A.24)}$$

Han et al. 1989

Validity ranges: Han et al. 1989
$10000 < Re < 60000$
$1/4 < A_r < 1$
$S_x/e = 10$
$0{,}05 < e/D_h < 0{,}08$
$30° < \alpha < 90°$

Table A.4 Han et al. 1989 [251] validity ranges

Friction Roughness Function:

$$R(e^+) = \left[12.31 - 27.07\left(\frac{\alpha}{90}\right) + 17.86\left(\frac{\alpha}{90}\right)^2\right] \cdot \left(\frac{W}{H}\right)^m$$

$$m \begin{cases} -0.5 & se\ 60° \le \alpha \le 90° \\ -0.5 \cdot \left(\frac{\alpha}{60}\right)^2 & se\ 30° < \alpha < 60° \\ 0 & se\ \alpha \le 30° \end{cases} \quad \textbf{(A.25)}$$

Friction Factor for two opposite ribbed walls:

$$f_{r2} = \left(f_{r4} + \frac{W}{H} f_{FD}\right)\left(\frac{W}{W+H}\right) \quad \textbf{(A.26)}$$

Friction Factor for four opposite ribbed walls:

$$f_{r4} = \frac{2}{\left(R(e^+) - 2{,}5ln\left(2\frac{e}{D_h} \cdot \frac{2W}{W+H}\right) - 2{,}5\right)^2} \quad \textbf{(A.27)}$$

Roughness Reynolds Number:

$$e^+ = \frac{e}{D_h} Re \left(\frac{f_{r4}}{2}\right)^{0,5} \tag{A.28}$$

Heat Transfer Roughness Function:

$$G(e^+) = C \cdot e^{+^n}$$

$$if \ \frac{1}{2} \leq \frac{W}{H} \leq 1: \begin{cases} n = 0.35 \\ C = 2.24 & if \ \alpha = 90° \\ C = 1.80 & if \ \alpha < 90° \end{cases}$$

$$if \ \frac{1}{4} \leq \frac{W}{H} < \frac{1}{2}: \begin{cases} n = 0.35 \cdot \left(\frac{W}{H}\right)^{0.44} \\ C = 2.24 \cdot \left(\frac{W}{H}\right)^{-0.76} & if \ \alpha = 90° \\ C = 1.80 \cdot \left(\frac{W}{H}\right)^{-0.76} & if \ \alpha < 90° \end{cases} \tag{A.29}$$

Stanton number on ribbed side, for two opposite ribbed walls:

$$St_{r2} = \frac{f_{r2}}{2 \cdot \left\{ [G(e^+) - R(e^+)] \cdot \left(\frac{f_{r2}}{2}\right)^{0.5} + 1 \right\}} \tag{A.30}$$

Average Stanton number in the center of the duct with two opposite ribbed walls:

$$St_m = \frac{f_{r4}}{2 \cdot \left\{ [1.2 \cdot G(e^+) - R(e^+)] \cdot \left(\frac{f_{r4}}{2}\right)^{0.5} + 1 \right\}} \tag{A.31}$$

Stanton number on the smooth side, for two opposite ribbed walls:

$$St_s = St_m + \frac{W}{H}(St_m - St_{r2}) \tag{A.32}$$

Dimple

Maithani & Kumar

Validity ranges: Maithani & Kumar 2019
$5000 < Re < 27000$
$15 < S_x/d_d < 35$
$15 < S_y/d_d < 25$
$0.5 < e/d_d < 1.5$

Table A.5 Maithani & Kumar 2019 [246] validity ranges

Average Nusselt number in the center of the duct with two opposite dimpled walls:

$$Nu = 2.98 \cdot 10^{-3} \cdot Re^{0.9899} \cdot \left(\frac{S_x}{d_d}\right)^{-0.1754} \cdot e^{-0.004\left(ln\left(S_x/d_d\right)\right)^2} \cdot \left(\frac{S_y}{d_d}\right)^{1.3085} \cdot e^{-0.248\left(ln\left(S_y/d_d\right)\right)^2} \cdot \left(\frac{e}{d_d}\right)^{0.0998} \cdot e^{-0.2385\left(ln\left(e/d_d\right)\right)^2} \quad \textbf{(A.33)}$$

Average Friction factor in the center of the duct with two opposite dimpled walls:

$$f_r = 366.46 \cdot Re^{-1.068} \cdot \left(\frac{S_x}{d_d}\right)^{0.6351} \cdot e^{-0.1641\left(ln\left(S_x/d_d\right)\right)^2} \cdot \left(\frac{S_y}{d_d}\right)^{1.4643} \cdot e^{-0.2968\left(ln\left(S_y/d_d\right)\right)^2} \cdot \left(\frac{e}{d_d}\right)^{0.1047} \cdot e^{-0.6009\left(ln\left(e/d_d\right)\right)^2} \quad \textbf{(A.34)}$$

Pin-Fin

Validity ranges: Pin-Fin
$2 < S_y/d_d < 4$
Metzger ($Z/d_d < 3$)
$1.5 < S_x/d_d < 5$
Faulkner ($Z/d_d > 3$)
$1.5 < S_x/d_d < 3.4$

Table A.6 Metzger [247] and Faulkner [248] validity ranges

Average Friction factor in the center of the duct:

$$if\ Re < 10000\ f_r = 0.317 \cdot Re^{-0.132}$$
$$if\ Re \geq 10000\ f_r = 1.760 \cdot Re^{-0.318} \quad \textbf{(A.35)}$$

Metzger

Average Nusselt number:

$$Nu = 0.135 \cdot Re^{0.69} \cdot \left(\frac{S_x}{d_d}\right)^{-0.34} \quad \textbf{(A.36)}$$

Faulkner

Average Nusselt number:

$$Nu = \left[0.023 + \left(\frac{4.143 \cdot e^{-3.094 \cdot \left({}^{S_x}/_{d_d}\right) - 0.89 \cdot \left({}^{S_y}/_{Z}\right)^{0.5075}}}{Re^{0.2946}}\right)\right] \cdot Re^{0.8} \cdot Pr^{1/3} \quad \textbf{(A.37)}$$

Jet Impingement

Florschuetz

Nusselt number:

$$Nu = A \cdot Re^{m} \cdot \left\{1 - B\left[\left(\frac{Z}{d_d}\right)\left(\frac{G_c}{G_j}\right)\right]^{n}\right\} \cdot Pr^{1/3} \quad \textbf{(A.38)}$$

where G_c is the crossflow mass flux and $G_j$is the jet mass flux.

$$A, B, m, n = C \cdot \left(\frac{S_x}{d_d}\right)^{nx} \cdot \left(\frac{S_y}{d_d}\right)^{ny} \cdot \left(\frac{Z}{d_d}\right)^{nz}$$

Friction factor:

$$f_r = 0.3475 \cdot Re^{-0.5244} \cdot \left(\frac{S_x}{D_h}\right)^{0.4169} \cdot \left(\frac{S_y}{D_h}\right)^{0.5321} \cdot \left(\frac{d_d}{D_h}\right)^{-1.4848} \cdot e^{-0.2210\left(ln\left(\frac{d_d}{D_h}\right)\right)^2} \quad \textbf{(A.39)}$$

	Inline Pattern				Inline Pattern			
	C	nx	ny	nz	C	nx	ny	nz
A	1.18	-0.944	-0.642	0.169	1.87	-0.771	-0.999	-0.257
n	0.612	0.059	0.032	-0.022	0.571	0.028	0.092	0.039
B	0.437	0.095	-0.219	0.275	1.03	-0.243	-0.307	0.059
n	0.092	0.005	0.599	1.04	0.442	0.098	-0.003	0.304

Table A.7 Coefficients for Florschuetz correlation [199]

Bibliography

[1] *Lefebvre, A. H., and Ballal, D. R., 2010,* Gas Turbine Combustion.

[2] *Mellor, A. M., 1990,* Design of Modern Turbine Combustors.

[3] *Acharya, S., and Kanani, Y., 2017, "Advances in Film Cooling Heat Transfer,"* Advances in Heat Transfer, *Elsevier Inc., pp. 91–156.*

[4] *Wilcock, R. C., Young, J. B., and Horlock, J. H., 2005, "The Effect of Turbine Blade Cooling on the Cycle Efficiency of Gas Turbine Power Cycles," J. Eng. Gas Turbines Power.*

[5] *KOFF, B., 1991, "Spanning the Globe with Jet Propulsion."*

[6] *Gad-Briggs, A., Pilidis, P., and Nikolaidis, T., 2017, "A Review of the Turbine Cooling Fraction for Very High Turbine Entry Temperature Helium Gas Turbine Cycles for Generation IV Reactor Power Plants," J. Nucl. Eng. Radiat. Sci.*

[7] *Bunker, R. S., 2009, "The Effects of Manufacturing Tolerances on Gas Turbine Cooling," J. Turbomach.,* ***131****(4).*

[8] *Stimpson, C. K., Snyder, J. C., Thole, K. A., and Mongillo, D., 2018, "Effectiveness Measurements of Additively Manufactured Film Cooling Holes," J. Turbomach.*

[9] *Stimpson, C. K., Snyder, J. C., Thole, K. A., and Mongillo, D., 2018, "Effects of Coolant Feed Direction on Additively Manufactured Film Cooling Holes," J. Turbomach.*

[10] *Redeker, G., Müller, R., Isaacs, D., and Hirdes, R., 1994, "A Selection of Experimental Test Cases for the Validation of CFD Codes - Volume II," Agard Ar-303.*

[11] *Massini, M., and Montomoli, F., 2018, "Manufacturing/in-Service Uncertainty and Impact on Life and Performance of Gas Turbines/Aircraft Engines,"* Uncertainty Quantification in Computational Fluid Dynamics and Aircraft Engines: Second Edition.

[12] *Massini, M., Miller, R. J., and Hodson, H. P., 2008, "A New Intermittent Aspirated Probe for the Measurement of Stagnation Quantities in High Temperature Gases,"* Proceedings of the ASME Turbo Expo.

[13] *Wilcox, D. C., 1993,* Turbulence Modeling for CFD.

[14] *Tietz, S., and Behrendt, T., 2011, "Development and Application of a Pre-Design Tool for Aero-Engine Combustors," CEAS Aeronaut. J.*

[15] *Andreini, A., Ceccherini, A., Facchini, B., Turrini, F., and Vitale, I., 2009, "Assessment of a Set of Numerical Tools for the Design of Aero-Engines Combustors: Study of a Tubular Test Rig,"*

Proceedings of the ASME Turbo Expo.

[16] *Iaccarino, G., 2008, "Quantification of Uncertainty in Flow Simulations Using Probabilistic Methods," Stanford.Edu.*

[17] *Andreini, A., Soghe, R. Da, Facchini, B., Mazzei, L., Colantuoni, S., and Turrini, F., 2014, "Local Source Based CFD Modeling of Effusion Cooling Holes: Validation and Application to an Actual Combustor Test Case," J. Eng. Gas Turbines Power.*

[18] *Le Maître, O. P., and Knio, O. M., 2010,* Spectral Methods for Uncertainty Quantification*, Springer Netherlands, Dordrecht.*

[19] *Carazas, F. J. G., and de Souza, G. F. M., 2012, "Reliability Analysis of Gas Turbine,"* Springer Series in Reliability Engineering.

[20] *Carazas, F. J. G., and De Souza, G. F. M., 2009, "Availability Analysis of Gas Turbines Used in Power Plants," Int. J. Thermodyn.*

[21] *Kappas, J., 2002, "Review of Risk and Reliability Methods for Aircraft Gas Turbine Engines," Report.*

[22] *Iooss, B., and Lemaître, P., 2015, "A Review on Global Sensitivity Analysis Methods," Oper. Res. Comput. Sci. Interfaces Ser.*

[23] *Borgonovo, E., and Plischke, E., 2016, "Sensitivity Analysis: A Review of Recent Advances," Eur. J. Oper. Res.*

[24] *Andreini, A., Carcasci, C., Ceccherini, A., Facchini, B., and Surace, M., "Combustor Liner Temperature Prediction : A Preliminary Tool Development and Its Application on Effusion Cooling Systems,"* First CEAS European Air and Space Conference Century Perspectives, Berlin*, CEAS, pp. 10–13.*

[25] *Lefebvre, A. H., and Herbert, M. V., 1960, "Heat-Transfer Processes in Gas-Turbine Combustion Chambers," Proc. Inst. Mech. Eng.*

[26] *Lefebvre, A. H., 1984, "Flame Radiation in Gas Turbine Combustion Chambers," Int. J. Heat Mass Transf.*

[27] *Norster, E. R., and Lefebvre, A. H., 1972, "INFLUENCE OF FUEL PREPARATION AND OPERATING CONDITIONS ON FLAME RADIATION IN A GAS TURBINE COMBUSTOR.,"* ASME Pap.

[28] *Kretschmer, D., and Odgers, J., 1978, "A Simple Method for the Prediction of Wall Temperatures in Gas Turbines,"* Proceedings of the ASME Turbo Expo.

[29] *Gosselin, P., De Champlain, A., and Kretschmer, D., 1999, "Prediction of Wall Heat Transfer for a Gas Turbine Combustor," Proc. Inst. Mech. Eng. Part A J. Power Energy.*

[30] *Facchini, B., Surace, M., and Zecchi, S., 2003, "A New Concept of Impingement Cooling for Gas Turbine Hot Parts and Its Influence on Plant Performance,"* American Society of Mechanical Engineers, International Gas Turbine Institute, Turbo Expo (Publication) IGTI.

[31] *Facchini, B., Surace, M., and Tarchi, L., 2005, "Impingement Cooling for Modern Combustors: Experimental Analysis and Preliminary Design,"* Proceedings of the ASME Turbo Expo.

[32] *Arcangeli, L., Facchini, B., Surace, M., and Tarchi, L., 2008, "Correlative Analysis of Effusion Cooling Systems," J. Turbomach.*

[33] Carcasci, C., Facchini, B., and Ferrara, G., 1995, "Rotor Blade Cooling Design Method for Heavy Duty Gas Turbine Applications," American Society of Mechanical Engineers (Paper).

[34] Carcasci, C., and Facchini, B., 1996, "A Numerical Procedure to Design Internal Cooling of Gas Turbine Stator Blades," Rev. Gen. Therm.

[35] Andreini, A., Ceccherini, A., Facchini, B., Turrini, F., and Vitale, I., 2009, "Assessment of a Set of Numerical Tools for the Design of Aero-Engines Combustors: Study of a Tubular Test Rig," Volume 2: Combustion, Fuels and Emissions*, ASME, pp. 421–433.*

[36] Farag, I. H., 1982, "NON LUMINOUS GAS RADIATION: APPROXIMATE EMISSIVITY MODELS.," Heat Transfer, Proceedings of the International Heat Transfer Conference.

[37] Andreini, A., Becchi, R., Facchini, B., Mazzei, L., Picchi, A., and Peschiulli, A., 2016, "Effusion Cooling System Optimization for Modern Lean Burn Combustor," Volume 5B: Heat Transfer*, American Society of Mechanical Engineers.*

[38] Gnielinski, V., 1976, "New Equations for Heat and Mass Transfer in Turbulent Pipe and Channel Flow," Int. Chem. Eng.

[39] L'Ecuyer, M. R., and Soechting, F. O., 1985, A Model for Correlating Flat Plate Film-Cooling Effectiveness for Rows of Round Holes.

[40] Baldauf, S., Scheurlen, M., Schulz, A., and Wittig, S., 2002, "Correlation of Film Cooling Effectiveness from Thermographic Measurements at Engine like Conditions," American Society of Mechanical Engineers, International Gas Turbine Institute, Turbo Expo (Publication) IGTI.

[41] Goldstein, R. J., 1971, "Film Cooling," Adv. Heat Transf.

[42] Colban, W. F., Thole, K. A., and Bogard, D., 2011, "A Film-Cooling Correlation for Shaped Holes on a Flat-Plate Surface," J. Turbomach.

*[43] SELLERS, J. P., 1963, "GASEOUS FILM COOLING WITH MULTIPLE INJECTION STATIONS," AIAA J., **1**(9), pp. 2154–2156.*

[44] Andreini, A., Carcasci, C., Gori, S., and Surace, M., 2005, "Film Cooling System Numerical Design: Adiabatic and Conjugate Analysis," Proceedings of the ASME Summer Heat Transfer Conference.

*[45] Kingman, J. F. C., and Moran, P. A. P., 1969, "An Introduction to Probability Theory.," J. R. Stat. Soc. Ser. A, **132**(1), p. 106.*

[46] Xiu, D., 2010, Numerical Methods for Stochastic Computations: A Spectral Method Approach.

[47] Rosenblatt, M., 1952, "Remarks on a Multivariate Transformation," Ann. Math. Stat.

[48] Karniadakis, G. E., Su, C. H., Xiu, D., Lucor, D., Schwab, C., and Todor, R. A., 2005, Generalzed Polynomial Chaos Solution for Differential Equations with Random Inputs*, Zurich, Switzerland.*

[49] Eldred, M. S., 2011, "DESIGN UNDER UNCERTAINTY EMPLOYING STOCHASTIC EXPANSION METHODS," Int. J. Uncertain. Quantif.

[50] Helton, J. C., Johnson, J. D., Sallaberry, C. J., and Storlie, C. B., 2006, "Survey of Sampling-Based Methods for Uncertainty and Sensitivity Analysis," Reliab. Eng. Syst. Saf.

[51] Adams, B. M., Ebeida, M. S., Eldred, M. S., Jakeman, J. D., Swiler, L. P., Stephens, J. A., Vigil, D. M., and Wildey, T. M., 2009, DAKOTA, A Multilevel Parallel Object-Oriented Framework for Design Optimization, Parameter Estimation, Uncertainty Quantification, and Sensitivity Analysis

Version 5.4 User's Manual SAND2010-2183.

[52] Eldred, M. S., Report, S., Giunta, A. A., Waanders, B. G. V. B., Wojtkiewicz, S. F., Hart, W. E., and Alleva, M. P., 2002, "DAKOTA, A Multilevel Parallel Object-Oriented Framework for Design Optimization, Parameter Estimation, Uncertainty Quantification, and Sensitivity Analysis (SAND 2001-3514)," Analysis.

[53] Gamannossi, A., Amerini, A., Poggiali, M., Elmi, C. A., Mazzei, L., and Andreini, A., 2019, "Uncertainty Quantification of an Aeronautical Combustor Using a 1-D Approach," AIP Conference Proceedings*, p. 020083.*

[54] Poggiali, M., Gamannossi, A., Langone, L., and Amerini, A., 2019, "Civil Aero-Engine Performance Prediction Using a Low-Order Code and Uncertainty Quantification Estimation," AIP Conference Proceedings*.*

[55] Eldred, M. S., and Burkardt, J., 2009, "Comparison of Non-Intrusive Polynomial Chaos and Stochastic Collocation Methods for Uncertainty Quantification," 47th AIAA Aerosp. Sci. Meet. Incl. New Horizons Forum Aerosp. Expo., pp. 1–20.

[56] Mueller, M. E., Iaccarino, G., and Pitsch, H., 2013, "Chemical Kinetic Uncertainty Quantification for Large Eddy Simulation of Turbulent Nonpremixed Combustion," Proc. Combust. Inst.

*[57] D'Ammaro, A., and Montomoli, F., 2013, "Uncertainty Quantification and Film Cooling," Comput. Fluids, **71**, pp. 320–326.*

[58] Babaee, H., Wan, X., and Acharya, S., 2014, "Effect of Uncertainty in Blowing Ratio on Film Cooling Effectiveness," J. Heat Transfer.

[59] Montomoli, F., Massini, M., Salvadori, S., and Martelli, F., 2010, "Geometrical Uncertainty and Film Cooling: Fillet Radii," Proceedings of the ASME Turbo Expo.

*[60] Shi, W., Chen, P., Li, X., Ren, J., and Jiang, H., 2019, "Uncertainty Quantification of the Effects of Small Manufacturing Deviations on Film Cooling: A Fan-Shaped Hole," Aerospace, **6**(4), p. 46.*

*[61] Gamannossi, A., Amerini, A., Mazzei, L., Bacci, T., Poggiali, M., and Andreini, A., 2019, "Uncertainty Quantification of Film Cooling Performance of an Industrial Gas Turbine Vane," Entropy, **22**(1), p. 16.*

[62] Wang, C., Sun, X., and Zhang, J., 2019, "Uncertainty Analysis of Trench Film Cooling on Flat Plate," Appl. Therm. Eng.

[63] Durocher, A., Versailles, P., Bourque, G., and Bergthorson, J. M., 2018, "Uncertainty Quantification of NOx Emissions Induced Through the Prompt Route in Premixed Alkane Flames."

[64] Zhao, Y., Guo, Z. P., and Niu, F. L., 2017, "The Uncertainty Analysis of Natural Circulation in Molten Salt Reactor Coupling Dakota with Genflow," International Conference on Nuclear Engineering, Proceedings, ICONE.

[65] Gamannossi, A., Amerini, A., Poggiali, M., Elmi, C. A., Mazzei, L., and Andreini, A., 2020, "Application of Uncertainty Quantification Methods To the Prediction of Effusion Cooled Combustor Liner Temperature," ASME 2020.

[66] Correa, S. M., 1998, "Power Generation and Aeropropulsion Gas Turbines: From Combustion Science to Combustion Technology," Symposium (International) on Combustion.

[67] Liu, Y., Sun, X., Sethi, V., Nalianda, D., Li, Y. G., and Wang, L., 2017, "Review of Modern Low

Emissions Combustion Technologies for Aero Gas Turbine Engines," Prog. Aerosp. Sci.

[68] Neumann, N., and Peitsch, D., 2020, "Pulsed Impingement Turbine Cooling and Its Effect on the Efficiency of Gas Turbines With Pressure Gain Combustion," Proceedings of ASME Turbo Expo 2020*, pp. 1–12.*

[69] McGuirk, J. J., 2014, "The Aerodynamic Challenges of Aeroengine Gas-Turbine Combustion Systems," Aeronaut. J., ***118****(1204), pp. 557–599.*

[70] von Neumann, J., 1942, Theory of Detonation Waves*, Institute for Advanced Study, Princeton, NJ.*

[71] Nordeen, C. A., Schwer, D., Schauer, F., Hoke, J., Barber, T., and Cetegen, B., 2014, "Thermodynamic Model of a Rotating Detonation Engine," Combust. Explos. Shock Waves.

[72] Stathopoulos, P., 2018, "Comprehensive Thermodynamic Analysis of the Humphrey Cycle for Gas Turbines with Pressure Gain Combustion," Energies, ***11****(12), p. 3521.*

[73] Offord, T., Miller, R. J., Dawson, J. R., Heffer, J. J. H., Mason, S., and Taylor, M., 2008, "Improving the Performance of a Valveless Pulse Combustor Using Unsteady Fuel Injection," 46th AIAA Aerospace Sciences Meeting and Exhibit.

[74] Ward, C. M., and Miller, R. J., 2012, "Performance Analysis of an Ejector Enhanced Pressure Gain Combustion Gas Turbine," 50th AIAA Aerospace Sciences Meeting Including the New Horizons Forum and Aerospace Exposition.

[75] Lefebvre, A. H., 1995, "The Role of Fuel Preparation in Low-Emission Combustion," J. Eng. Gas Turbines Power.

[76] Wulff, A., and Hourmouziadis, J., 1997, "Technology Review of Aeroengine Pollutant Emissions," Aerosp. Sci. Technol.

[77] Bertini, D., Mazzei, L., Andreini, A., and Facchini, B., 2019, "Multiphysics Numerical Investigation of an Aeronautical Lean Burn Combustor," Volume 5B: Heat Transfer*, American Society of Mechanical Engineers.*

[78] Rankin, B. A., Fotia, M. L., Naples, A. G., Stevens, C. A., Hoke, J. L., Kaemming, T. A., Theuerkauf, S. W., and Schauer, F. R., 2017, "Overview of Performance, Application, and Analysis of Rotating Detonation Engine Technologies," J. Propuls. Power.

[79] Theuerkauf, S. W., Schauer, F. R., Anthony, R., and Hoke, J. L., 2014, "Average and Instantaneous Heat Release to the Walls of an RDE," 52nd Aerospace Sciences Meeting.

[80] Theuerkauf, S. W., King, P. I., Schauer, F. R., and Hoke, J. L., 2013, "Thermal Management for a Modular Rotating Detonation Engine," 51st AIAA Aerospace Sciences Meeting Including the New Horizons Forum and Aerospace Exposition 2013.

[81] Warnatz, J., Maas, U., and Dibble, R. W., 2006, Combustion: Physical and Chemical Fundamentals, Modeling and Simulation, Experiments, Pollutant Formation.

[82] Boyce, M. P., 2006, Gas Turbine Engineering Handbook.

[83] Lutoschkin, E., "Pressure-Gain Combustion for Gas Turbines Based on Shock-Flame Interaction," Institute of Aircraft Propulsion Systems, University of Stuttgart.

[84] Paxson, D., and Kaemming, T., 2012, "Foundational Performance Analyses of Pressure Gain Combustion Thermodynamic Benefits for Gas Turbines," 50th AIAA Aerospace Sciences Meeting Including the New Horizons Forum and Aerospace Exposition*, American Institute of Aeronautics*

and Astronautics.

[85] Rasheed, A., Tangirala, V., Dean, A., Vandervort, C. L., and Haubert, C., 2004, "Interactions of a Pulsed Detonation Engine with a 2D Blade Cascade," 42nd AIAA Aerospace Sciences Meeting and Exhibit*, American Institute of Aeronautics and Astronautics.*

[86] Suresh, A., Hofer, D. C., and Tangirala, V. E., 2011, "Turbine Efficiency for Unsteady, Periodic Flows," J. Turbomach.

[87] Van Zante, D., Envia, E., and Turner, M. G., 2007, "The Attenuation of a Detonation Wave By an Aircraft Engine Axial Turbine," ISABE.

[88] Roy, A., Bedick, C., Strakey, P., Sidwell, T., Ferguson, D., Sisler, A., and Nix, A., 2016, "Development of a Three-Dimensional Transient Wall Heat Transfer Model of a Rotating Detonation Combustor," 54th AIAA Aerospace Sciences Meeting.

[89] Meyer, S. J., Polanka, M. D., Schauer, F. R., and Hoke, J. L., 2018, "Parameter Impact on Heat Flux in a Rotating Detonation Engine," AIAA Aerospace Sciences Meeting, 2018.

[90] Lee, J. H. S., 2008, The Detonation Phenomenon.

[91] Zel'dovich, Y. B., 1950, On the Theory of the Propagation of Detonation in Gaseous Systems*, National Advisory Committee for Aeronautics, Washington, DC, United States.*

[92] Anand, V., and Gutmark, E., 2018, "Rotating Detonations and Spinning Detonations: Similarities and Differences," AIAA Journal.

[93] Driscoll, R. B., Anand, V., St. George, A. C., and Gutmark, E. J., 2015, "Investigation on RDE Operation by Geometric Variation of the Combustor Annulus and Nozzle Exit Area," 9th U.S. Natl. Combust. Meet.

[94] Ma, J. Z., Zhang, S., Luan, M., and Wang, J., 2019, "Experimental Investigation on Delay Time Phenomenon in Rotating Detonation Engine," Aerosp. Sci. Technol.

[95] Kailasanath, K., 2009, "Research on Pulse Detonation Combustion Systems: A Status Report," 47th AIAA Aerospace Sciences Meeting Including The New Horizons Forum and Aerospace Exposition*, American Institute of Aeronautics and Astronautics.*

[96] Rasheed, A., Tangirala, V. E., Vandervort, C. L., Dean, A. J., and Haubert, C., 2004, "Interactions of a Pulsed Detonation Engine with a 2D Turbine Blade Cascade," AIAA Paper.

[97] Kailasanath, K., 2011, "The Rotating-Detonation-Wave Engine Concept: A Brief Status Report," 49th AIAA Aerospace Sciences Meeting Including the New Horizons Forum and Aerospace Exposition.

[98] Voitsekhovskii, B. V., Mitrofanov, V. V., and Topchiyan, M. E., 1969, "Structure of the Detonation Front in Gases (Survey)," Combust. Explos. Shock Waves.

[99] Bykovskii, F. A., and Vedernikov, E. F., 2009, "Heat Fluxes to Combustor Walls during Continuous Spin Detonation of Fuel-Air Mixtures," Combust. Explos. Shock Waves.

*[100] Bykovskii, F. A., Zhdan, S. A., and Vedernikov, E. F., 2006, "Continuous Spin Detonations," J. Propuls. Power, **22**(6), pp. 1204–1216.*

[101] Theuerkauf, S. W., "Heat Exchanger Design and Testing for a 6-Inch Rotatind Detonation Engine," p. 79.

[102] Theuerkauf, S. W., Schauer, F. R., Anthony, R., Paxson, D. E., Stevens, C. A., and Hoke, J. L., 2016,

"Comparison of Simulated and Measured Instantaneous Heat Flux in a Rotating Detonation Engine," 54th AIAA Aerospace Sciences Meeting.

[103] Theuerkauf, S. W., Schauer, F. R., Anthony, R., and Hoke, J. L., 2015, "Experimental Characterization of High-Frequency Heat Flux in a Rotating Detonation Engine," 53rd AIAA Aerospace Sciences Meeting.

[104] Frolov, S. M., Dubrovskii, A. V., and Ivanov, V. S., 2013, "Three-Dimensional Numerical Simulation of Operation Process in Rotating Detonation Engine."

[105] Roy, A., Strakey, P., Sidwell, T., and Ferguson, D., 2015, "Unsteady Heat Transfer Analysis to Predict Combustor Wall Temperature in Rotating Detonation Engine," 51st AIAA/SAE/ASEE Joint Propulsion Conference.

[106] Meyer, S. J., Polanka, M. D., Schauer, F. R., Anthony, R. J., Stevens, C., Hoke, J. L., and Rein, K., 2017, "Experimental Characterization of Heat Transfer Coefficients in a Rotating Detonation Engine," AIAA SciTech Forum - 55th AIAA Aerospace Sciences Meeting.

[107] Zhou, S., Ma, H., Liu, C., Zhou, C., and Liu, D., 2018, "Experimental Investigation on the Temperature and Heat-Transfer Characteristics of Rotating-Detonation-Combustor Outer Wall," Int. J. Hydrogen Energy.

[108] Yi, T. H., Turangan, C., Lou, J., Wolanski, P., and Kindracki, J., 2009, "A Three-Dimensional Numerical Study of Rotational Detonation in an Annular Chamber," 47th AIAA Aerospace Sciences Meeting Including the New Horizons Forum and Aerospace Exposition.

[109] Schwer, D. A., and Kailasanath, K., 2015, "Physics of Heat-Release in Rotating Detonation Engines," 53rd AIAA Aerospace Sciences Meeting.

[110] Le Naour, B., Falempin, F., and Miquel, F., 2011, "Recent Experimental Results Obtained on Continuous Detonation Wave Engine," 17th AIAA International Space Planes and Hypersonic Systems and Technologies Conference 2011.

[111] Kindracki, J., Wolański, P., and Gut, Z., 2011, "Experimental Research on the Rotating Detonation in Gaseous Fuels-Oxygen Mixtures," Shock Waves.

[112] Randall, S., St George, A., Driscoll, R., Anand, V., and Gutmark, E. J., 2015, "Numerical and Experimental Study of Heat Transfer in a Rotating Detonation Engine," 53rd AIAA Aerospace Sciences Meeting.

[113] Roy, A., Strakey, P., Sidwell, T., and Ferguson, D., 2015, "Unsteady Heat Transfer Analysis to Predict Combustor Wall Temperature in Rotating Detonation Engine," 51st AIAA/SAE/ASEE Joint Propulsion Conference.

[114] Cocks, P. A. T., Holley, A. T., and Rankin, B. A., 2016, "High Fidelity Simulations of a Non-Premixed Rotating Detonation Engine," 54th AIAA Aerospace Sciences Meeting.

[115] Goto, K., Nishimura, J., Kawasaki, A., Matsuoka, K., Kasahara, J., Matsuo, A., Funaki, I., Nakata, D., Uchiumi, M., and Higashino, K., 2019, "Propulsive Performance and Heating Environment of Rotating Detonation Engine with Various Nozzles," J. Propuls. Power.

[116] Stevens, C. A., Fotia, M. L., Hoke, J. L., and Schauer, F. R., 2019, "An Experimental Comparison of the Inner and Outer Wall Heat Flux in an Rde," AIAA Scitech 2019 Forum.

[117] Kailasanath, K., 2020, "Recent Developments in the Research on Pressure-Gain Combustion

Devices," Innovations in Sustainable Energy and Cleaner Environment. Green Energy and Technology, *S. Springer, ed., pp. 3–21.*

[118] Andrews, G. E., and Bazdidi-Tehrani, F., 1989, "Small Diameter Film Cooling Hole Heat Transfer: The Influence of the Number of Holes," Proceedings of the ASME Turbo Expo.

[119] Andrews, G. E., Khalifa, I. M., Asere, A. A., and Bazdidi-Tehrani, F., 1995, "Full Coverage Effusion Film Cooling with Inclined Holes," Proceedings of the ASME Turbo Expo.

[120] Bernhard Gustafsson, K. M., and Gunnar Johansson, T., 2001, "An Experimental Study of Surface Temperature Distribution on Effusion-Cooled Plates," J. Eng. Gas Turbines Power.

[121] Kelly, G. B., and Bogard, D. G., 2003, "An Investigation of the Heat Transfer for Full Coverage Film Cooling," American Society of Mechanical Engineers, International Gas Turbine Institute, Turbo Expo (Publication) IGTI.

[122] Sen, B., Schmidt, D. L., and Bogard, D. G., 1996, "Film Cooling with Compound Angle Holes: Heat Transfer," J. Turbomach.

[123] Andrews, G. E., Asere, A. A., Gupta, M. L., and Mkpadi, M. C., 1985, "FULL COVERAGE DISCRETE HOLE FILM COOLING: THE INFLUENCE OF HOLE SIZE.," American Society of Mechanical Engineers (Paper).

[124] Martiny, M., Schulz, A., and Wittig, S., 1995, "Full-Coverage Film Cooling Investigations: Adiabatic Wall Temperatures and Flow Visualization," American Society of Mechanical Engineers (Paper).

[125] Mutiny, M., Schulz, A., and Wittig, S., 1997, "Mathematical Model Describing the Coupled Heat Transfer in Effusion Cooled Combustor Walls," Proceedings of the ASME Turbo Expo.

[126] Kumada, M., Hirata, M., and Kasagi, N., 1981, "Studies of Full-Coverage Film Cooling Part 2: Measurement of Local Heat Transfer Coefficient," Proceedings of the ASME Turbo Expo.

*[127] Scrittore, J. J., Thole, K. A., and Burd, S. W., 2006, "Investigation of Velocity Profiles for Effusion Cooling of a Combustor Liner," J. Turbomach., **129**(3), pp. 518–526.*

[128] Ligrani, P., Goodro, M., Fox, M., and Moon, H. K., 2012, "Full-Coverage Film Cooling: Film Effectiveness and Heat Transfer Coefficients for Dense and Sparse Hole Arrays at Different Blowing Ratios," J. Turbomach.

[129] Scrittore, J. J., Thole, K. A., and Burd, S. W., 2005, "Experimental Characterization of Film-Cooling Effectiveness near Combustor Dilution Holes," Proceedings of the ASME Turbo Expo.

[130] Tarchi, L., Facchini, B., Maiuolo, F., and Coutandin, D., 2012, "Experimental Investigation on the Effects of a Large Recirculating Area on the Performance of an Effusion Cooled Combustor Liner," J. Eng. Gas Turbines Power.

[131] Metzger, D. E., Takeuchi, D. I., and Kuenstler, P. A., 1973, "Effectiveness and Heat Transfer with Full-Coverage Film Cooling," J. Eng. Gas Turbines Power.

[132] Martinez-Botas, R. F., and Yuen, C. H. N., 2000, "Measurement of Local Heat Transfer Coefficient and Film Cooling Effectiveness through Discrete Holes," Proceedings of the ASME Turbo Expo.

[133] Hu, Y., and Ji, H., 2004, "Numerical Study of the Effect of Blowing Angle on Cooling Effectiveness of an Effusion Cooling," Proceedings of the ASME Turbo Expo 2004.

[134] Facchini, B., Maiuolo, F., Tarchi, L., and Coutandin, D., 2010, "Combined Effect of Slot Injection,

Effusion Array and Dilution Hole on the Heat Transfer Coefficient of a Real Combustor Liner - Part 1 Experimental Analysis," Proceedings of the ASME Turbo Expo.

[135] Facchini, B., Maiuolo, F., Tarchi, L., and Coutandin, D., 2011, "Experimental Investigation on the Effects of a Large Recirculating Area on the Performance of an Effusion Cooled Combustor Liner," Proceedings of the ASME Turbo Expo.

[136] Andreini, A., Ceccherini, A., Facchini, B., and Coutandin, D., 2010, "Combined Effect of Slot Injection, Effusion Array and Dilution Hole on the Heat Transfer Coefficient of a Real Combustor Liner Part 2: Numerical Analysis," Proceedings of the ASME Turbo Expo.

*[137] Andreini, A., Facchini, B., Picchi, A., Tarchi, L., and Turrini, F., 2014, "Experimental and Theoretical Investigation of Thermal Effectiveness in Multiperforated Plates for Combustor Liner Effusion Cooling," J. Turbomach., **136**(9).*

[138] Andreini, A., Bonini, A., Caciolli, G., Facchini, B., and Taddei, S., 2011, "Numerical Study of Aerodynamic Losses of Effusion Cooling Holes in Aero-Engine Combustor Liners," J. Eng. Gas Turbines Power.

[139] Lin, Y., Song, B., Li, B., Liu, G., and Wu, Z., 2003, "Investigation of Film Cooling Effectiveness of Full-Coverage Inclined Multihole Walls with Different Hole Arrangements," American Society of Mechanical Engineers, International Gas Turbine Institute, Turbo Expo (Publication) IGTI.

[140] Lin, Y., Song, B., Li, B., and Liu, G., 2006, "Measured Film Cooling Effectiveness of Three Multihole Patterns," J. Heat Transfer.

*[141] Krewinkel, R., 2013, "A Review of Gas Turbine Effusion Cooling Studies," Int. J. Heat Mass Transf., **66**, pp. 706–722.*

[142] Yellu Kumar, K. R., Qayoum, A., Saleem, S., and Qayoum, F., 2020, "Effusion Cooling in Gas Turbine Combustion Chambers - A Comprehensive Review," IOP Conference Series: Materials Science and Engineering.

[143] Leger, B., Miron, P., and Emidio, J. M., 2003, "Geometric and Aero-Thermal Influences on Multiholed Plate Temperature: Application on Combustor Wall," Int. J. Heat Mass Transf.

[144] Andreini, A., Champion, J. L., Facchini, B., Mercier, E., and Surace, M., 2007, "Advanced Liner Cooling Numerical Analysis for Low Emission Combustors," ICAS-Secretariat - 25th Congress of the International Council of the Aeronautical Sciences 2006.

[145] Miron, P., Berat, C., and Sabelnikov, V., 2004, "Effect of Blowing Rate on the Film Cooling Coverage on a Multi-Holed Plate: Application on Combustor Walls," Computational Studies.

[146] Michel, B., Gajan, P., Strzelecki, A., Wagner, B., Savary, N., Kourta, A., and Boisson, H. C., 2008, "Full Coverage Film Cooling: Comparison of Experimental and Numerical Data," 44th AIAA/ASME/SAE/ASEE Joint Propulsion Conference and Exhibit.

[147] Zhong, F., and Brown, G. L., 2009, "Experimental Study of Multi-Hole Cooling for Integrally-Woven, Ceramic Matrix Composite Walls for Gas Turbine Applications," Int. J. Heat Mass Transf.

[148] Johnson, B., Tian, W., Zhang, K., and Hu, H., 2014, "An Experimental Study of Density Ratio Effects on the Film Cooling Injection from Discrete Holes by Using PIV and PSP Techniques," Int. J. Heat Mass Transf.

[149] Kakade, V. U., Thorpe, S. J., and Gerendás, M., 2012, "Effusion-Cooling Performance at Gas

Turbine Combustor Representative Flow Conditions," Proceedings of the ASME Turbo Expo.

[150] Andreini, A., Becchi, R., Facchini, B., Picchi, A., and Peschiulli, A., 2017, "The Effect of Effusion Holes Inclination Angle on the Adiabatic Film Cooling Effectiveness in a Three-Sector Gas Turbine Combustor Rig with a Realistic Swirling Flow," Int. J. Therm. Sci., ***121****, pp. 75–88.*

[151] Andreini, A., Caciolli, G., Facchini, B., Tarchi, L., Coutandin, D., Peschiulli, A., and Taddei, S., 2012, "Density Ratio Effects on the Cooling Performances of a Combustor Liner Cooled by a Combined Slot/ Effusion System," Proceedings of the ASME Turbo Expo.

[152] Most, A., Savary, N., and Bérat, C., 2007, "Reactive Flow Modelling of a Combustion Chamber with a Multiperforated Liner," Collection of Technical Papers - 43rd AIAA/ASME/SAE/ASEE Joint Propulsion Conference.

[153] Harrington, M. K., McWaters, M. A., Bogard, D. G., Lemmon, C. A., and Thole, K. A., 2001, "Full-Coverage Film Cooling with Short Normal Injection Holes," J. Turbomach.

[154] Errera, M. P., and Chemin, S., 2004, "A Fluid-Solid Thermal Coupling Applied to an Effusion Cooling System," 34th AIAA Fluid Dynamics Conference and Exhibit.

[155] Mendez, S., and Nicoud, F., 2008, "Large-Eddy Simulation of a Bi-Periodic Turbulent Flow with Effusion," J. Fluid Mech.

[156] Zhong, F., and Brown, G. L., 2007, "A 3-Dimensional, Coupled, DNS, Heat Transfer Model and Solution for Multi-Hole Cooling," Int. J. Heat Mass Transf.

[157] Cottin, G., Laroche, E., Savary, N., and Millan, P., 2011, "Modeling of the Heat Flux for Multi-Hole Cooling Applications," Proceedings of the ASME Turbo Expo.

[158] Florenciano, J. L., and Bruel, P., 2016, "LES Fluid-Solid Coupled Calculations for the Assessment of Heat Transfer Coefficient Correlations over Multi-Perforated Walls," Aerosp. Sci. Technol.

[159] Andrei, L., Andreini, A., Bianchini, C., Facchini, B., and Mazzei, L., 2013, "Numerical Analysis of Effusion Plates for Combustor Liners Cooling with Varying Density Ratio," Proceedings of the ASME Turbo Expo.

[160] Incropera, F. P., and De Witt, D. P., 1981, "Fundamentals of Heat Transfer."

[161] Ligrani, P., 2013, "Heat Transfer Augmentation Technologies for Internal Cooling of Turbine Components of Gas Turbine Engines," Int. J. Rotating Mach.

[162] Ligrani, P. M., Oliveira, M. M., and Blaskovich, T., 2003, "Comparison of Heat Transfer Augmentation Techniques," AIAA J.

[163] Burgess, N. K., Oliveira, M. M., and Ligrani, P. M., 2003, "Nusselt Number Behavior on Deep Dimpled Surfaces within a Channel," J. Heat Transfer.

[164] Gromov, P. R., Zobnin, A. B., Rabinovich, M. I., and Sushchik, M. M., 1986, "Formation of Solitary Vortices in Flow over Small Spherical Depressions," PZhTF, ***12****, pp. 1323–1328.*

[165] Kesarev, V. S., and Kozlov, A. P., 1993, "Convective Heat Transfer in Turbulized Flow Past a Hemispherical Cavity," Heat Transf. Res.

[166] Afanasyev, V. N., Chudnovsky, Y. P., Leontiev, A. I., and Roganov, P. S., 1993, "Turbulent Flow Friction and Heat Transfer Characteristics for Spherical Cavities on a Flat Plate," Exp. Therm. Fluid Sci.

[167] Kimura, T., and Tsutahara, M., 1991, "Fluid Dynamic Effects of Grooves on Circular Cylinder

Surface," AIAA J.

[168] Chyu, M. K., Yu, Y., Ding, H., Downs, J. P., and Soechting, F. O., 1997, "Concavity Enhanced Heat Transfer in an Internal Cooling Passag," Proceedings of the ASME Turbo Expo.

[169] Gortyshov, Y. F., Popov, I. A., Amirkhanov, R. D., and Gulitsky, K. E., 2019, "STUDIES OF HYDRODYNAMICS AND HEAT EXCHANGE IN CHANNELS WITH VARIOUS TYPES OF INTENSIFIERS."

[170] Moon, H. K., O'Connell, T., and Glezer, B., 1999, "Channel Height Effect on Heat Transfer and Friction in a Dimpled Passage," Proceedings of the ASME Turbo Expo.

[171] Isaev, S. A., Leont'ev, A. I., and Baranov, P. A., 2000, "Identification of Self-Organized Vortexlike Structures in Numerically Simulated Turbulent Flow of a Viscous Incompressible Liquid Streaming around a Well on a Plane," Tech. Phys. Lett.

[172] Kithcart, M. E., and Klett, D. E., 1996, "Heat Transfer and Skin Friction Comparison of Dimpled versus Protrusion Roughness," J. Enhanc. Heat Transf.

[173] Metzger, D. E., Berry, R. A., and Bronson, J. P., 1982, "Developing Heat Transfer in Rectangular Ducts with Staggered Arrays of Short Pin Fins," J. Heat Transfer.

[174] Metzger, D. E., and Haley, S. W., 1982, "Heat Transfer Experiments and Flow Visualization for Arrays of Short Pin Fins," Volume 4: Heat Transfer; Electric Power*, American Society of Mechanical Engineers.*

[175] Sparrow, E. M., Ramsey, J. W., and Altemani, C. A. C., 1980, "Experiments on In-Line Pin Fin Arrays-and Performance Comparisons with Staggered Arrays," J. Heat Transfer.

[176] Brigham, B. A., and VanFossen, G. J., 1984, "Length to Diameter Ratio and Row Number Effects in Short Pin Fin Heat Transfer," J. Eng. Gas Turbines Power.

[177] Chyu, M. K., and Goldstein, R. J., 1991, "Influence of an Array of Wall-Mounted Cylinders on the Mass Transfer from a Flat Surface," Int. J. Heat Mass Transf.

[178] Chyu, M. K., Hsing, Y. C., Shih, T. I. P., and Natarajan, V., 1999, "Heat Transfer Contributions of Pins and Endwall in Pin-Fin Arrays: Effects of Thermal Boundary Condition Modeling," J. Turbomach.

[179] Chyu, M. K., Hsing, Y. C., and Natarajan, V., 1998, "Convective Heat Transfer of Cubic Fin Arrays in a Narrow Channel," J. Turbomach.

[180] Chyu, M. K., and Natarajan, V., 1996, "Heat Transfer on the Base Surface of Three-Dimensional Protruding Elements," Int. J. Heat Mass Transf.

[181] Hwang, C. C., 2001, "Lateral-Flow Effect on Endwall Heat Transfer and Pressure Drop in a Pin-Fin Trapezoidal Duct of Various Pin Shapes," J. Turbomach.

[182] Uzol, O., and Camci, C., 2001, "Elliptical Pin Fins as an Alternative to Circular Pin Fins for Gas Turbine Blade Cooling Applications: Part I: Endwall Heat Transfer and Total Pressure Loss Characteristics," Proceedings of the ASME Turbo Expo.

[183] Won, S. Y., Mahmood, G. I., and Ligrani, P. M., 2004, "Spatially-Resolved Heat Transfer and Flow Structure in a Rectangular Channel with Pin Fins," Int. J. Heat Mass Transf.

[184] Ligrani, P. M., and Mahmood, G. I., 2003, "Variable Property Nusselt Numbers in a Channel with Pin Fins," J. Thermophys. Heat Transf.

[185] Han, J. C., Dutta, S., and Ekkad, S., 2012, Gas Turbine Heat Transfer and Cooling Technology.

[186] Casarsa, L., Çakan, M., and Arts, T., 2002, "Characterization of the Velocity and Heat Transfer Fields in an Internal Cooling Channel with High Blockage Ratio," American Society of Mechanical Engineers, International Gas Turbine Institute, Turbo Expo (Publication) IGTI.

[187] Ligrani, P. M., and Mahmood, G. I., 2003, "Spatially Resolved Heat Transfer and Friction Factors in a Rectangular Channel with 45-Deg Angled Crossed-Rib Turbulators," J. Turbomach.

[188] Cho, H. H., Lee, S. Y., and Wu, S. J., 2001, "The Combined Effects of Rib Arrangemets and Discrete Ribs on Local Heat/Mass Transfer in a Square Duct," Proceedings of the ASME Turbo Expo.

[189] Al-Qahtani, M., Chen, H. C., and Han, J. C., 2003, "A Numerical Study of Flow and Heat Transfer in Rotating Rectangular Channels (AR = 4) with 45 Deg Rib Turbulators by Reynolds Stress Turbulence Model," J. Heat Transfer.

[190] Iacovides, H., 1998, "Computation of Flow and Heat Transfer through Rotating Ribbed Passages," Int. J. Heat Fluid Flow.

[191] Jia, R., Saidi, A., and Sundén, B., 2002, "Heat Transfer Enhancement in Square Ducts with V-Shaped Ribs of Various Angles," American Society of Mechanical Engineers, International Gas Turbine Institute, Turbo Expo (Publication) IGTI.

[192] Stephens, M. A., and Shill, T. I. P., 1997, "Computation of Compressible Flow and Heat Transfer in a Rotating Duct with Inclined Ribs and a 180-Degree Bend," Proceedings of the ASME Turbo Expo.

[193] Al-Qahtani, M., Jang, Y. J., Chen, H. C., and Han, J. C., 2002, "Prediction of Flow and Heat Transfer in Rotating Two-Pass Rectangular Channels with 45-Deg Rib Turbulators," J. Turbomach.

[194] Rigby, D. L., 1998, "Prediction of Heat and Mass Transfer in a Rotating Ribbed Coolant Passage with a 180 Degree Turn," Proceedings of the ASME Turbo Expo.

[195] Martin, H., 1977, "Heat and Mass Transfer between Impinging Gas Jets and Solid Surfaces," Adv. Heat Transf.

[196] Bradbury, L. J. S., 1965, "The Structure of a Self-Preserving Turbulent Plane Jet," J. Fluid Mech.

[197] Goldstein, R. J., and Seol, W. S., 1991, "Heat Transfer to a Row of Impinging Circular Air Jets Including the Effect of Entrainment," Int. J. Heat Mass Transf.

[198] Goldstein, R. J., and Behbahani, A. I., 1982, "Impingement of a Circular Jet with and without Cross Flow," Int. J. Heat Mass Transf.

*[199] Florschuetz, L. W., Truman, C. R., and Metzger, D. E., 1981, "Streamwise Flow and Heat Transfer Distributions for Jet Array Impingement with Crossflow," J. Heat Transfer, **103**(2), pp. 337–342.*

[200] Bunker, R. S., Dees, J. E., and Palafox, P., 2014, "Impingement Cooling in Gas Turbines: Design, Applications, and Limitations."

[201] Bertini, D., Mazzei, L., Puggelli, S., Andreini, A., Facchini, B., Bellocci, L., and Santoriello, A., 2018, "Numerical and Experimental Investigation on an Effusion-Cooled Lean Burn Aeronautical Combustor: Aerothermal Field and Metal Temperature," Proceedings of the ASME Turbo Expo.

[202] Silverman, B. W., 2018, Density Estimation: For Statistics and Data Analysis.

[203] Montomoli, F., D'Ammaro, A., and Uchida, S., 2013, "Uncertainty Quantification and Conjugate

Heat Transfer: A Stochastic Analysis," J. Turbomach., ***135****(3).*

[204] Avila, G., and Carrington, T., 2015, "A Multi-Dimensional Smolyak Collocation Method in Curvilinear Coordinates for Computing Vibrational Spectra," J. Chem. Phys.

[205] Helman, D., 1984, Detonation Pulse Engine*, National Research Council, 2101 Constitution Avenue, Washington, D.C., 20418.*

[206] Patil, S., Sedalor, T., Tafti, D., Ekkad, S., Kim, Y., Dutta, P., Moon, H. K., and Srinivasan, R., 2011, "Study of Flow and Convective Heat Transfer in a Simulated Scaled up Low Emission Annular Combustor," J. Therm. Sci. Eng. Appl.

[207] Patil, S., Abraham, S., Tafti, D., Ekkad, S., Kim, Y., Dutta, P., Moon, H. K., and Srinivasan, R., 2009, "Experimental and Numerical Investigation of Convective Heat Transfer in a Gas Turbine Can Combustor," Proceedings of the ASME Turbo Expo.

[208] Wurm, B., Schulz, A., and Bauer, H. J., 2009, "A New Test Facility for Investigating the Interaction between Swirl Flow and Wall Cooling Films in Combustors," Proceedings of the ASME Turbo Expo.

[209] Andreini, A., Becchi, R., Facchini, B., Mazzei, L., Picchi, A., and Turrini, F., 2016, "Adiabatic Effectiveness and Flow Field Measurements in a Realistic Effusion Cooled Lean Burn Combustor," J. Eng. Gas Turbines Power, ***138****(3).*

[210] Andreini, A., Facchini, B., Becchi, R., Picchi, A., and Turrini, F., 2016, "Effect of Slot Injection and Effusion Array on the Liner Heat Transfer Coefficient of a Scaled Lean-Burn Combustor with Representative Swirling Flow," J. Eng. Gas Turbines Power.

[211] Picchi, A., Andreini, A., Becchi, R., and Facchini, B., 2020, "A New Test Facility For Investigation Thermal Behaviour of Effusion Cooling Test Plates for RQL Combustors," pp. 1–12.

[212] Caciolli, G., Facchini, B., Picchi, A., and Tarchi, L., 2013, "Comparison between PSP and TLC Steady State Techniques for Adiabatic Effectiveness Measurement on a Multiperforated Plate," Exp. Therm. Fluid Sci.

[213] Shih, T. H., Liou, W. W., Shabbir, A., Yang, Z., and Zhu, J., 1995, "A New K-ϵ Eddy Viscosity Model for High Reynolds Number Turbulent Flows," Comput. Fluids.

[214] Fluent, A., 2013, "Ansys Fluent Theory Guide," ANSYS Inc., USA.

[215] Mazzei, L., Puggelli, S., Andreini, A., and Facchini, B., 2017, "Numerical Investigation of Optimized Arrangements for Effusion Cooling in Gas Turbine Combustor Applications," Proceedings of the ASME Turbo Expo.

[216] Mazzei, L., Andreini, A., Facchini, B., and Turrini, F., 2016, "Impact of Swirl Flow on Combustor Liner Heat Transfer and Cooling: A Numerical Investigation with Hybrid Reynolds-Averaged Navier Stokes-Large Eddy Simulation Models," J. Eng. Gas Turbines Power.

[217] Chterev, I., Foley, C. W., Foti, D., Kostka, S., Caswell, A. W., Jiang, N., Lynch, A., Noble, D. R., Menon, S., Seitzman, J. M., and Lieuwen, T. C., 2014, "Flame and Flow Topologies in an Annular Swirling Flow," Combust. Sci. Technol.

[218] Gupta, A. K., Lilley, D. G., and Syred, N., 1984, "Swirl Flows Abacus Press," Tunbridge Wells, Engl.

[219] Bunker, R. S., 2006, "Cooling Design Analysis," Gas Turbine Handb.

[220] Gustafsson, K. M. B., 2001, "Experimental Studies of Effusion Cooling," Doktorsavhandlingar vid Chalmers Tek. Hogsk.

[221] Bogard, D. G., and Thole, K. A., 2006, "Gas Turbine Film Cooling," J. Propuls. Power.

[222] Thole, K., Sinha, A., Bogard, D., and Crawford, M., 1990, "Mean Temperature Measurements of Jets with a Crossflow for Gas Turbine Film Cooling Application," Third Int. Symp. Transp. Phenom. Dyn. Rotating Mach.

[223] Yusop, N. M., Andrews, G. E., Ingham, D. B., Khalifa, I. M., Mkpadi, M. C., and Pourkashanlan, M., 2007, "Predictions of Adiabatic Film Cooling Effectiveness for Effusion Film Cooling," Proceedings of the ASME Turbo Expo.

[224] Thomas, M., and Povey, T., 2016, "A Novel Scalar Tracking Method for Optimising Film Cooling Systems," Proc. Inst. Mech. Eng. Part A J. Power Energy.

[225] Walton, M., and Yang, Z., 2014, "Numerical Study of Effusion Cooling Flow and Heat Transfer," Int. J. Comput. Methods Exp. Meas.

[226] Sobol', I. M., 1993, "Sensitivity Estimates for Nonlinear Mathematical Models," Math. Model. Comput. Exp.

[227] Heiser, W. H., and Pratt, D. T., 2002, "Thermodynamic Cycle Analysis of Pulse Detonation Engines," J. Propuls. Power.

[228] Hishida, M., Fujiwara, T., and Wolanski, P., 2009, "Fundamentals of Rotating Detonations," Shock Waves.

[229] Wolański, P., 2013, "Detonative Propulsion," Proc. Combust. Inst.

[230] DUNLAP, R., BREHM, R. L., and NICHOLLS, J. A., 1958, "A Preliminary Study of the Application of Steady-State Detonative Combustion to a Reaction Engine," J. Jet Propuls.

[231] Bluemner, R., Bohon, M. D., Paschereit, C. O., and Gutmark, E. J., 2018, "Single and Counter-Rotating Wave Modes in an RDC," AIAA Aerospace Sciences Meeting, 2018.

[232] Shank, J. C., King, P. I., Karnesky, J., Schauer, F. R., and Hoke, J. L., 2012, "Development and Testing of a Modular Rotating Detonation Engine," 50th AIAA Aerospace Sciences Meeting Including the New Horizons Forum and Aerospace Exposition.

[233] Bach, E., Bohon, M. D., Paschereit, C. O., and Stathopoulos, P., 2018, "Development of an Instrumented Guide Vane Set for Rdc Exhaust Flow Characterization," 2018 Joint Propulsion Conference.

[234] 2020, "SSINA: Stainless Steel: Composition/Properties."

[235] Randall, S., Anand, V., St. George, A. C., and Gutmark, E. J., 2015, "Numerical Study of Heat Transfer in a Rotating Detonation Combustor," 53rd AIAA Aerospace Sciences Meeting, American Institute of Aeronautics and Astronautics.

[236] Schwer, D., and Kailasanath, K., 2011, "Numerical Investigation of the Physics of Rotating-Detonation-Engines," Proc. Combust. Inst., **33**(2), pp. 2195–2202.

[237] Nordeen, C., 2013, "Thermodynamics of a Rotating Detonation Engine," Univ. Connect. Dr. Diss.

[238] Braun, J., Sousa, J., and Paniagua, G., 2018, "Numerical Assessment of the Convective Heat Transfer in Rotating Detonation Combustors Using a Reduced-Order Model," Appl. Sci.

[239] Valencia, J. J., and Quested, P. N., 2008, "Thermophysical Properties, ASM Handbook," Asm.

[240] Dittus, F. W., and Boelter, L. M. K., 1985, "Heat Transfer in Automobile Radiators of the Tubular Type," Int. Commun. Heat Mass Transf.

[241] Blasius, H., 1913, "Das Aehnlichkeitsgesetz Bei Reibungsvorgängen in Flüssigkeiten," Mitteilungen Über Forschungsarbeiten Auf Dem Gebiete Des Ingenieurwesens.

[242] Han, J. C., Glicksman, L. R., and Rohsenow, W. M., 1978, "An Investigation of Heat Transfer and Friction for Rib-Roughened Surfaces," Int. J. Heat Mass Transf.

*[243] Han, J. C., Park, J. S., and Lei, C. K., 1985, "Heat Transfer Enhancement in Channels With Turbulence Promoters," J. Eng. Gas Turbines Power, **107**(3), pp. 628–635.*

[244] Han, J. C., and Park, J. S., 1988, "Developing Heat Transfer in Rectangular Channels with Rib Turbulators," Int. J. Heat Mass Transf.

[245] Kumar, V., 2019, "Nusselt Number and Friction Factor Correlations of Three Sides Concave Dimple Roughened Solar Air Heater," Renew. Energy.

[246] Maithani, R., and Kumar, A., 2020, "Correlations Development for Nusselt Number and Friction Factor in a Dimpled Surface Heat Exchanger Tube," Exp. Heat Transf.

[247] Metzger, D. E., Shepard, W. B., and Haley, S. W., 1986, "ROW RESOLVED HEAT TRANSFER VARIATIONS IN PIN-FIN ARRAYS INCLUDING EFFECTS OF NON-UNIFORM ARRAYS AND FLOW CONVERGENCE.," American Society of Mechanical Engineers (Paper).

[248] Faulkner, F. E., 1971, "ANALYTICAL INVESTIGATION OF CHORD SIZE AND COOLING METHODS ON TURBINE BLADE COOLING REQUIREMENTS," NASA CR-120882.

*[249] Bunker, R. S., 2007, "Gas Turbine Heat Transfer: Ten Remaining Hot Gas Path Challenges," J. Turbomach., **129**(2), pp. 193–201.*

[250] Bunker, R. S., 2010, "Gas Turbine Engines: Turbine Cooling," Encyclopedia of Aerospace Engineering.